Max-Planck-Institute für Kolloid- und Grenzflächenforschung

Reactive eutectic media based on ammonium formate for the valorization of bio-sourced materials

Dissertation

zur Erlangung des akademischen Grades

"doctor rerum naturalium"

(Dr. rer. nat.)

in der Wissenschaftsdisziplin "Kolloid- und Polymerchemie"

eingereicht an der

Mathematisch-Naturwissenschaftlichen Fakultät

der Universität Potsdam

von

Helen Schneider

Hauptbetreuer*in: Prof. Dr. Dr. h.c. Markus Antonietti
Betreuer*innen: Prof. Dr. Andreas Taubert
Gutachter*innen: Dr. Mika Sipponen

Published online on the
Publication Server of the University of Potsdam:
https://doi.org/10.25932/publishup-61302
https://nbn-resolving.org/urn:nbn:de:kobv:517-opus4-613024

Table of Contents

Introduction

Motivation

Deep eutectic solvents (DES) are promising and versatile systems that can function as solvents, reagents, and catalysts in many applications and possibly also in natural systems. In contrast to conventional solvents, DES distinguish themselves by being imperatively composed of mixtures of simple molecules or salts. Often these compounds are solid at room temperature but become liquid upon mixing with each other at an apposite composition. The reason for this is suspected to be connected to hydrogen bond interactions between the different components, which results in a freezing point depression. Because of the vast number of possible components and their almost countless possible combinations, DES are considered so-called "designer solvents" as their physical and chemical properties can be adapted by the choice and composition of components.[1] Their role as solvents is however just one aspect of their possible functions. If one of the DES components is reactive (i.e., undergoes chemical transformation upon the appropriate triggering), then the DES becomes the medium in which the reaction is taking place as well as the reactant itself. Such unconventional media are also known as reactive eutectic media (REM), and they have been used for a wide range of (bio)chemical or material synthesis.

This thesis will investigate a variety of different REM, based on ammonium formate. Ammonium formate is insofar interesting, as it has mostly been neglected in previous research on DES in favor of quaternary ammonium salts. This is due to its comparably much higher reactivity which does not correspond to the role of a traditional solvent. However, this property of ammonium formate can also be exploited in its favor, in order to perform unusual chemical reactions. Such reaction will take place in the REM, which implicates the absence of a traditional solvent and thereby promises the benefits of solvent-free reactions.

Furthermore, the thesis will investigate the use of microwave heating to run chemical reactions in REM, as those two approaches offer a great synergy.[2,3] Microwave heating offers the potential to be generated from green electricity and can enable rapid reaction rates and higher yields compared to conventional heating. Prerequisites for this are reaction media with high polarities for an efficient absorption of microwave irradiation. Furthermore, it requires reaction media with low vapor pressures in order to avoid the risks of rapid pressure build up due to high heating rates. Both of these properties are fulfilled by REM.

The investigated REM will consist of ammonium formate as well as a range of different components that can all be bio-sourced. The thesis thereby aspires to put a focus on renewable starting materials. Ammonium formate itself is currently produced from fossil fuels as one of the cheapest bulk chemicals. However, its basic components – ammonia and formic acid – are both essential to the chemical industry and promising research is underway to produce them from renewable sources. E.g. formic acid is can be obtained by the two-electron reduction of CO_2

either through hydrogenation or electrolysis (the later being currently under pilot development).[4] Ammonia production is currently developed via electrochemical nitrogen reduction.[5,6]

The focus of research in this thesis is thereby very much in line with the guidelines of green chemistry. Green chemistry is not a subdivision of chemistry like organic or physical chemistry but instead has environmental, technological and societal objectives and is thereby linked to the wider goals of sustainability. Already coined in the 1990s, the term has become the catchphrase of a lot of research that has been published in recent years. Considering the current state of the world where the lifestyle of our so-called Western civilization appears to consume its own basis of existence (together with that of countless other animate beings), this by intention is certainly a good sign. However, there also has been some criticism of the term, as well as some urgent calls to give all of its guidelines the appropriate attention. The thesis will therefore also contain a closer inspection of the terminology of green chemistry.

Objectives and outline

The overall objective of this thesis is to explore the potential of REM based on ammonium formate as well as the synergy between REM and microwave heating. For this purpose, a number of different reactions in REM will be investigated and will be compared to conventional solvent-based procedures. Furthermore, the role of water as a third component of the REM is studied, and its influence on the respective reaction is investigated. Lastly, the possibility of using such REM for biomass treatment will be explored.

The thesis will begin with some necessary background information on the relevant subjects. CHAPTER 1 will therefore start with an introduction to DES (and the subfield of REM) and will give an overview on their applications in the literature up to date. Furthermore, it will introduce the mechanism of microwave heating and discuss its state of the art as well as pros and cons compared to conventional heating. Finally, it will define the approach of green chemistry, with a focus on its history as well as on contemporary discussions.

The subsequent chapters will discuss the specific experiments that were performed within this thesis. The chapters are structured in the way that each chapter presents a different REM and the reaction of ammonium formate with a different reaction partner. Each chapter will therefore start with relevant background information on the respective reaction, followed by an experimental section, the presentation of results and corresponding discussion as well as a conclusion.

CHAPTER 2 presents REM between ammonium formate and different monosaccharides. Their Maillard type reaction yields a range of pyrazine derivatives with potential antimicrobial properties.

CHAPTER 3 presents REM between ammonium formate and levulinic acid in a Leuckart reaction for the synthesis of 5-methyl-2-pyrrolidone.

CHAPTER 4 presents REM between ammonium formate and different organic acids for lignocellulosic biomass treatment. Thereby, the potential of such REM in the context of the biorefinery is investigated.

CHAPTER 5 presents REM between ammonium formate and citric acid. The endeavored product characterization points toward a yet undiscovered reaction pathway and the findings will be discussed within the research field of fluorophores and bottom-up carbon nanodots from citric acid.

CHAPTER 6 contains the overall conclusion of the thesis, based on the presented results.

The applied analysis techniques throughout the thesis are discussed in detail in the first chapter of the supplementary information (SI), chapter S1. They are ordered alphabetically and each analysis technique is shortly introduced from a general viewpoint and then with respect to the experimental procedure that is applied in the thesis. The subsequent chapters of the SI are paired with the chapters of the main text, so for example supplementary information of CHAPTER 2 can be found in chapter S2 of the SI.

CHAPTER 1
Theoretical background

1.1. Deep eutectic solvents (DES)

1.1.1. Definition

The concept of eutectic systems has gained much attention in the last two decades by the emergence of so-called deep eutectic solvents (DES). Such solvents are eutectic mixtures between two or more components, which are capable of associating with each other through hydrogen bond interactions. By changing the nature and the ratio of components, DES are tunable in a broad range of physical and physiochemical properties and are considered so-called designer solvents. In this sense, they are similar to ionic liquids but its constituents are in many cases cheaper, less toxic and biodegradable.[1]

The components of DES are typically divided into hydrogen-bond acceptors (HBAs) and hydrogen-bond donors (HBDs) as both types of components are typically present to ensure sufficient hydrogen bond formation for an excess melting point depression. Typical HBAs are halide salts or quaternary ammonium salts such as choline chloride[1] or betaine[7], but also uncharged molecules such as menthol have been used[8]. Typical HBDs include sugars, alcohols, carboxylic acids, amines, amides or amino acids.[9] From these components, DES are prepared by mixing. Often the formation is facilitated by moderate heating or preparing a water solution of the different components, which is then freeze-dried or vacuum dried and desiccated.[10]

The term "deep" in DES refers to the fact these eutectic mixtures possess abnormally low eutectic points – much lower than what would be predicted from their ideal liquid mixtures. This phenomenon has first been reported by Abbott et al.[1] in 2004[1] for a 1:2 mol fraction combination of choline chloride [Melting temperature (T_m) ≈ 302 °C] with crystalline urea [T_m ≈ 133 °C], which results in a liquid at room temperature [T_m = 12 °C]. The reason for this "deepness" is not finally understood but there is evidence that points towards the role of hydrogen bonding. A computational study by Ashworth et al.[11] on the choline chloride/ urea system found an "alphabet soup" of many different types of hydrogen bonds between the different functional groups. These bonds varied in number and strength, with a majority of ionic and doubly ionic

[1] Strictly speaking DES were used before in a few cases, e.g. to reduce the lattice energy of halide salts by addition of urea[287]. However, Abbott et al. were the first to investigate the phenomenon in viewpoint of a new solvent class.

hydrogen bonds being present so that the neutral bonding was only encountered in urea-urea interactions.

The research on fundamental aspects of DES is highly relevant as there is still a lack of understanding of structure-property relationships in this class of solvent. As a result, many systems have been described under the headline of DES, which do not deviate from ideal liquid mixtures and which can be described as ordinary eutectic mixtures.[12,13] Several researchers are therefore calling for a more coherent definition of the terms.[13,14] At the moment, e.g. DES are often defined as melts, that are liquid at a low enough temperature to make them practically usable. The temperature that is considered "low enough" is sometimes set to room temperature, sometimes to 70°C but also definitions of 150°C have been encountered. The research field would certainly gain rigor from a cleared differentiation, e.g. by differentiating true DES from low melting mixtures (LMM) that do not deviate from ideal mixtures. Nevertheless, it is still unclear whether there would be an appreciable difference between the two when it comes to practical applications. In the following, I will thus stick to the current definition and will include all eutectic mixtures in the discussion – also mixtures that are labeled as DES but might not be truly "deep". Very often, there is also no investigation on the matter.

1.1.2. Properties

With respect to practical applications, there are a number of properties that make DES appealing. The first one is obviously its high tunability of physical and chemical properties by selecting the appropriate components. In this way, one can achieve e.g. very high solubilities of solutes. Another advantage is that DES components are often biodegradable, low in toxicity and well characterized in this respect. However, it should be noted that research on the toxicological properties of DES itself has only recently started and for certain DES a potential toxicity was identified due to synergetic effects of the mixtures.[15–17] More research along these lines will therefore be required. One more advantage of DES is that they often feature very low vapor pressures. In a chemical process, evaporation is a major route for the loss of classical solvents into the atmosphere. The use of solvents with low vapor pressures can thereby make a significant contribution to reduce volatile organic compound (VOC) emissions. However, it should be noted that this will also impede separation procedures in certain cases, especially in organic synthesis.[18]

One property of DES, that is often a problem for industrial applications, is that they typically possess high viscosities. It has been rationalized that the high viscosity results from the large size of the constituent molecules or ions and the extensive network of hydrogen bonds which results in a low molar volume and a small free volume in the DES. However, this issue has been tackled in recent years by the use of "solvent in DES". This means that water or another solvent were used as constituents of the DES but at a relatively low concentration. In this way the viscosity of some DES could be drastically reduced while still retaining their characteristic properties [19–22].

1.1.3. Applications

Applications of DES are very wide, as they have been used as solvents, reagents or catalysts in different fields. As a result, I can only give a very brief overview over applications in order to demonstrate the promise and versatility that is offered by DES.

One important application for DES is in extraction and separation. Examples are the separation of azeotropic mixtures[23–25], extraction for metal recovery[26–28], the extraction of natural products from plants[29–32] or the extraction of proteins (while preserving protein structure)[33–35]. There have also been publications on the preparation of hydrophobic DES, based on menthol or other terpenes[8,36], which will certainly open up the application range of DES even further. In addition, DES have been used for gas adsorption such as CO_2 capture.[37,38] Another application is the use of DES for biomass fractionation as some DES showed the ability to cleave lignin-carbohydrate complexes while dissolving lignin.[39–41] Furthermore, they are used in the conversion of biomass to value-added products.[42,43]

A new term that has been established within the solvent class of DES is "natural DES" (NADES). This emphasizes that such solvents consist solely of abundant cellular constituents such as sugars, alcohols, amino acids, organic acids, and choline derivatives. This concept was introduced by Choi et al.[44] in 2011 as he proposed that such NADES systems might form a third liquid phase of intermediate polarity in living systems apart from water and lipids. He arrived at this hypothesis after nuclear magnetic resonance metabolomics showed that certain NADES components are present in all organisms as major compounds and often keep a constant molar ratio to some others. This hypothesis would explain a great number of biological processes that are otherwise difficult to explain, such as the biosynthesis of poorly water-soluble metabolites and macromolecules in the aqueous environment of cells, as well as the survival of organisms in extreme drought and cold conditions. Such NADES systems can also contain water as a constituent but it is so strongly retained in the liquid that it cannot be evaporated.[45] Furthermore, water content in these media is also hypnotized to be a way to regulate properties such as enzyme activity or viscosity (and thereby flow).[46]

Under the headline of NADES one can find further applications in pharmacology[47–51] A popular example for the use of NADES in drug solubilization is honey. Honey can be considered a naturally occurring NADES that is liquid at room temperature, although it consists predominantly of glucose and fructose in about equal molar ratios. It has been shown that honey is an excellent solvent for medium polar bioactive compounds (for some of these compounds much higher than water) and that honey can also enhance their stability. The improved bioavailability of bioactive compounds in honey is a potential explanation why honey has long been used as a traditional medicine additive and rationalizes the application of honey and honey-like substances in pharmaceuticals.[52,53]

Another important application area for DES is in material synthesis.[18] One of the first applications that sparked interest in DES was for metallurgy when it was discovered that metals and metals salts exhibit high solubilities and electrical conductivities as part of DES.[54] Furthermore, electrochemical windows are relatively wide, e.g. choline chloride based DES were found to offer electrochemical windows not quite as large as in some conventional ionic liquids but much wider than one might expect from a protic solvent.[55] As a results DES were successfully

used as electrolytes in electrodeposition[56,57], electropolishing[58,59], and energy storage[60]. In this way also promising results in battery recycling were obtained.[61] Other uses for DES in material synthesis are e.g. as solvent for polymerization or in ionothermal synthesis where DES can function as solvents as well as a structure directing agents.[62–64]

DES as reaction media for chemical synthesis is the last research area I want to highlight. Already a substantial number of organic reactions have been carried out in DESs (mostly choline chloride based), such as Knoevenagel condensation[65], Michael addition[65], Suzuki-Miyaura[66] cross-coupling and a number of selective addition reactions.[67–70] Furthermore, there are several reports on one-pot reactions in choline chloride based DES for products such as pyrimidines[71], pyrazines[72], quinazolinones[73] and pyrroles[74]. Those reactions give high yields and can be performed under milder conditions compared to traditional solvents. Another interesting approach is a synthesis in which DES serves as both a solvent and a catalyst. One example for this are oxidation reactions, were $FeCl_3$ is the catalyst as well as the HBA in the DES. Such reactions are e.g. the conversion of cellulose into gluconic acid[75], oxidation of toluene into benzaldehyde[76] and a number of C–C bond formation reactions through C-H activation[77,78]. Lastly, also in biocatalysis DES have been successfully employed as reaction media due to their ability to support a wide variety of substrates and enzymes.[79,80]

1.1.4. Reactive eutectic media (REM)

In the above-mentioned applications, the DES mostly takes the role of a solvent – sometimes one of its components also plays a catalytic role. However, if one of the DES components is reactive, the DES can serve as the reaction medium as well as the reactant. This realization has enabled a number of innovative approaches that I want to highlight here. In the corresponding publications, such systems are referred to by various names, DES, reactive DES (RDES) or reactive eutectic media (REM) are commonly encountered. In the following discussion, I will use the term “REM” since these mixtures do not necessarily show a “deep” eutectic behavior, as discussed before.

Applications of REM in material synthesis can be found in carbonization as well as polymerization. An example for carbonization is the use of resorcinol-based DES as both carbonaceous precursors and templating agents, which resulted in the preparation of carbon monoliths with hierarchical pores. By adjusting the counterparts in the resorcinol-based DES it was possible to adjust the mesopore diameters in the final material.[81] In polymer science, many publications on REM can be found for polymerization reactions, where this approach avoids the use of organic solvent and can yield novel materials.[82–86] Furthermore, REM are used in the preparation of eutectogels.[87] One such example is a choline chloride: acrylic acid: malic acid mixture, which was polymerized via UV initiation and which showed good self-healing properties as well as increased conductivity – presumably due to the role of choline chloride in the gel. Other eutectogels are reported to form via self-assembly and are envisioned to be used as solid electrolytes.[88]

The concept of REM also works for biocatalysis, were the eutectic components can function as the reaction medium as well as the substrate for microbes.[89–91] This approach has shown to achieve high substrate conversion and high atom efficiency.

For biomass treatment, the use of REM enabled various methods for cellulose derivatization. This includes the functionalization[92] of cellulose but also the preparation of charged nanocellulose. A variety of REM has been investigated to this end. While treatment with REM based on choline chloride and carboxylic acid[41,93,94], but also sulfamic acid with urea[95,96], enables the preparation of negatively charge nanocellulose, positively charged samples were obtained by treatment with REM based of ammonium formate with different carboxylic acids.[97]

In organic synthesis, REM have been successfully employed in a few cases, e.g. in heterocyclic synthesis where different urea derivatives were used as reactants.[98] Furthermore, the modification of phospholipids in REM was reported, using glycerol or ethylene glycol as reactive components.[99] Finally, a photocatalytic reductive formylation of nitroarenes was achieved by employing an ammonium formate based REM, where ammonium formate also acted as the formylation agent.[100] These examples all have in common that only one of the components of the REM reacts with a substance that is dissolved in the media. If all components of the REM also act as reactants, we basically end up with a solvent-free reaction that is also referred to as a solid-state melt reaction (SSMR), outside the research field of DES. Such reactions have been successfully used in the synthesis of biologically active molecules, ranging from two- to four components syntheses.[101–106] These kind of reactions offer remarkable advantage, when compared to solution reactions because they typically enable higher reaction rates. This is because collisions between the reactants are much more frequent and often gives high purity of the products with high selectivity. As a result, these reactions have been shown to give high product yields in short reaction times. Another advantage of these reactions is that no solvent is required, which improves their reactive mass efficiency as well as energy efficiency of the reaction (no energy is required to heat or remove the solvent). Furthermore, many reactions rely on toxic or potentially explosive solvents, making solvent-less reactions additionally valuable (although solvents may obviously still be required for isolation and purification of products[2]). The downside of these solvent-free reactions is that such melts often form at elevated temperatures and with high viscosities, which can make them unfavorable for industrial applications.

1.2. Microwave heating for chemical synthesis

1.2.1. History

Microwave irradiation is electromagnetic irradiation in the frequency range 0.3 to 300 GHz, corresponding to wavelengths between 1 mm to 1 m. The use of microwave energy for heating applications was discovered in the 1940's in the course of research on radar systems during World War II. The technology was originally applied for heating food and by the late 1970's the microwave oven became a common kitchen appliance in industrial countries. In the years to come, microwave technology also found applications in different industrial processes, ranging from all sorts of uses in the food industry (heating, drying, cooking, baking, sterilization, and pasteurization) to the processing of other materials such as ceramic sintering, nanotechnology[107], photovoltaics or paper, wood and textile processing. Apart from materials, the technology also found uses in extraction processes as well as in distillation or treatment of soil, sludge, or wastewater.[108] With respect to chemical synthesis, research on microwave heating started to appear in the mid-1980s[109,110] and opened a period of very intensive investigation of the mechanism of microwave heating and its influence on chemical reactions. Since then, thousands of research papers have been published on the subject as microwave heating offers an alternative approach to conventional heating (based on convective and conductive heat transfer).

1.2.2. Theory

In general, microwave heating is based on three phenomena: dielectric heating, magnetic heating, and conduction loss heating and it is thereby based on the dielectric, magnetic and electric properties of a material. In chemical synthesis, the later two terms become relevant e.g. for heterogeneous catalysis.[111] However, in the scope of this thesis I will not be dealing with such materials and solely work with media that are susceptible for dielectric heating[2]. The presented theory will therefore focus on this phenomenon, which is based on two effects:

- *Dielectric polarization:* Polar molecules can be oriented along an electric field. In the absence of this phenomenon, dipoles are orientated at random and molecules are submitted to Brownian motion only. In the presence of microwave radiation, the dipoles attempt to align with the oscillating electric field. This alignment causes rotation, which induces friction and ultimately dissipates as internal heating.
- *Ionic conduction:* Under the influence of microwave irradiation, dissolved ions oscillate back and forth with the electric field. This oscillation causes friction and collisions of the charged particles with neighboring molecules or ions, which ultimately results in heat energy. This is also known as ion-drag.

[2] This is not quite correct, as ionic conduction (which is mentioned as a phenomenon of dielectric heating) is actually a phenomenon that contributes to conduction-loss heating. However, it usually only makes sense to dive into the theory of conduction-loss heating, when dealing with metals where skin effects also have to be considered. For media that feature dielectric polarization as well as ionic conduction it is usually more elegant to integrate both phenomena under the term of dielectric heating as it is often done in literature. The influence of conduction loss due to ion-drag is then simply included in the loss factor ε''.

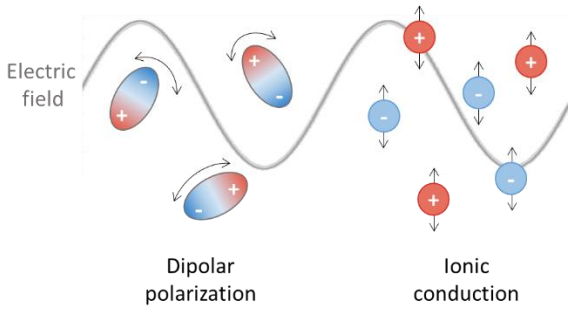

Figure 1. *Schematic illustration of the relevant heating mechanisms during dielectric heating with microwave irradiation.*

This illustrates why microwave are in the suitable range of the electromagnetic spectra to make use of these effects. If the frequency is much lower, the dipoles and ions will follow the electric field almost instantaneously and their motion will not result in substantial losses that dissipate into heat energy. Contrary, if the frequency is much higher, dipoles and ions will not be able to follow the oscillation of the electric field. Instead, the energy will be partly absorbed in the form of resonant molecular vibrations (infrared frequencies) or at higher frequencies (such as UV and above) for electron excitation.

How well a media converts microwave energy into heat can be derived from its permittivity, which represents the electric polarizability of the media. As we are dealing with a time-varying electromagnetic field, the permittivity has a real and imaginary component and is frequency as well as temperature dependent. It is given by:

$$\varepsilon = \varepsilon' - j\varepsilon'' \tag{1}$$

where ε' is the real part of the permittivity[3] and is a representation of the ability of the material to store electric energy and ε'' is the imaginary part of the permittivity and represents the loss factor which reflects the ability of the material to dissipate electric energy.

The ability of the medium to convert microwave energy into heat at a given frequency and temperature is given by the ratio of those two terms in the form of the loss tangent:

$$\tan\delta = {}^{\varepsilon''}/_{\varepsilon'} \tag{2}$$

The loss tangent is the dissipation factor of the medium and describes how efficiently microwave energy is converted into thermal energy. This explains why it is not sufficient to consider simply

[3] The real part of the permittivity is sometimes also referred to as dielectric constant. However, this term holds some ambiguity, as some older reports used it for the absolute permittivity (ε) or relative permittivity (ε/ ε_0). This only makes sense if we are dealing with dielectric materials – good electric insulators where the dielectric loss (ε") can be neglected and the real part of the permittivity and the absolute permittivity become equivalent.

the permittivity of a medium as a relative measure of its polarity in order to evaluate its efficiency to absorb microwave irradiation. Liquid water, for example has one of the highest permittivities of conventional solvents, but its dielectric loss values are lower compared to other solvents for a commercial 2.45 GHz microwave reactor. When comparing its loss tangent values water is therefore classified as a medium absorber of microwave energy. This also explains why materials such as quartz or Teflon are some of the preferred materials for microwave reaction vessels – their dielectric loss values are so small that that they are practically transparent for microwave radiation and do not heat up as such.

Having defined the main characteristics of microwave heating, the last parameter to consider is the penetration depth. This is defined as the depth of the medium where the microwave power drops to 1/ e (about 37%) of its initial value and is given by:

$$Dp = \frac{c_0}{4\pi f}\sqrt{\frac{2}{\varepsilon'}}\left[\sqrt{1+\tan^2\delta}-1\right]^{-\frac{1}{2}} \quad (3)$$

where c_0 is the speed of light in free space and f is the applied frequency.

The penetration depth is obviously dependent on the ability of the medium to convert microwave energy into heat but as this is a frequency and temperature dependent property, so is the penetration depth. For example, in the case of water in a commercial 2.45 GHz microwave reactor, the penetration depth is about 1.8 cm at 25 °C and increases to 3.1 cm at 50 °C and 5.4 cm at 90 °C. If ions are added to the water, its penetration depth decreases as the dielectric loss of the media increases. For example, the penetration depth of water at 25°C changes from 1.8 cm to 0.5 cm in a 0.25M NaCl solution.

1.2.3. Microwave vs. conventional heating

With this theoretical background in mind, it should be clear that microwave heating is substantially different from conventional heating. In the remains of this chapter, the most important differences of microwave heating compared to conventional heating with respect to chemical synthesis and process design will be highlighted:

- *Volumetric and rapid heating:* Microwaves interact directly with the reaction medium and can thereby provide rapid heating of the bulk. On the contrary, conventional heating comprises a combination of conductive and convective heat transfer, which results in non-uniform heating via the reactor wall and lower heating rates (Figure 2). As shown in many cases, microwave heated reactions can therefore give higher yields and less side reactions.[112–115]

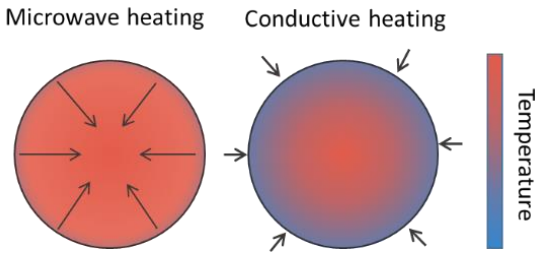

Figure 2: *Schematic illustration of different heating profiles during microwave heating and conventional heating.*

The rapid heating that microwaves cause can allow liquid solvents within closed vessels to be heated well above their normal boiling point. In some cases, this is desired, as it may be favorable to the reaction outcome. However, in other cases this is less desirable as it can induce safety issues. This is the case when the boiling points of solvents are reached and exceeded so rapidly that explosions due to rapid pressure built-up cannot be excluded. For this reason, microwave heating and solvent-free reaction of eutectic mixtures offer a great synergy. Eutectic mixtures often exhibit low-vapor pressures and thereby eliminate the risk of rapid pressure built-up. Furthermore, they are typically composed of polar or ionic components and therefore promise a highly efficient absorption of microwave irradiation.[2,3]

- *Other microwave-specific effects:* In the past, there have been numerous reports on reactions where the reaction rate increased dramatically under microwave heating compared to conventional heating.[116–118] In some of these cases, the observed rate enhancement was so high that is could not be predicted from the Arrhenius equation for a particular temperature. This has sparked a lively debate over the cause of this rate increase but also over proper experimental set-ups for such experiments.[119–123] This is because many reported rate enhancements could be traced back to improper temperature measurement inside the microwave cavity.[124] The reason is that the IR sensors measure the temperature on the outside of the vessel but microwaves heat the inside. As shown by Kappe et al., fiber optics are therefore the better choice for temperature measurements if reaction rates are to be determined.[124] Nevertheless, there are still controversies about the effects of microwave heating amongst researchers in the field. Many experts argue in favor of so-called selective heating effects. They hypothesize that the measured system temperature does not fully reflect the thermal energy of the selectively heated components. Examples for this may be reagents in a less polar reaction medium or strongly microwave-absorbing heterogeneous catalysts that lead to hot spot formation.[125–129] However, there are also experts who claim that such phenomena, which are not connected to macroscopic bulk temperature effects, are greatly overestimated due to erroneous temperature measurements. They therefore doubt that such phenomena will ever contribute to useful chemical processes.[121,130] While the argument of selective

heating and hot spot formation is still based on thermal effects there are also some researchers (although they appear to be in the minority) who argue in favor of so called non-thermal effects which are instead connected to the polarizing electric field. While most of these earlier explanations have already been rejected, there are some more recent hypothesis, which have not yet been challenged. These include for example the hypothesis that microwave polarization may change the spatial orientation of collisions[131] or enhance the diffusion of reactants in certain systems[132].

- *Ease of operation:* One factor that distinguishes microwave heating, is the facile reaction control that it can offer. It can be described with "instant on-instant off", because when the microwave energy is turned off there is only latent heat left in the reaction medium. Superficial overheating, which is relevant in conventional heating, is therefore not an issue.

- *Reactor design:* The fact that microwaves interact directly with the reaction medium and have a limited penetration depth sets certain constrains on the reactor design. The most promising options with respect to scale-up are continuous flow system, which have already been used for a few commercial applications. Examples include the pyrolysis of biomass or waste materials by Bionic Laboratories BLG GmbH (Germany)[133] as well as the production of fatty acid esters with a production capacity of 3200t/year by Microwave Chemical Co., Ltd. (Japan)[134]. Microwave-assisted continuous flow systems can also allow for solid treatment such as biomass as shown, e.g. by the use of rotary, fixed bed reactors or the use of an Archimedes-type screw which moves the material.[135]
  Concerning penetration depth, it may also be beneficial to use lower microwave frequencies. The most common frequency that is used in domestic microwaves but also for industrial and scientific purposes is 2450 MHz. However, for some applications it is beneficial to lower the frequency to 915 MHz, which allows for an increase in penetration depth. Applicable frequencies are regulated by legislations in order to avoid any interference with broadcast and communication bands.[111] Finally, an important part of the reaction design is the choice of microwave reactor (mono/multi frequency), which will influence the homogeneity of the field as well as the energy efficiency and scalability of the process. Here is much room for optimization[136], also under the consideration that novel solid state radio frequency transmitters might be an alternative to classic magnetrons altogether[137]. However, as this is above the scope of this chapter, the interested reader is referred to the primary literature.[138–140]

- *Energy efficiency:* Microwave heating offers the advantage of rapid and volumetric heating. This means that heat is generated from the inside out and less heat is lost compared to conventional heating. Nevertheless, when it comes to the energy consumption of the overall process, judgement needs to be rendered on a case-to-case basis as microwave technology is still under development. When comparing several different microwave processes, one study found that energy efficiency is mainly dependent on scale and that the optimization of the microwave reactor (i.e., frequency,

reactor geometry, field density, and homogeneity) has an immense impact.[141] Another study also found that simple process optimizations could increase energy savings up to 93% compared to earlier reports for the same process of microwave heated pretreatment for bioethanol production.[142] Considering, that microwave heated chemical processes just start to appear for large-scale production, there are naturally not many examples of mature and optimized process designs that allow a fair comparison between microwave and conventionally heating. One such example is the production of biodiesel, where a large-scale process in the continuous mode has been developed based on microwave heating.[143,144] For this process, one study[144] claimed ca. 48% energy savings, comparing the optimized microwave process with a total energy consumption of 116.7 Wh/L to the energy consumption of 222 Wh/L for a similar conventionally heated process.[145] More studies on energy efficiency can be found on the medium reactor size scale, where one research group compared several different reactions in different microwave reactors.[146] They observe the trend that microwave -heating is generally more energy-efficient for short reactions at high temperatures and proportionately less so for longer reactions at lower temperatures. This is also in agreement with an earlier study on smaller scales.[147]

- *Process decarbonization:* The burning of fossil fuels to supply process heat is a major contribution to direct carbon dioxide emission for industrial processes. For example in Germany, process heat was responsible for 67% of the energy consumption of the industrial sector and thereby contributed more than 20% of the country's total energy demand in 2020.[148] Considering that 72% of this process heat was supplied by fossil fuels[149], alternative heat supplies are in high demand. Assuming that Germany will eventually achieve the production of sufficient renewable electricity (2020 renewables had a share of 45%[150]), the electrification of process heat appears to be one promising approach. Obviously, there are multiple technologies, worthwhile to discuss here, but beyond the scope of this chapter. It should suffice to note that the expansion of microwave technology could be one building block in the decarbonization of process heat via electrification.[151,152]

1.3. On the concept of green chemistry

1.3.1 History

Green chemistry can be described as a conceptual framework for the design of chemical reactions, with the intent to minimize chemical pollution and resource depletion. The concept emerged in the 1990s from various existing ideas and research efforts (such as catalysis and atom economy), in the context of an ever-growing environmental movement. The development of green chemistry was linked to a paradigm shift in environmental policy in the OECD countries, which started to focus on pollution prevention instead of so-called command and control regulations that simply mandate the level of industrial emissions at the "end of the pipe".[153] In the United States, this culminated in the Pollution Prevention Act of 1990, which aimed towards the active prevention of pollution through innovation of production technology. As a result, the US Environmental Protection Agency (EPA) and the chemical industry started to cooperate more and more in developing new processes, in order to meet their shared environmental and economic goals.[154] Furthermore, US EPA engaged in extensive networking activities, involving actors from industry, academia and government, which cumulated in a number of symposia on the subject of "*Benign by design*". During these meetings, it was also that the term "green chemistry" emerged as a conscious choice. The alternative terminology "benign chemistry" was eventually abandoned, due to the assessment that it is very difficult (or mostly impossible) to design a truly benign process.[155] One of the outcomes of the professional coordination of US EPA and the knowledge exchange between the different actors was the first handbook on green chemistry[156], which was published in 1998. The book includes topics, such as renewable feedstocks, the design of safer synthesis procedures and chemical products, alternative solvents and catalysts and the use of biosynthesis and biomimetic principles. Furthermore, it serves as an introduction to the chemical philosophy that was envisioned by US EPA, which is best described in the chapter on the 12 principles of green chemistry, written by Paul Anastas (the US EPA representative at the time) and John Warner (from Polaroid Cooperation). These 12 principles (or better guidelines) are probably the quintessence of the green chemistry approach, which is today known by most chemists. They are summarized below in **Table 1**.

Table 1: *Summary of the 12 principles of Green Chemistry by Anastas and Warner*

1. *Prevention:* It is better to prevent waste than to treat or clean up waste after it has been created.
2. *Atom Economy:* Design synthetic methods to maximize incorporation of all materials used in the process into the final product.
3. *Less Hazardous Chemical Syntheses:* Synthetic methods should, where practicable, use or generate materials of low human toxicity and environmental impact
4. *Designing Safer Chemicals:* Chemical product design should aim to preserve efficacy whilst reducing toxicity.
5. *Safer Solvents and Auxiliaries:* The use of auxiliary substances (e.g., solvents, separation agents, etc.) should be made unnecessary wherever possible and innocuous when used.
6. *Design for Energy Efficiency:* Energy requirements should be minimized. If possible, synthetic methods should be conducted at ambient temperature and pressure.

7. *Use of Renewable Feedstocks:* A raw material or feedstock should be renewable whenever technically and economically practicable.
8. *Reduce Derivatives:* Unnecessary derivatization (such as use of blocking groups, protection/ deprotection, temporary modification of physical/chemical processes) should be avoided, where possible.
9. *Catalysis:* Catalytic reagents (as selective as possible) are superior to stoichiometric reagents.
10. *Design for Degradation:* Chemical products should be designed so that at the end of their function they break down into innocuous degradation products and do not persist in the environment.
11. *Real-time analysis for Pollution Prevention:* Process monitoring should be used to avoid excursions leading to the formation of hazardous materials.
12. *Inherently Safer Chemistry for Accident Prevention:* Substances and the form of a substance used in a chemical process should be chosen to minimize hazard and risk.

From this period onwards, the use of green chemistry as a terminology really took off. This can be illustrated by a steady rise in citation statistics but also by the establishments of awards (e.g. Presidential Green Chemistry Challenge Award), conferences (e.g. Green & Sustainable Chemistry Conference) or journals (e.g. Green Chemistry (RSC)). A detailed account on this development can be found in [157] by Linthorst.

1.3.2 Critique (and reform)

Linthorst's analysis shows that the success of the term "green chemistry" was really a networking effort from political and industrial actors. Some authors have made the case that this has brought a cohesion to the field and has thereby enabled scientific breakthroughs and new kinds of synergies.[158,159] Others have also raised the question whether the practitioners of green chemistry can be considered as actors of a social movement that may eventually transform the chemical sector.[160] Nevertheless, there has also been critique of the terminology. Lindhorst argues that a large part of the success of "green chemistry" lies in the "user-friendliness" of the term, as he calls it. What he means is that it is relatively easy to label research as green chemistry, because the only prerequisite is that it "strives to incorporate one or more of the 12 Principles of Green Chemistry".[161] This is one of the major weaknesses of the term and has been pointed out repeatedly. For example, Winterton has criticized the term on the basis that it encourages a lot of research to make unsupported or selective claims on being "green".[162,163] Furthermore, he claims that far too little attention is paid to the larger context such as scalability, economics, and environmental impact. Such assessments require much more multidisciplinary approaches (and they obviously do exist). Finally, Winterton also warns that the focus on green chemistry may result in an over-simplistic analysis of pollution – which is in fact a complex societal problem and ultimately results from the human overshoot of the biophysical carrying capacity of the earth. A truly sustainable way of living will therefore require changes far and beyond the discipline of chemistry.

Another issue, which has been put into the spotlight by chemists, is the toxicological footprint of the chemical industry. This has often been overshadowed by the discussion on its carbon footprint, when talking about green processes and products. However, it has been observed that

the number of chemical substances on the market has increased to the degree that risk assessments for many of them have never been performed adequately. According to Fanner and Scheringer, the sheer number of chemicals that are marketed globally (which currently are estimated around 350.000) as well as their continuing increase has rendered it impossible to adequately study all substances on the market with respect to their toxicological profile. They are therefore calling for a "simplification of chemistry" and the utilization of much fewer chemicals, which can thereby studied much more thoroughly on their environmental toxicity.[164] The ban (or stern restriction) of PFAS, for example, would thus only be the tip of the iceberg.[165] Another study also attests that the level of pollution is outside the safe operating space of the planetary boundary with unknown effects on ecosystem and human health and proposes a cap of production.[166]

To sum up, the philosophy of green chemistry has undoubtedly affected the discipline of chemistry and has supplied useful guidelines for the approach and discussion on sustainability. However, its vague requirements have also undermined its concept and often claims on green procedures need to be approached with caution. A more holistic approach on the subject of sustainability would therefore be required. This means in particular also the coercive consideration of toxicology, which is e.g. also acknowledged by Anastas (who is sometimes also known as the founding father of green chemistry) and who calls for the integration of toxicology deeply into the curriculum of chemistry students.[167,168]

CHAPTER 2
The reaction with monosaccharides for the synthesis of Maillard reaction products

2.1. Overview

This chapter investigates REM based on ammonium formate and monosaccharides for the synthesis of bioactive substituted pyrazines. This Maillard type reaction is optimized with respect to reaction temperature and time, and the influence of microwave heating (vs. conventional heating) is investigated. Furthermore, water is included in the REM as a third component in order to decrease the viscosity of the mixture, analogous to the solvent-in-DES approach (discussed in chapter 2.1). The influence of water on the reaction yield as well as on the physical properties of the REM is studied. Finally, the major reaction products are separated via chromatographic methods, chemically analyzed and tested on their antimicrobial activity via high-throughput screening.

Maillard reaction products (left) and purified substituted pyrazines (right)

This chapter is an adapted version of the article: Schneider, H., Merbouh, N., Keerthisinghe, S., & Filonenko, S., Microwave-irradiated rapid synthesis of antimicrobial pyrazine derivatives in reactive eutectic media. *Green Chem.* **24**, 9745-9754 (2022).

This study was a collaboration with Dr. Nabyl Merbouh and Dr. Sandra Keerthisinghe from the Simon Fraser University, Canada, who performed the antimicrobial testing of the samples.

2.2. Background

In 1912, Louis-Camille Maillard discovered that mixtures of amino acids and sugars become intensively brown upon heating. He thereby laid the basis for understanding the non-enzymatic browning reactions that occurs during cooking, roasting, and baking of foods that now carries his name: the Maillard reaction. This reaction is known as one of the most complex processes in food chemistry as it forms a vast variety of intermediate products such as furfurals, pyrazines, imidazoles and other heterocyclic molecules and eventually results in a brown polymeric substance that is known as melanoidin. In this way, the reaction is a major contributor to colour and characteristic flavour in food.[169]

One specific type of Maillard reaction is the reaction between sugars with aqueous ammonia and ammonium salts. The final reaction mixture features a pleasant smell and low odor threshold, which is why the food as well as the Tobacco industry have made use of this reaction for years.[170,171] Furthermore, the reaction is also extensively used to prepare brown food-colorants, which are known under the name of ammonia caramel.[172,173] This substance is prepared with an excess of sugar so that Maillard as well as caramelization reactions take place, and the resulting product is used in many commercially produced foods and beverages - from beer to sauces, bread and pastry.

Despite the commercial importance of such reactions, it is still rather challenging to understand the underlying reaction chemistry due to its complexity. Much fundamental work goes back to the 50's and 60's when it was first possible to analyze and isolate the major reaction products.[174] Since then it is understood that the reaction between sugars and aqueous ammonia results in a mixture of heterocyclic products – predominantly substituted imidazoles and pyrazines as well as in the darkly colored substance melanoidin. These reactions can take place at room temperature but the reaction time will be in the order of days. At elevated temperatures (most studies use at least 90°C) the reaction time can be reduced to a few hours. However, if the temperature is increased much further, a large part of the substitution on imidazole and pyrazine fractions will undergo thermal cleavage. As a result, there is a substantial increase in the methyl-pyrazine and -imidazole fraction. A range of different heterogeneous catalysts were tested but did not appear to change the reaction significantly. So far, the mechanisms for the formation of imidazoles and pyrazines are however much better understood then the polymerization into melanoidin, which has been described as the "most enigmatic food macromolecule today"[175].

What has caused a recurring interest in this reaction over the past years is the biological activity that was identified in pyrazine derivatives in the reaction mixture. The compounds are known under the name of deoxyfructosazine (DOF) and fructosazine (FZ) for fructose- based reactions (as shown in Scheme 1) but other sugars may also be used to produce similar derivatives. DOF and FZ belong to the non-volatile poly(hydroxyalkyl)pyrazines and occur naturally in food products[176–178]. The biological activity of these compounds was investigated in different studies were they showed, e.g. antimicrobial activity for heat resisting *E. coli* [179,180] as well as promising pharmaceutical activity for the treatment of diabetes[181], cancer[182] and as immunomodulators[183].

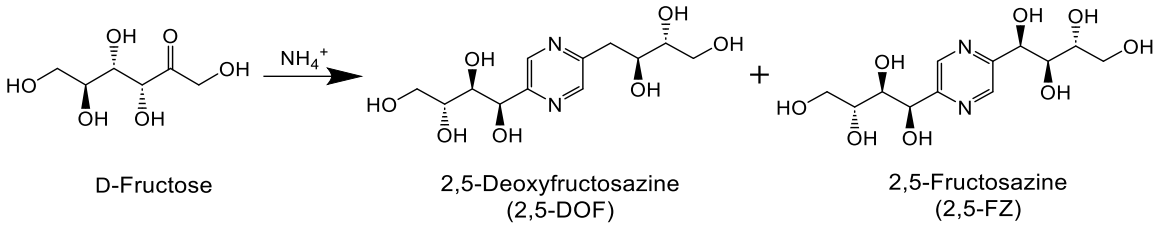

Scheme 1: *Reaction of ammonium formate with fructose into substituted pyrazines*

These findings spurred the development of synthesis routes for such substituted pyrazines. However, the great number of competing reactions that occur during the Maillard reaction make it difficult to achieve good yields. Wu *et al.* used cellobiose and inulin as biomass based starting materials, which were hydrolyzed to glucose and fructose respectively and then reacted with an excess of ammonium formate in aqueous solution. They optimized reaction conditions in the later step and obtained DOF in 33% yield from glucose and 28% yield from fructose with a temperature of 150°C for 2 hours[184]. Similarly long reaction times and high temperature conditions were reported in a pending patent by Shanxi Institute of Coal Chemistry of CAS from 2019. The patent used different ammonium salts for the reaction with fructose, again with a large excess of the ammonium salt in aqueous solution. The highest yield of DOF of 60% was reported, using ammonium chloride and with reaction conditions of 120°C for 2 hours[185]. Another approach to synthesize DOF was via the self-condensation of glucosamine and fructosamine. The synthesis was performed in ionic liquids by Jia *et al.* and required reaction times of 3 hours[186]. Faster rates were only reported when catalysts such as boric acid were used[187] or by homogeneous catalysis with ionic liquids based on amino acids [186]. Without a catalyst, the yields of FZ are only minor in the aforementioned studies and amount to a few percent.

In summary, the synthesis routes for DOF either suffer from long reaction times and the excessive use of ammonium salts or require the use of much more expensive reagents and catalysts. In this chapter, I tackle these issues by using REM between monosaccharides, ammonium formate and water. Regarding the choice of monosaccharides, fructose is used to optimize the reaction conditions and to investigate the eutectic mixture. After reaction conditions and water content have been optimizes, the products from other monosaccharides are investigated. For this purpose, glucose and the two deoxy sugars, fucose and rhamnose are used. The latter two have been investigated much less for this reaction. The diversity of the saccharides covers isomers and molecules with various functionality and hydrophobicity.

2.3. Experimental procedure

2.3.1. General reaction procedure

REM are prepared by mixing 0.47g of ammonium formate with different monosaccharides to obtain a molar ratio of 1.5:1. Water is added in different amounts, using molar ratios ranging from 0 to 50. A table of the educts in molar ratio as well as in weight percentages can be found in S2.1 of the SI. Samples are transferred into 10 ml quartz glass vials and after addition of a

magnetic stir bar, sealed with a Teflon-lined cap. Vials are heated under vigorous stirring with a laboratory microwave (Discover SP) with a power of 5 Watt for mixtures without water. The power is increased with water addition to enable comparable heating rates. The temperature is monitored by infrared technology. Zero time is taken when the desired temperature is reached. Experiments are conducted at 80°C, 100°C and 120°C and performed for 5 to 90 minutes. For comparison, experiments are also performed with thermal heating in an oil bath, otherwise keeping the same reaction set-up (same reaction vessel and stirring bar).

2.3.2. Analytical methods

Characterization and reaction yield

The crude mixtures are analyzed on reaction product by ^{1}H NMR, ^{13}C NMR and HPLC-MS. Quantitative ^{1}H NMR is applied to calculate the substrate conversion and yields of products using pyrazine as an internal standard. The exact procedures are described in S1 of the SI.

Characterization of eutectic mixtures

REM are characterized prior to reaction with DSC, falling ball viscometer and ^{1}H NMR. The later is used to investigate hydrogen bonding within the REM, which is why the media is physically separated from the NMR solvent by a capillary. The exact procedures are described in S1 of the SI.

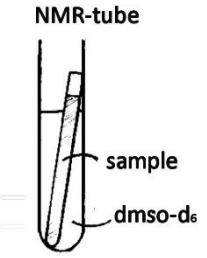

Separation of DOF derivatives and testing on their antimicrobial activity

The separation of DOF derivatives is performed via column chromatography for the reaction mixtures from fructose and rhamnose. The following procedure is used: The reaction mixture is extracted several times with diethyl ether and dichloromethane until a clear extract is obtained. Afterwards the reaction mixture is reduced by vacuum evaporation at 45°C and separated on a silica column (0.040-0.063 mm) eluted with ethyl acetate / 2-propanol / water (4/2/1 by volume). Fractions containing the product were combined and concentrated under reduced pressure at 45°C. The oil thus obtained is chromatographed again on a silica column (0.040-0.063 mm) eluted with 1-butanol / ethanol/ water / ammonium hydroxide (25%) (8/2/2/1 by volume). Fractions containing the expected product were combined, concentrated under reduced pressure at 45°C and freeze dried overnight. For fructose, the dried product is washed with ethanol, while for rhamnose the product is washed with acetone. After drying in a vacuum oven at 40°C, the resulting white powder is identified to be the desired product as shown by ^{1}H NMR. DOF from fructose and deoxyrhamnosazine (DOR) from rhamnose were both obtained with a purity above 97%.

In order to simplify the separation procedure, another method is developed, based on semi-preparative HPLC. The reaction mixtures from glucose and from fucose were separated as follows: The reaction mixtures were extracted with ethanol and concentrated under reduced pressure. The resulting oil is injected into a HPLC, using semi-preparative C18 column (ACE 5, C18 250x21.2) with a flow rate of 15 mL min^{-1}. The mobile phase consists of 0.1% formic acid in

water (A) and 0.1% formic acid in methanol (B). The gradient program is as follows: 95% A (0–5 min), 95–0% A (15–40 min), 0% A (40–50 min) and 0-95% A (50-60 min). UV-vis is used at a wavelength of 280 nm. The method is thereby analogous to the one applied for analytical HPLC, so products could be readily identified. Fractions containing the desired product are combined. For glucose, the product is washed with ethanol, for fucose the product is washed with acetone. The resulting powder is identified to be DOF from glucose (>95% purity) and deoxyfucosazine (DOFu) from fucose (>93% purity).

Each compound is characterized by NMR techniques as well as HR-MS. After at least 40 mg are prepared for each compound, they are tested on their antimicrobial activity. Test are performed with high-throughput screening on 19 different microbial strains. Gram-negative bacteria include *E. coli, K. aerogenes, K. pneumonia, S. enterica, A. baumanii, P. alcalifaciens, S. sonnei, V. cholera, P. aeruginosa, Y. pseudotuberculosis and O. anthropi.* Gram-positive bacteria include *B. Subtilis, MSSA, MRSA, S. epidermidis, L. Ivanovii, E. faecium, E. faecalis and S. Pneumoniae.* The test protocol can be found in chapter S2.2 of the SI.

2.4. Results and discussion

2.4.1. Reaction conditions

The products from sugar-ammonia reactions have been systematically studied since the 50's[188,189] and the mechanism of formation of DOF and FZ has been elucidated in a number of papers by Komoto and co-workers[190–192]. Therefore, characterization of the main products with HPLC-MS and ^{1}H NMR is straightforward and is shown in chapter S2.3 of the SI.

Out of all the tested monosaccharides, fructose is chosen for optimization of reaction conditions because it gives a good reference point; it has been used in multiple studies for this reaction.[184,185,187] The influence of molar ratio of reagents on the reaction yield has been investigated previously by our group.[193] The previous study showed that an excess of ammonium formate is only slightly increasing the yields of the main products. The present study therefore relies on a molar ratio of 1.5:1 between ammonium formate and monosaccharide. Since microwave heating is used in the present study, the reaction parameters with respect to temperature and time are optimized (Figure 3, left). The reaction features relatively fast reaction rates as the maximum yield is reached in less than 3 minutes at 120°C, in 15 minutes at 100°C and in 40 minutes at 80°C. While the reaction at 80°C seems to reach a plateau in product yield, products at 100°C and 120°C undergo degradation with sustained reaction conditions. Interestingly, no FZ is detected in the reaction mixture, which is typically observed as a minor product for this reaction when performed in water.[192,194] Presumably, the fast reaction rates favor solely the formation of DOF.

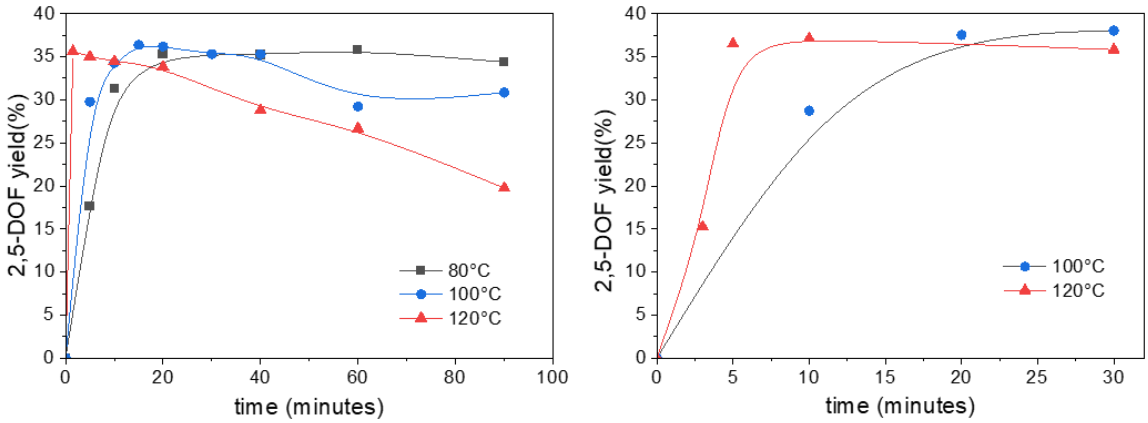

Figure 3: *Yields of 2,5-DOF from fructose at different reaction temperatures, under microwave heating (left) and under conventional heating in an oil bath (right). No additional water is added to the eutectic mixture.*

To my knowledge, such fast rates are unprecedented for this reaction and might be traced back to two explanations, which present the novelty of this approach: the use of REM, or the use of microwave heating during the reaction.

Regarding microwave heating, it has been observed that organic reactions ran in a microwave can exhibit unexpectedly high reaction rates (as discussed in CHAPTER 2.2). Therefore, the influence of the heating method on reaction rate is investigated by repeating experiments under thermal heating, as shown in Figure 3, right. This investigation does reveal a rate enhancement, but none that would suggest a substantial influence of the heating method. With conventional heating, maximum yields are reached in 5 minutes at 120°C and in 30 minutes at 100°C. The slightly faster rates during microwave heating can easily be explained by different heating profiles. While microwaves can provide rapid heating of the bulk by a direct energy transfer to the reaction mixture, conventional heating comprises a combination of conductive and convective heat transfer, which results in non-uniform heating via the reactor wall and lower heating rates.

These results suggest that the effect of the heating method is only minor with respect to the reaction rate. That means that the REM and the resulting high concentration of (both) reactants must be the reason for the faster rates observed.

2.4.2. Water addition to the reaction mixture

Subsequently, the effect of water as a third component in the REM is investigated. Figure 4 shows that small amounts of water are beneficial for the overall reaction yield; however, at a water content above a molar ratio of 7, the yield suffers from the presence of water, presumably due to lower reaction rates. The interesting aspect of this finding, is that the addition of water in such small amounts can already greatly reduce the viscosity of the medium, as has been shown previously for other eutectic systems[21,195]. Indeed, this mixture also features a drastic decrease in viscosity due to water addition as shown in Figure 5. The decrease of viscosity can also serve to rationalize the slide increase of the reaction yields if only little water is added. In this case, the mass transport in the reaction mixture will also increase, thereby increasing the reaction rate.

However, further water addition will barely affect viscosity and therefore only result in dilution and lower concentration of reactants. The measurement also shows that the viscosity of the mixtures decreases during the reaction. The drop of viscosity after the reaction can be explained by water formation in the course of the Maillard reaction.

A reduction of viscosity is a great benefit for the use of this reaction on a larger scale, e.g. it would allow the reaction to be performed in a microwave-assisted continuous flow system which is one of the most promising approaches for scale-up of microwave technology in organic synthesis (as discussed in CHAPTER 2.2).

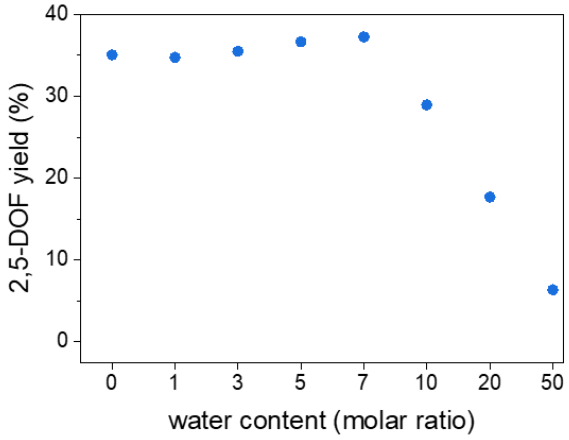

Figure 4: *Yields of 2,5-DOF with varying amounts of water in the REM. Experiments are performed at 100°C for 15 minutes. The microwave power for heating is increased with water addition to enable comparable heating rates.*

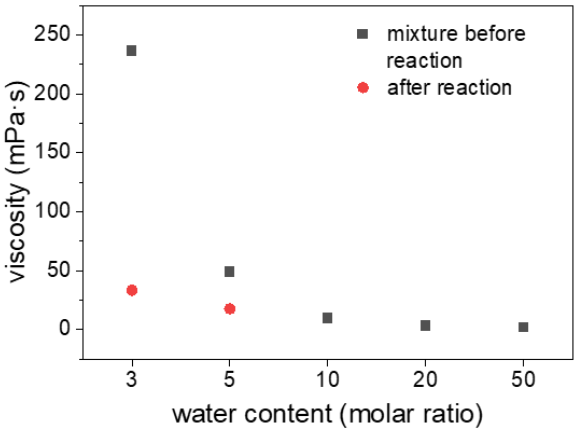

Figure 5: *Viscosity of ammonium formate/fructose mixtures with different amounts of water at 25°C. Samples with a water content of 0 and 1 in molar ratio were not measured because they do not form a homogenous liquid at room temperature.*

Another advantage of this approach is the efficient heating of the REM, compared to dilute systems. This is shown in Figure 6A, which compares the heating rate of different mixtures by heating 0.5g of sample for 60 seconds with fixed 20 W applied power. Pure water is considered a moderate absorbing solvent to convert microwave energy into heat. Its performance increases with increasing salt concentration as ionic conduction is one of the two fundamental mechanism for absorbing microwave energy (the other one being dipole rotation). The results show that the applied REM are indeed very good absorbing solvents for microwave energy. Furthermore, samples with the highest concentration of reactants also show the highest heating rates, which means that microwave energy for heating is used with maximum efficiency. In this way, most of the energy goes into the heating of reactants and less into the solvent molecules. This is visualized in Figure 6B, which shows that samples with high water content barely react while samples with the lowest water content (:3 and :5) are close to completion (considering the fast reaction rates at 120°C in Figure 3, left). Interestingly, samples :3 and :5 show a different heating profile compared to more diluted samples, indicating that these mixtures are in a different dilution regime and do not form aqueous solutions but tertiary eutectic mixtures instead.

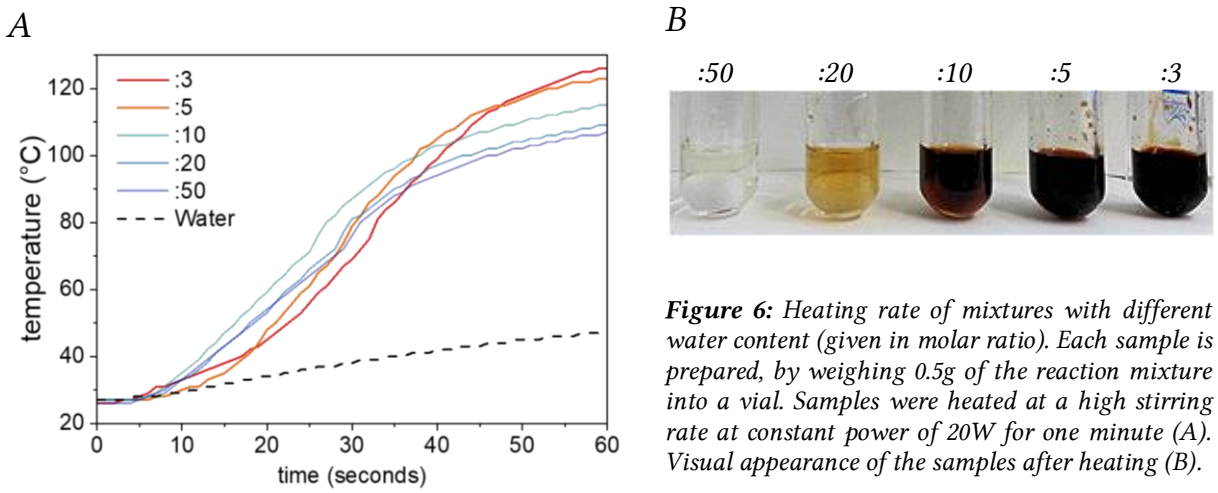

Figure 6: *Heating rate of mixtures with different water content (given in molar ratio). Each sample is prepared, by weighing 0.5g of the reaction mixture into a vial. Samples were heated at a high stirring rate at constant power of 20W for one minute (A). Visual appearance of the samples after heating (B).*

2.4.3. Further characterization of the REM

DSC measurements are performed for a better understanding of the influence of water content on the eutectic mixture (Figure 7). Indeed, eutectic mixtures seem to have formed for water contents below a water ratio of 10. These samples lack the typical melting and crystallization peaks of water but feature glass transitions. Glass transition (due to frustrated crystallization) is a typical phenomenon of DES and has been connected to the transient nature of hydrogen bonds (compared to other intermolecular forces), which allows molecules to readily switch between bonding sites. However, this phenomenon is not ultimately understood.[10] Compared to those so-called "glass formers", the sample with a water molar ratio of 10 displays a borderline behavior – it still exhibits a glass transition temperature (which is fluctuating with each cycle) but is also showing signs of the melting peak of water. The two samples with the highest dilution do not behave as eutectic mixtures but rather as aqueous solutions and exhibit the typical melting and freezing peaks of water. The decrease of the freezing point from sample :50 to :20 can be explained by the well-known freezing-point depression due to increased solute concentration.

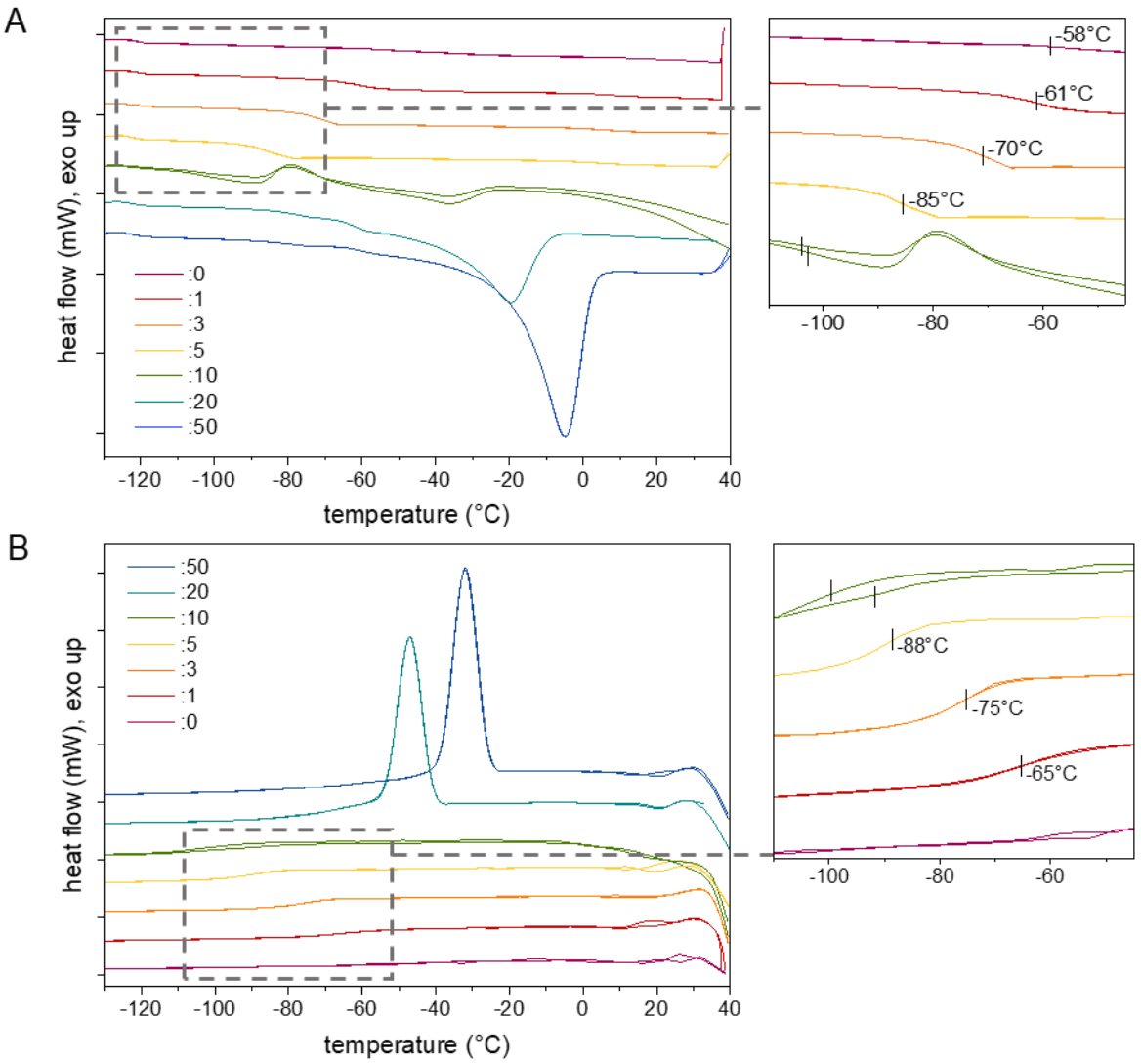

Figure 7: *DSC measurement with A) heating and B) cooling profiles for ammonium formate/fructose mixtures with different water content, given in molar ratio. The glass transition temperatures are noted in the graphs on the right-hand side.*

^{1}H NMR is used to take a closer look at hydrogen bonding in the eutectic mixtures. By using DMSO-d_6 as a standard but keeping the mixtures separated in a sealed capillary tube, it is possible to investigate proton shifts as a function of water dilution (Figure 8). A change in the chemical shift is a consequence of the change in the electron environment of the proton and thereby the strength of hydrogen bonding. Downfield shift indicates less shielding and thereby stronger hydrogen bonding, upfield shift indicates weaker hydrogen bonds. Under typical dilution (:50-:1000) there is no change for water and very little change for the protons of fructose and formate ion, meaning that the chemical environment barely changes. However, when the water content decreases further (< :50), molecules start to see each other instead of being surrounded by a hydration shell. The chemical shift indicates that the liquid state can be maintained for reduced water content because the hydrogen bonds in water strongly increase, while hydrogen bonds of fructose and the formate ion weaken to a lesser extent. It seems likely that the increasing ionic

strength of the solution enables stronger polarization of the water molecules, thereby enabling stronger hydrogen bonds. This explanation is also supported by the DSC results. As the strength of hydrogen bonding increases, water cannot exhibit its typical melting/ crystallization behavior but is incorporated into the eutectic mixture instead.

The broadening of the NMR peaks for lower water contents can be attributed to the increase in viscosity. It is a known phenomenon in NMR that viscous samples will have low tumbling rates of molecules which will make them less effective in causing relaxation. This results in longer T1 values and thereby signal broadening.

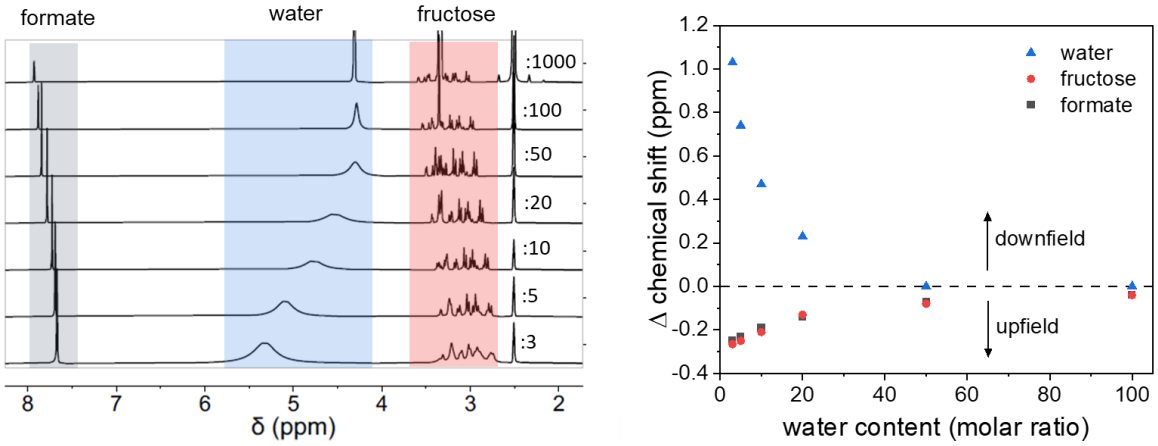

Figure 8: *^{1}H NMR of ammonium formate/ fructose mixtures with different amounts of D_2O (given in molar ratio) using DMSO-d6 as a reference standard (left). The difference in chemical shift compared to the sample with highest dilution (:1000) (right). Samples with a water content of 0 and 1 in molar ratio could not be measured because they do not form a homogenous liquid at room temperature.*

2.4.4. Changing the saccharide reactants

After the reaction conditions are optimized for the fructose reaction, the same reaction is performed with several other monosaccharides. Products and yields are shown below in Table 2, while their characterization using NMR and HPLC-MS is presented in chapter S2.3 of the SI. It is in accordance with previous studies that aldoses predominantly yield the 2,6-isomers while ketoses predominantly yield the 2,5-isomers. However, the respective other isomer is also observed in small amounts[192]. Products from rhamnose and fucose have been less investigated but have been reported before by Basiardes *et al.*[17]. These products are DOF derivatives that differ by the lack of hydroxyl groups on the terminal carbon. In the following, I will call them deoxyrhamnosazine (DOR) and deoxyfucosazine (DOFu), following a scheme by Komoto[191].

Considering the effect of the increasing water content (Figure 9) it can be observed that the reactions all follow a similar trend: for water dilution above a molar ratio of 7, yields drop drastically for the chosen reaction conditions. A slightly earlier decrease of yields from rhamnose and fucose might be related to their terminal methyl groups, which increases the hydrophobic nature of the product.

Table 2: *Products from reaction with ammonium formate: monosaccharide: water in a 1.5:1:7 ratio for fructose and glucose and in a 1.5:1:3 ratio for rhamnose and fucose. Experiments are performed at 100°C for 15 minutes.*

Monosaccharide	Major product	Yield	Minor product	Yield
D-Fructose	2,5-Deoxyfructosazine	37.2%	2,6-isomer	9.3%
D-Glucose	2,6-Deoxyfructosazine	26.1%	2,5-isomer	5.9%
L-Rhamnose	2,6-Deoxyrhamnosazine	32.5%	2,5-isomer	11.2%
L-Fucose	2,6-Deoxyfucosazine	23.9%	2,5-isomer	6.0%

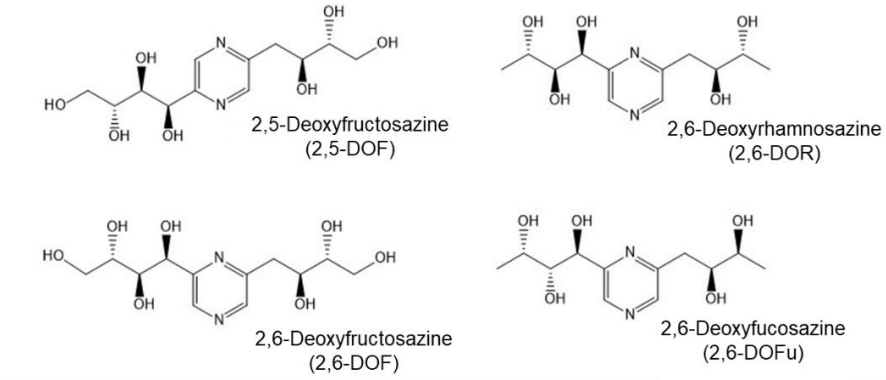

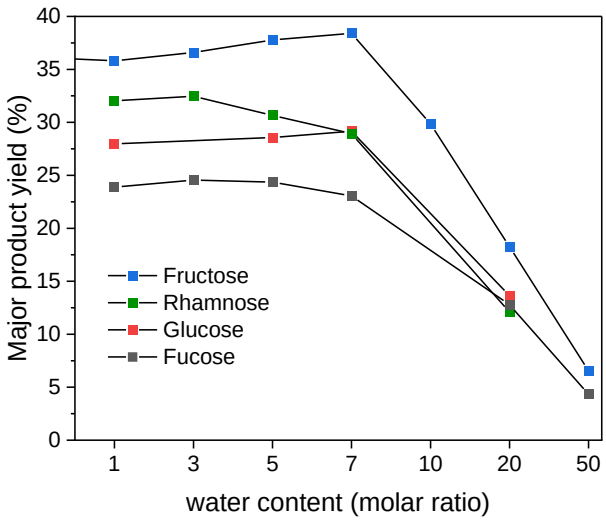

Figure 9: *Yields of DOF derivatives from different monosaccharides with varying amounts of water in the reaction mixture. Experiments are performed at 100°C for 15 minutes.*

2.4.5. Study on separation and antimicrobial activity of DOF derivatives

The separation of the crude mixtures is performed by two approaches: the previously reported use of column chromatography as well as the use of reversed-phase HPLC. The later appears

highly promising as it offers a much easier approach compared to previously reported methods that require two runs of column chromatography. It also enables a much more straightforward approach for separation of by-products for future investigations. After the separation of the major product from each reaction mixture, the respective compounds are thoroughly characterized, using NMR and HR-MS as shown in chapter S2.4 of the SI.

The antimicrobial properties of the separated DOF derivatives show several hits in the high-throughput screening as shown below in Figure 10. 1,5-DOF for *O. anthropi* (TSB) as well as 1,6-DOR for *S. pneumoniae* (BHI) show cumulative hits, with inhibition above 50%. They will be investigated in further testing, in order to quantify their antimicrobial effect on the respective strain[36].

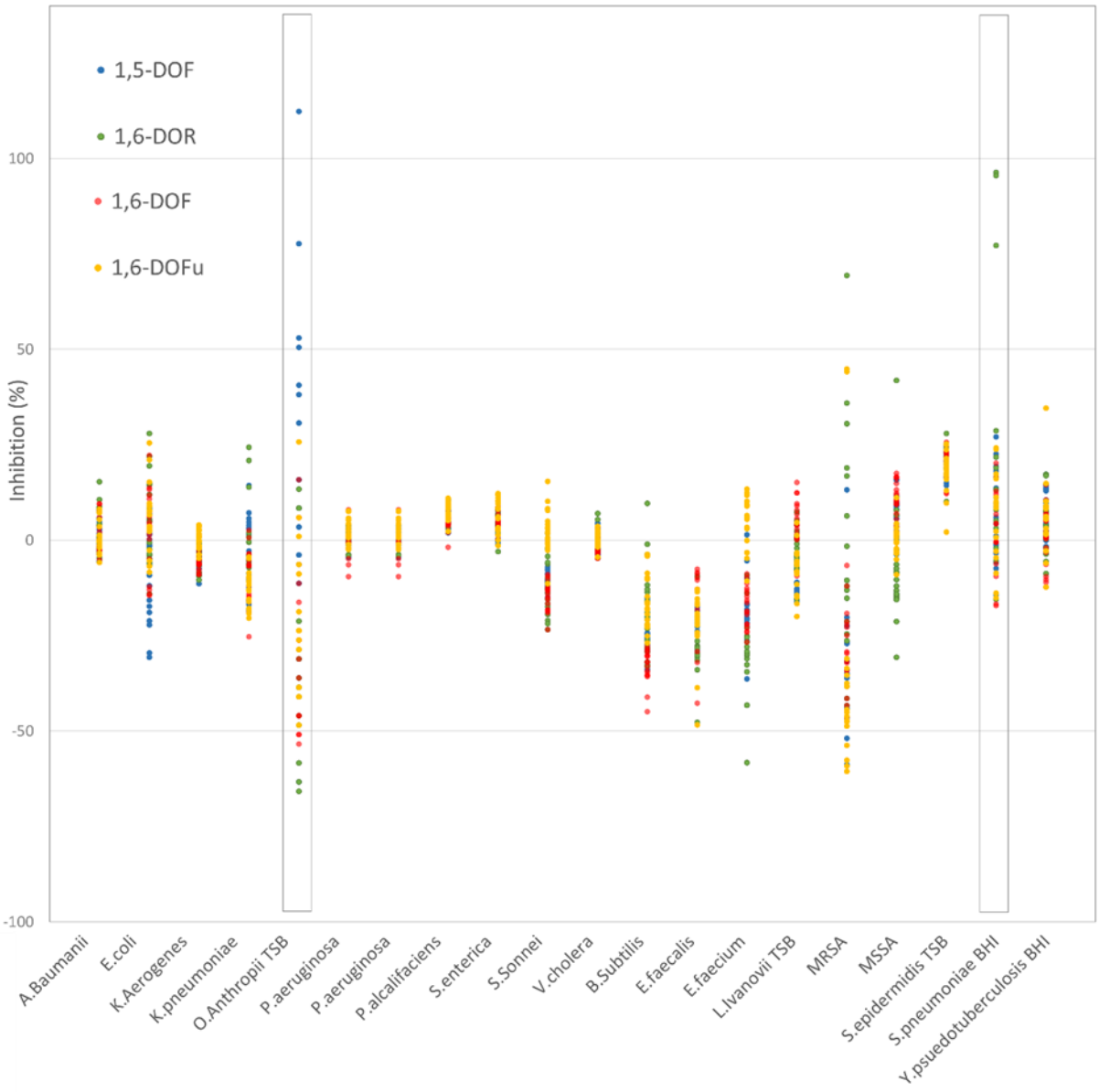

Figure 10: *Graphical representation of the high-throughput screening for four different DOF derivative compounds.*

2.5 Conclusion and outlook

This work showed that fructose and ammonium formate form a eutectic mixture where water can be incorporated as a third component. This approach results in a much better reaction mass efficiency compared to previously reported synthetic routes. This is because reactants were used in an almost stoichiometric ratio (1.5:1) instead of using one compound in great excess. The high concentration of reactants led to unprecedented fast reaction rates with a yield up to 37.2% of 2,5-DOF and 9.3% of 2,6-DOF, while the incorporation of water also retained relatively low viscosities. Applying the microwave energy directly to the reaction mixture led to a highly energy efficient heating method, making this approach attractive for microwave-assisted continuous flow systems.

In addition to fructose, other monosaccharides were successfully used as reactants, showing the same trend as fructose with respect to water addition. The respective reaction mixtures were successfully separated, with HPLC proving to be a straightforward method for the final compound purification. The separated DOF derivative compounds were thoroughly characterized and successfully tested for their antimicrobial activity via high throughput screening. Promising candidates were identified and will undergo additional antibacterial screening: 2,5-DOF for *O. anthropi* as well as 1,6-DOR for *S. pneumoniae*.

CHAPTER 3
The reaction with levulinic acid for the synthesis of 5-methyl-2-pyrrolidone

3.1. Overview

This chapter investigates REM based on ammonium formate and levulinic acid for the synthesis of 5-methyl-2-pyrrolidone. This Leuckart-Wallach type reaction is optimized with respect to reaction temperature and the influence of microwave heating (vs. conventional heating) is investigated. Furthermore, water is included in the REM as a third component in order to study its influence on the reaction yield as well as on the physical properties of the REM. The results are also discussed with respect to the use of the alternative Leuckart reagent based on formamide and formic acid.

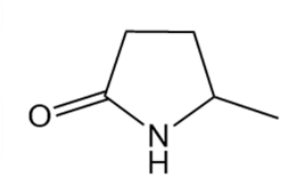

Structural formular of 5-methyl-2-pyrrolidone

3.2. Background

N-substituted-2-pyrrolidones have a variety of industrial uses, e.g. as intermediates in pharmaceutical products, fiber dyes and printing ink as well as in form of the solvent N-methyl-2-pyrrolidone (NMP) and the precursor N-vinyl-2-pyrrolidone for the production of polyvinylpyrrolidone (PVP). However, currently these compounds are fossil-derived, which means that bio-based production schemes are in high demand. Furthermore, NMP is a reproductive toxicant and has recently been classified as a "Substance of Very High Concern" by the European Chemical Agency (EChA), which means that's its use needs to be restricted.[197] Yet, as a dipolar, aprotic solvent NMP features favorable solvent properties, making it the solvent of choice for high-profile technologies such as the production of graphene by exfoliation of graphite or for the fabrication of lithium-ion battery electrodes.

Different solvents are considered for NMP replacement but dipolar aprotic solvents with negligible hazardous statements are hard to find.[198] One solvent class that is increasingly investigated are N-substituted-5-methyl-2-pyrrolidones (N-substituted-5MPs) which show similar solvent properties than NMP and can also be tailored to relevant applications according to their N-substitution. They promise a different toxicological profile than NMP and derivatives due to the additional methyl group. Nevertheless, there is obviously a need for toxicological studies on the subject, which have – to my knowledge – never been performed for such compounds.

Another advantage of N-substituted-5MPs is that they can be synthesized from levulinic acid, generated from biomass. This is therefore an attractive strategy to abandon fossil-based production schemes, also for other N-substituted-2-pyrrolidones such as N-vinyl-2-pyrrolidone for PVP.

For several decades, heterogeneous and homogeneous catalysts have been developed for the reductive amination of levulinic acid to produce unsubstituted 5MP with molecular hydrogen. The patented method relies on a mix of H_2 and NH_3 gas but has several drawbacks, such as the need for expensive noble catalysts, a high excess of H_2 gas and hazardous organic solvents.[199,200] Therefore, other approaches have been explored, based on transfer hydrogenation. Promising results were achieved by using levulinic acid and ammonium formate (or different amines and formic acid, depending on the N-substitution) in water and relying on catalysts such as RHC-Ru[201], Raney-Ni[202] or Pd/C[203]. However, all these approaches suffer from common issues related to metal catalysts such as the need for high loadings and relatively fast deactivation (Raney-Ni) or the use of expensive noble materials with potential toxicity[204] (Pd/C). In the last decade, other studies could circumvent these issues by avoiding a catalyst entirely while still obtaining good yields. Ledoux et al. could synthesize a series of N-substituted-5MP derivatives from levulinic acid by the addition of amines and formic acid under isochoric conditions at 160°C. It was thereby possible to avoid any additive, catalyst or solvent. Obviously, the use of a catalyst still has advantages mostly because milder reaction temperatures can be applied. However, Ledoux et al. could show imposingly in the subsequent E-factor calculation of 0.2 (kg waste per kg product) that this approach performed much better, compared to other approaches, reliant on catalysts or additives with respect to this paramter.[205] Furthermore, N-substituted-5MP derivatives were prepared by Ma et al. in a continuous flow reactor, using formic acid as a hydrogen source and

acetonitrile as the reaction solvent.[206] Lastly, Wu et al. relied on this catalyst-free approach and optimized the reaction by using an excess of formamide and formic acid as reagents. [207] They were able to reach 95% yield of (unsubstituted) 5MP after 2h at 160°C (which is the highest report for catalyst-free approaches for this synthesis) and developed a synthesis procedure from hexose sugars to the final purified product.

This last reaction is known as a Leuckart reaction, where formamide and formic acid are used as reagents for the reductive amination of a carbonyl group. Another reagent, which can be used alternatively, is ammonium formate. While the choice of reagent gives the same product, it cannot be predetermined which will give the better outcome. This will depend on the specific reaction and reaction conditions.[208–210] In this chapter, I will therefore investigate REM based on levulinic acid and ammonium formate for the synthesis of 5MP (as shown in Scheme 2) and compare the results to the data reported by Wu et al.. Furthermore, I will also investigate the influence of water on the reaction.

Finally, Leuckart reactions generally need relatively long reaction times in the order of hours. There has been a report on a profound enhancement of reaction time by using microwave heating.[211] The influence of microwave heating will therefore also be considered.

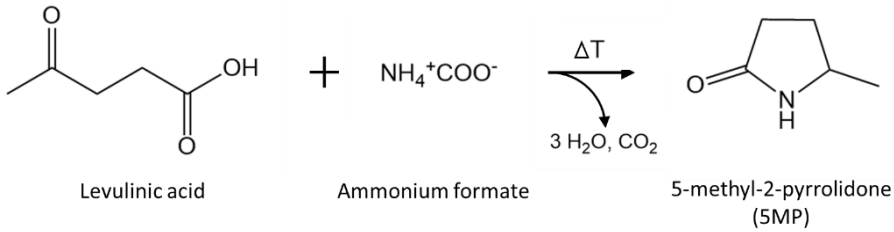

Scheme 2: *Reaction of ammonium formate with levulinic acid into 5MP.*

3.3. Experimental

REM are prepared by mixing 1.5g of levulinic acid with varying amounts of ammonium formate, to cover molar ratios from 1:1 to 1:5. Water is added in different amounts, using molar ratios ranging from 0 to 30. Samples are prepared in 35 ml quartz glass vials and after addition of a magnetic stir bar, sealed with a Teflon-lined cap. Vials are heated under vigorous stirring with a laboratory microwave (Discover SP) with a power of 40 Watt. The pressure is monitored and temperature is measured by infrared technology. Zero time is taken when the desired temperature is reached. Experiments are conducted at 150-180°C and performed for 20 to 120 minutes.

^{1}H NMR is used for product characterization of the crude mixture and is also applied quantitatively to calculate the substrate conversion and yields of products using DMSO as an internal standard. Eutectic mixtures after water dilution are characterized, using DSC, a falling ball viscometer and by investigating hydrogen bonding by ^{1}H NMR (using a capillary to physically separate the media from the NMR solvent). The exact procedures are described in chapter S1 of the SI.

3.4. Results and discussion

An initial screening of the reaction conditions for the synthesis of 5MP is shown in Figure 11. It shows that a slight access (2:1) of ammonium formate is beneficial for reaction yields but a higher excess brings only minor benefits. Furthermore, increasing the temperature is slightly beneficial for the reaction, so in the course of this study, 170°C will be used. This is also in accordance with previously reported catalyst-free approaches for this synthesis, which relied on similar temperatures.[205,207] The same holds for the necessity of isochoric reaction conditions - yields drop drastically when the reaction is performed under reflux. This is commonly observed for Leuckart reactions due to reduced reaction rates in an open system.[208,210] The consequence of such isochoric conditions is that CO_2 accumulates as a by-product in the reaction vessel and results in a pressure build-up during the reaction. As shown in Figure 12, this pressure build-up can be correlated to the reaction yields and is thereby a useful tool to monitor the reaction. These results also shows that the use of microwave heating has no meaningful influence on the reaction rate as these time scales are comparable to the ones reported by Wu et al.[207] as well as Ledoux et al. [205] under conventional heating.

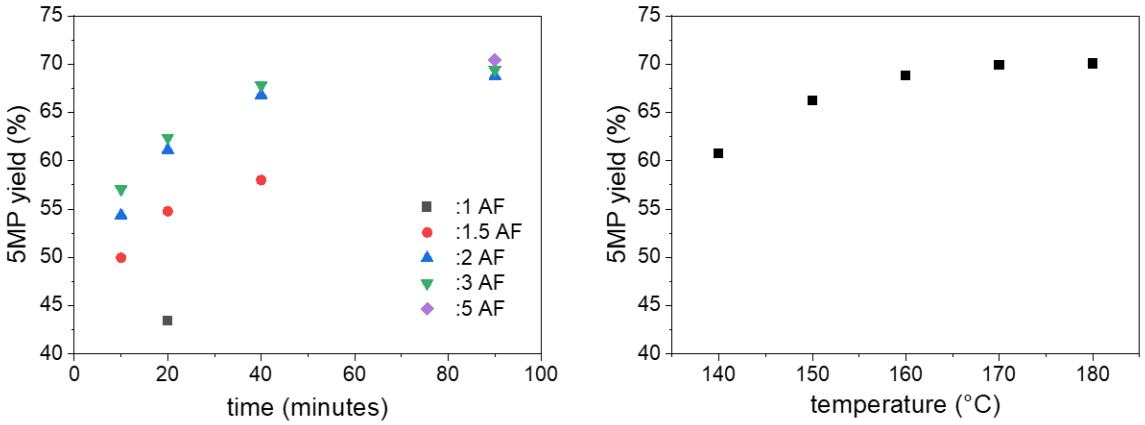

Figure 11: *Reaction yields of 5MP for varying molar equivalents of ammonium formate (AF) for 1 mole of levulinic acid. Reactions are performed at 170°C (left). Reaction yields of 5MP for varying reaction temperature. Reactions are performed for 90 minutes with a molar ratio of 2:1 for ammonium formate to levulinic acid.*

In the next step, the addition of water on the reaction yield is investigated. As shown in Figure 13, this has a profound influence on the reaction yield, which goes up to 83.3% with the addition of 3 mole equivalents of water. This is supported by a previous study by Pollard and Young from the 1950s. [208] They investigated the reaction mechanism of the Leuckart reaction and found that a minimum of water is beneficial in order to convert formamide (which forms from ammonium formate under heating) back to ammonium formate. This increases the concentration of reducing agent (i.e. formic acid) that is required by the reaction and can thereby increase reaction yields. This is supported by NMR analysis of reaction mixtures, which indeed shows that the conversion of ammonium formate into formamide is reduced for increasing water concentration (S3.2 in the

SI). The results in Figure 13 also show that further water addition, beyond 3 mole equivalents results in a drop of reaction yields. The explanation that suggests itself is that little water addition is incorporated in the REM and concentration of reactants is still high. However, if more water is added the reaction takes place in solvent and reaction rates are reduced. This is also confirmed by the reduction of levulinic acid conversion.

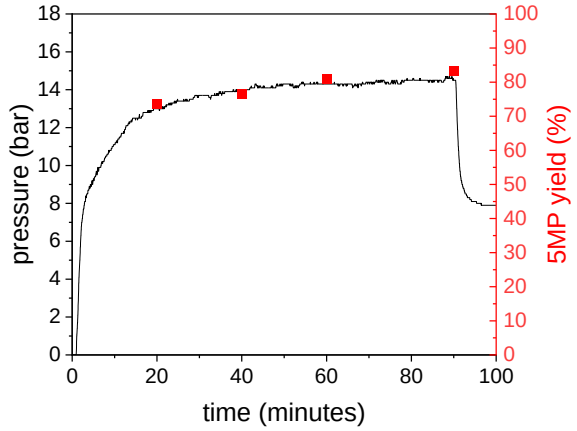

Figure 12: *Pressure build-up over time vs. reaction yield. The reaction is performed at 170˚C with a molar ratio of 2:1:3 for ammonium formate to levulinic acid to water.*

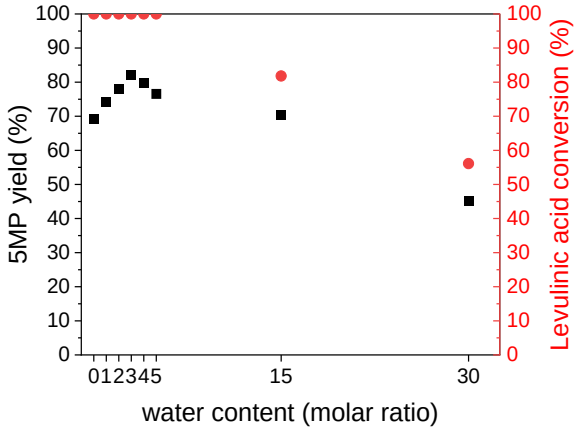

Figure 13: *The influence of water addition on the reaction yield. Reactions are performed for 90 minutes at 170˚C with a molar ratio of 2:1 for ammonium formate to levulinic acid.*

This is supported by consideration of the pressure build-up during the reaction, which is used as a tool to monitor reaction progress. As shown in Figure 14, the pressure profiles for different water contents indicate two different dilution regimes, according to the difference in shape which is due to formation of CO_2 as well as solubility of CO_2 in the reaction media. Samples with little water content appear to be in a different dilution regime and do not form aqueous solutions but tertiary eutectic mixtures instead.

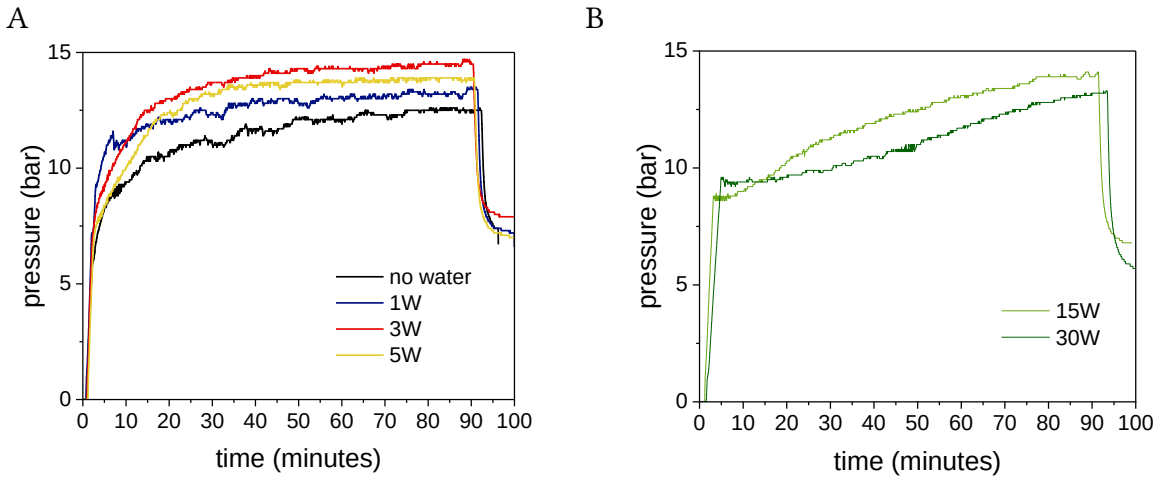

Figure 14: *Pressure build up over time for two different regimes: reactive mixture regime (A) and solvent regime (B). Reactions are performed for 90 minutes at 170˚C with a molar ratio of 2:1 for ammonium formate to levulinic acid and varying addition of water (W) in molar ratio.*

This is supported by DSC measurement (Figure 15), which indicate the inclusion of water in the REM for samples with a water content of :5 or less. Such samples feature only a glass transition temperature (which is often observed for eutectic mixtures) but lack the characteristic melting and crystallization peaks of water. However, such peaks can be observed for samples with a water content of :15 or more, were indeed aqueous solutions are formed. The shift of these peaks can be explained by a freezing-point depression due to increased solute concentration.

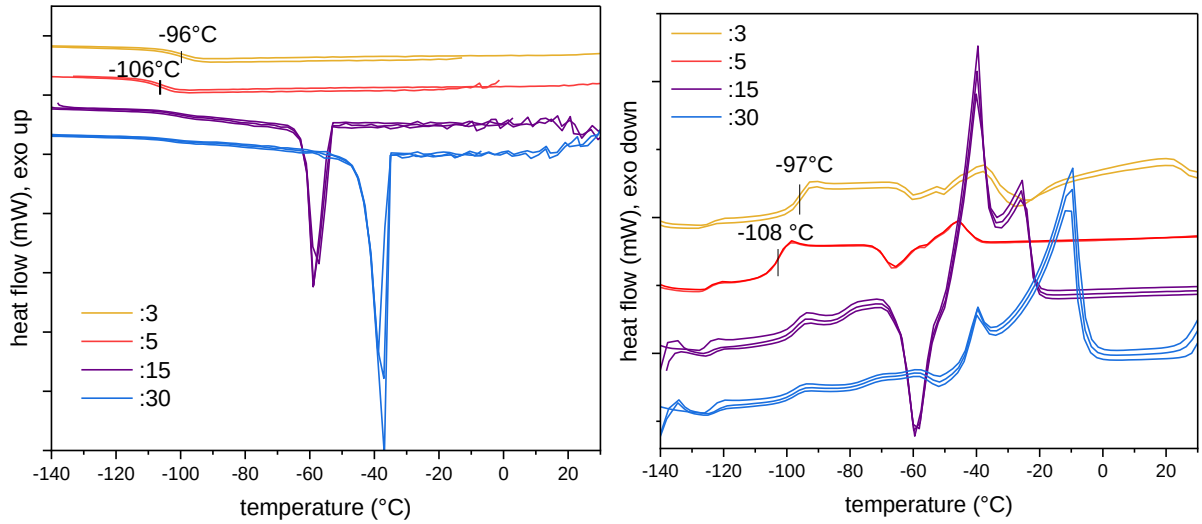

Figure 15: *DSC measurements of ammonium formate/ levulinic acid mixtures with different amounts of water, given in molar ratio.*

The role of water in the REM is also investigated by NMR measurement, as shown in Figure 16. The pronounced downfield shift of water protons, indicates the strong polarization of water molecules for samples with water addition of :5 (in molar ratio) or less. This indicated the incorporation of water as a third component in the REM for these samples.

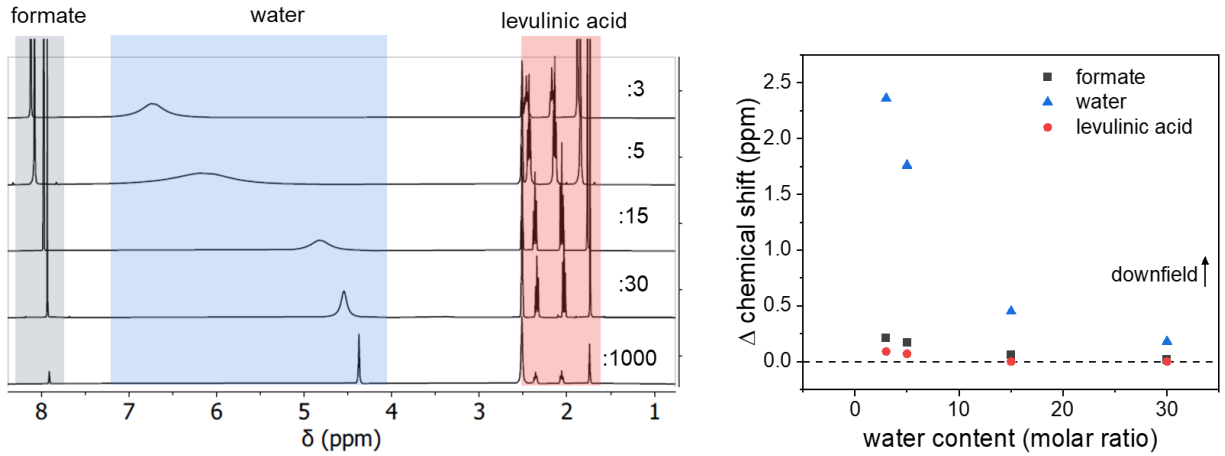

Figure 16: *^{1}H NMR of ammonium formate/ levulinic acid mixtures with different amounts of D_2O, given in molar ratio (left). The difference in chemical shift compared to the sample with highest dilution (:1000) (right). I could not measure samples with a water content below 3 in molar ratio because they do not form a homogenous liquid at room temperature. DMSO-d6 is used as a reference standard.*

The addition of water also affects the physical properties of the REM, such as the viscosity. As can be seen in Figure 17, water addition leads to a reduction in viscosity. However, the extend is only minor compared to the effect that is observed for REM based on monosaccharides and ammonium formate in CHAPTER 2.

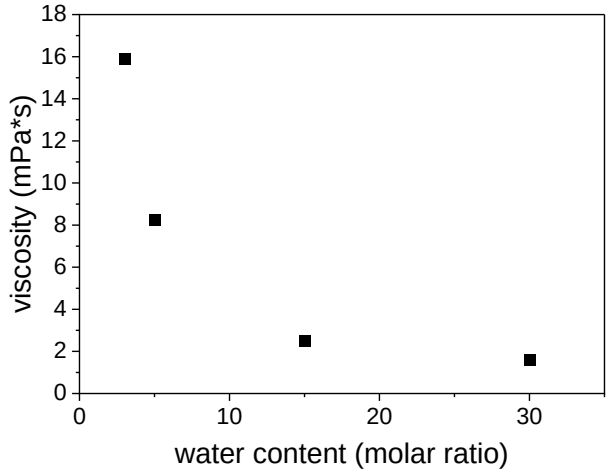

Figure 17: *Influence of water addition on the viscosity of the REM at room temperature. I did not measure samples with a water content below 3 in molar ratio as they do not form homogenous liquids at room temperature.*

3.5. Conclusion and outlook

In this chapter, the reaction in REM between levulinic acid and ammonium formate was described and the optimization parameters were rationalized. The use of synthesis in REM appeared highly beneficial for reaction rates, while the heating method (microwave vs. conventional) was found to have little effect on the reaction. Small amounts of water appeared necessary in order to increase yields, by shifting the chemical equilibria towards a higher concentration of ammonium formate. The best results were obtained for molar ratios of 2:1:3 between ammonium formate, levulinic acid and water, which gave a 5MP yield of 83.3% after 90 minutes at 170°C. The yields are thereby lower to the same reaction that was performed by Wu et al., which relied on the alternative Leuckart reagent formamide/ formic acid. They reached yields of 95% for 5MP under comparable conditions, by using a molar ratio of 1:10:3:15 for levulinic acid, formamide, formic acid and water. The results are in agreement with an early study on the Leuckart reaction[208] which found that ammonium formate is the better Leuckart reagent when stoichiometric ratios are used. However, having it in greater access has less impact on the reaction yield – in this case formamide with formic acid becomes superior. Nevertheless, it should be highlighted that the use of ammonium formate has the advantage of a much better reaction mass efficiency and resulting energy and material savings during the purification procedure. A scaled-up synthesis of 5MP, along with its separation by vacuum distillation and subsequent E-factor calculation will thus be the subject of future work.

CHAPTER 4
The reaction with organic acids and its use in the biorefinery

4.1. Overview

This chapter investigates REM based on ammonium formate and different organic acids for the treatment of lignocellulosic biomass. The separated cellulose fraction is analyzed on its remaining lignin content and is studied with respect to surface charge and fiber length. The isolated lignin fraction is investigated with respect to its structure and composition. Finally, the influence of REM composition on the reaction products is studied.

Cellulose (left) and lignin (right) from beech wood after REM treatment

4.2. Background

The REM between levulinic acid and ammonium formate, which was discussed in the previous chapter, has an interesting additional use beside the synthesis of 5MP. A eutectic containing ammonium formate and organic acids such as levulinic acid has recently been used as a REM for the treatment of cellulose for nanocellulose isolation.[97] Another recent paper has found that NMP (which is a close analogue to 5MP) shows excellent properties for lignin dissolution and biomass treatment.[212] Both these findings combined, have led to the concept of REM for lignocellulosic biomass treatment, which will be pursued in this chapter. According to this idea, this would not only lead to the pulping of cellulose from lignin, but also to the synthesis of the value-added product 5MP. This implies a substantial process intensification and presents a novel approach for the implementation to biorefinery schemes.

The biorefinery presents an alternative to today's petroleum refinery and is a cornerstone of a future chemical industry that should serve the circular economy and strives to operate sustainably. In the case of lignocellulosic biomass as starting material, this means that its three main components (cellulose, hemicellulose and lignin) should be exploited to produce value-added fuels, chemicals and materials. However, currently this is not the case for all of its components. Annually, over 100 million tons of lignin are produced as a byproduct from traditional pulp mills and modern cellulosic ethanol industry but only 2% of lignin are used for applications different from energy-production through burning. [213] On the other hand, lignin is the largest naturally available source of aromatic building blocks and can be used to produce bulk, fine, and functionalized aromatic compounds.[214] What is standing in the way of the large-scale utilization of lignin-derived chemicals or materials is the recalcitrant chemical nature of the macromolecule.

Unlike cellulose, which has a single repeating linkage of β-1,4 glucosidic bonds, lignin contains several different types of linkages between its aromatic units, including C–O–C bonds (β-O-4/4′, α-O-4/4′, 4-O-5/5′, etc.) and C–C bonds (5–5/5′, β-β, β-1, β-5, etc.) [215]. Lignin fractions during depolymerization conditions in traditional pulping processes are usually highly reactive and therefore undergo substantial side reactions, which are hard to control. Such side reactions include repolymerization or condensation, which results in very heterogeneous structures. This makes direct production of well-defined compounds from lignin very challenging.[216] Furthermore, the cross-linked structure often results in low solubility in most conventional solvents, which is the bottleneck for further processing.

New fractionation treatments for biomass have been investigated in order to tackle some of these issues. One approach is the use of alternative solvent systems, which manage to yield reactive and less condensed types of lignin after treatment. Methods which rely on this approach include ammonia-based fractionation[217,218], ionic liquid (IL)-assisted fractionation[219,220], treatment with deep eutectic solvents (DES)[221], γ-valerolactone-assisted hydrolysis[222] and ethylenediamine pretreatment[223,224]. While these methods give promising results, they also come with the drawback of much higher solvent costs compared to organosolv treatment with ethanol.

In this chapter, I make use of REM based on ammonium formate and organic acids for biomass fractionation. In the treatment of biomass, I hypothesize that the organic acid catalyzes the lignin

depolymerization while ammonium formate acts as an amination agent to introduce nitrogen-containing functional groups into the lignin structure. Additionally, the REM components react within each other to form a solvent for improved lignin dissolution. This last point is important, as this allows the production of higher value products from the starting materials. This enables a better utilization of the process energy for a wider product range and thereby holds the potential to drive the modern biorefinery toward economic viability. Besides, levulinic acid, I will also employ lactic acid as well as acetic acid in the REM as they have also given good results for cellulose treatment with REM.[97] However, since it is unknown how capable these REM are for lignin dissolution, I will also investigate the addition of ethylene glycol and propylene glycol to the REM to facilitate lignin dissolution. Both of these solvents have shown to be good lignin solvents in previous studies[225,226], can be bio-derived[227,228] and offer low vapor pressures.

4.3. Experimental

4.3.1. REM reaction

The REM are prepared by simply mixing the components, which are shown below in Table 3. All REM employed in this work, consist of ammonium formate and an organic acid. The different organic acids used are levulinic acid (LvAc), lactic acid (LacAc) and acetic acid (AcAc). Furthermore, some REM contain the additional components propylene glycol (PG) and ethylene glycol (EG) as part of the REM. In the following, the respective REM will be referred to by the employed organic acid (LvAc, LacAc or AcAc) as well as by the use of additional solvent (n, PG or EG). They are all prepared, based on 3 g of ammonium formate.

Table 3: Composition of employed REM. The molar ratios are kept constant.

REM components	Ammonium formate	Organic acid • Levulinic acid (LvAc) • Lactic acid (LacAc) • Acetic acid (AcAc)	Additional components • None (n) • Propylene glycol (PG) • Ethylene glycol (EG)
Molar ratio	3	1	4

For the REM reaction, the components are transferred to a 35 ml quartz vial, facilitated with a magnetic stirrer and sealed with a Teflon lined cap. The vial is heated in a microwave oven (Discover SP) with a power of 100 Watt under vigorous stirring and kept at 160°C for 30 minutes to 2 hours.

After synthesis, the REM is qualitatively analyzed, using GC-MS and NMR. Quantitative ^{1}H NMR is applied to calculate the substrate conversion and yields of products using DMSO as an internal standard and D_2O solvent, analogous to the procedure described in CHAPTER 3. The detailed procedures can be found in chapter S1 of the SI.

4.3.2. REM treatment of biomass

10 wt% of dried beech wood sawdust is mixed with the respective REM. After treatment at 160°C for 2h in the microwave oven, the cellulose fraction can be separated by vacuum filtration. The filter cake is mechanically pressed to remove as much of the filtrate as possible and consecutively washed with ethanol and acetone. The filtrate is collected and concentrated by rotary evaporation at 45°C. Water is added, five times the volume of the filtrate, and the solution is stored in the fridge at 5 °C overnight. The filter cake is washed with water and dried in the vacuum oven at 45°C overnight, yielding dried cellulose pulp. The following day, the diluted filtrate is centrifuged to yield the precipitated lignin and the supernatant is collected and stored. Lignin is washed with water several times and dried in the freeze drier overnight.

The cellulose fraction is analyzed on the residual lignin content, using Klason lignin quantification, according to the NREL analytical procedure. Furthermore, the fiber length is investigated with TEM after homogenization as well as with GPC in NMP after carbanilation. Finally, the samples are analyzed by Zeta-potential measurements and crystallinity index (CI) is determined, using PXRD.

The lignin fraction is analyzed with NMR analysis, using HSQC techniques. Furthermore, samples are studied with elemental analysis, FTIR as well as with GPC in NMP. In addition, lignin is extracted via organosolv (OS) treatment from the same beechwood sawdust, in order to compare it to lignin from REM extraction, according to [229].

The detailed procedures for the analysis techniques can be found in chapter S1 of the SI.

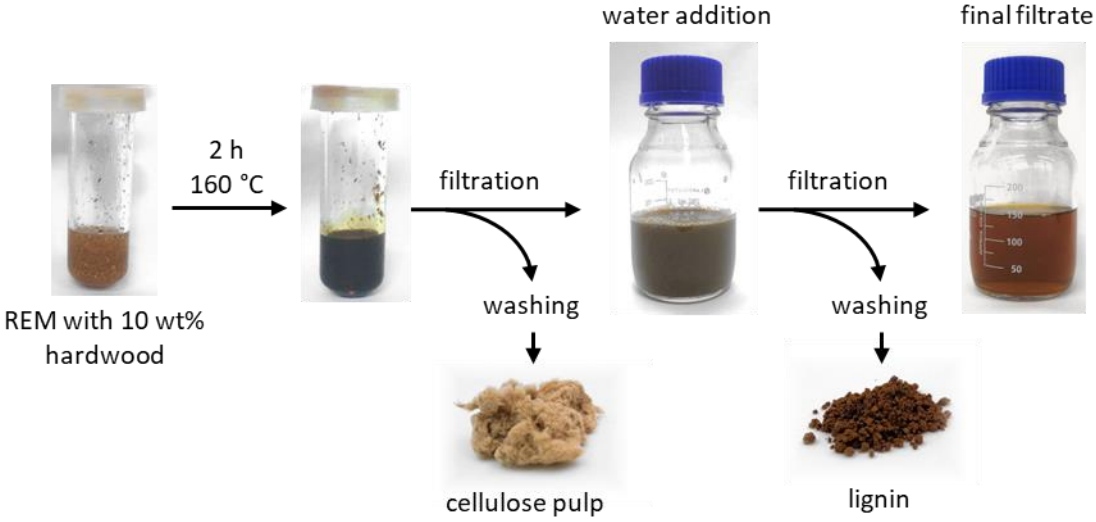

Figure 18: *Process scheme of lignocellulosic biomass treatment with REM.*

4.4. Results and discussions

4.4.1. Investigating the REM

Investigation of the REM reveals that the employed organic acids undergo different reactions with ammonium formate. The products are identified by ^{1}H NMR and GC-MS (see S4.1 in the SI) and are summarized below in Table 4 for the reaction conditions that are also employed during biomass treatment.

Reactions of LacAc or AcAc with ammonium formate form the respective amides. Presumably, the carboxylic acid is first converted into its ammonium salt, which then produces the primary amide upon heating. Primary amides feature extensively in organic synthesis as they can be found in pharmaceuticals, natural products and biologically-active molecules.[230] The most common synthetic methods currently used for the direct amidation of carboxylic acids require harsh reaction conditions and long reaction times[231]. The fact that this approach generates them simultaneously with biomass treatment can also be described as an upgrading of the biomass solvent.

The reaction of LvAc with ammonium formate proceeds via a different mechanism due to the carbonyl group on LvAc. The main reaction product here is 5MP as discussed in CHAPTER 3. 5MP and N-substituted derivatives are a highly promising class of substances, considering that they can be produced from bio-based sources and can be used as solvents (e.g. NMP substitutes), surfactants or precursors of pharmaceuticals.[232,233]

It should be highlighted here, that the reactions have not been optimized. E.g. as discussed in CHAPTER 3, the synthesis of 5MP can reach yields as high as 95% by optimization of reactants, as shown by Wu et al.[207] However, this work just aims towards a proof of concept for the simultaneous synthesis of 5MP with the treatment of biomass.

Table 4: *Reaction of different organic acids with ammonium formate at 160°C for 2h. Yields and conversions are measured with quantitative NMR.*

Organic acid	Main product	Yield (%)	Conversion (%)
Levulinic acid (LvAc)	5-methyl-2-pyrrolidone (5MP)	70	100
Lactic acid (LacAc)	Lactamide	47	47
Acetic Acid (AcAc)	Acetamide	56	56

4.4.2. Cellulose fraction

The separated cellulose fractions are shown in Figure 19 and are analyzed on their remaining content of Klason lignin. REM without additional solvent show the widest divergence in their capacity for extracting lignin. LacAc-n and AcAc-n seem to be only moderate extraction solvents (which is why they will not be considered any further) but LvAc-n appears to be an excellent solvent and removes 92% of lignin. One should keep in mind here that LvAc-n is mainly converted to 5MP during the reaction as explained above. If additional solvent is added to the

REM, the type of organic acid appears to have little influence on the lignin extraction. However, REM with additional PG appear to work better than EG and extract on average 86% of lignin compared to 74% for REM with additional EG. What would be interesting to investigate in the future is how theses REM perform for higher biomass loading.

In CHAPTER 3 it was shown that synthesis of 5MP profits from catalytic amounts of water. Therefore, I also tested its effects in the treatment of biomass by adding 3 mole equivalents of water to the REM of LvAc-n. The results show that lignin removal remains high, with a lignin removal of 89%. This is a positive indication that also wet biomass might be used in the process (instead of pre-dried).

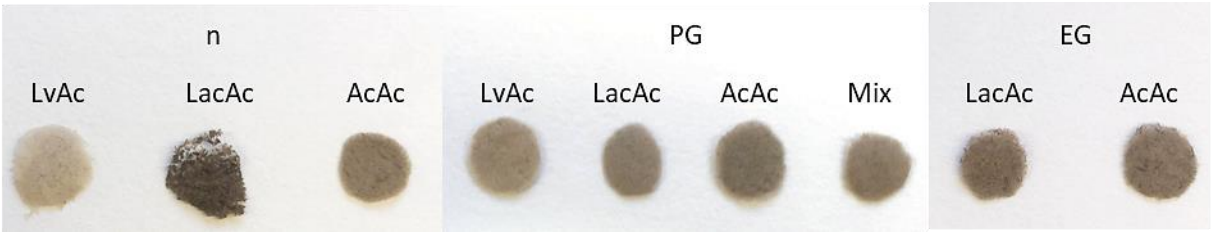

Figure 19: *Cellulose fractions, after REM treatment.*

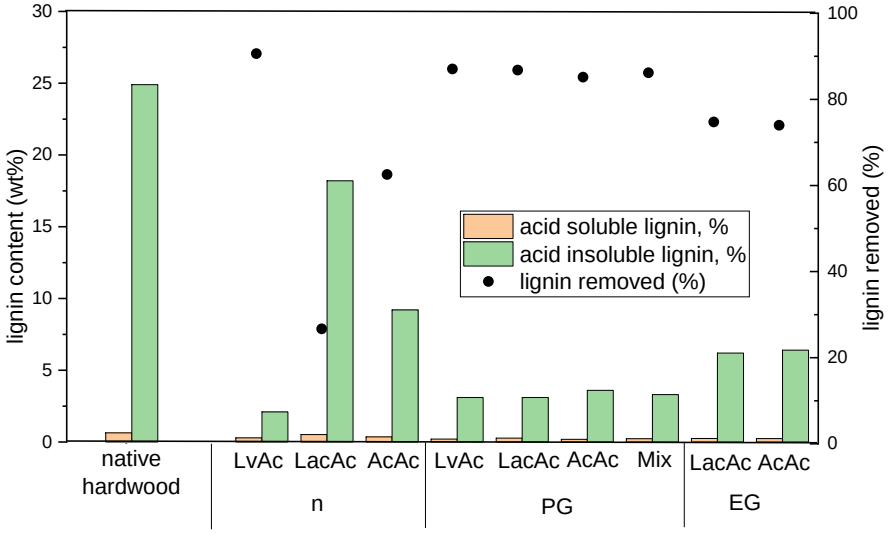

Figure 20: *Lignin content and lignin removal for cellulose samples, obtained after beech wood treatment with different REM. Sample Mix-PG are obtained from treatment with a REM based on a 50/50 mix of LacAc and AcAc.*

In the previous work by Jaekel et al., the employed REM were used for treatment of pure cellulose and the generation of cationic cellulose nanocrystals.[97] However, in the present case, TEM measurements in Figure 21 reveal much longer fibers (>1µ). The observed differences of cellulose properties may be explained with the different starting materials. While the previous relied on pure cellulose, this method employs raw lignocellulosic biomass, which means that the REM need to dissolve lignin first, before they can reach and act on the single cellulose fibers. Therefore, the fibers remain much longer. This is confirmed by reacting two of the obtained

cellulose fractions one more time in the respective REM. They are referred to as 2xLv-n and 2xLc-PG. These samples do feature lengths below 500 nm as shown by TEM imaging.

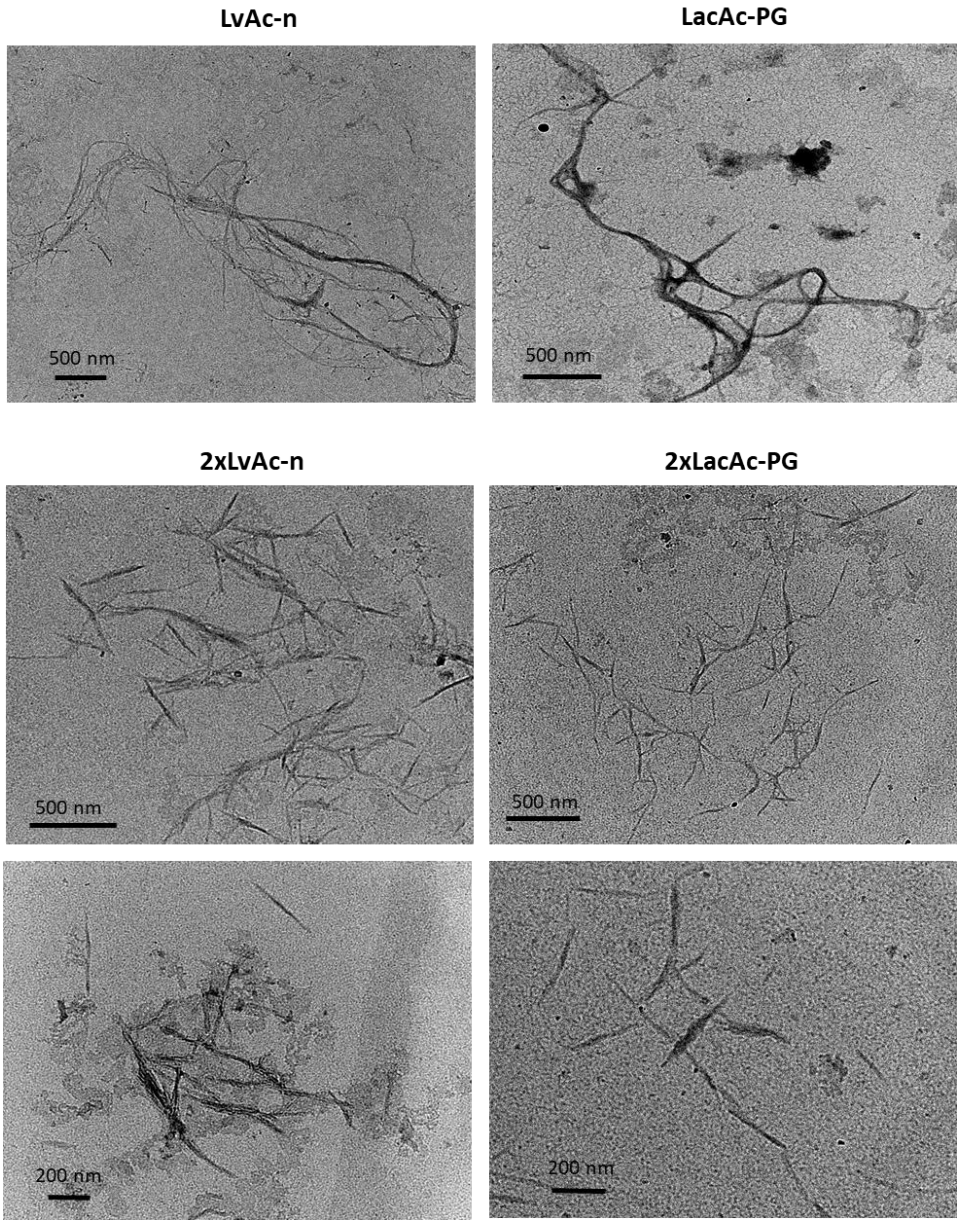

Figure 21: *TEM images of cellulose pulp, after homogenization of the samples.*

This observation is confirmed by GPC measurements of derivatized cellulose. As shown in Figure 22, the molecular weight (thereby the fiber length) becomes shorter for repeated treatment with REM. Another observable difference between REM treatment of pure cellulose vs. lignocellulosic biomass is the surface charge. As shown in Figure 23, Zeta-potential measurements reveal a negative surface charge on the cellulose samples but repeated treatment in REM yields a positive

surface charge. This indicates the formation of cationic nanocellulose, with nitrogen-containing functional groups on its reducing ends.

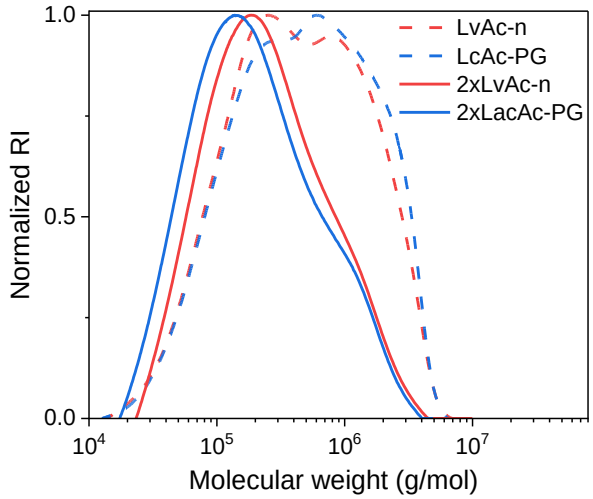

Figure 22: *GPC of cellulose samples, after carbanilation.*

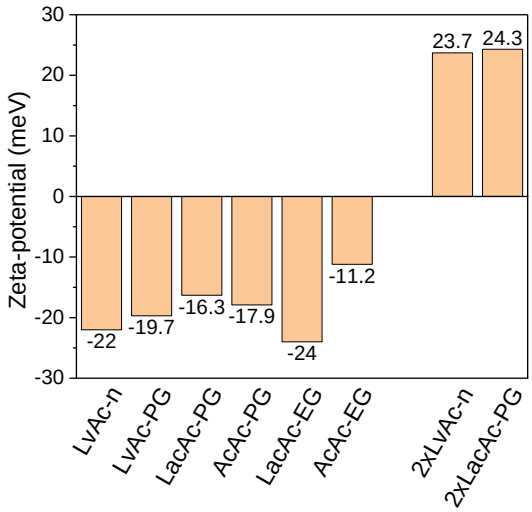

Figure 23: *Zeta-potential of cellulose samples in water.*

Finally, the crystallinity index (CI) of the cellulose samples is measured using X-Ray Diffraction (XRD) and peak height analysis. All samples featured a relatively high crystallinity, with a CI between 72 and 76% (Table 5) which increases for the samples, which were treated twice in the REM to around 78%. This is supporting the observation of nanocrystal generation in is such samples.

Table 5: *Crystallinity index (CI) of cellulose samples, using the peak height analysis of XRD data*

Sample	LvAc-n	LvAc-PG	LacAc-PG	AcAc-PG	LacAc-EG	AcAc-EG	2xLvAc-n	2xLacAc-PG
CI (%)	75.8	72.3	75.0	71.8	72.5	73.0	78.1	78.4

4.4.3. Lignin fraction

The amount of lignin that is removed from the respective cellulose samples can be compared to the amount of lignin that is actually recovered. As it turns out, only a portion of the lignin is precipitated and a part remains in the final filtrate (Figure 24). This can also be noticed by simply looking at the final filtrate solution, which shows lignin precipitation at the bottom of the flask after several days. This indicates the formation of lignin nanoparticles by water addition. The preperation of lignin nanoparticles through the addition of an anti-solvent is in fact a common method for this material.[234] However, in our case a better recovery would be desirable, meaning that the method for lignin recovery from the filtrate should be refined. Relevant factors to investigate would be e.g. adding more water, adapting the pH of the solution, changing the anti-solvent or changing the recovery method entirely (e.g. nanofiltration, vacuum distillation of

5MP[235]). The difficulty of recovering the extracted lignin by water addition already points to a possible modification of the lignin towards more amphiphilic systems.

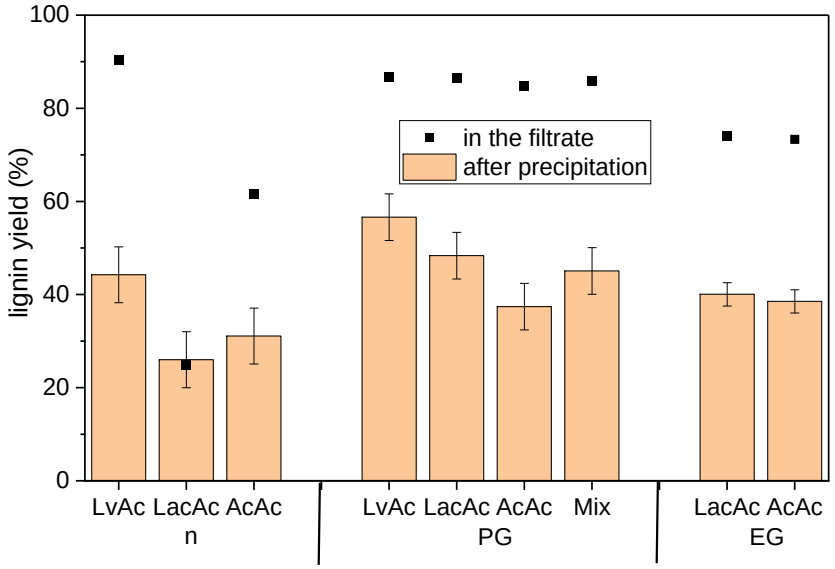

Figure 24: *Recovery of lignin after precipitation vs. the content of lignin in the filtrate according to Klason analysis of cellulose samples.*

Elemental analysis of the recovered lignin indicates the presence of nitrogen as shown in Table 6. According to FTIR (Figure 25), this nitrogen can be assigned to imine groups with an emerging stretching vibration at 1690cm^{-1}, which is absent in the organosolv lignin that was prepared from the same wood for comparison. In addition, the C-H stretch of the imine can be found at 3285 cm^{-1}. Otherwise, the lignin features the typical signals on FTIR.[236] The three peaks associated with aromatic skeletal vibrations are found at 1590, 1505, and 1420 cm^{-1} and are all readily visible. The band at 1460 cm^{-1} belongs to C-H deformations of methyl and methylene. The dominant lignin monomers in hardwood can be identified by bands at 1267 cm^{-1} (C-O of the G ring) and 1315 cm^{-1} (C-O of the S ring). In addition, a band shared by the two monomers (C-H of the G and S ring) is located at 1113 cm^{-1}. The peak at 1215 cm^{-1} as well as at 1030 cm^{-1} are assigned to the C-O stretching. The band observed at 3450 cm^{-1} is attributed to O-H stretching, while 2935 and 2845 cm^{-1} are assigned to methyl and methylene bond stretching.

Table 6: *Elemental analysis of lignin samples as well as the average C9 composition. The later can be calculated after considering the amount of methoxy groups per sample, which is revealed by analysis of HSQC-NMR data.*

Sample	N (%)	C (%)	H (%)	O (%)	OCH_3	C9 formula
LvAc-n	5.1	61.0	6.2	27.7	1.56	$N_{0.76}C_9H_{8.25}O_{2.0}(OCH_3)_{1.54}$
LvAc-PG	5.3	61.6	6.3	26.8	1.56	$N_{0.78}C_9H_{8.25}O_{1.86}(OCH_3)_{1.56}$
LacAc-PG	5.2	61.9	5.9	27.0	1.51	$N_{0.75}C_9H_{7.39}O_{1.89}(OCH_3)_{1.51}$
AcAc-PG	4.8	61.6	5.8	27.7	1.51	$N_{0.71}C_9H_{7.42}O_{2.01}(OCH_3)_{1.51}$
LacAc-EG	4.4	60.5	5.9	29.3	1.58	$N_{0.66}C_9H_{7.65}O_{2.21}(OCH_3)_{1.58}$
AcAc-EG	4.3	61.5	6.0	28.2	1.59	$N_{0.64}C_9H_{7.73}O_{2.02}(OCH_3)_{1.59}$

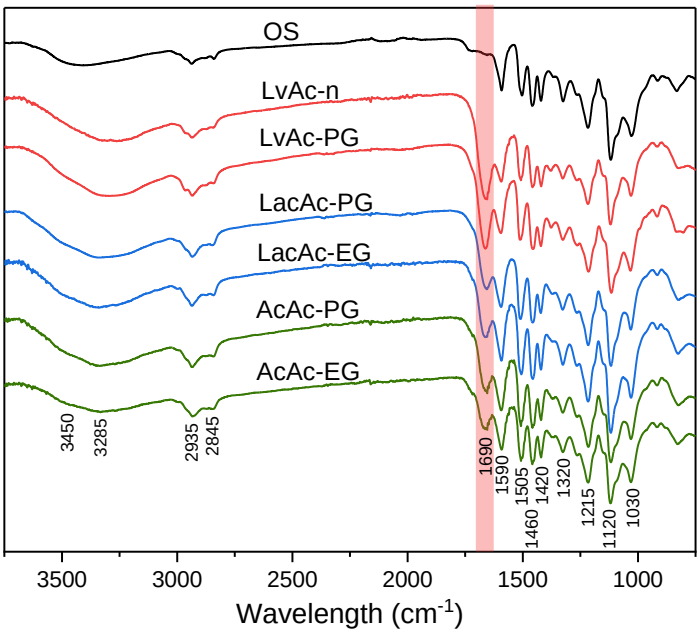

Figure 25: *FTIR of lignin samples, obtained from treatment of beech wood with different REM. For comparison, lignin from organosolv (OS) extraction is investigated as well.*

The formation of imine bonds is also supported by HSQC NMR, shown on the example of lignin from LvAc-PG in Figure 26a. The cross-peaks at δC/δH 161/8.0 ppm corresponds to the imine bond (–CH=N–), more specifically an aldimine from the reaction of a primary amine with an aldehyde. This type of signal was also observed previously for lignin, extracted with ethylenediamine.[223] Otherwise, the typical lignin signals are observed in the spectra, while only traces of hemicellulose are detected. The integration of the signals enables a comparison between the samples and how the different REM affect the extracted lignin structure. A complete table of the integration results of HSQC NMR can be found in S4.2 of the SI. Figure 26b depicts the number of linkages per 100 C9 units (/ 100 C9) for each lignin sample. It shows that the number of β-β linkages remains relatively consistent throughout the samples but the β-5 linkages are present in the organosolv lignin but almost disappear for REM treated lignin. The number of β-O-4/4′ linkages can be correlated to the acid used, during extraction. Since organosolv treatment does not employ any additional acid, it gives the highest amount of β-O-4/4′ linkages. Second rank is taken by the treatment with LvAc based REM. Here the acid is consumed completely during the reaction. LacAc based REM feature the lowest amount of β-O-4/4′ linkages, reflecting that LacAc is the strongest acid out of the employed organic acids and also shows the lowest conversion during the reaction.

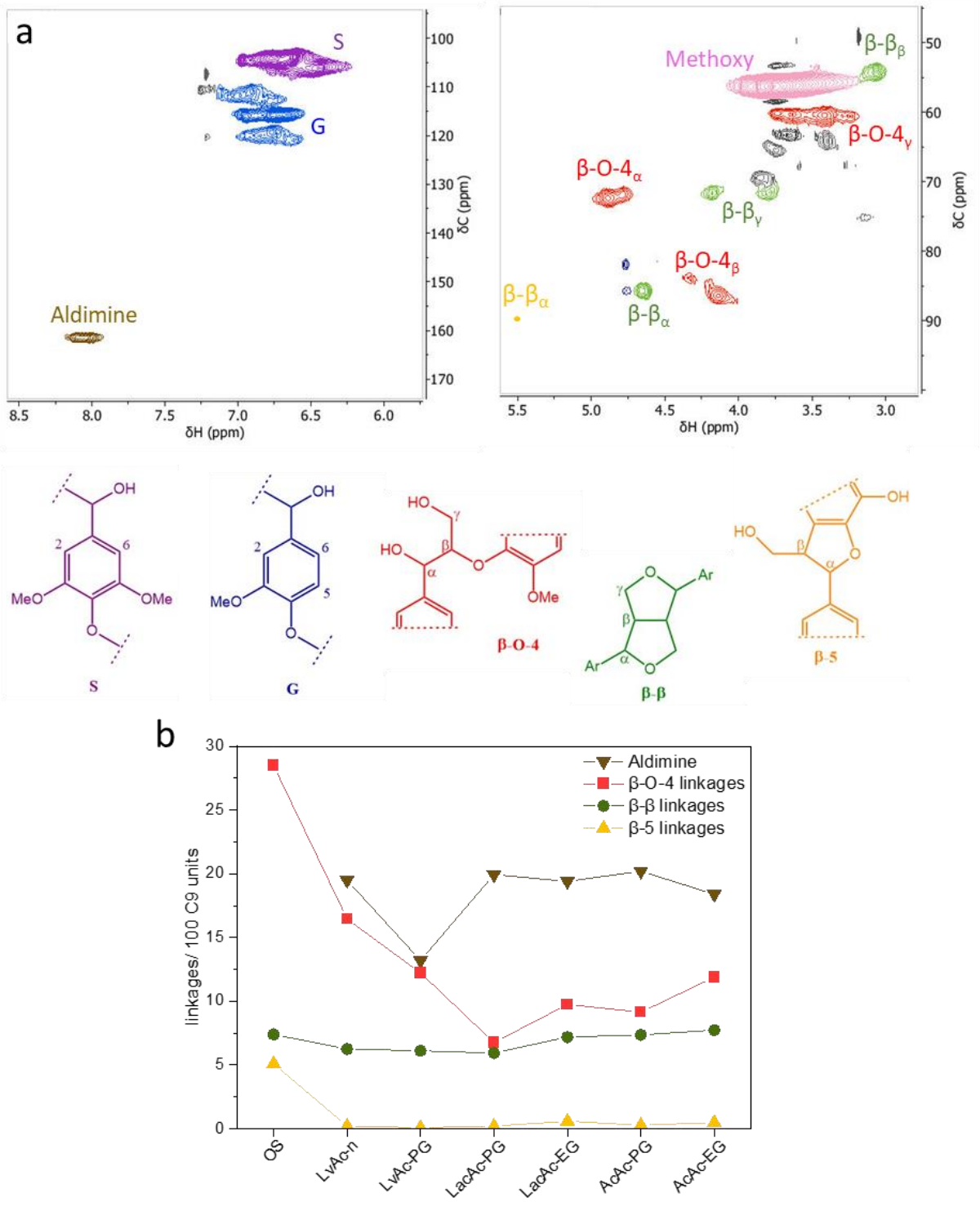

Figure 26: *HSQC-NMR on the example of lignin from LvAc-PG (a). The integration of the corresponding signals enables the analysis of the identified linkages per 100 aromatic units (b). For comparison, lignin from organosolv (OS) extraction is investigated as well.*

The imine linkage exhibits a proton on the imine carbon, otherwise it would not be detectable in HSQC NMR. It can therefore be described as an aldimine group, which is formed by the reaction between a primary amine with an aldehyde. The proposed reaction is shown in Scheme 3, where ammonium formate acts as an amination agent and reacts in a Leuckart reaction with a carbonyl group, present in lignin of native wood. In a second step this amine reacts with and aldehyde group for aldimine formation. According NMR results in Figure 26, the lignin structure features approximately 20 of such aldimine linkages for 100 C9 units. These results can be compared to the total amount of nitrogen in the lignin structure according to CHN analysis (Table 6), which amounts to approximately 70 molecules of nitrogen per 100 C9 units. That means that aldimines can only partly account for the total nitrogen content in the lignin structure. Other functional groups, that are likely to have formed, are ketimines (where a ketone instead of an aldehyde participates in imine formation) or amides (where the introduced amine group reacts with the organic acid, present in the REM). However, both of these propositions cannot be detected with HSQC NMR, due to the absence of C-H bonds.

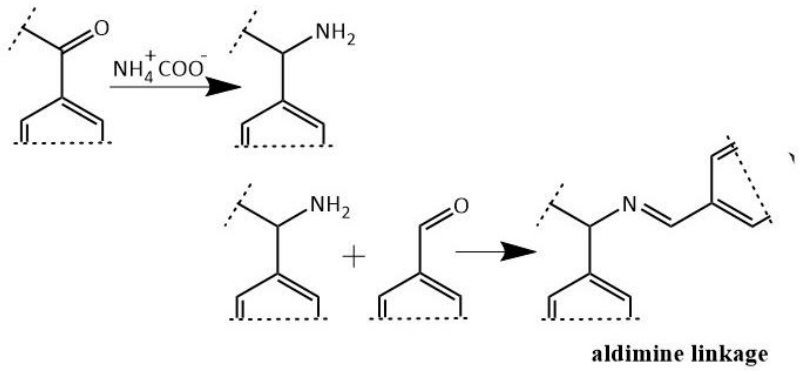

Scheme 3: *Amination reaction between ammonium formate and a carbonyl group in lignin and subsequent aldimine formation.*

According to the literature, native lignin in hard wood contains around 15-20 carbonyl groups per 100 C9 units and only a smaller part of these are aldehyde groups.[237] Native carbonyl groups are therefore not numerous enough to account for the high number of nitrogen containing function groups (ca. 70 /100 C9 units) and the amount of aldimine groups (ca. 20 /100 C9 units) that are detected in the lignin structure after REM treatment. One possible explanation is that additional carbonyl groups are formed via the acid catalyzed cleavage reaction of β-O-4 bonds and that such groups contribute to imine formation. It has been shown in numerous studies that β-O-4 bonds indeed form aldehyde groups upon acid catalyzed cleavage but such groups are usually unstable and prone to repolymerization with C-C bond formation. The inclusion of these groups in imine formation would therefore be a great benefit of lignin extraction via REM treatment as is would preserve a relatively higher reactivity of the lignin structure.

If one acts on the assumption of imine groups in the lignin structure, it should be possible to subject them to a hydrolysis reaction. For this, a portion of lignin from LacAc-PG is dissolved in aqueous NaOH (pH 11) and refluxed at 80 °C for 24 hours. After neutralization with HCl it can be noticed, that the lignin becomes less soluble in organic solvents but its water solubility is greatly increased. The execution of the ninhydrin test reveals the presence of primary amine

groups due to the purple colour of the resulting solution (Figure 27). This indicates a successful hydrolysis of the imine bond and the presence of amine groups.

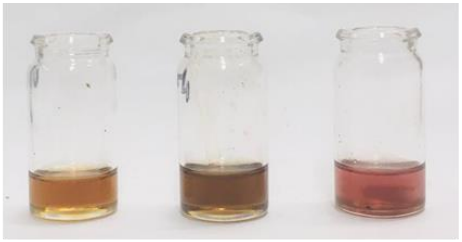

Figure 27: *Ninhydrin test on different lignin samples from beech wood. Obtained from organosolv extraction (left), obtained from REM treatment (middle) and obtained from REM treatment with subsequent alkaline treatment for hydrolysis of imine bonds (right).*

Finally, lignin is measured on its molecular weight, using GPC (Figure 28). It can be seen that the samples from treatment with LvAc have lower molecular weight, compared to samples with other organic acids. Presumably, this is because LvAc as well as its reaction product 5MP can both participate in reaction with lignin due to their keto group and amide bond, respectively. This means that not only two lignin fractions react to form an imine bond, but lignin fraction can also be "capped" by reacting with LvAc or 5MP for imine or enamine formation. This hypothesis is supported by the FT-IR measurement in Figure 25, which reveals a stronger peak at 1690 cm^{-1} for lignin samples from LvAc based REM compared to the other samples.

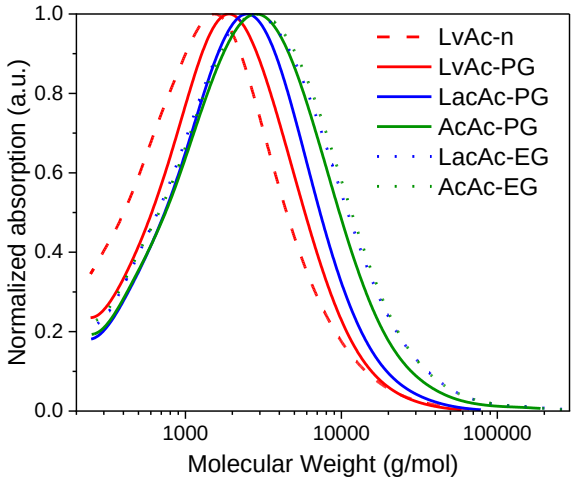

Figure 28: *GPC in NMP of different lignin samples, obtained from beech wood treatment with different REM.*

4.5. Conclusion and outlook

In this chapter, lignocellulosic biomass was treated with a number of different REM, based on ammonium formate and organic acids. The method could thereby isolate cellulose and lignin as well as generate value added chemicals from the REM itself and thus demonstrates an opportunity for process intensification.

The different REM varied in their ability for lignin extraction. While REM with LvAc showed excellent performance, REM with other organic acids could be boosted on their ability to extract lignin, by facilitating the REM with an additional component such as propylene glycol or ethylene glycol. The generated cellulose fractions showed low lignin contents with (relatively) long fibers. By repeated treatment of the cellulose pulp, cationic nanocellulose could be obtained, which is in accordance with previous studies that could generate such material by the same treatment of pure cellulose.

The method also produced high-purity lignin, although the method for lignin isolation needs to be refined. Water addition only precipitated a portion of the dissolved lignin. Furthermore, lignin was analyzed on its structural composition and featured a nitrogen content around 5%. This was (partly) attributed to imine functionalities. By hydrolysis, it was also possible to generate amine groups in the structure, which present a promising opportunity to use the material for further applications.

The study underlines the excellent solvent properties of pyrrolidones for lignin extraction. In this work 5MP from LvAc was investigated but a previous study attested similar properties to NMP[212]. Considering, that LvAc can be used to produce a wide range of N-substituted-5MP there is certainly an opportunity for further investigations in this direction with respect to biomass treatment.

What has not been considered in this study is the fate of hemicellulose in this method. Most likely it has ended up in the final filtrate (as it also has in the study, based on NMP[212]) but further investigation will be necessary. Furthermore, the separation of the final filtrate and the purification of REM reaction products have not been ventured but will be the subject of future work. Finally, it would be interesting to study lignocellulosic biomass from differ sources and to investigate the influence of different molar ratios of the REM.

CHAPTER 5
The reaction with citric acid for the synthesis of an oligocitrazinic acid dye

5.1. Overview

This chapter investigates REM based on ammonium formate and citric acid for the isochoric synthesis of a deeply purple reaction product with fluorescent properties. This brings this reaction in the realm of bio-based fluorophores and bottom-up carbon nanodots from citric acid. The reaction conditions are optimized in terms of UV-vis spectroscopic properties and, subsequently, the main reaction product is separated. While the structural analysis does not give any indication for carbon nanodots in a general sense, it points towards the formation of molecular fluorophores that consist of oligomerized citrazinic acid derivatives. Furthermore, EPR spectroscopy reveals the presence of unpaired electrons in the structure. This is an important finding as it may benefit the overall quest for the structural analysis of citric acid-based fluorophores. Finally, the product is characterized with respect to its optical and fluorescent properties.

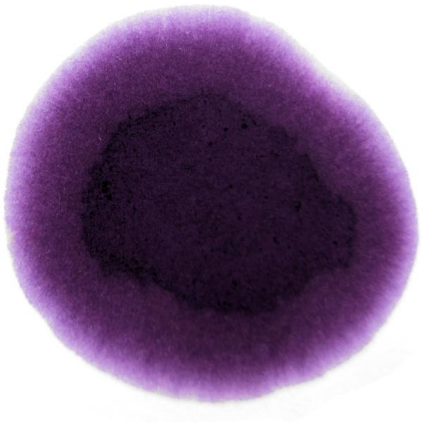

A drop of the purple reaction product on paper.

This chapter is an adapted version of the article: Schneider, H., Strauß, V., Vogl, S., Antonietti, M., & Filonenko, S., Eutectic media open a synthetic route to oligocitrazinic acid fluorophores of purple hue. *ChemPhysChem.* e202300180 (2023).

The study was performed in collaboration with Dr. Sarah Vogel from the department of Chemistry/ Functional Materials, TU Berlin, who performed XPS measurements and data fitting.

5.2. Background

Research on fluorophores from citric acid (CA) and reactive nitrogen precursors has been a flourishing subject in recent years. Such materials are promising due to their sustainable, bio-based precursors and their intriguing fluorescent properties, which make them attractive for many applications such as in biomedical imaging[238–241], fluorescent inks[242,243], solar cells[244–246] or fluorescent probes for detection of metals and biomolecules[247–251].

The starting point for the research on CA derived fluorophores was already marked in the late 19th century by the discovery of the molecular fluorophore citrazinic acid (CzA). Behrmann and Hoffmann synthesized it in 1884 by the addition of sulphuric acid to a water solution of citric acid amide.[252] Two years later, Sell and Easterfield obtained CzA by the reaction of CA with ammonia via melt formation by evaporation of water. Heating the resulting melt to 130 °C led to transformation of ammonium citrate into its amide and substantially to CzA. [253,254]This method was widely used to synthetize CzA, particularly for colour photography films processing such as Kodak Ektachrome E-6 process.[255] After those early synthesis, it has been observed that CA can form many fluorescent structures, using different amines instead of ammonia as reactants. Many of such CzA derivatives have been reported by Kaspzyk et al..[256]

In recent years, considerable research on fluorescent materials form CA has been performed under the headline of carbon nanodots (CNDs).[257] Currently, the structure of CNDs is typically depicted as a core/shell model, where a carbon core with graphitic elements is equipped with various functional groups on its surface.[258–260] CNDs from CA and various amines are typically formed by heating to temperatures between 140 and 200 °C, where solvent-free as well as hydro- and solvothermal approaches have been reported.[261,262]

The fluorescent properties of bottom-up CNDs from CA are still a matter of debate. They have been attributed to the graphitic core as well as to molecular fluorophores – namely CzA and its derivatives. However, it is still an open question how these fluorophores are connected to the cores of CNDs or with each other, or whether they are chemically connected at all.[257,263,264] Firstly, separation is an issue and in several cases the observed fluorescence could be attributed to a specific molecular species rather than CNDs after careful separation of the product mixture.[265,266] Secondly, aggregation plays an important part in the fluorescent properties of such molecules. For example, in 2017 Reckmeier et. al.[267] analyzed amorphous aggregates of CzA derivatives and showed that such aggregates could absorb and emit at wavelengths over a wide range of the visible spectra. The emission spectra were overall very similar to those typically reported for CNDs. In summary, one can say that fluorophores and CNDs from CA still pose a puzzle with respect to their structural analysis.

In this chapter, I report on a novel synthesis, using CA and ammonium formate in a REM synthesis. This synthesis is especially interesting as it produces a dye substance with an intense purple colour, indicating a yet undiscovered reaction pathway. In most of the reported syntheses with CA so far, the reaction mixture has usually a brownish colour and is pale-yellow after dilution and purification.[268] I hypothesize that formic acid plays a pivotal catalytic role in the system, which results in subsequent oligomerization of CzA derivatives.

5.3. Experimental

Synthesis in autoclave: 3.78 g of ammonium formate is mixed with 5.76 g of citric acid to result in a molar ratio 2:1. The mixture is thoroughly grinded in an agar mortar to obtain homogeneous viscous paste. The viscous mixture is transferred into the Teflon beaker and sealed with the Teflon cap. The beaker is placed into a high-pressure stainless-steel reactor from Parr. The reactor is kept at 180 °C for 4 hours. The reaction is stopped by cooling the autoclave in an ice bath. The product is a viscous solution with the dark violet colour.

Microwave synthesis: Synthetic procedure is also performed in a laboratory microwave reactor, which allows for stirring during the reaction. The precursors are mixed in the same ratio (2:1 ammonium formate: citric acid), but the quantity is decreased by half to fit the smaller reactor volume. The reactants are transferred into a 35 ml quartz vial, sealed with a Teflon-lined cap. The vial is heated with a laboratory microwave (Discover SP), using a power of 50 Watt. The reaction is performed at 180 °C, but the reaction time is decreased to 40 min since stirring could be applied.

Purification procedure: The viscous liquid product is transferred to a plastic centrifuge tube and ethanol is added. The mixture is thoroughly shaken and subsequently sonicated for 15 minutes. The product is insoluble in ethanol and can be separated by centrifuging at 6000 RPM for 5 min. The washing procedure with ethanol is repeated several times, until no organic molecules are detected in the washing solution by NMR. The washed powder is dried in the oven at 60 °C overnight. For 1.5 g of CA, approximately 0.7g of purified product could be obtained (after microwave synthesis).

Preparation of NH_4-CzA: CzA is dissolved in a minimum amount of ammonium hydroxide solution and dried in the oven at 60 °C overnight.

Analytical methods are described in chapter S1 of the SI.

5.4. Results and Discussion

5.4.1. Synthesis in eutectic mixture

Ammonium formate and CA (2:1) form a eutectic mixture that is liquid at room temperature. According to DSC the mixture features at glass transition temperature at -37.1 °C and starts reacting at elevated temperatures (Figure S35). The REM can be prepared by dissolving the components in a minimal required amount of water, and subsequently freeze-drying the solution. The resulting mixture appears as a colorless transparent liquid with a high viscosity.

Considering, that formic acid and CA are acids both of similar strength we can assume that the ammonium cation is shared between both acids. If the temperature is high enough, the ammonium salt of CA can then form CzA. Indeed, at 120 °C a colour change of the reaction mixture into yellow is observed, which is in agreement with the reported preparation of CzA from CA and ammonia or urea at 120-130 °C.[269] At 150 °C, the mixture starts to get a purple hue while at 180 °C an intense purple colour is observed (Figure 1, left). This is a common synthesis

temperature for fluorophores from CA.[266] Furthermore, ammonium formate decomposes at 180 °C, so at this temperature a maximum concentration of ammonia can be expected. It is thus important to maintain isochoric conditions as the reaction does not work in an open vessel. Furthermore, the solvent-free approach appears to be essential for the synthesis –the same reaction in water results in a completely different reaction pathway, while the same reaction in ethylene glycol gives only traces of the relevant product, according to UV-vis (Figure S36).

Reaction kinetics, monitored over time by UV-vis absorption spectroscopy (Figure 29, right), show a similar trend. The band at 340 (associated with CzA) develops initially but decreases over time in favor of an increasing band intensities at 520 and 560 nm. This reflects the purple colour of the resulting compound, reaching its maximum after a reaction time of four hours. Prolonged heating reduces the brilliance of colour.

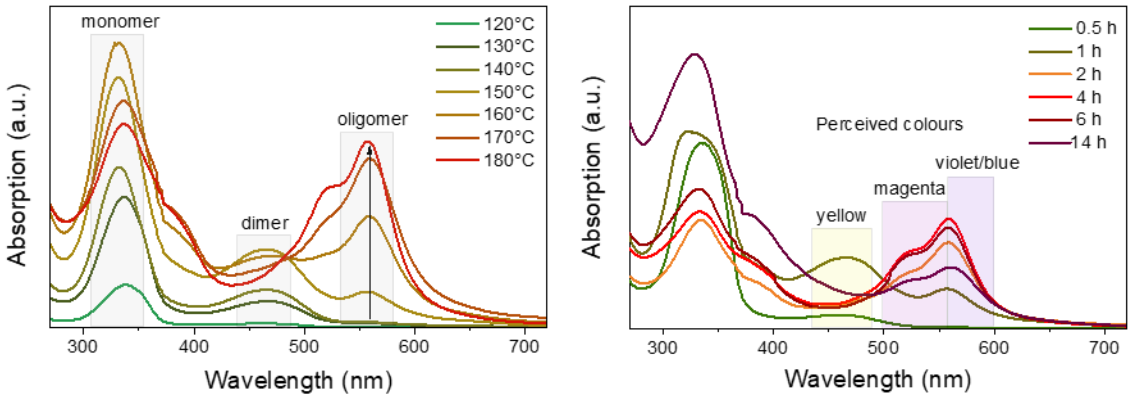

Figure 29: *UV-vis spectra of the reaction kinetics of the reactive eutectics in water. Left: prepared at different temperatures from 120 to 180 °C and reacted for 40 min in a microwave oven. Right: prepared with different reaction times at a temperature of 180 °C in an autoclaved system without stirring. The absorption maxima at ~340 nm corresponds to the spectra of CzA.*

Overall, the kinetic study shows that the reaction proceeds in at least two clearly distinguishable steps. The first one can be attributed to the formation of CzA (and derivatives), and the second one corresponds to the oligomerization of the formed monomer into oligomers of purple hue. Based on these observations, I propose the following reaction products, depicted in Figure 30, as a starting point for discussion. That products from CA are able to form such conjugated structures has long been known by the biosynthesis of indigoidine.[270,271] Furthermore, indigoidine derivatives have recently been identified as reaction products from CA and urea by including a photo oxidation step during the synthesis.[272]

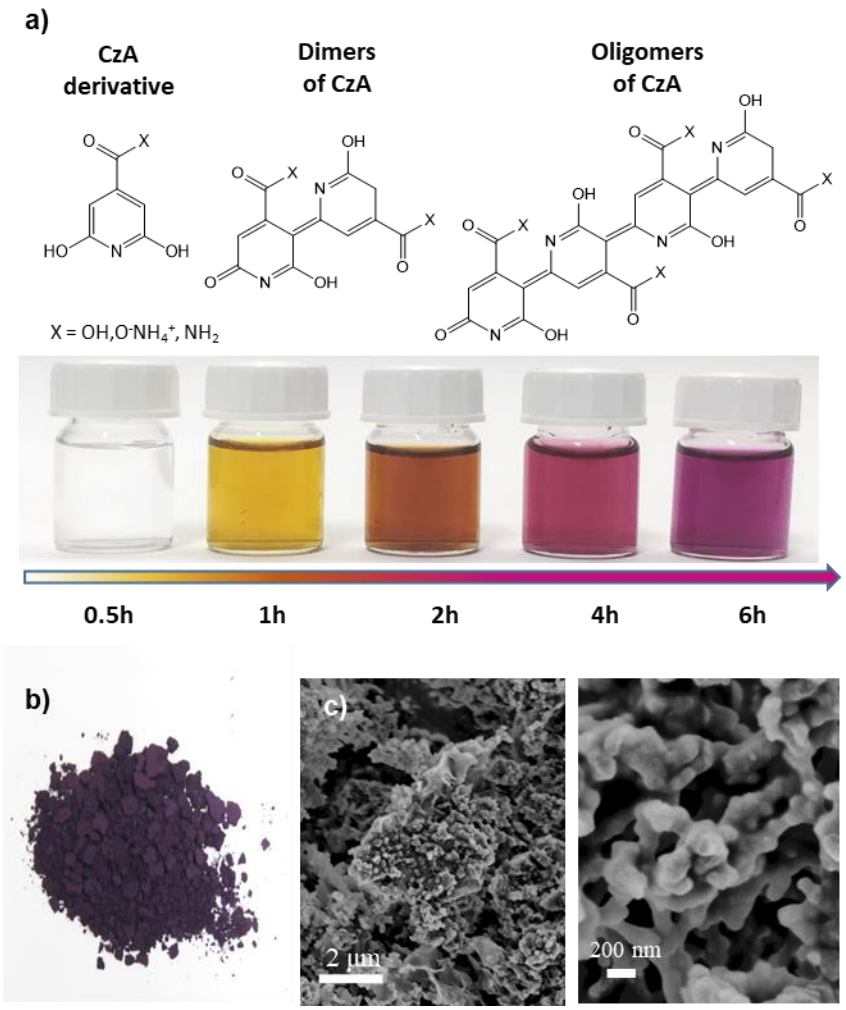

Figure 30: *(a) Schematic representation of the formation kinetics of CzA and polymerization in the reactive eutectic media at 180 °C supported by the colour change of the reaction mixture, (b) visual appearance of the purified product* ***oligo-CzA*** *in powder form, (c) SEM images of the purified product.*

5.4.2. Structural analysis of the fluorophores

In the following, the purple reaction product is investigated which is termed **oligo-CzA** in the further discussion. Maximum yields are obtained in an autoclaved synthesis at 180 °C for 4 h as shown by UV-vis analysis (or in 40 minutes in the microwave, which enables stirring). The reaction work-up can be easily achieved by repeated washing with ethanol. This precipitates the product and removes by-products such as formamide and formic acid as confirmed by NMR (Figure 31A). After drying, a purple powder of **oligo-CzA** is obtained (Figure 30B).

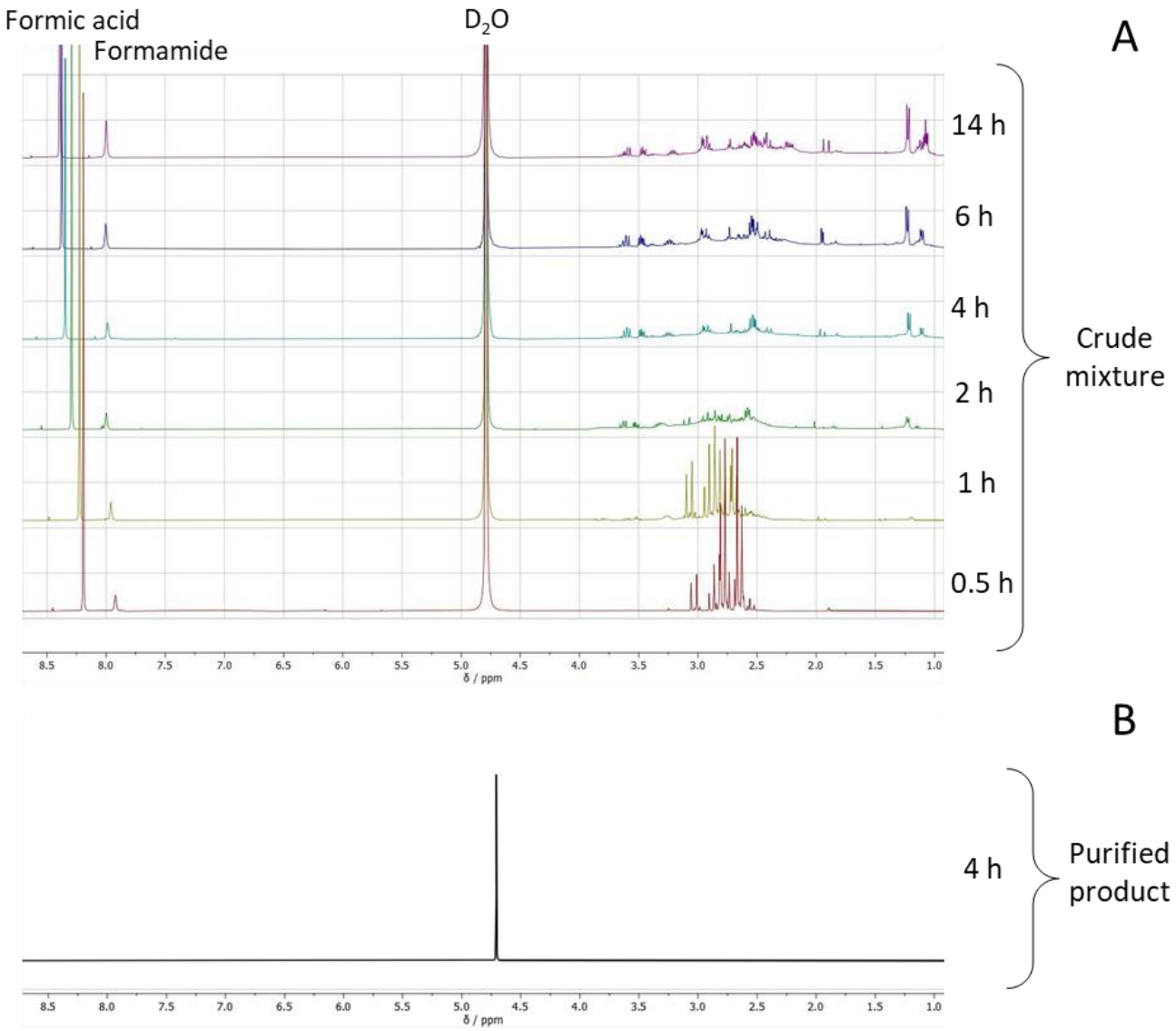

Figure 31: *^{1}H NMR spectra in D_2O of (A) the reaction mixture heat-treated at 180°C in an autoclave over different times and (B) heat-treated at 180°C for 4h and purified by washing with ethanol.*

In the further analysis of the product, I did not find any indication of CNDs. Gel-permeation chromatography (GPC) shows only small sized molecules below the smallest standard of 1250 Da. Moreover, scanning electron microscopy (SEM) and transition electron microscopy (TEM) measurements (Figure 31C and Figure S37) do not reveal any crystalline particles, instead show amorphous agglomerates. This is in agreement with the finding of Reckmeier et al.[268], who obtained similar TEM images for the reaction of CA and supercritical ammonia. They also attributed the observed particles to aggregated CzA derived fluorophores instead of CNDs.

NMR analysis of the product is not possible as the sample turns out to be completely NMR silent (**Figure 31**B). EPR measurements (Figure 34 left) reveal that this is due to the paramagnetic nature of the product. The number of unpaired electrons in **oligo-CzA** is calculated to be 1.6×10^{18} spins/g and increases slowly over time (Table S6). EPR measurements for variable

temperatures reveal that the signal increases linearly with temperature, which means that the behavior is Curie like (Figure 32, right). In order to determine the ground state spin multiplicities of the system, more analysis will be needed. It is not the first time that EPR active CNDs or fluorophores from citric acid have been reported.[273,274] Interestingly, the ammonium salt of CzA (**NH_4-CzA)** also gives a weak EPR signal (Figure 34, left). The concentration of unpaired electrons is significantly lower at 5.1×10^{16} spins/g. Both samples have very similar g-factors: 2.0036 for **oligo-CzA** and 2.0038 for **NH_4-CzA** (Figure S38). This indicates a similar chemical environment of the free radical in the two samples. Considering this result from a broader perspective, it may have important implications. If such open-shell structures also form in other syntheses with CA in the realm of CNDs, a portion of molecules may have been systematically overlooked in NMR analysis.

Regarding the cause of the observed radical stability I can only speculate here, but it must ultimately be traced back to the delocalization of spin density in the molecular structure.[275] This is known e.g. to be possible by extension of π-conjugates[276] (which is in fact featured by the proposed structure of **oligo-CzA**) but also possible by non-covalent mechanisms such as electrostatic interactions[277] or π–π interaction and molecular aggregates[278]. Also such non-covalent mechanisms seem worth to consider, taking into account that molecular aggregation of CzA has been identified as a crucial factor for understanding its fluorescent properties.[267]

For a better understanding of the observed radical stability, more analysis will be needed. E.g. it would be very interesting to perform magnetic susceptibility measurements in order to determine the ground state spin multiplicities of the system. In order to suppress paramagnetic properties, it is also attempted to reduce **oligo-CzA** with sodium sulphite or to oxidize it with sodium hypochlorite– however the NMR remain silent in both cases. While reduction does not do anything to the colour, oxidation leads to a change in colour from purple to orange to yellow to colorless. This is exactly the reversal of the formation kinetics, observed during synthesis.

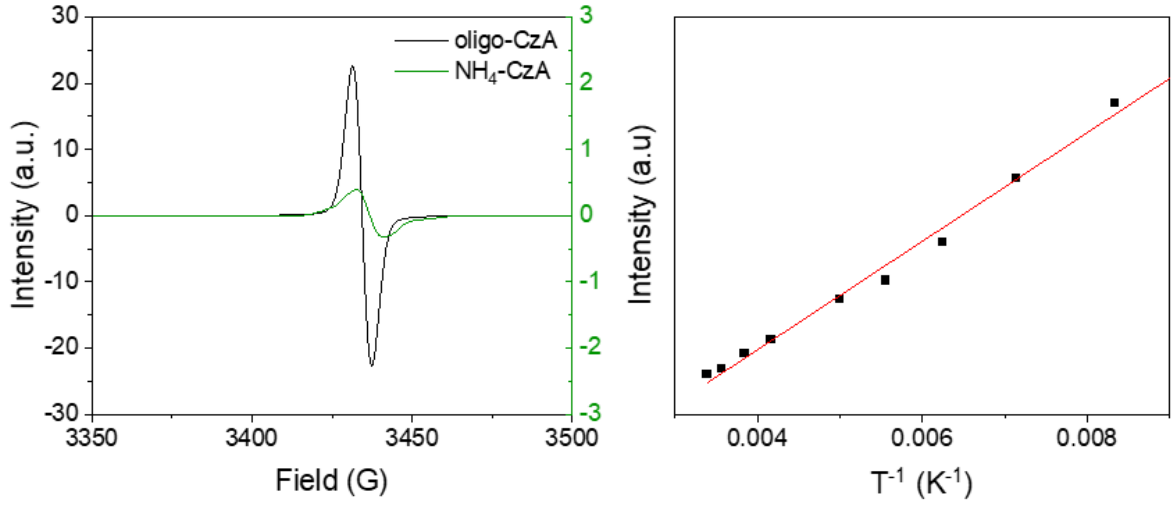

Figure 32: *(left) EPR measurement of 20 mg of* ***oligo-CzA*** *and* ***NH_4-CzA****, (right) variable temperature EPR of* ***oligo-CzA****.*

The product is structurally investigated by X-ray photoelectron spectroscopy (XPS) in reference to **NH_4-CzA**, since similarities between the structures are presumed. The tautomeric forms of both structures are presented in Figure 33 to make it easier to follow the discussion.

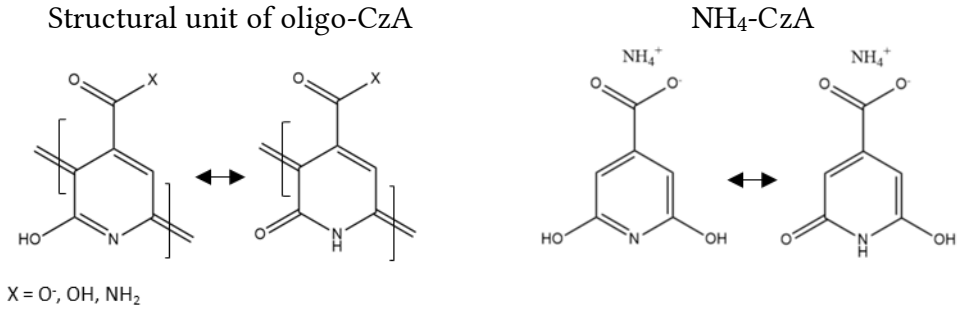

Figure 33: *Tautomeric structures.*

The XPS C_{1s} spectra show four species of carbons within the compounds. For **oligo-CzA** they appear at 284.8, ~286, ~287.5 and ~288.5 eV and are assigned to carbon-carbon (C-C/C=C), hydroxy and carbon-nitrogen (C-O/C-N), carbonyl as well as lactam (C=O) and carboxy groups (O-C=O), respectively. For **NH_4-CzA** a significantly higher signal at 287.8 eV is observed in comparison to the oligomer suggesting that the lactam form is favored over the pyridinic tautomer. This assumption is supported by the N_{1s} XPS spectrum presenting an intense signal at 400.6 eV which is characteristic for pyrrolic nitrogen and which is also in accordance with previous observations.[279] The N_{1s} spectrum of **oligo-CzA** shows a signal at 399.9 eV which indicates a mixture of pyridinic N which range between 399.0-399.6 eV as well as pyrrolic N at ~ 400.2 eV. This means that both tautomeric forms are present. Furthermore, the signals between 401.9-402.0 eV in both N_{1s} spectra prove the presence of ammonium ions. Due to the measurement under high vacuum, the amount of ammonia groups was possibly reduced to some extent for both compounds. Nevertheless, the small signal for **oligo-CzA** may also hint to the formation of primary amides from ammonium carboxylates which can be expected under such high synthesis temperatures. Primary amides occur at ~399.7 eV and are therefore be part of the major signal at 399.9 eV. The O_{1s} spectra show two species at 531.7 and 533.2-533.4 eV which correspond with carbonyl as well as lactam groups (C=O/NH-C=O) and carboxyl as well as hydroxyl groups (O-C=O/C-OH), respectively. For **oligo-CzA** the reduction in intensity of the carboxyl/hydroxyl group signals at 533.2 eV is in accordance with the proposed structure and a decrease in hydroxyl groups as well as amide formation.

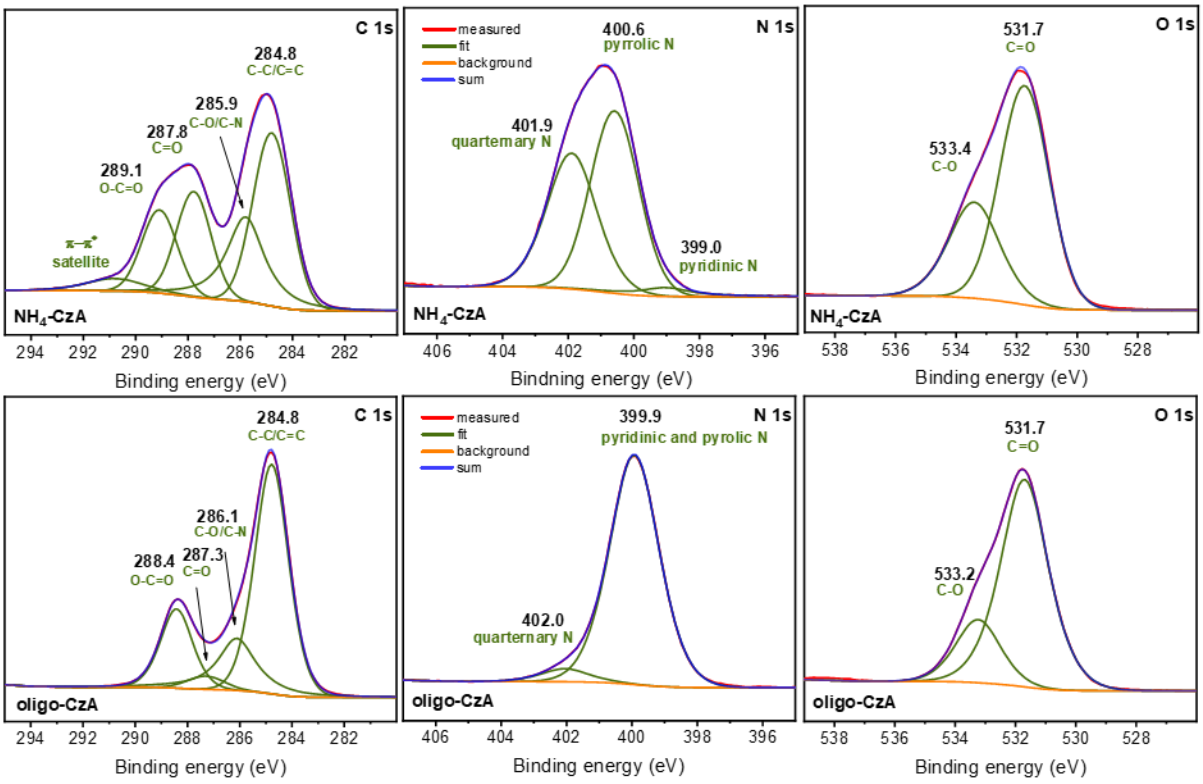

Figure 34: *XPS spectra of* ***NH₄-CzA*** *(top) and purified* ***oligo-CzA*** *(bottom) with emphasis on the* C_{1s}*,* N_{1s}*, and* O_{1s} *regions.*

Similarities between **NH₄-CzA** and **oligo-CzA** are also observed with Fourier-transform infrared spectroscopy (FTIR), as shown in Figure 35. What can clearly be distinguished in the **oligo-CzA** spectra are different C=O stretching vibrations. The peak at 1570 cm^{-1} corresponds with the peak of **NH₄-CzA** and is therefore assigned to the asymmetric stretch of the carboxylate group. The signal at 1690 cm^{-1} is assigned to the C=O stretching from carboxylic acid. Presumably, there were not sufficient ammonium ions present in order to ionize all carboxylic acid groups. This is supported by performing the synthesis of **oligo-CzA** with an excess of AF (4:1 ratio). In this case the signal at 1690 cm^{-1} from carboxylic acid disappears in favor of a stronger band from carboxylate stretching vibrations (Figure S39).

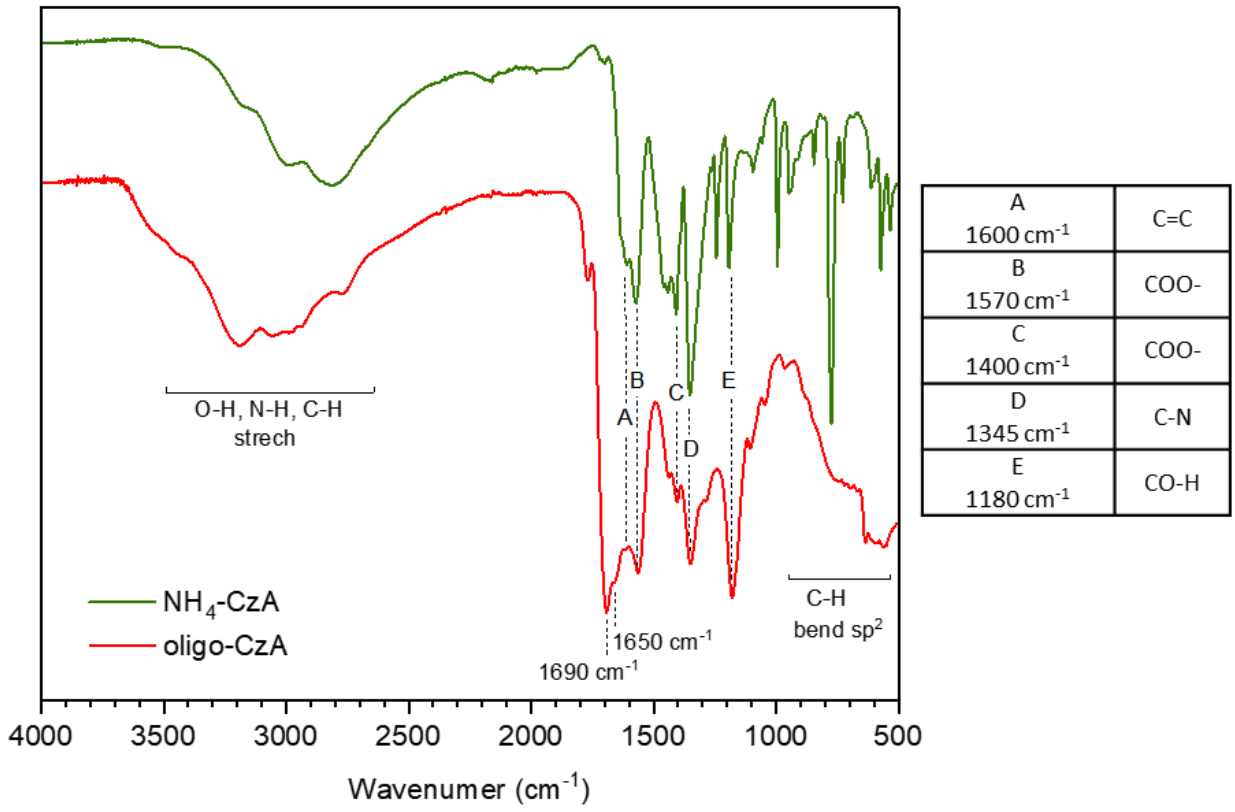

Figure 35: *FTIR of* ***NH₄-CzA*** *and* ***oligo-CzA.***

The same can be achieved, when **oligo-CzA** is treated with an alkali salt such as potassium or sodium hydroxide. This does not only result in salt formation of carboxylic acids but also in the cation exchange of ammonium ions as wells as hydrolysis of primary amides. In this way all derivatives of carboxylic acid groups are converted to the carboxylate salt of the respective alkali metal and the elemental analysis of these materials gives insightful results. While untreated **oligo-CzA** gives a nitrogen/carbon ratio of 1.6/6, the ratio of the alkali treated compound approaches 1:6, while the ratio between nitrogen and counter cation approaches 1:1 (Table 7). That means that each pyridine unit is connected to one carboxylate group, which reflects the structure of **NH₄-CzA**. This is in agreement with the proposed structure for **oligo-CzA** of polymerized CzA derivatives into oligomers.

Table 7: *Elemental analysis of* ***oligo-CzA*** *as well as for* ***alkali salt treated oligo-CzA****. The results are normalized to six carbon atoms, which corresponds to one unit of CzA.*

	CHNX analysis			**ICP analysis**		**-**
(per unit CzA)	**N**	**C**	**H**	**K**	**Na**	**O**
K-oligo-CzA	1.01	6.00	7.19	0.92	-	3.59
Na- oligo-CzA	1.04	6.00	7.35	-	1.06	3.69
oligo-CzA	1.60	6.00	7.56	-	-	3.14
oligo-CzA, prepared with excess AF	1.94	6.00	7.24			2.90

For information on the molecular mass, MALDI-TOF (matrix-assisted laser desorption-ionization - time of flight) mass spectrometry experiments were performed. Although mostly used for large molecules such as synthetic polymers and proteins, this technique is also suitable for small molecular analytes. Soltzberg et al. successfully used MALDI-TOF mass spectrometry for the identification of a range of anionic dye molecules.[280] The applied matrix 9-aminoacridin (9AA) appears to be a good choice for such analytes; it allows for measurements in negative ion mode and only exhibits a low background. Measured species in MALDI-TOF mass spectrometry are virtually always singly charged. Multiply charged species therefore most often lose all of their counter ions but they will be compensated by protons from the MALDI plume to result in a singly charged ion (e.g. $[M - NH_4]^-$, $[M - 2\ NH_4 + H]^-$, $[M - 3\ NH_4 + 2H]^-$, etc.).

Figure 36 shows the results of **oligo-CzA** sample. The measurements are reproducible but for older samples, the spectra feature peaks with lower molecular weight. The results suggest that the product consists of several molecular species, which are decomposing over time. This is supported by preparative HPLC (Figure S40) where three different hues of purple are separated from the fresh dye sample. An older sample, that has been stored for a few weeks, gives a wider palette of colors and at least six different fractions are identified.

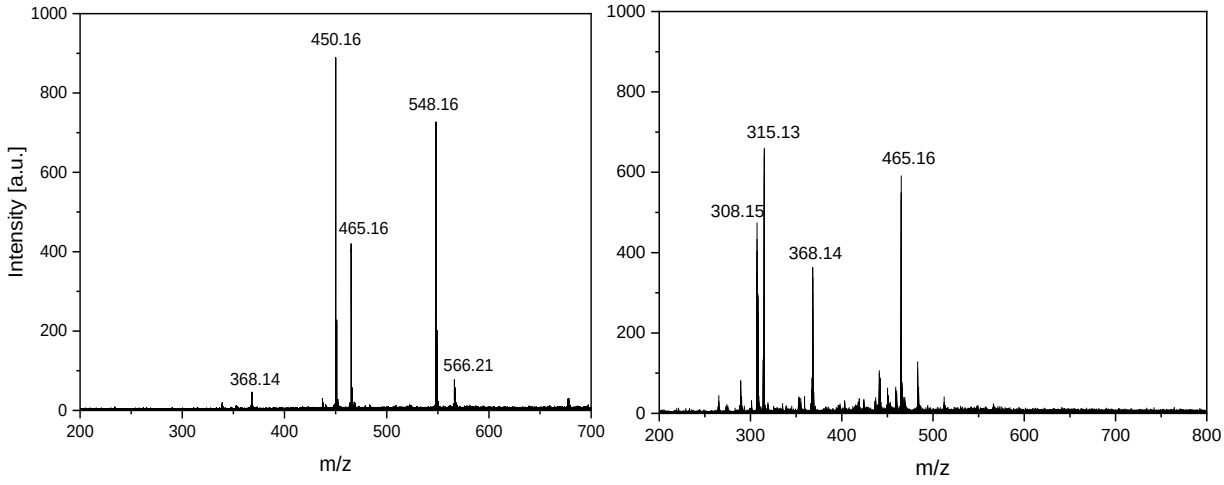

Figure 36: *MALDI-TOF mass spectrometry measurements of oligo-CzA, freshly prepared (left) and after a few weeks, stored as powder (right). The measurement took place in negative ion mode and by using 9AA as a matrix. The laser intensity was 40%.*

Taking the results from MALDI-TOF and the structural analysis into consideration, we can make a few suggestions on the molecular structure. For examples the major peak at 548.16 m/z in the fresh sample corresponds closely the original structure suggested (**Figure 37**, left). However, we do not know on which position the individual CzA units are connected, so the structure might

also resemble the right proposal in Figure 37. This would also account for the radical character of the product in form of a non-Kekulé structure. However, it should be stressed, that more work will be required to advance on this subject and the nature of the stable free radical. For example, in the present investigation we did not resolve weather we are dealing with a monoradical or diradicals.

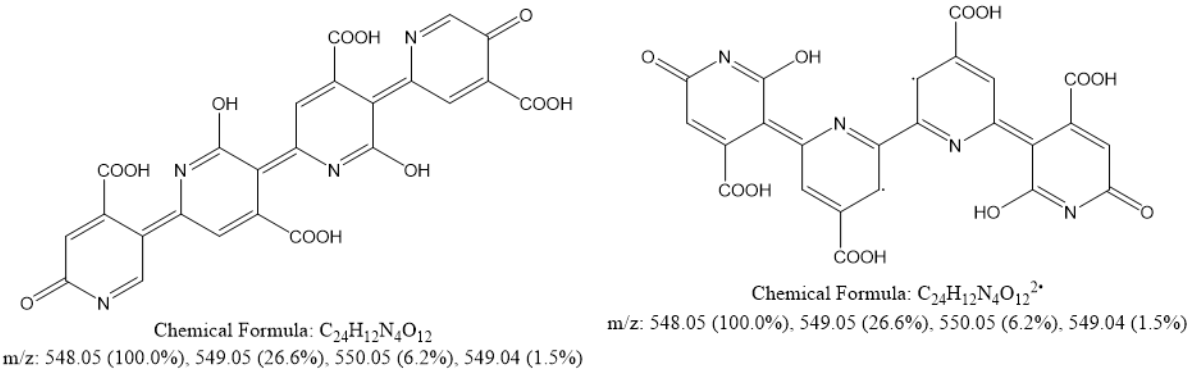

Figure 37: *Proposals for the structure of the major component of oligo-CzA.*

5.4.3. Spectral properties

The purified product features high solubility in water and results in a solution with an intense purple colour, which is even stronger in ammonia solution. However, the colour of the solution fades over time - a process which is even faster in ammonia solution as well as under light illumination (**Figure 38**a). We presume that the highly substituted structure of **oligo-CzA** has little stability in solution due to steric hindrance within the molecules. What can also be observed in water solution, is precipitation of a purple powder. I attribute this to molecular aggregation, which is a phenomenon that is well known in dye chemistry.[281,282] This is supported by XRD measurements of the precipitate, which gives the typical signal from π-stacking at 26 °2Θ (Figure S42) as well as by the broadening of absorption band in the UV-vis spectra. Precipitation is not observed in ammonia solution. As a result, no material is retained by a dialysis tube (molecular weight cut-off 1000 Da) in case **oligo-CzA** is dissolved in ammonia solution. However, dialysis of **oligo-CzA** in water results in an initial yellow dialysate. The solution shows a single absorption peak at 340 nm which correlates to the absorption peak of CzA (Figure S43).

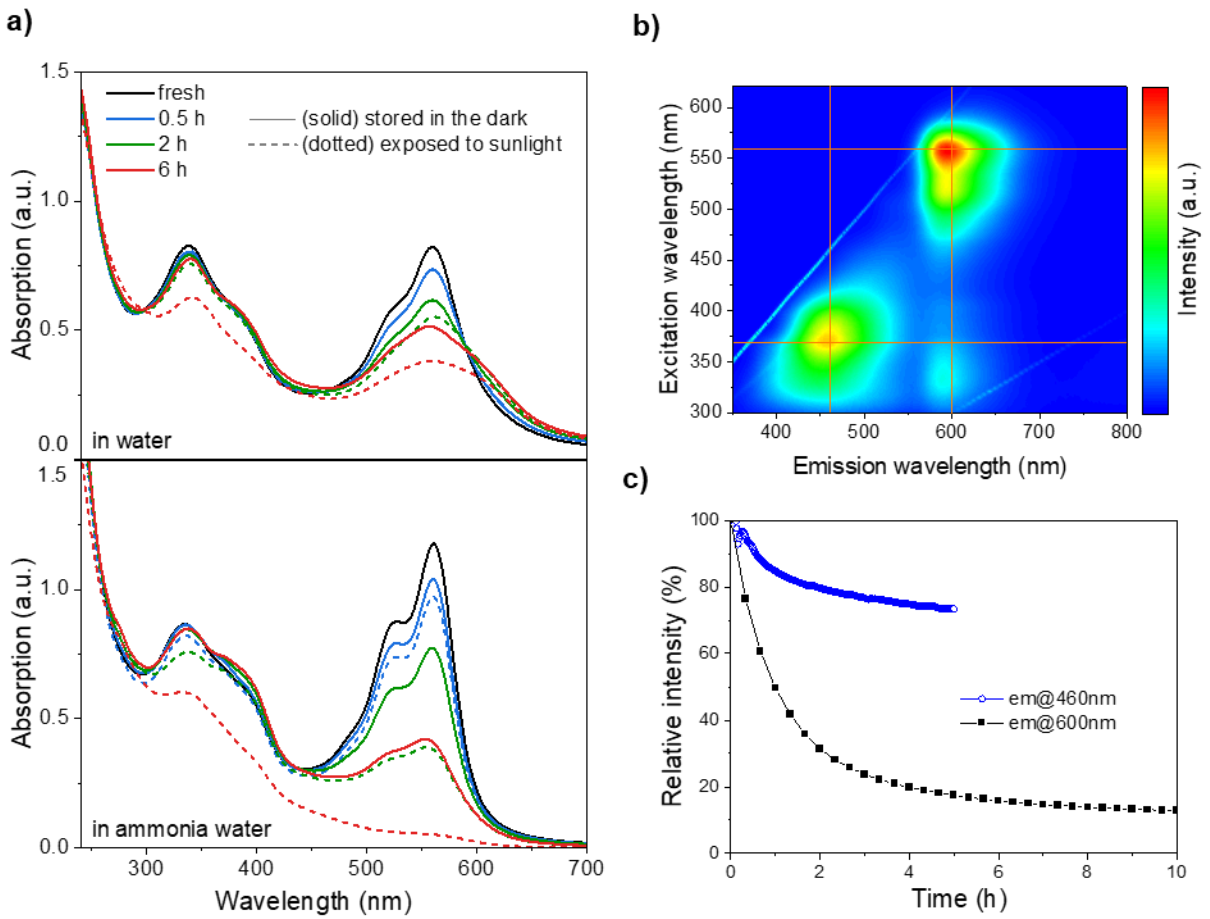

Figure 38: *a) Absorption spectra of* ***oligo-CzA*** *in water as well as in ammonia water (5%). The solutions were freshly prepared (black) and then stored under dark (solid) as well as light exposed (dotted) conditions; b) 2D-photoluminescence plot of* ***oligo-CzA*** *in ammonia water; c) Fluorescence intensity decay of* ***oligo-CzA*** *in ammonia water at 460 nm (blue) and at 600 nm (black) under continuous illumination at 370 or 560 nm respectively.*

The fluorescent properties of the product in solution are shown in **Figure 38**b. There are two fluorescent centers so we assume to be dealing with two main species. The two emission maxima appear at 462 and 594 nm corresponding to excitation maxima at 370 or 558 nm, respectively. The rather large Stokes shifts of 92 and 36 nm, respectively, are related to the highly polar solvation environment (Figure S44). Notably, the fluorescence intensity decays rapidly after the product is dissolved. For example, upon continuous emission measurement at the excitation wavelength of 520 nm, a significant decay down to ~15% after 10 h is measured (**Figure 38**c). A decay takes place irrespective whether or not the solution was exposed to light. However, the respective emission curves differ slightly (Figure S45), which again points towards the contribution of photodegradation. The decrease of the molecular species that emits at 460 nm is less pronounced. The fluorescence quantum yields (QY_{fl}) of **oligo-CzA** were determined by the gradient method using Rhodamine B (RhB) as a reference. In ammonia in water solutions the fluorescence quantum yields are only 1.9% while in ammonia in methanol the QY_{fl} is ten times higher, namely 19% (Figure S46).

5.5. Conclusion and outlook

In this chapter, the isochoric synthesis in a REM between ammonium formate and citric acid was investigated. Reaction kinetics were analyzed with UV-vis spectroscopy and optimized with respect to the purple colored reaction product. This product was not observed when any solvent was used during the reaction so that the reaction appeared to rely on the pure REM.

Structural similarities between the purified product and the ammonium salt of citrazinic acid were detected with several analysis techniques such as XPS, FTIR, and elemental analysis. With EPR spectroscopy unpaired electrons were detected in the structure as well as in the ammonium salt of citrazinic acid. It was therefore not possible to conduct a conclusive structural analysis with NMR. However, the results give rise to the hypothesis that such paramagnetic properties may be a prevalent property in fluorophores based on citrazinic acid and that certain structures may have been systematically overlooked by relying on NMR analysis.

By use of other analysis techniques, I hypothesized that the product consists of oligomerized structures of citrazinic acid derivatives. Further analysis (such as magnetic susceptibility measurements) will be needed in order to understand these paramagnetic properties and to gain confidence with respect to the exact molecular structure of the product. This may also contribute to a better understanding of the formation of fluorophores and CNDs from citric acid in general. For the future, it would be most interesting to check on the paramagnetic properties of previously reported fluorophores from citric acid.

CHAPTER 6
Overall conclusions

In this thesis, REM based on ammonium formate were investigated in a number of different reactions, highlighting the versatility of ammonium formate as reactant as well as the utility of REM.

The reaction in REM featured some expected benefits of solvent-free reactions such as a high reaction mass efficiency, higher yields and faster rates compared to the reaction in solution. This was evident in CHAPTER 2 and 3 for the synthesis of DOF derivatives and 5MP respectively. Furthermore, REM proofed useful for process intensification, as shown in CHAPTER 4, where REM could be successfully employed for biomass treatment as well as the for the synthesis of value-added products from REM. Finally, CHAPTER 5 investigated the synthesis of a newly discovered reaction product, based on oligomerized citrazinic acid derivatives and showed that REM can even offer distinct reaction pathways that are closed under solvent conditions.

One factor, that was investigated, was the inclusion of water as a third component in the REM. As shown in CHAPTER 2 and 3, this proofed to be greatly beneficial for decreasing the viscosity of the media. Furthermore, it showed to be beneficial for the reaction yield due to different reasons. In the Maillard reaction in CHAPTER 2, this was presumably due to the reduced viscosity, which was affecting the reaction rate by limiting mass transport of reactants. In the Leuckart reaction in CHAPTER 3, water presumably shifted the chemical equilibrium in favor for the reaction. However, both studies showed that the precise control of water content was necessary, as further increase in water content resulted in lower yields, due to a considerable reduction of reaction rates. The concept of two different dilution regimes (tertiary REM and in solvent) appeared useful for investigation of this phenomenon.

Another factor that was investigated was the influence of microwave heating on reactions in REM. In CHAPTER 2, it could be shown that the heating of REM was highly beneficial in terms of energy efficiency, as no heating energy had to be used to heat additional solvent. Furthermore, a beneficial influence of microwave heating compared to conventional heating was detected due to the direct energy transfer to the reaction mixture. However, a meaningful (although minor) impact on reaction rate was only observed in CHAPTER 2, which featured a reaction with relatively short reaction times. The Leuckart reaction in CHAPTER 3 relied on relatively long reaction times that were comparable to the ones reported for similar reactions with conventional heating. In this case, no influence of the heating method was detected. Nevertheless, the use of the microwave oven proved very useful in the laboratory context because it monitored the pressure built up during the reaction and because it could be employed for relatively small amounts of sample (the smallest reactor has a volume of 10 ml).

Finally, a number of analysis techniques were used and developed, that proofed useful for the analysis of REM. They comprise DSC, the investigation of the heating profiles in microwave synthesis as well as the analysis of proton shifts in NMR by keeping the REM physically separated from the NMR solvent. Furthermore, care has to be taken in the preparation of REM

since heating (which is often used for DES preparation) has to be carefully employed due to the reactivity of the media. It is therefore beneficial to employ freeze-drying during the REM preparation due to reduced reactivity.

Supplementary information

S1. Analysis techniques

CHNS analysis

CHNS analysis is one type of elemental analysis that is used for determination of mass fractions of carbon, hydrogen, nitrogen, and sulfur. The technique relies on the combustion of the sample at elevated temperatures (>1000°C), and the use of gas-specific adsorption columns that are used to catch and concentrate CO_2, SO_2 and H_2O. N_2 is fed directly to the detector. The amount of the different gases is then determined by measuring thermal conductivity.

CHNS analysis was used in CHAPTER 4 for analysis of lignin samples as well as in CHAPTER 5 to study the separated reaction product. The analysis was performed with a vario MICRO cube CHNOS elemental analyzer by Elementar Analysensysteme GmbH.

Differential scanning calorimetry (DSC)

DSC can be used to study physical transformation of a sample with respect to temperature. Most importantly, it is used to observe phase transitions such as melting, crystallization or glass transitions but can also be used to observe oxidation stability or other chemical reactions. The technique relies on measuring the amount of heat that is necessary to increase the sample temperature in comparison to a reference material with a well-defined heat capacity. In this way, exothermic or endothermic processes within the sample can be detected and are used to draw conclusions on the type of physical transformation.

DSC measurements were employed in CHAPTER 2 and 3 for analysis of REM with varying water content. In CHAPTER 5, it was used to analyze the REM after varying reaction temperatures. For DSC measurements, samples were prepared shortly before the measurement in order to keep chemical reactions to a minimum. DSC was performed on a DSC 204 F1 Phoenix (Netzsch, Selb, Germany) using a platinum crucible at a heating rate of 10° C min^{-1}. The mixtures were cooled to -150°C and then heated to 50 °C with a heating/cooling rate of 10 °C min^{-1}. Three cycles of heating and cooling were conducted.

Electron paramagnetic resonance (EPR) spectroscopy

EPR spectroscopy can be used to study unpaired electrons in a sample. It relies on the electron's magnetic moment, which aligns itself either antiparallel or parallel to an applied magnetic field. Each alignment has a specific energy (according to its spin quantum number and thereby its magnetic moment) and the difference in energy between these two states (is directly proportional to the strength of the applied magnetic field (known as the Zeeman effect). This means that free electrons can change their magnetic moment by absorbing or emitting a photon of energy resonance condition, obeyed. This leads us to the fundamental equation of EPR spectroscopy:

$$h\nu = g\mu_B B_0 \quad (S1)$$

where g is the electrons g-factor, μ_B is the Bohr magneton and B_0 is the strength of the applied exteral magnetic field.

In EPR spectroscopy, the sample is typically exposed to microwaves of a fixed frequency (so is kept costant) the strength of the external magnetic field (B_0) is changed. When the discussed resonance conditions are obeyed, the unpaired electrons can move between their two spin states, also known as an EPR transition. Therefore, at appropriate B_0 a net absorption of energy is observed (since more electrons are usually is their lower energy state according to the Maxwell–Boltzmann distribution). This absorption of energy is monitored and converted into a spectrum along B_0. EPR spectra are usually reported with the first derivative of the absorption spectrum since this is the signal that is directly measured by field modulation. The position and shape of the EPR signal contain a number of information about the chemical environment of the unpaired electrons:

- Firstly, the g-factor of the unpaired electron denotes the position in the magnetic field where an EPR transition takes place. The g-factor is sensitive to the electronic structure of the molecule (by so-called spin-orbit coupling) and will therefore differ from the g-factor of the free electron. This is particularly relevant for metal-based radicals where the change in g-factor is significant. For organic radicals the g-factor is typically very close to the g-factor of the free electron of 2.0023. Furthermore, for crystal EPR, the g-factor will consist of three space coordinates due to anisotropic effects. However, in solution EPR such effects are typically averaged out.
- Secondly, the intensity of absorption by the sample is directly proportional to the relative numbers of unpaired electrons. Double integration of the obtained spectrum can therefore be used to estimate radical concentration by prior calibration with a known standard.
- As already mentioned, the unpaired electron is affected by so-called spin-orbit coupling which means that its spin will couple with nearby nuclear spins (a phenomenon analogous to J-coupling in NMR). The result is so-called hyperfine coupling, which results in the splitting of the EPR signal into doublets, triplets etc. This hyperfine structure is particularly useful for analysis of the chemical environment of the radical.
- For systems with multiple unpaired electrons, also electron–electron interactions will have an effect and will feature in the so-called fine structure of the spectra (meaning its effect can be relatively large in magnitude compared to hyperfine coupling)

It is helpful to understand EPR spectroscopy by knowing that the basic concepts are analogous to those of nuclear magnetic resonance (NMR), but the excited spins are those of the electrons instead of the atomic nuclei. Because of the mass difference between electrons and nuclei, the magnetic moment of an electron is substantially larger so that a much higher electromagnetic frequency is needed to observe spin resonance.

In CHAPTER 5, EPR spectroscopy was used to study unpaired electrons in the separated reaction product as well as in the ammonium salt of citrazinic acid. EPR spectroscopy was performed on

a Bruker EMXnano benchtop X-Band EPR spectrometer, where the samples where measured as powder in EPR tubes (ID 3 mm, OD 4 mm, length 250 mm). Samples were measured using a receiver gain of 40 dB an attenuation of 35 dB and 5 number of scans. Cooling during EPR measurements was conducted with liquid nitrogen.

Falling ball viscometer

The falling ball viscometer is one way of measuring the viscosity of a fluid sample. It is based on the steady state settling velocity of a sphere of known diameter and density within the fluid.

In CHAPTER 2 and 3 the falling ball viscometer was used to determine REM viscosity for changing water content. The measurements took place at at 25°C and were evaluated with an Automated Microviscometer (AMVn, Anton Paar, Graz), a capillary with a diameter of 1.6mm at 70° angle and repeated runs.

Fluorescence spectroscopy

Fluorescence spectroscopy is used to analyze the fluorescence from a sample. It relies on a beam of light that is directed towards the sample (at the excitation wavelength), which excites the electrons in the sample and causes them to emit light (at the emission wavelength).

In CHAPTER 5, fluorescence measurements were performed on the separated reaction product. For this purpose, sample were dissolved in ammonia water and transferred into 10 mm quartz cuvettes. Measurements were performed on a FP-8300 fluorescence spectrometer.

Fourier-transform infrared spectroscopy (FTIR)

FTIR relies on the interaction of matter with electromagnetic radiation in the infrared region. It relies on the fact that molecules absorb frequencies that are characteristic to their structure. These absorptions translate into vibrational modes of the molecule, where each molecular bond absorbs at characteristic resonance frequencies. Functional groups can therefore be associated with characteristic bands both in terms of frequency and intensity. FTIR is thus useful for structural analysis and identification of compounds.

FTIR was used in CHAPTER 4 for analysis of lignin samples and in CHAPTER 5 for characterization of the purified reaction product. FTIR measurements were performed using a Nicolet iS 5 FT-IR-spectrometer in conjunction with an iD5 ATR unit from Thermo Fisher Scientific.

Gas chromatography – mass spectrometry (GC-MS)

GC-MS enables the analysis of compound mixtures by separation via gas chromatography (GC) and consequent identification with a mass spectrometer (MS). The later relies on the ionization and fragmentation of the compound in order to obtain a characteristic fragmentation pattern. The most common form for ionization is electron ionization, where molecules are bombarded

with free electrons in order to fragment in a characteristic and reproducible way. This is also known as "hard ionization", contrary to “soft ionization” where charge is created by molecular collision with an introduced gas. The result of hard ionization is the creation of more fragments of low mass-to-charge ratio (m/z) and few to none molecules that approach the actual molecular weight. However, since the applied electron energy is standardized to 70 eV it is possible to identify compounds by their characteristic fragmentation pattern by comparing them to library spectra of already known compounds. One limit of GC-MS is that compounds must be volatilized in order to enter the system. Molecular weights are therefore limited, roughly to about 1000 Dalton (but often lower, depending on volatility)

GC-MS was used in CHAPTER 4 for identification of REM reaction product. Measurements were performed, using the Agilent GC 6890 gas chromatograph, equipped with an HP-5MS column (inner diameter=0.25 mm, length=30 m, and film=0.25 μm) and coupled with the Agilent MSD 5975 mass spectrometer (electron ionization). The MS method has been set with a run time of 15 min, injection volumes of 1.0 μL, and He as carrier gas with a flow of 1 mL min^{-1}. The injection has been set in Split mode with a split ratio of 10 while the inlet has been kept at 553 K to evaporate the injection. The temperature program for the column oven has been set as following: start at 323 K and maintaining for 1 min, then increasing to 573 K with a heating rate of 10 K min^{-1} and maintaining at 573 K for 6 min. The MS detector has been set to scan between 50 and 300 m/z with a gain factor of 1.1. The solvent delay has been set at 2 min, while the MS detector and the quadrupole has been kept at 503 K and 423 K, respectively. The mass spectra of the compounds were analyzed integrating the peak area using the Agilent MassHunter Qualitative Analysisi 10.0 software from and comparing with the NIST 17 mass spectral database.

Gel permeation chromatography (GPC)

GPC separates macromolecules based on their size or more precisely based on their hydrodynamic volume. It relies on a chromatography column that is filled with porous beads, where common materials include e.g. agarose, dextran or polyacrylamide polymers. Samples are dissolved in an eluent, where water but also organic solvents are commonly used (for water-based systems the technique is more accurately known as gel filtration chromatography (GFC)). The separation of molecules relies on the differently sized pores of the stationary phase. As the eluent flows through the column, larger molecules cannot enter into as many pores and will therefore elute first. By contrast, the smaller the molecule, the longer its retention time. Modern GPC columns, typically contain a mixture of pores so that they separate rather linear with the hydrodynamic volume of analytes. One important requirement for this separation is that the analyte molecules do not interact with the stationary phase (e.g. by electrostatic or chemical interactions) but are solely separated on their size. The eluting analytes are then detected, typically with an RI- and UV-detector. If a suitable calibration is performed, the respective data (detector signal vs. elution volume) can be converted into the molar mass distribution of the analyte. Such calibration is performed by measuring the elution time of several polymer standards with known molecular weight and low dispersity. However, for this it is important to choose standards that closely resemble the analyte as the shape of the molecule and its hydrodynamic volume will have a large impact on the elution time.

In CHAPTER 4, GPC was used for analysis of derivatized cellulose as well as for lignin samples. For derivatization of cellulose, the method of Evans et al[283] was applied. For this purpose, 25 mg of oven-dried cellulose was mixed with 10 ml of DMSO and 1 ml of phenyl isocyanate. The vials with the mixture were placed into the oil bath and heated at 70°C under stirring during 48 h. After cooling of the mixture, 2 ml of methanol was added to eliminate the unreacted phenyl isocyanate. The excess of methanol was removed via rotary evaporator. After removal of undissolved cellulose fragments with 0.45 mkm syringe filter, GPC measurements were performed in NMP/LiBr (0.05 mol/L) at 70 °C on a GRAM-100/1000-7μ column (PSS Polymer Standards Service GmbH, Mainz, Germany). RI and UV signals were collected using PSS SECcurity-RI-1260 and PSS SECcurity-UV-1260 detectors were the RI signal was used for further data analysis. The molecular weight was evaluated against a pullulan standard.

For measurement of lignin samples, 1 mg/ml of lignin was dissolved in NMP/LiBr (0.05 mol/L) and stirred for three days. The sample was then measured on the same GCP set-up as described for cellulose samples, but using a polystyrene standard and further analysis by using the UV-vis signal.

In CHAPTER 5, GPC was used to investigate the molecular weight of the separated reaction product. Analysis was carried out in $H_2O/NaNO_3$ on a SUPREMA 30/3000-10 μm column. The sample was detected with a RI- as well as a UV-detector at 350 nm. The molecular weight was evaluated against a poly(acrylic acid sodium salt) standard. The measurement was performed for freshly dissolved samples (in order to avoid degradation) as well as for samples that were stirred for one day.

High performance liquid chromatography - mass spectrometry (HPLC-MS)

HPLC-MS enables the analysis of compound mixtures by separation via high performance liquid chromatography (HPLC) and consequent identification with a mass spectrometer (MS). The crux in developing HPLC-MS was the interface between both techniques, as MS typically operates under high vacuum and does not allow for the direct injection of pressurized liquid. Today's systems therefore only feed a small portion of the mobile phase into the MS and then rely on various, specifically developed ionization techniques. One of the most popular ones is electrospray ionization (ESI) in which a high voltage is applied to a liquid in order to create an aerosol. This results in small and highly charged liquid droplets, where solvent from the droplets progressively evaporates, ultimately resulting in ions with various charge states. Due to the soft-ionization process there is very little fragmentation (as opposed to typical GC-MS) and the techniques is suitable for macromolecules. Furthermore, the detected ions may be multiply charged, making this technique different from other soft-ionization processes such as MALDI.

In CHAPTER 2, HPLC-MS was used for product identification. It was performed on a separation column (Thermo Scientific Accucore C18, 2.6 μm, 100 × 3) with a flow rate of 0.5 mL min^{-1} and a mobile phase consisting of 0.1% formic acid in water (A) and 0.1% formic acid in methanol (B). The gradient program was as follows: 95% A (0–5 min), 95–0% A (15–40 min), 0% A (40–50 min)

and 0-95% A (50-60 min). UV-vis was used at a wavelength of 280 nm. The components were detected using an LTQ Orbitrap XL (Thermo Scientific) linear ion trap quadrupole mass spectrometer equipped with an Ion Max electrospray ionization (ESI) source (Thermo Fisher Scientific).

Inductively Coupled Plasma Optical Emission spectroscopy (ICP-OES)

ICP-OES can be used for the detection and quantification of chemical elements. It relies on the fact that atoms and ions can be excited in order to move electrons from a lower to higher energy level. In ICP-OES, the source of energy is an argon plasma that operates at high temperatures up to 10 000 Kelvin. Upon relaxation of the electrons back to their ground state, energy is emitted in the form of photons at characteristic wavelengths. The identification of elements thus relies on their unique emission spectra. The intensity of emissions can then be used for quantitative measurements after calibration with known concentrations of the respective element.

ICP-OEC was used in CHAPTER 5 for quantification of sodium and potassium in the cation-exchanged reaction product. Analysis was performed on an ICP-OES Optima 8000.

Klason lignin analysis

The Klason method is the most commonly-used method for quantitative analysis of lignin in lignocellulosic material. It is a gravimetric method to measure insoluble material (predominantly lignin) after hydrolysis with 72% H_2SO_4. It is typically coupled with UV-vis spectroscopy for the determination of acid dissolved lignin.

In CHAPTER 4 the remaining lignin content within the generated cellulose pulp was quantified using NREL analytical procedure.[284] Due to analysis of previously pretreated cellulose samples the steps of extractives removal was skipped. The procedure of acid hydrolysis of the cellulosic residuals was as follows: 300 mg of oven-dried sample was placed into the pressure tube and 3 ml of 72% sulfuric acid was added. The mixture was stirred with a Teflon stir rod and placed into the ultrasound bath set at 30 °C. During the 60-minute hydrolysis, the mixture was stirred every 5 – 10 min. The tube was removed from the ultrasound bath and 84 ml of deionized water was added. The tube was placed into the oven and incubated for one hour at 121 °C. After slow cooling at room temperature the undissolved Klason lignin fraction was separated via vacuum filtration using 0.45 mkm nylon filter membrane. Few milliliters of filtrate were collected for acid soluble lignin quantification. After that, the lignin fraction was washed with distilled water and dried in the oven at 80 °C overnight. The percentage of residual lignin in the cellulose fraction was calculated based on the mass of dried Klason lignin obtained after hydrolysis and the mass of started material. The aliquot of previously collected filtrate was analyzed for acid soluble lignin using UV spectrophotometry. The UV absorbance intensity at 320 nm was recorded and the percentage of acid soluble lignin was calculated on the base of the Lambert–Beer law using an attenuation coefficient of 30 $l \cdot g^{-1} \cdot cm^{-1}$.

Matrix assisted laser desorption ionization - time of flight (MALDI-TOF) mass spectrometry

MALDI-TOF mass spectrometry relies on a laser energy-absorbing matrix for the ionization of analyte molecules. For this purpose, samples are mixed with a chosen matrix material (typically in solution but solvent-free grinding is also possible) and applied onto a metal plate. The spotted sample is then irradiated with a pulsed laser, which will ultimately lead to a hot plume of ablated gases where the analyte molecules are ionized by protonation or deprotonation. The generated ions are then separate based on their mass-to-charge ratio via TOF mass spectrometry, which is determined by accelerating them in an electric field and measuring their time of flight. This technique is superior with respect to the accurate mass and high resolution compared to standard ion traps or quadrupoles and particularly compatible with MALDI due to the pulsed measurement. MALDI-TOF mass spectrometry produces relatively little fragmentation, which means that there is usually a pronounced molecular ion peak of $[M - H]^-$ or $[M + H]^+$. Furthermore, ions are typically single charged, distinguishing this technique from other soft-ionization techniques such as ESI-MS. The analysis technique is particularly popular for macromolecules such as biopolymers, which tend to fragment with other ionization techniques. However, it is also possible to measure molecules with low molecular weights. What is crucial for the detection of analyte molecules is the choice of a compatible matrix material.

MALDI-TOF mass spectrometry was performed in CHAPTER 5 for analysis of the purified reaction product. For this purpose, 9-aminoacridin (9AA) was used as a matrix and was dissolved in methanol for the preparation of a saturated solution. A drop of this solution was mixed with the dissolved sample material and spotted onto a metal plate. After the solvent had evaporated, the spot was irradiated with a nitrogen laser operating at 337 nm and the analyte molecules were detected with an Autoflex speed detector from Bruker in negative mode. Each spectra was the average of at least five laser shots. Prior to these measurements, the spectra were calibrated using the $[M - H]^-$ peaks from picric acid and erythrosin B as external standards and the matrix 9AA was measured without sample for determination of the background peaks.

Ninhydrin test

Ninhydrin is an organic compound that can be used for identification of ammonia and primary or secondary amines. Upon reaction with such amines, ninhydrin forms a dye that is typically purple in colour and that is known as Ruhemanns's purple.

In CHAPTER 4, the ninhydrin test was used for detection of amine groups in lignin. For this, a few milliliters of pyridine were mixed with a few drops of 80 wt% of phenol in ethanol and a few drops of 5 v/v% of ninhydrin in ethanol. The dried lignin sample was added and the mixture was boiled for few minutes. The solution was cooled to room temperature and the colour of the lignin samples were compared.

Nuclear-magnetic resonance (NMR) spectroscopy

NMR spectroscopy is the preeminent technique for determining the chemical structure of organic compounds. The technique relies on the magnetic moment of the atomic nucleus and can therefore be applied for atomic nuclei with non-zero spin, such as ^{1}H, ^{13}C, ^{19}F and ^{31}P. It is thereby analogous to EPR spectroscopy (which relies on the magnetic moment of the electron) so that the underlying theory will not be repeated here. What is additionally useful in NMR, is that it can be performed as a two-dimensional technique (2D-NMR). In this way it can be used e.g. to investigate nuclei that correlate through chemical bonds or through space and it can also be used to investigate heteronuclear correlation.

In CHAPTER 2, NMR spectroscopy was used for analysis of the crude mixture by ^{1}H and DEPT 135 (Distortionless Enhancement by Polarization Transfer) ^{13}C NMR. Furthermore, it was used for characterization of the purified DOF derivatives by ^{1}H NMR, APT (Attached Proton Test) ^{13}C, H^{1} COSY (Correlated Spectroscopy), HSQC (Heteronuclear Single Quantum Coherence) and HMBC (Heteronuclear Multiple Bond Correlation) NMR using DMSO-d_6 as NMR solvent. Furthermore, quantitative ^{1}H NMR was applied to calculate the substrate conversion and yields of DOF derivatives using pyrazine as an internal standard. For this, pyrazine was added to the NMR solvent in the range of 1.5 g/ml. The amount of product was calculated, based on the following equation:

$$m(x) = m(std) \cdot \frac{mw(x)}{mw(std)} \cdot \frac{nH(std)}{nH(x)} \cdot \frac{A(x)}{A(std)} \qquad (S2)$$

Where m(x) and m(std) are the weights in g, mw(x) and mw(std) are the molecular weights in g/mol, A(x) and A(std) are the integration areas of the selected peaks of the product and the internal standard.

DOF content was quantified based on its aromatic proton peaks, shown below for the example of DOF products from fructose. Fructose and fucose were measured in D_2O, glucose and rhamnose in DMSO- d_6 to avoid overlap between the pyrazine and product peaks. In the case of water as a third component of the reaction mixture, the method was applied in exactly the same way. There reactions were performed under isochoric conditions but according to the microwave monitoring, there was no sign of pressure build-up. Thus, the weight of the reaction mixture remained constant before and after synthesis.

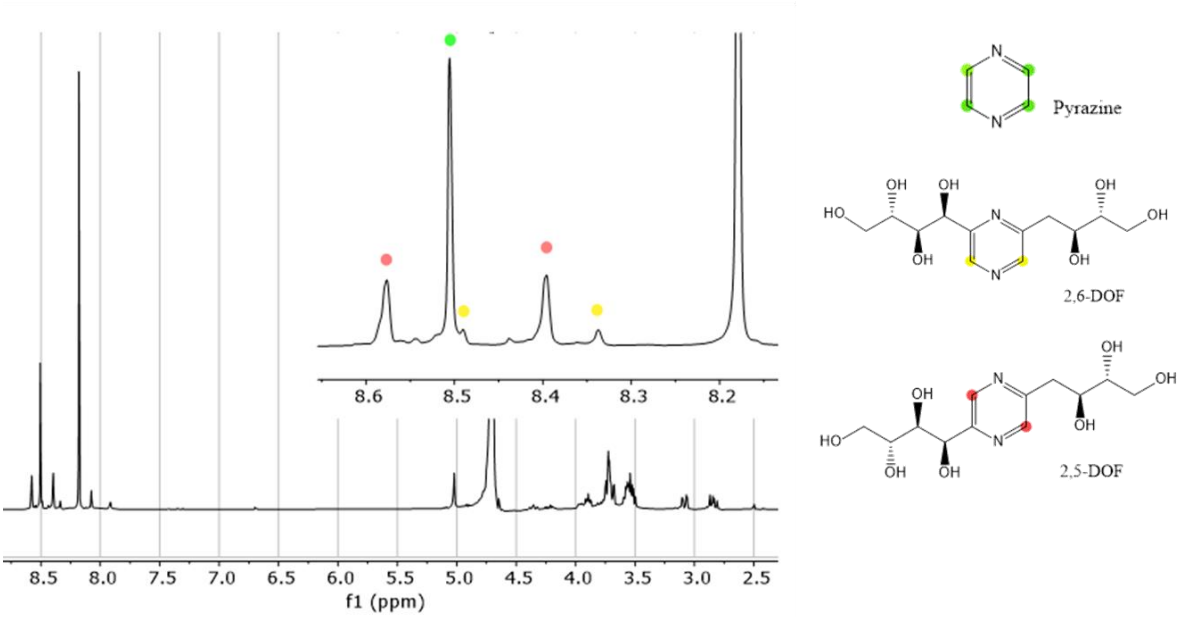

Figure S1: Proton assignment for quantitative ^1H NMR

Lastly, in CHAPTER 2 ^1H NMR was used for analysis of hydrogen bonding in REM by keeping the media physically separated from the NMR solvent. For this purpose, the REM was filled into a sealed capillary, which was then transferred to the NMR tube, filled with DMSO-d_6. Instead of normal water, D_2O was used for REM preparation, in order to avoid a large water peak.

In CHAPTER 3, ^1H NMR was used for product characterization of the crude mixture. Furthermore, it was used for quantitative analysis to calculate the substrate conversion and yields according to equation S2. For this purpose, DMSO was used as an internal standard and D_2O as NMR solvent. For yield calculations, the peak at (CH, 3.7 ppm) of 5MP was integrated, conversion was calculated based on the peak area of (CH_2, 2.7 ppm) of levulinic acid. Since, the reaction involved a substantial pressure build-up due to CO_2 formation, the mass loss of the reaction mixture was taken into account. Lastly, ^1H NMR was used for analysis of hydrogen bonding in REM by keeping the media physically separated from the NMR solvent (in this case DMSO-d_6), just as described for the previous chapter.

In CHAPTER 4, ^1H NMR was used for quantitative analysis of REM reaction products, using DMSO as an internal standard. Furthermore, NMR spectroscopy was used for structural analysis of lignin. For this purpose, around 80 mg of sample was dissolved in 450 µl of DMSO-d_6. The vial was immersed in an ultrasound bath for 30 minutes and solution was transferred to a NMR tube. For HSQC NMR measurements the *hsqcedetgpsisp* method was applied, using 32 number of scans and fixing the F1 axis to 220 ppm.

In CHAPTER 5, ^1H NMR in D_2O was used for analysis of the crude mixtures as well as for measurement of the separated reaction product.

All measurements were performed on an Agilent 400 MHz (at 400 MHz for Protons and 101 MHz for Carbon-13).

Powder X-ray diffraction (PXRD) to obtain the crystallinity index of cellulose

PXRD is based on the constructive interference of monochromatic X-rays and a crystalline sample that acts as a three-dimensional diffraction grating. While single crystal XRD relies on a single, well-ordered crystal structure and is especially useful for solving crystal structures, PXRD can be performed on powder or microcrystalline samples. It thereby finds wide applications in material characterization, most importantly to determine crystallinity or perform phase identification.

The crystallinity index (CI) of cellulose is described as the relative amount of crystalline regions in the material, according to the traditional two-phase model of cellulose. This model describes cellulose chains as containing both crystalline (ordered) and amorphous (less ordered) regions. The CI of cellulose is typically determined by solid-state ^{13}C NMR or PXRD. The most popular method, which will also be used here, is the peak height analysis of PXRD data. The CI is calculated from the height of the 002 peak (I_{002}) and the height of the minimum (I_{am}) between the 002 and the 101 peak, according to the following equation:

$$CI = \frac{I_{002} - I_{am}}{I_{002}} \qquad (S3)$$

The peak height analysis of PXRD data allows for rapid comparison of cellulose samples. However, since the relative height can only be taken as a rough approximation of the contribution of amorphous cellulose to the cellulose diffraction spectrum it is best be used for comparison of relative difference between sample. For determination of more accurate CI values it is better to rely on more laborious methods such as peak deconvolution of PXRD data or by taking an amorphous standard into account.

PXRD with peak height analysis was used in CHAPTER 4 for measuring the crystallinity of cellulose samples. Measurements were performed on a Bruker D8 Advance diffractometer at the Cu Kα wavelength. Cellulose samples were grinded and pressed flat onto the sample holder. Scans were obtained from 10 to 40 degrees 2θ in 0.1 degree steps for 15 seconds per step. Peak height were measured after subtraction of the background signal that was measured without cellulose.

Scanning electron microscopy (SEM)

SEM describes an electron microscope that can magnify a sample by scanning it with a focused beam of electrons in a raster scan pattern. Such electrons interact with the atoms of the sample and a part of their energy is converted into various alternative forms of energy. The most common imaging mode in SEM is the collection of so-called secondary electrons that are ejected by inelastic scattering from valence or conduction bands of atoms in the sample. Another mode is the collection of backscattered electrons, which are beam electrons that are reflected by the sample due to elastic scattering interactions. Irrelevant of detection mode, SEM generally creates images by mapping the intensity of collected signal for each spot of the raster patter. The

technique is surface sensitive and therefore useful for investigating topology with a high depth of focus.

SEM was used in CHAPTER 5 to study the separated reaction product. SEM images were obtained on a LEO 1550-Gemini microscope at an accelerating voltage of 3.00 kV.

Transmission electron microscopy (TEM)

The most important difference between TEM and SEM is that TEM creates images by detecting transmitted electrons that pass through the sample (as opposed to reflected or knocked-off electrons in SEM). As a result, sample preparation for TEM is more demanding because samples need to be very thin (typically below 100 nm). However, for materials that are small enough to be electron transparent (such as fibers or powders) it is sufficient to deposit a diluted solution or suspension onto a support grid. As opposed to SEM, TEM can offer more information on the inner structure of the sample, such as crystal structure and morphology. Furthermore, its spatial resolution is typically higher, whereas its maximum field of view is much lower. That means that TEM can usually only image a smaller part of the sample in the same amount of time.

TEM was used in CHAPTER 4 to study the fiber dimensions of the cellulose pulp. For this purpose, cellulose fibers were stained prior to analysis with uranyl acetate. TEM was also used in CHAPTER 5 to study the separated reaction product. The measurements were performed using an EM 912 Omega from Zeiss operating at 120 kV.

Ultraviolet-visible (UV-vis) spectroscopy

UV-vis spectroscopy is used to investigate the interactions of a sample with electromagnetic radiation in the ultraviolet and visible region. The resulting absorbance spectra can potentially provide information on the molecular structure of the sample as well as on its concentration.

UV-vis measurements were performed in CHAPTER 5 for analysis of the crude reaction mixtures as well as for the separated reaction product. Measurements were performed in solution with a Specord 210 plus from Analytik Jena using 10 mm quartz cuvettes.

X-ray photoelectron spectroscopy (XPS)

XPS relies on the photoelectric effect for investigating energy levels of atomic core electrons in solid samples. This enables the identification of the present elements and gives information on their chemical state. XPS is one type of photoemission spectroscopy that distinguishes itself by the use of X-rays as the radiation source. Such a beam of X-rays is directed towards a sample under ultra-high vacuum conditions, which allows the detection of ejected electrons from the material. XPS is a surface sensitive technique, since only electrons that have escaped the sample will be detected. Such electrons are measured with respect to their kinetic energies and quantities, making it possible to draw conclusions on their binding energies. XPS spectra plot the number of detected electrons vs. their binding energy. Every element produces a set of characteristic peaks, which correspond to the electron configuration within the atom. This can

be used for the determination of elemental composition. Furthermore, the binding energy of an atom will be influenced by its local bonding environment. That means that so-called chemical shifts from the nominal binding energy (analogous to the use in NMR) can be used to provide information on the chemical state of the atom. However, since such peaks often overlap, the process of peak fitting during data analysis is crucial for determination of chemical states.

In CHAPTER 5 XPS was performed for the analysis of the separated reaction product. For the measurement, the prepared powder samples were loaded on carbon taps. Measurements were performed on a K-Alpha™ + X-ray Photoelectron Spectrometer System Thermo Scientific) with Hemispheric 180 ° dual-focus analyzer with 128-channel detector. X-ray monochromator was Micro-focused Al-Kα radiation.

Zeta potential measurement

The zeta potential describes the electrical potential that arises between different phases in a colloidal dispersion and is thereby an indicator of the colloidal stability. Its exact location is defined by the theory on the interfacial double layer and is known under the name of the slipping plane. This name arises because it describes the layer that separates mobile fluid from fluid that remains attached to the surface of the dispersed particle. The measurement of zeta potential is based on electrophoresis, which describes the motion of dispersed particles under the influence of a uniform electric field. Particles will migrate toward the electrode of opposite charge to their zeta potential and will do so with a velocity that is proportional to the magnitude of their zeta potential. The velocity is measured, using the phase shift of a laser beam that is passed through the solution by exploiting the laser Doppler effect. By application of the Smoluchowski theory, the zeta potential can be generated from the measurement data.

Zeta potential measurements were performed in CHAPTER 4 for analysis of cellulose fibers. Samples were directly taken after biomass fractionation, so the fibers never dried out. Measurements were carried out on a Zetasizer Nano ZS, Malvern Instruments (Malvern Panalytical, United Kingdom) in an aqueous colloidal solution.

S2. The reaction with monosaccharides for the synthesis of Maillard reaction products

S2.1. Educts in molar ratio as well as in weight percent

Table S1: Each sample is prepared with a constant amount of ammonium formate and fructose, with a molar ratio of 1.5:1. Water is added in changing amounts as shown below.

Ammonium formate [g]	Fructose [g]	Water [g]	Molar ratio of water	Wt% water
0.47	0.90	0.00	**:0**	0.0
0.47	0.90	0.09	**:1**	6.2
0.47	0.90	0.27	**:3**	16.4
0.47	0.90	0.45	**:5**	24.7
0.47	0.90	0.63	**:7**	31.5
0.47	0.90	0.90	**:10**	39.6
0.47	0.90	1.80	**:20**	56.7
0.47	0.90	4.50	**:50**	76.6
0.47	0.90	9.01	**:100**	86.8

Table S2:: For comparison, educts for the synthesis of DOF from previous papers, which are discussed in the introduction.

Reference	***Reactants***			***Molar ratio***	***Wt% water***
Wu[184]	*Ammonium formate [g]*	*Fructose [g]*	*Water [g]*		
	0.39	*0.1*	*2*	***10:1:179***	*95.2*
Shanxi Institute[185]	*Ammonium chloride [g]*	*Fructose [g]*	*Water [g]*		

	15	*5*	*500*	***10:1:1000***	*96.2*
		Glucosamine	*Ionic liquid*		
Jia[186]		*[g]*	*[g]*		
		0.2	*2*	***1:100***	*90.9*

S2.2. Procedure of high throuput screening

Antimicrobial susceptibility tests are performed via the antiBiotic Mode of Action Profile (BioMAP) assay.[285,286] BioMAP utilizes high-throughput screening methodology in order to screen the effect of compounds on a panel of 19 pathogenic bacterial strains, including both Gram negative and Gram positive strains (Table S3).

The assay was performed according to Clinical & Laboratory Standards (CLSI) protocols, and as per Hawkins et al. with the following exceptions: during compound incubation cation-adjusted Muller Hinton Broth (CAMHB; Millipore-Sigma) was used as the growth media for 12 bacterial strains, a 1:1 mixture of CAMHB and brain heart infusion (BHI; Millipore Sigma); (CAMHB:BHI) was used as the growth media for 3 strains, and 4 strains were grown in appropriate complete media (Table S3).

Briefly, each bacterial strain was inoculated in 3 mL of sterile media, as in Hawkins et al. (2022), and grown overnight with shaking (200 rpm) at 37°C, with the exception of Streptococcus pneumonia, which was placed in a 5% CO_2 incubator set to 37°C, overnight, without shaking. Saturated overnight cultures were diluted in the appropriate media (Table S3) to achieve approximately 5 x 10^5 CFU of final inoculum density and dispensed via a Matrix dispenser into sterile clear polystyrene 384-well assay microplates (Greiner 781186, Sigma-Aldrich) with a final screening volume of 30 µL. Solutions of test compounds and antibiotic controls were prepared as a 1:1 dilution series in 384-well storage microplates (NUNC 264573, Thermo Fisher Scientific). Two hundred nanoliters of the compound, or antibiotic control, was pinned into each assay plate using a Tecan Freedom EVO 100 equipped with a 384 well pintool. Post-pinning test compounds had a final concentration ranging from 40 to 4 mM per compound, while antibiotic controls had a final concentration ranging from 128 µM to 3.91 nM per compound.

In each 384-well plate, controls were placed in lanes 1, 2, 23 and 24. For the controls, lane 1 contained vehicle (DMSO) and culture medium only; lane 2 contained vehicle (DMSO), culture medium and target bacteria; and lanes 23 and 24 contained vehicle (DMSO), culture medium, target bacteria and antibiotic controls. Ciprofloxacin and gentamicin were used as controls for Gram negative bacteria, while azithromycin and vancomycin were used as controls for Gram positive bacteria.

After pinning and dispensing, absorbance values were obtained at OD600 for timepoint T_0 using an automated plate reader (Synergy Neo2, BioTek). Plates were then sealed with a lid and placed in a 37°C incubator. S. pneumoniae was incubated in a separate incubator (37°C; 5% CO2). After an incubation period of 18-20 hours absorbance measurements were obtained for timepoint T_{20}.

MIC90 values were calculated using GRAPHPAD PRISM (version 8). Percent growth (PG) was calculated via the following equation:

$$PG = [(TreatT_{20} - TreatT_0)/(Cpos - Cneg)] \times 100 \quad (S4)$$

Where, Treat represents absorbance values at T_0 and T_{20}; Cneg and Cpos are the averaged absorbance values of the controls in Lane 1 (DMSO + culture media) and lane 2 (DMSO + culture media + bacteria), respectively. Percent inhibition was calculated as 100 − PG.

Table S3: Tested microbial strains, alongside their strain designation and employed growth media.

Strain Name	Strain Designation	Growth Media
Gram-Positive		
Bacillus subtilis	ATCC 6051	CAMHB
Enterococcus faecalis	ATCC 29212	CAMHB:BHI
Enterococcus faecium	ATCC 6569	CAMHB:BHI
Listeria ivanovii	BAA-139	TSB
Staphylococcus aureus (Methicillin-Resistant)	BAA-44	CAMHB
Staphylococcus aureus (Methicillin-Sensitive)	ATCC 29213	CAMHB
Staphylococcus epidermidis	ATCC 14990	TSB
Streptococcus pneumoniae	ATCC 49619	CAMHB:BHI
Gram-Negative		
Acinetobacter baumanii	ATCC 19606	CAMHB
Escherichia coli	K-12 MG1655	CAMHB
Klebsiella aerogenes	ATCC 35029	CAMHB
Klebsiella pneumoniae	ATCC 700603	CAMHB
Ochrobactrum anthropi	ATCC 49687	TSB
Providencia alcalifaciens	ATCC 9886	CAMHB
Pseudomonas aeruginosa	ATCC 27853	CAMHB
Salmonella enterica	ATCC 13311	CAMHB
Shigella sonnei	ATCC 25931	CAMHB
Vibrio cholera	A1552 El Tor	CAMHB
Yersinia pseudotuberculosis	ATCC 6904	BHI

S2.3. Characterization of products

Major products are depicted below. The respective isomers (2,5 vs. 2,6) are also detected in smaller amounts. I did not aim to identify the byproducts of the Maillard reaction. The typical products are recognizable by the dark brown color as well as by the pleasant smell of the crude samples.

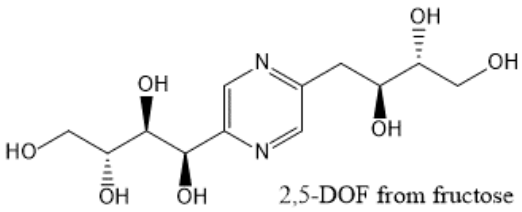

2,5-DOF from fructose

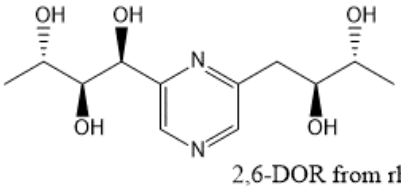

2,6-DOR from rhamnose

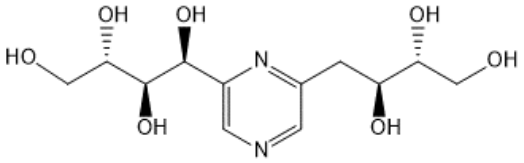

2,6-DOF from glucose

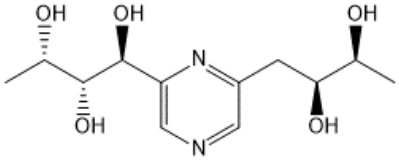

2,6-DOFu from fucose

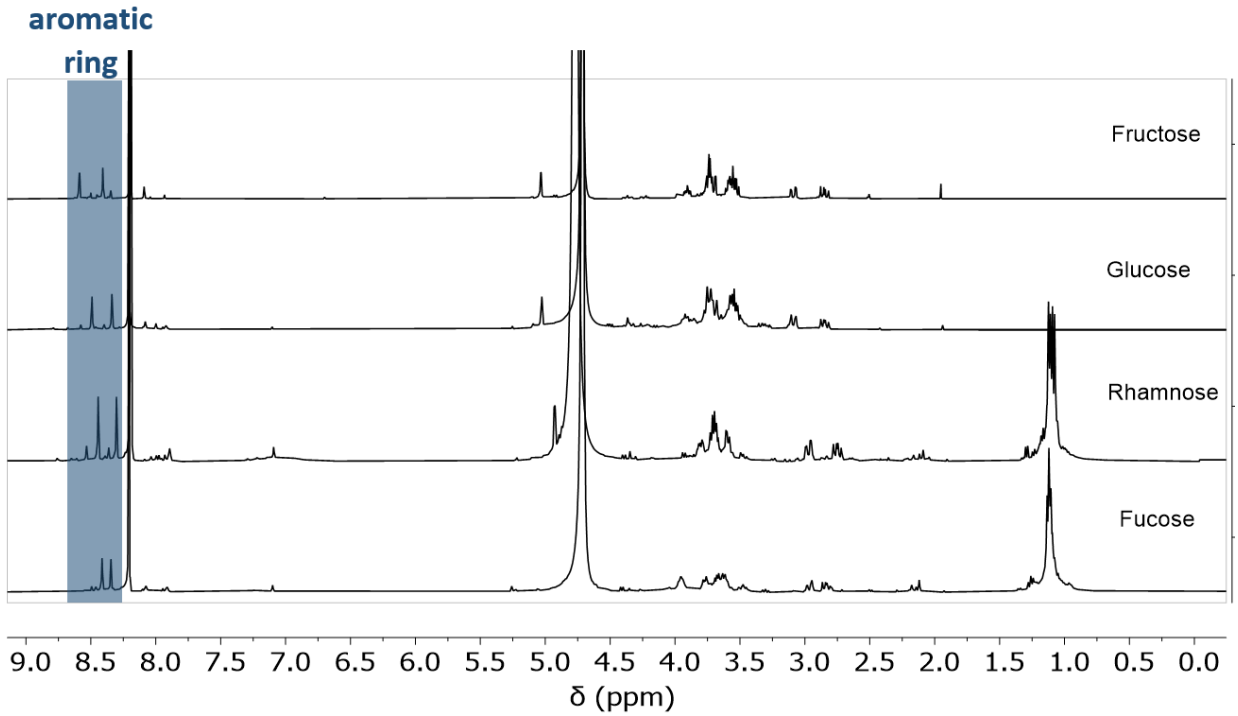

Figure S2: [1]H-NMR in D2O of the crude reaction mixture from different monosaccharides.

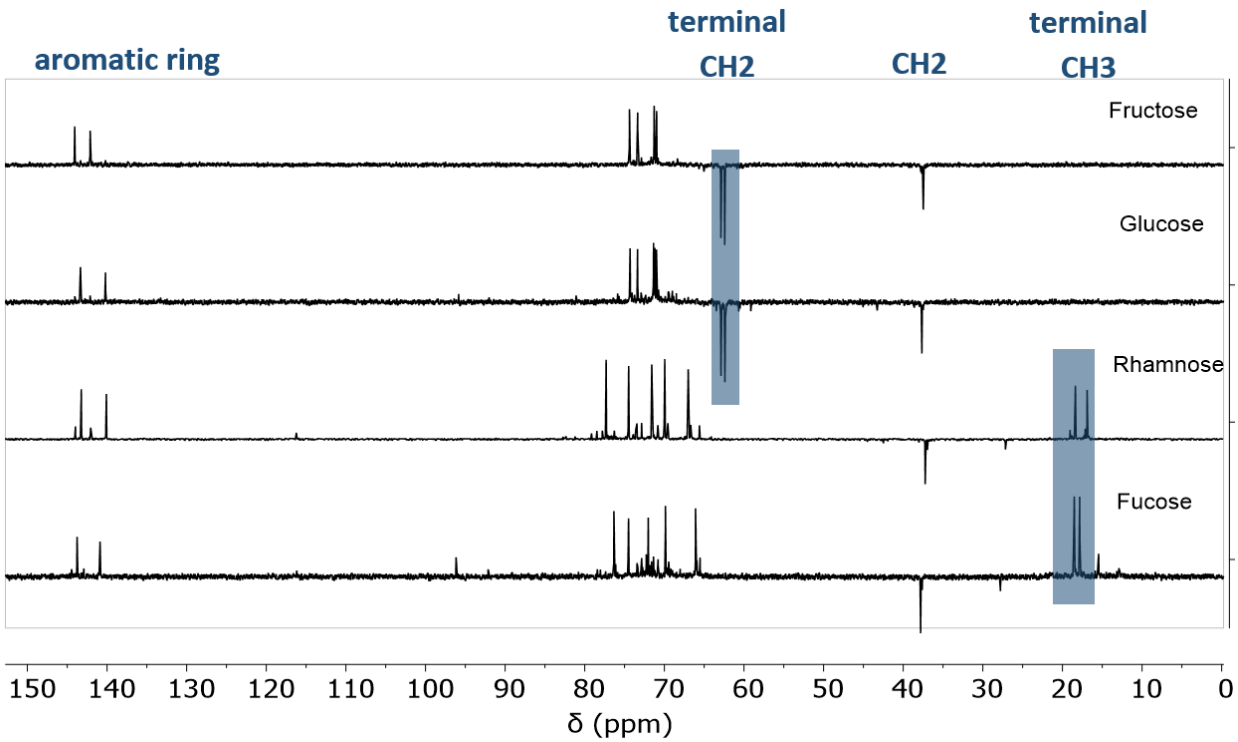

Figure S3: DEPT 135 [13]C NMR in D2O of the crude reaction mixture from different monosaccharides.

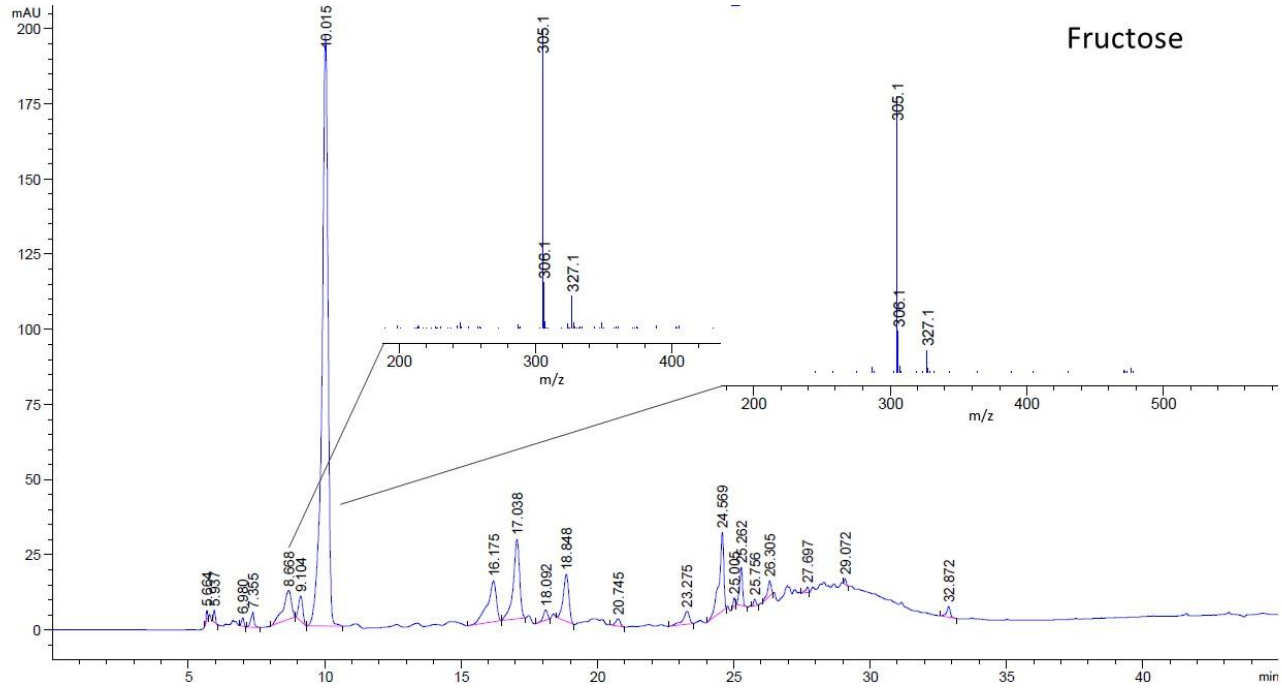
Fructose
mAU
10.015
395.1
306.1
327.1
m/z
5.664
5.931
6.980
7.355
8.668
9.104
16.175
17.038
18.092
18.848
20.745
23.275
24.569
25.005
25.262
25.756
26.305
27.697
29.072
32.872
min

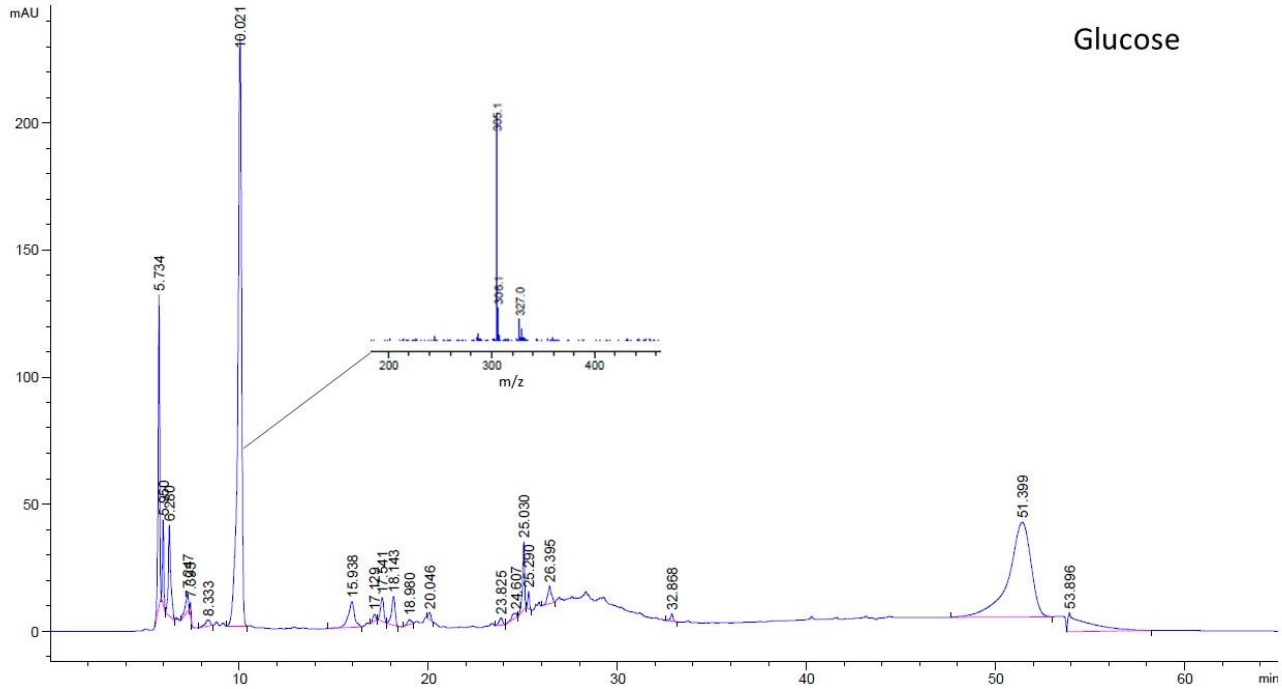
Glucose
mAU
10.021
395.1
306.1
327.0
m/z
5.734
6.260
6.350
7.847
8.333
15.938
17.129
17.341
18.143
18.980
20.046
23.825
24.607
25.030
25.290
26.395
32.868
51.399
53.896
min

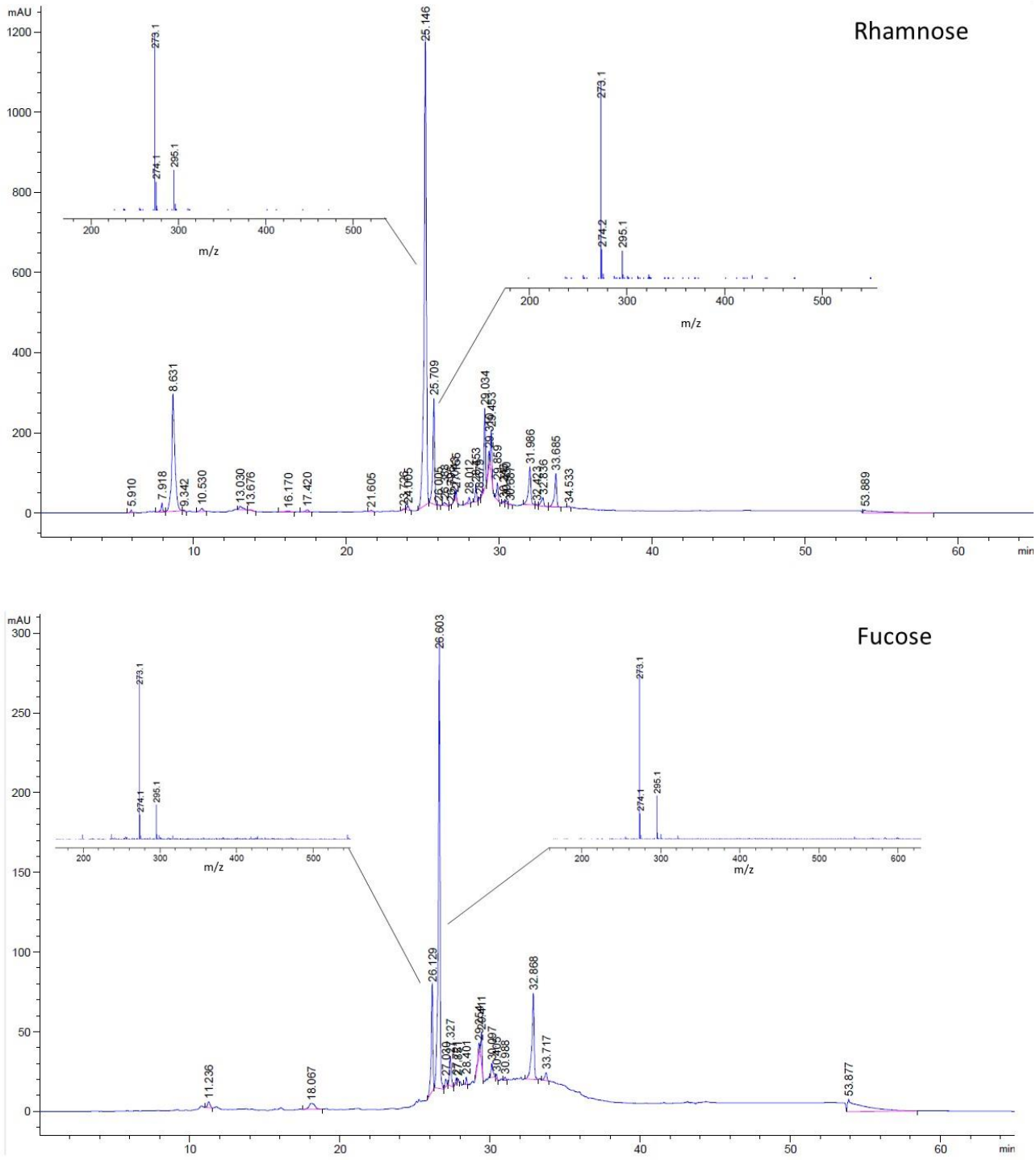

Figure S4: HPLC-MS of the crude reaction mixture from different monosaccharides.

S2.4. Characterization of separated DOR derivatives

Analytical data for 2,6-DOR from Rhamnose

^{1}H NMR (400 MHz, DMSO-d_6) δ = 8.60 (s, 1H), 8.40 (s, 1H), 5.33 (d, $\mathcal{J}$ = 6.5 Hz, 1H), 5.06 – 4.97 (d looking m, 1H), 4.73 – 4.62 (m, 3H), 4.50 (d, $\mathcal{J}$ = 8.1 Hz, 1H), 3.77 – 3.61 (m, 1H), 3.62 – 3.52 (m, 1H), 3.47 (q, J = 6.0 Hz, 1H), 3.38 – 3.23 (m, 1H), 3.02 (dd, J = 13.8, 2.8 Hz, 1H), 2.65 2.68 – 2.60 (dd, J = 13.8, 9.7 Hz, 1H), 1.14 (d, J = 6.2 Hz, 3H), 1.11 (d, J = 6.1 Hz, 3H) ppm.

^{13}C NMR (101 MHz, DMSO-d_6) δ = 19.95, 21.15, 39.25, 66.64, 70.39, 71.97, 75.38, 78.37, 141.01, 143.29, 154.38, 158.45 ppm.

HRMS (ESI^{+}): Calculated for $C_{12}H_{21}N_2O_5$: 273.1445, Found: 273.1453

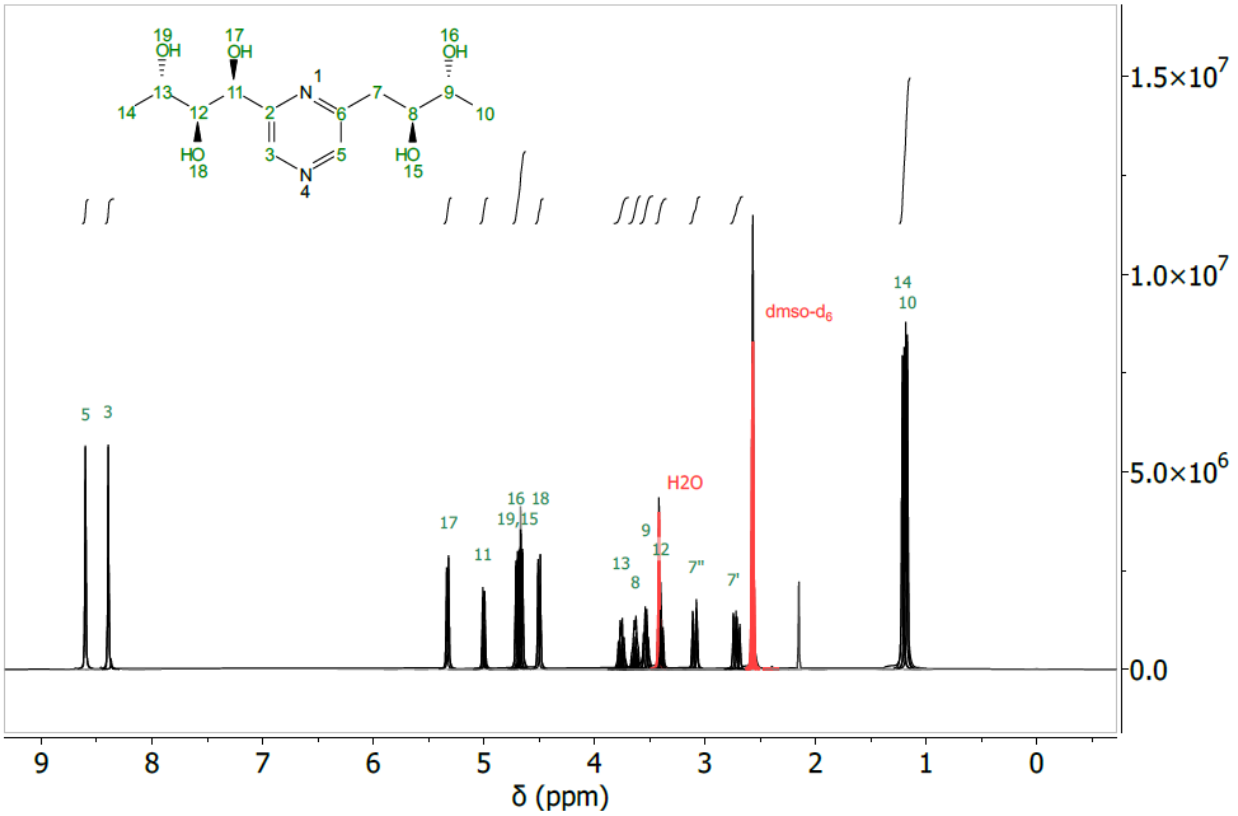

Figure S5: ^{1}H -NMR (400MHz, DMSO-d_6) for 2,6-DOR from rhamnose

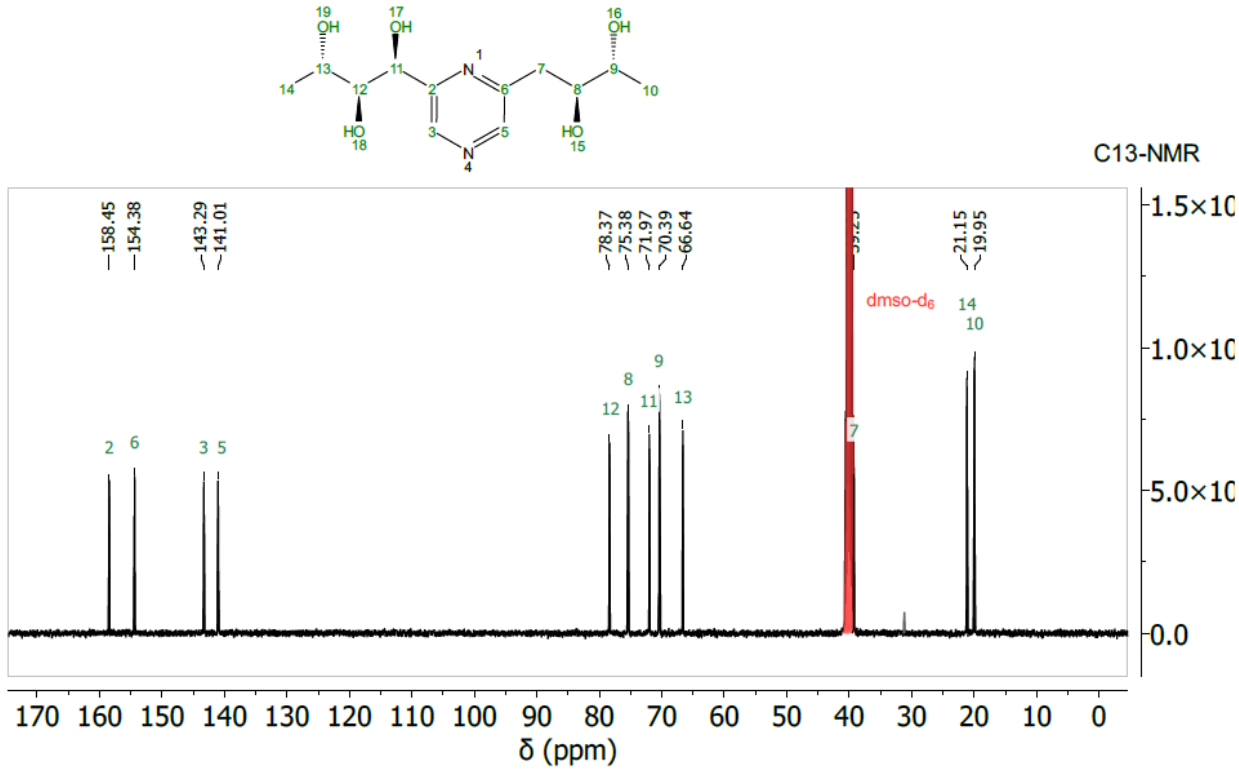

Figure S6: [13]C -NMR (400MHz, DMSO-d6) for 2,6-DOR from rhamnose

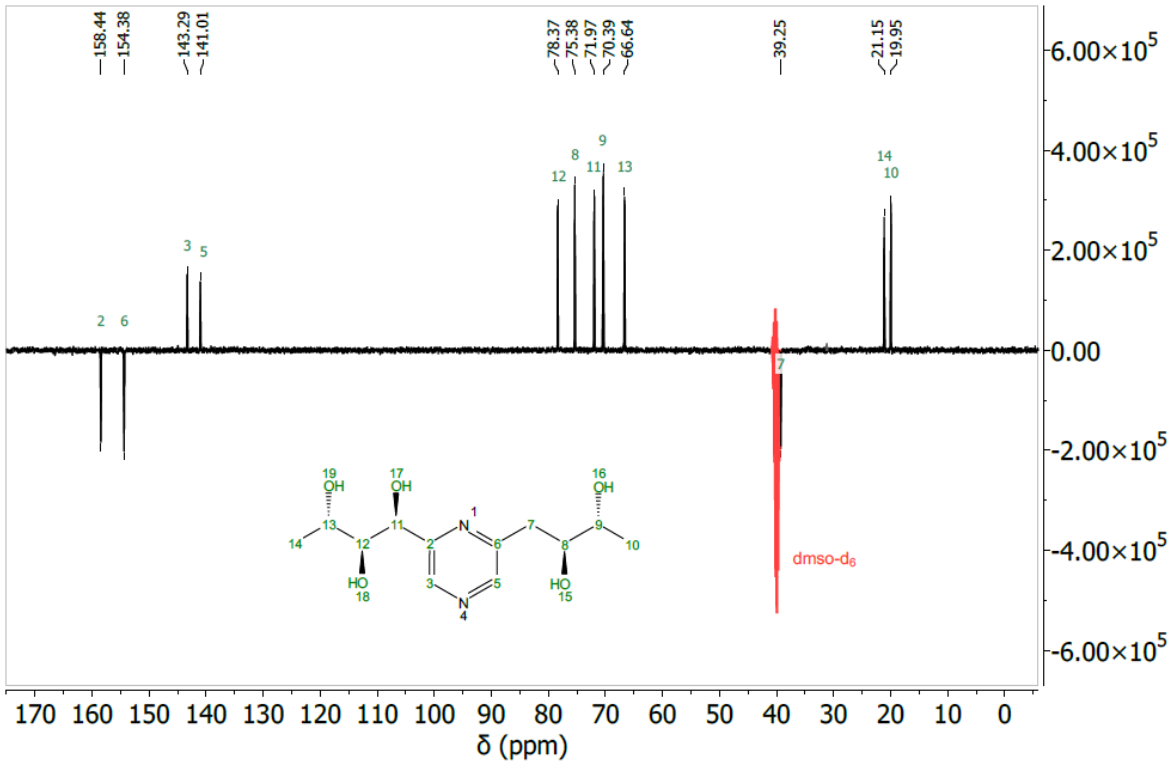

Figure S7: [13]C-APT-NMR (400MHz, DMSO-d6) for 2,6-DOR from rhamnose

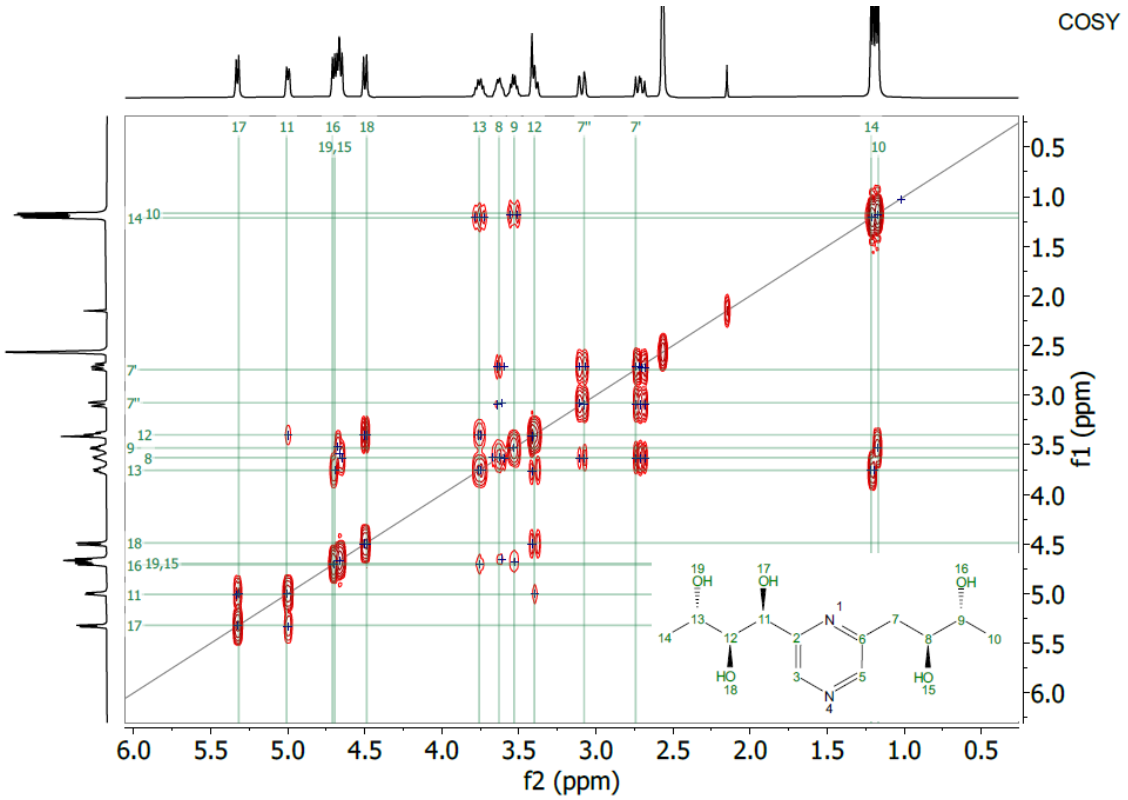

Figure S8: COSY -NMR (400MHz, DMSO-d₆) for 2,6-DOR from rhamnose

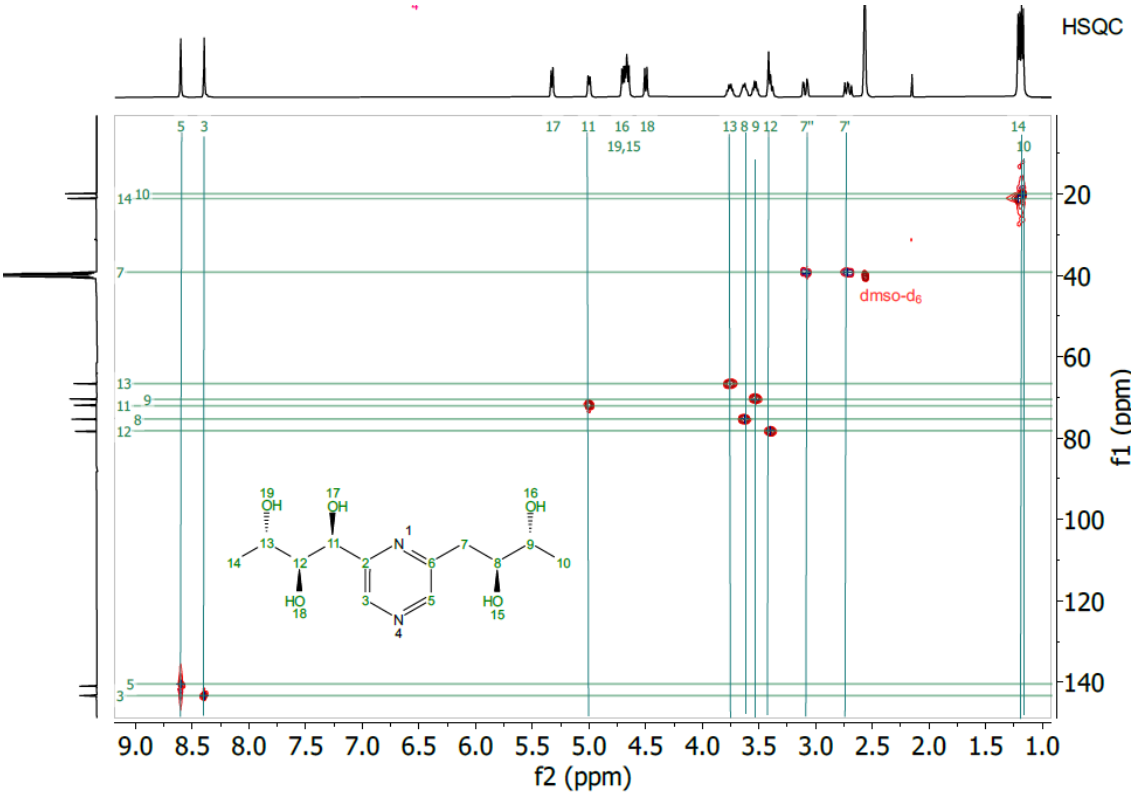

Figure S9: HSQC -NMR (400MHz, DMSO-d₆) for 2,6-DOR from rhamnose

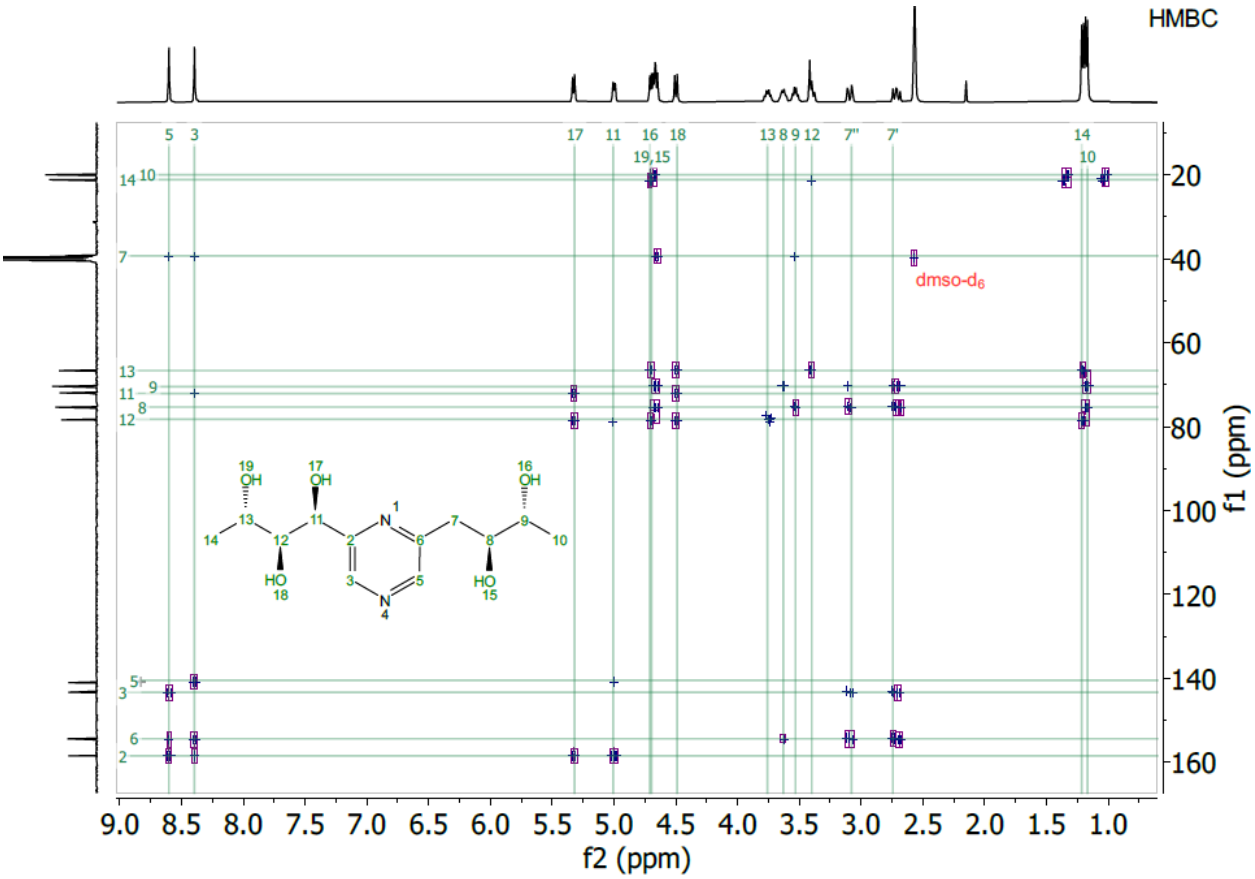

Figure S10: HMBC -NMR (400MHz, DMSO-d_6)

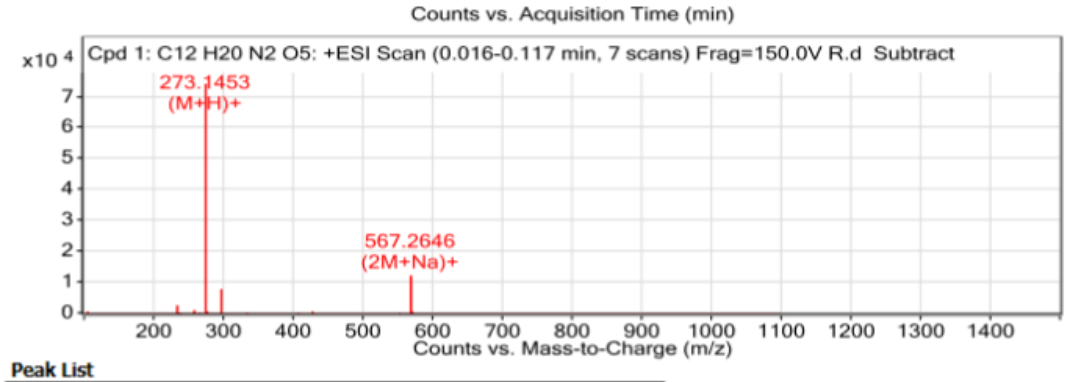

Peak List

m/z	z	Abund	Formula	Ion
255.1336	1	134	C12 H19 N2 O4	(M+H)+[-H2O]
273.1453		75954	C12 H21 N2 O5	(M+H)+
273.3493		993		
274.1483		7596	C12 H21 N2 O5	(M+H)+
275.15		925	C12 H21 N2 O5	(M+H)+
295.1273	1	8129	C12 H20 N2 Na O5	(M+Na)+
296.1307	1	1059	C12 H20 N2 Na O5	(M+Na)+
567.2646	1	13067	C24 H40 N4 Na O10	(2M+Na)+
568.2678	1	3006	C24 H40 N4 Na O10	(2M+Na)+
569.2701	1	621	C24 H40 N4 Na O10	(2M+Na)+

Figure S 11: HR-MS of for 2,6-DOR from rhamnose

Analytical data for 2,5-DOF from fructose.

^{1}H NMR (400 MHz, DMSO-d_6) δ = 8.62 (s, 1H), 8.39 (s, 1H), 5.31 (d, $\mathcal{J}$ = 6.4 Hz, 1H), 4.93 (d, $\mathcal{J}$ = 5.9 Hz, 1H), 4.67 (dd, $\mathcal{J}$ = 15.9, 4.7 Hz, 2H), 4.62 (d, $\mathcal{J}$ = 6.6 Hz, 1H), 4.42 (d, $\mathcal{J}$ = 7.0 Hz, 2H), 4.37 (d, $\mathcal{J}$ = 5.9 Hz, 1H), 3.75 (dtd, $\mathcal{J}$ = 9.5, 6.4, 6.3, 2.9 Hz, 1H), 3.69 – 3.52 (m, 5H), 3.44-3.37 (m, 2H, overlapping with H_2O peak in DMSO-d_6), 3.06 (dd, $\mathcal{J}$ = 14.0, 3.0 Hz, 1H), 2.72 (dd, $\mathcal{J}$ = 13.9, 9.5 Hz, 1H) ppm.

^{13}C NMR (101 MHz, DMSO-d_6) δ = 38.39, 63.25, 63.62, 71.29, 71.36, 71.40, 73.84, 74.96, 142.30, 143.31, 153.26, 155.77 ppm.

HRMS (ESI$^+$): Calculated for $C_{12}H_{21}N_2O_7$: 305.1343, Found: 305.1356.

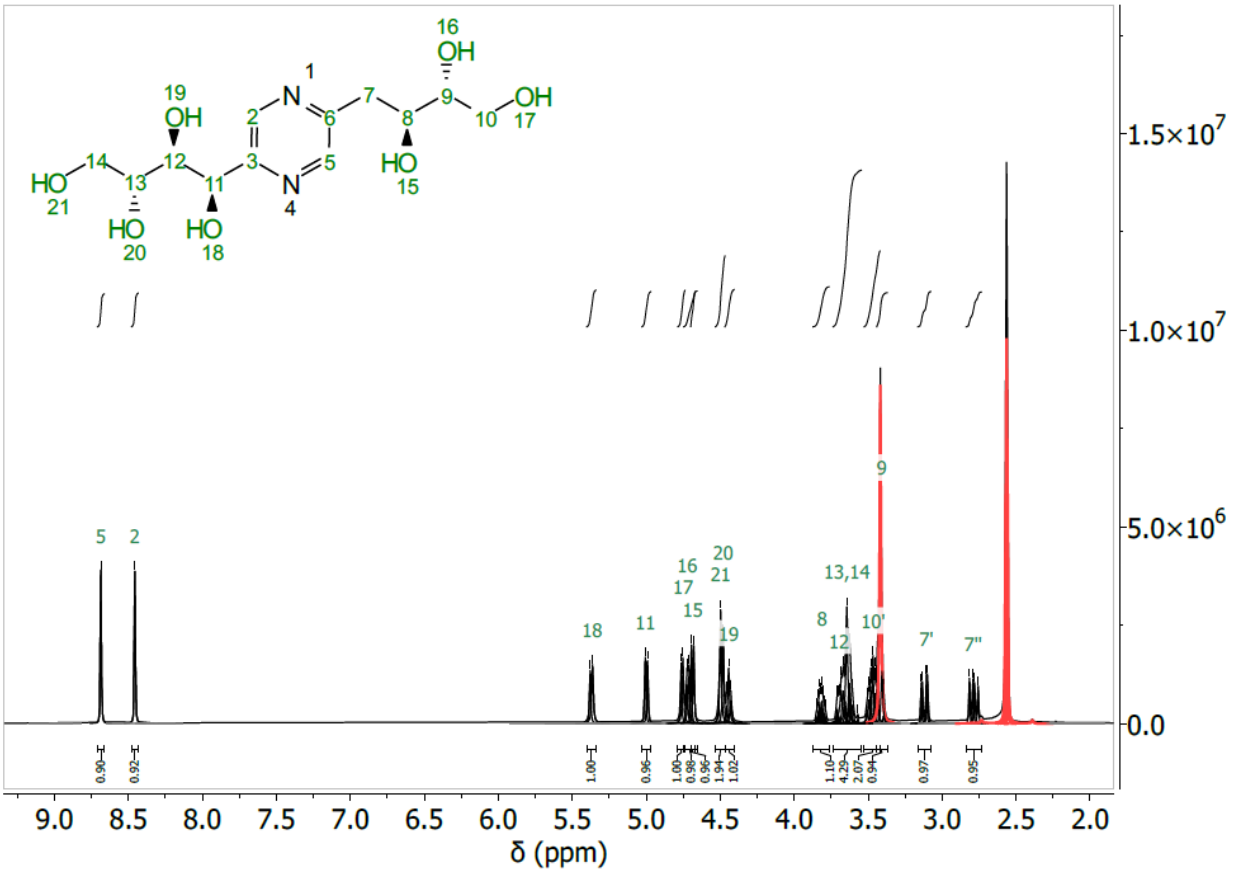

Figure S12: ^{1}H -NMR (400MHz, DMSO-d_6) for 2,5-DOF from fructose

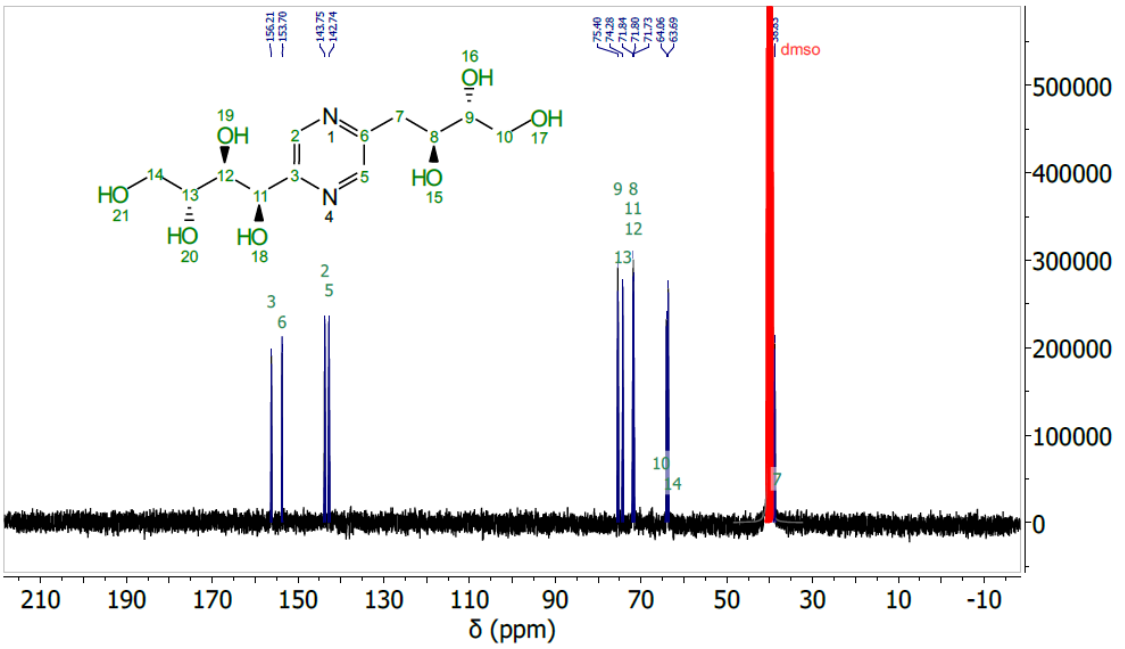

Figure S13: ^{13}C -NMR (400MHz, DMSO-d_6) for 2,5-DOF from fructose

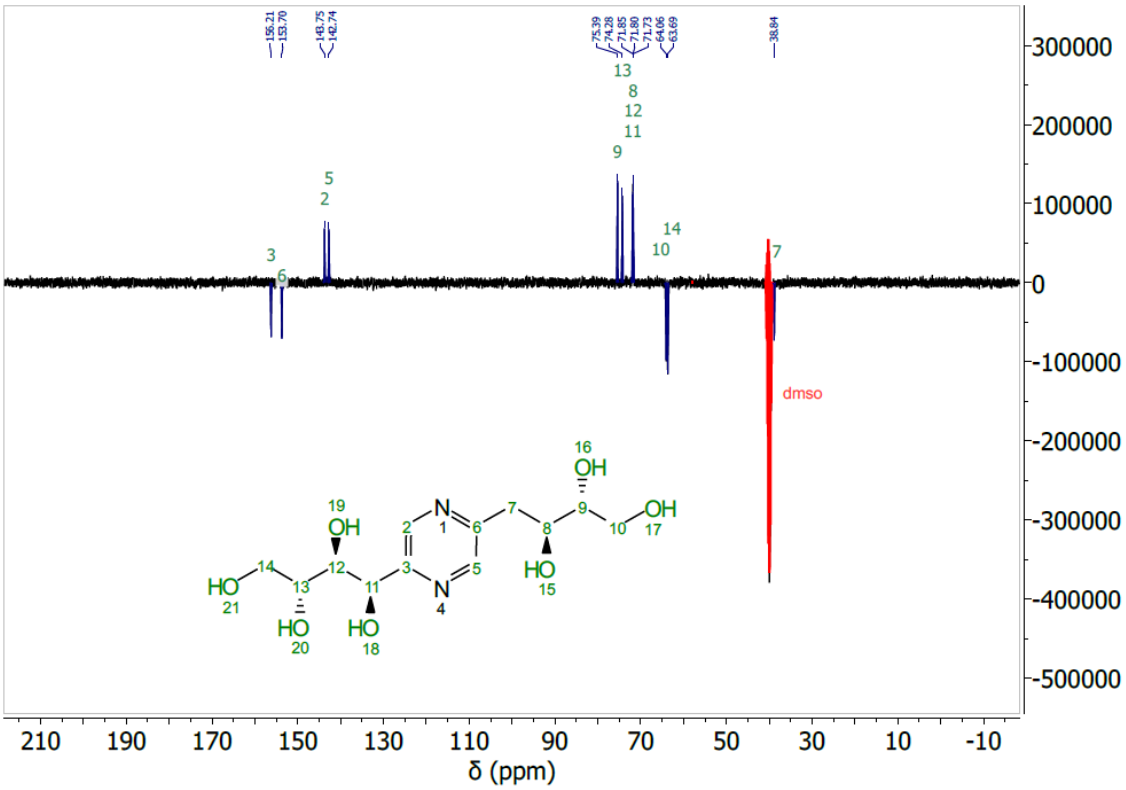

Figure S14: ^{13}C-APT -NMR (400MHz, DMSO-d_6) for 2,5-DOF from fructose

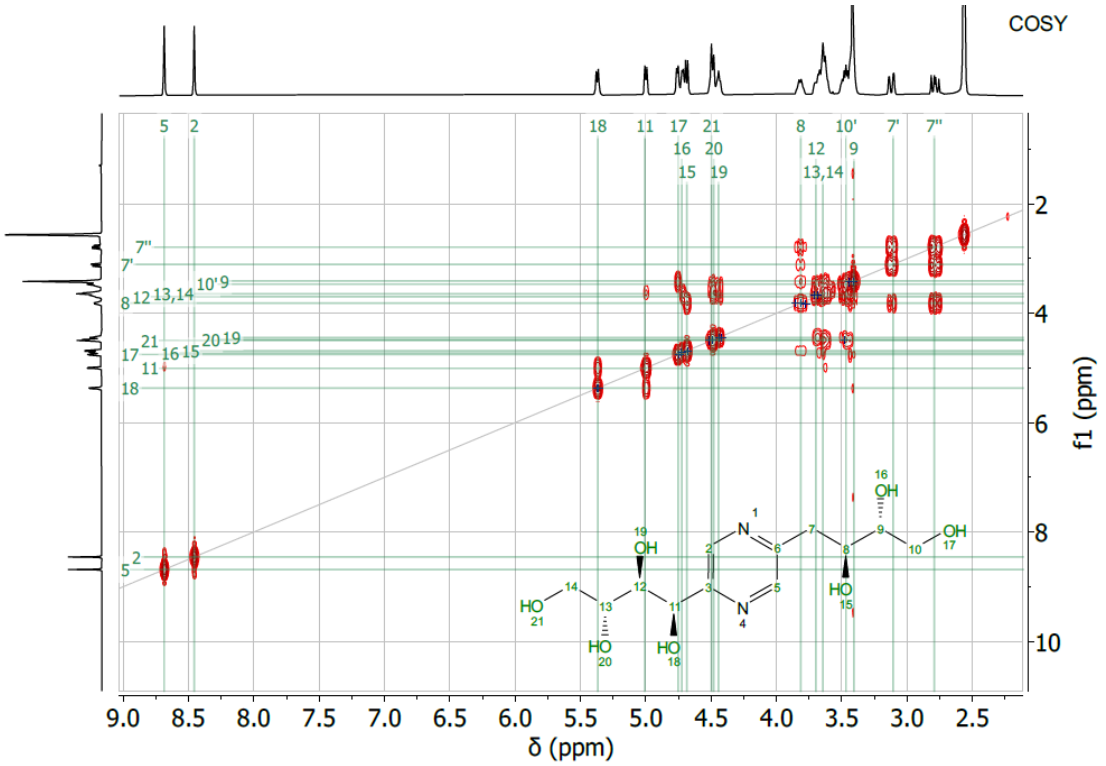

Figure S15: COSY -NMR (400MHz, DMSO-d_6) for 2,5-DOF from fructose

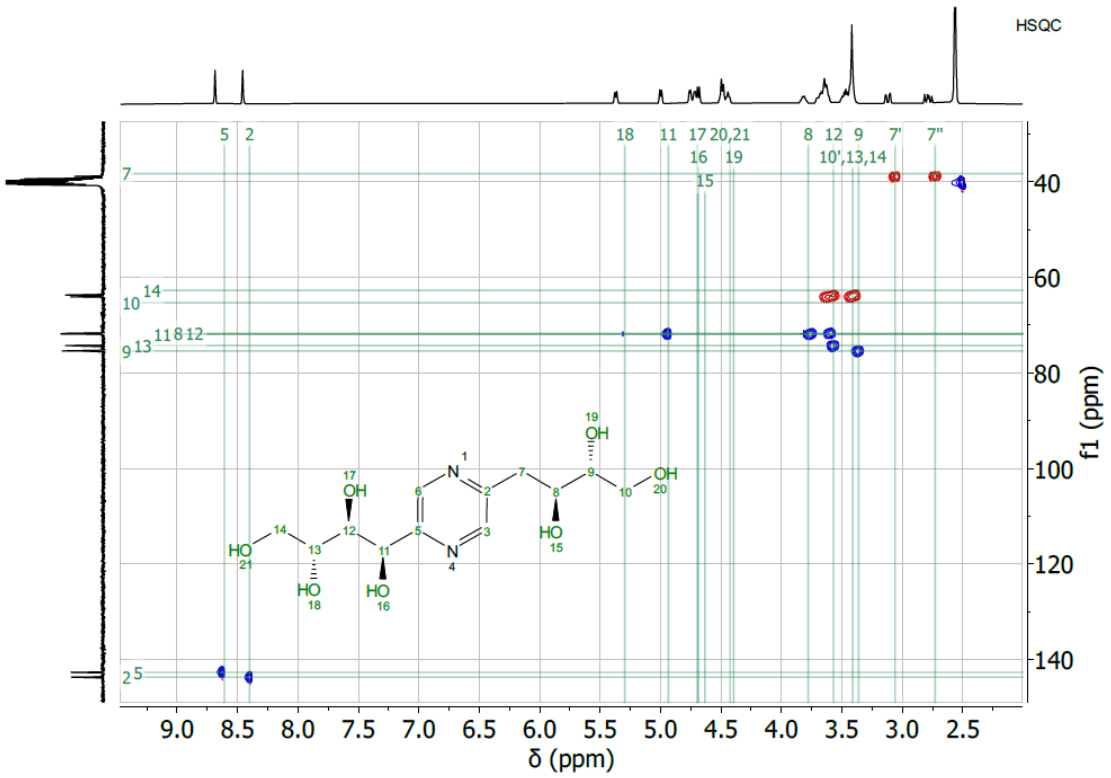

Figure S16: HSQC -NMR (400MHz, DMSO-d_6) for 2,5-DOF from fructose

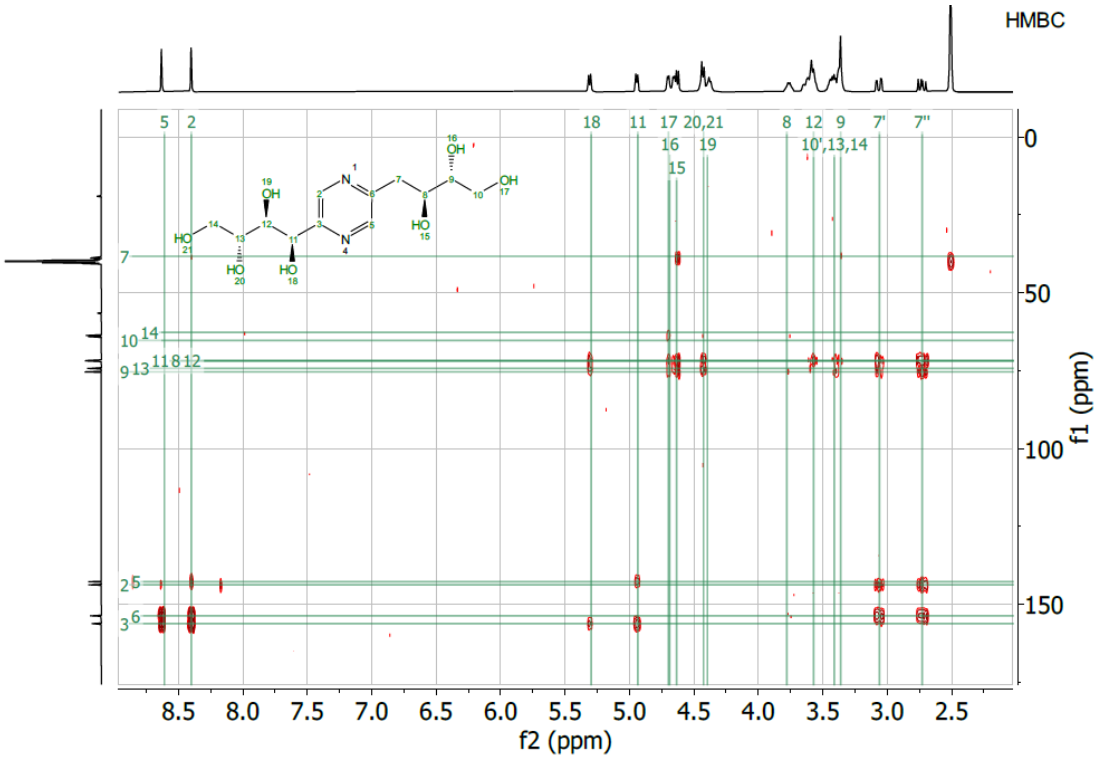

Figure S17: HMBC-NMR (400MHz, DMSO-d_6) for 2,5-DOF from fructose

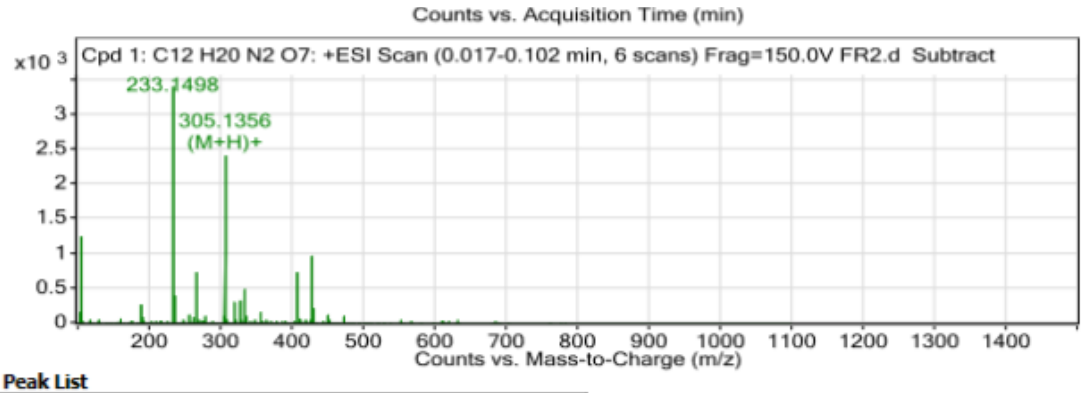

Peak List

m/z	z	Abund	Formula	Ion
233.1498		3426		
233.3431		14		
233.635		12		
233.7796		8		
234.1526		417		
235.1552		54		
305.1356	1	2455	C12 H21 N2 O7	(M+H)+
306.1377	1	381	C12 H21 N2 O7	(M+H)+
307.1458	1	57	C12 H21 N2 O7	(M+H)+

Figure S18: HR-MS for 2,5-DOF from fructose

Analytical data for 2,6-DOF from glucose

^{1}H NMR (400 MHz, DMSO-d_6) δ = 8.54 (s, 1H), 8.33 (s, 1H), 5.34 (d, J = 6.4 Hz, 1H), 4.94 (d, J = 4.3 Hz, 1H), 4.78 – 4.55 (m, 3H), 4.53 – 4.32 (m, 3H), 3.75 (dt, J = 6.5, 3.3, 3.3 Hz, 1H), 3.68 – 3.54 (m, 5H), 3.06 (dd, J = 13.8, 2.7 Hz, 1H), 2.71 (dd, J = 13.9, 9.9 Hz, 1H) ppm.

^{13}C NMR (101 MHz, DMSO-d_6) δ = 22.56, 63.24, 63.62, 71.25, 71.36, 71.59, 73.79, 75.07, 140.59, 142.93, 153.97, 157.90 ppm.

HRMS (ESI$^+$): Calculated for $C_{12}H_{21}N_2O_7$: 305.1343, Found: 305.1350

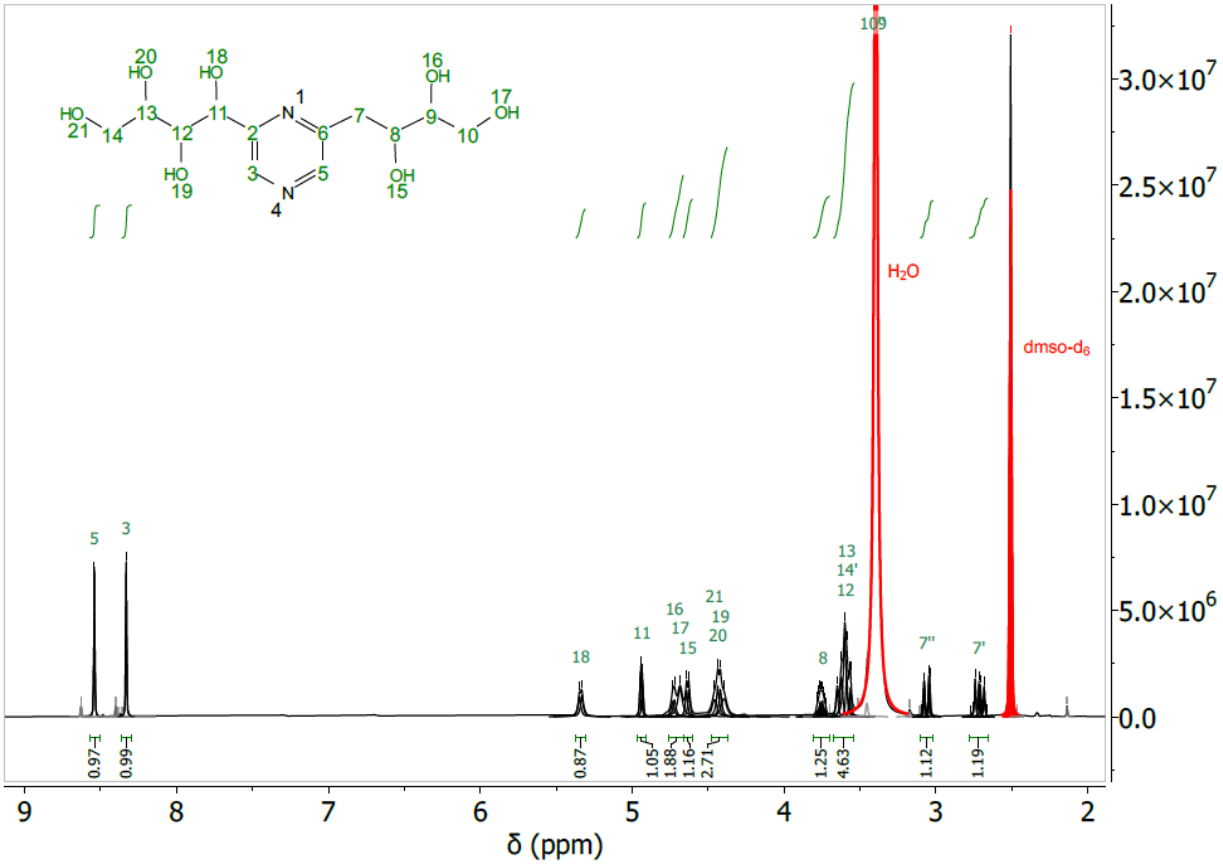

Figure S19: ^{1}H -NMR (400MHz, DMSO-d_6) for 2,6-DOF from glucose. The integration misses the proton peaks from 9 and 10. These are hidden behind the water peak as shown by HSQC spectra.

13

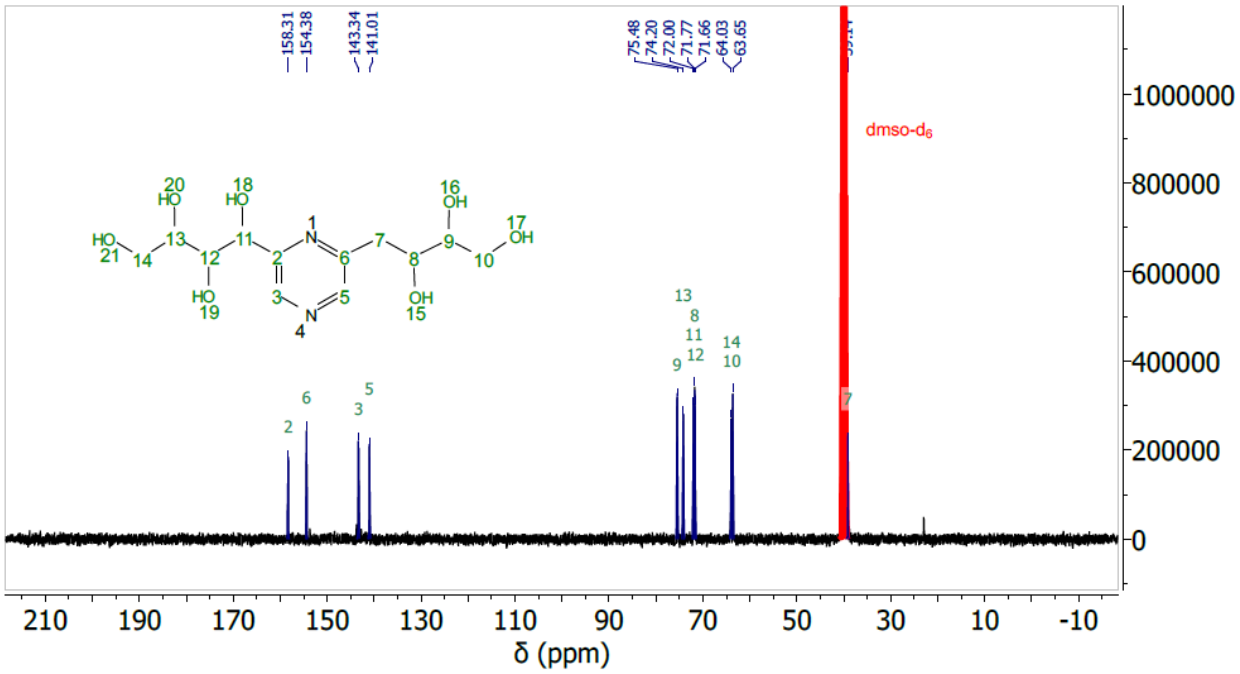

Figure S20: C -NMR (400MHz, DMSO-d₆) for 2,6-DOF from glucose

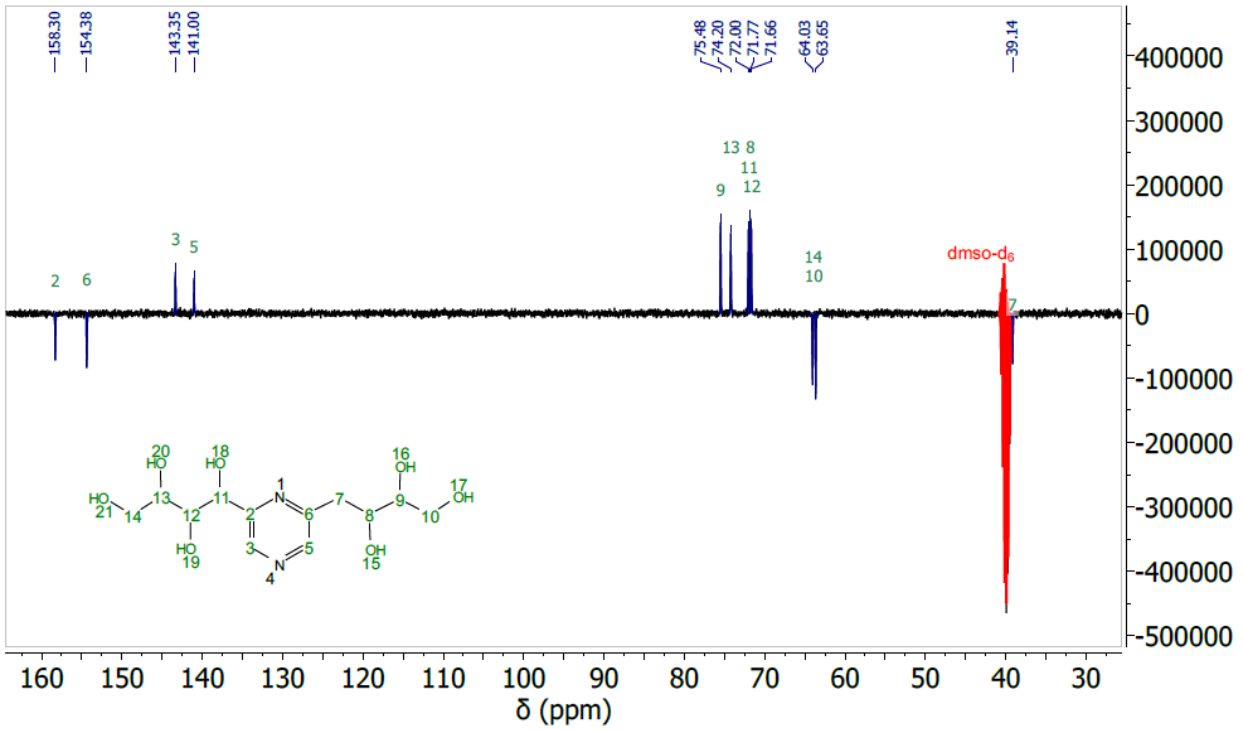

Figure S21: [13]C-APT-NMR (400MHz, DMSO-d₆) for 2,6-DOF from glucose

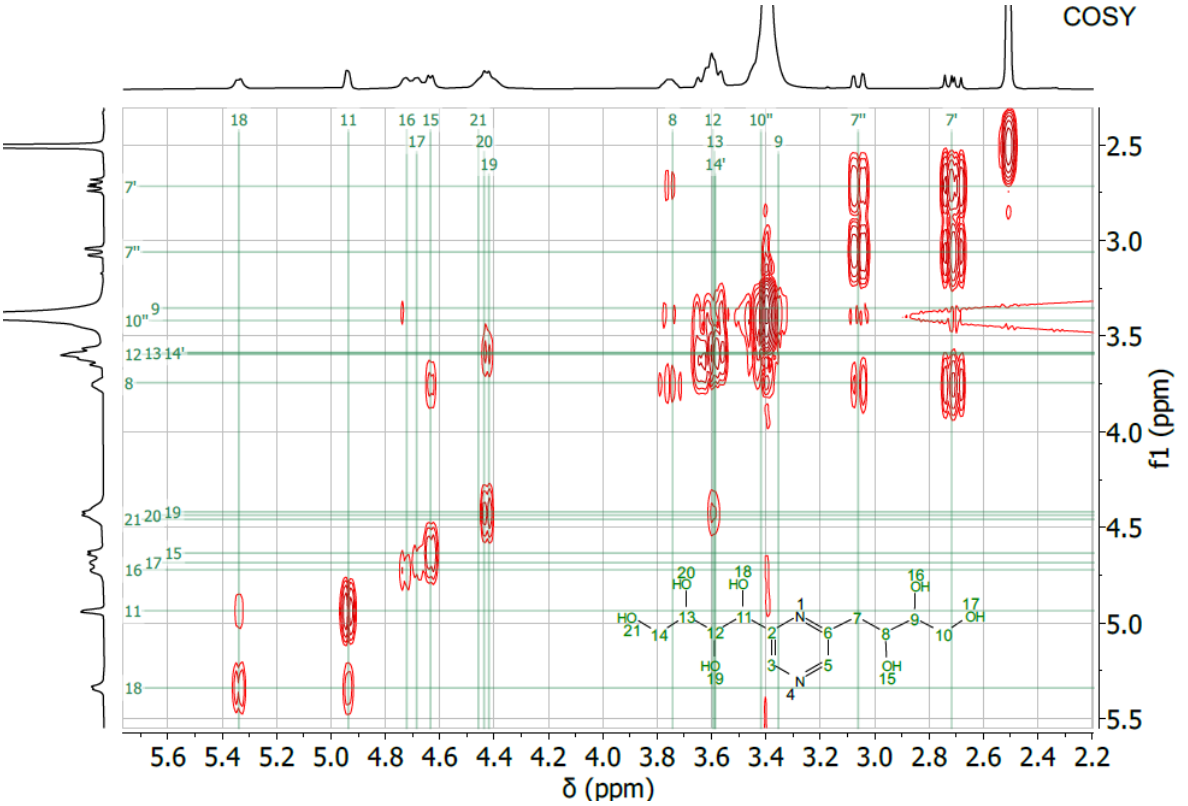

Figure S 22: COSY-NMR (400MHz, DMSO-d_6) for 2,6-DOF from glucose

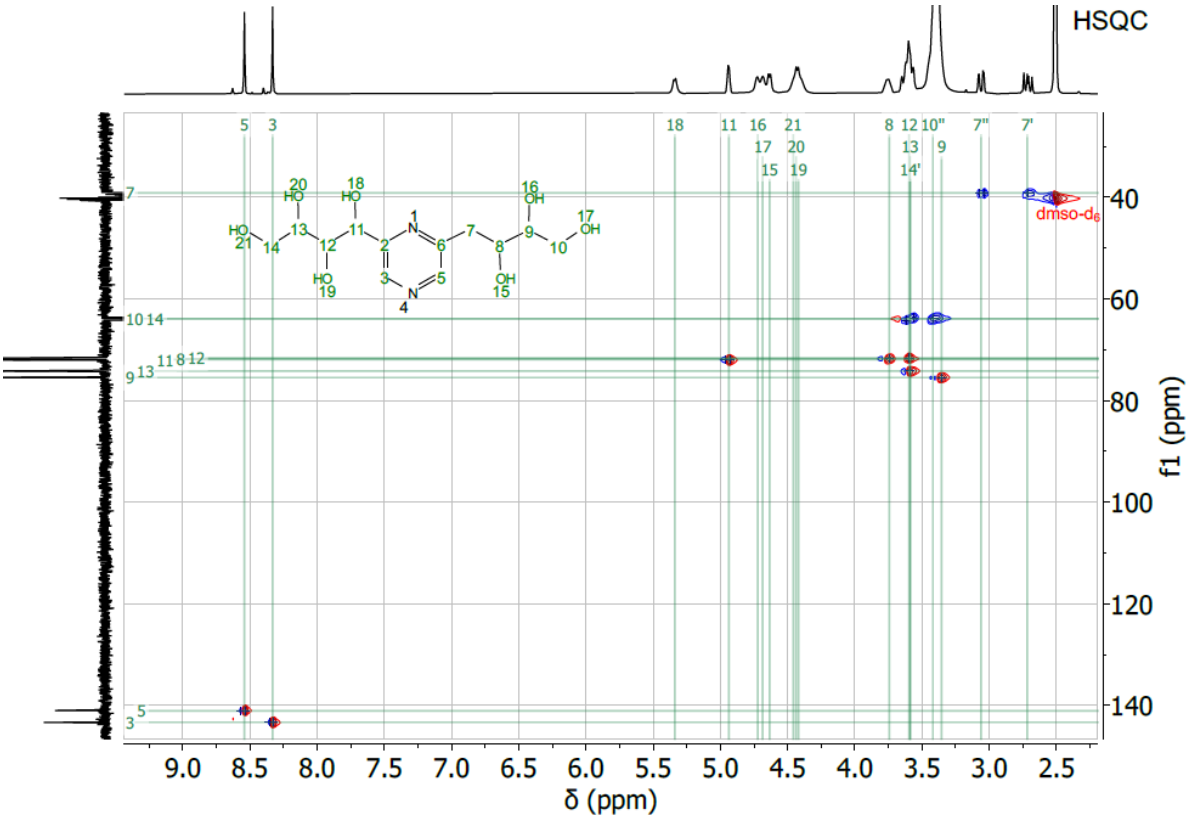

Figure S23: HSQC-NMR (400MHz, DMSO-d_6) for 2,6-DOF from glucose

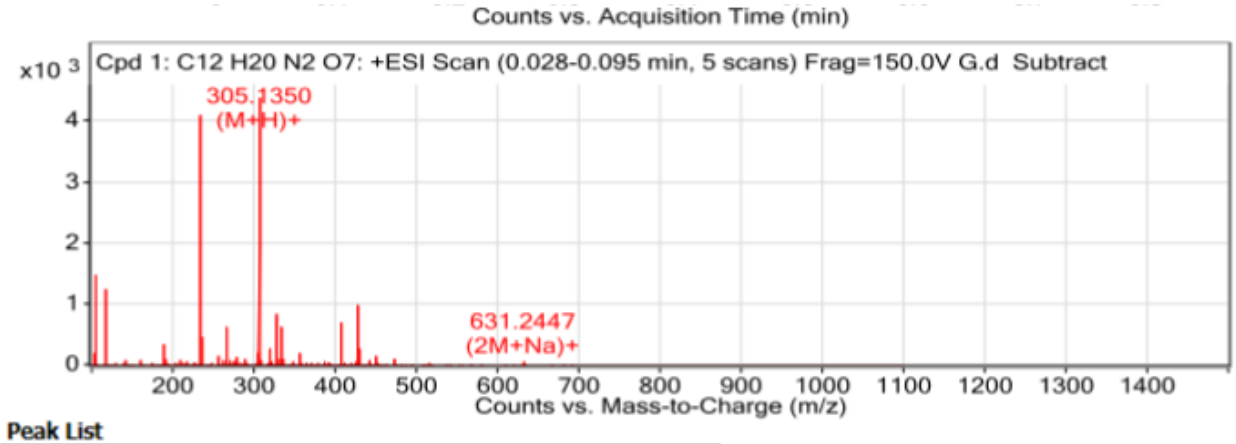

Peak List

m/z	z	Abund	Formula	Ion
302.2089		39		
304.1678		25		
305.135		4450	C12 H21 N2 O7	(M+H)+
306.1388		591	C12 H21 N2 O7	(M+H)+
307.1347		104	C12 H21 N2 O7	(M+H)+
327.1176	1	869	C12 H20 N2 Na O7	(M+Na)+
328.1261	1	121	C12 H20 N2 Na O7	(M+Na)+
329.1256	1	27	C12 H20 N2 Na O7	(M+Na)+
631.2447	1	75	C24 H40 N4 Na O14	(2M+Na)+
632.2437	1	23	C24 H40 N4 Na O14	(2M+Na)+

Figure S24: HR-MS for 2,6-DOF from glucose

Analytical data for 2,6-DOFu from fucose

^{1}H NMR (500 MHz, DMSO-d_6) δ = 8.45 (s, 1H), 8.38 (s, 1H), 5.48 (d, $\mathcal{J}$ = 5.7 Hz, 1H), 4.59 (dd, $\mathcal{J}$ = 7.5, 5.6 Hz, 1H), 4.54 (dd, $\mathcal{J}$ = 5.5, 3.5 Hz, 2H), 4.41 (d, $\mathcal{J}$ = 6.9 Hz, 1H), 4.29 (d, $\mathcal{J}$ = 6.1 Hz, 1H), 3.87-3.81 (m, 1H), 3.73 – 3.64 (m, 1H), 3.59-3.56 (m, 1H), 3.47 (td, $\mathcal{J}$ = 7.2, 3.0 Hz, 1H), 2.88 (dd, $\mathcal{J}$ = 13.8, 3.3 Hz, 1H), 2.73 (dd, $\mathcal{J}$ = 13.8, 9.5 Hz, 1H), 1.10 (d, J = 6.5 Hz, 3H) 1.08 (d, J = 6.3 Hz, 3H).

^{13}C NMR (101 MHz, DMSO-d_6) δ = 18.58, 20.09, 37.81, 65.49, 69.04, 72.76, 73.97, 76.66, 141.31, 143.31, 154.09, 156.97ppm.

MS (ESI^{+}): Calculated for $C_{12}H_{21}N_2O_5$: 273.1445, Found: 273.1450

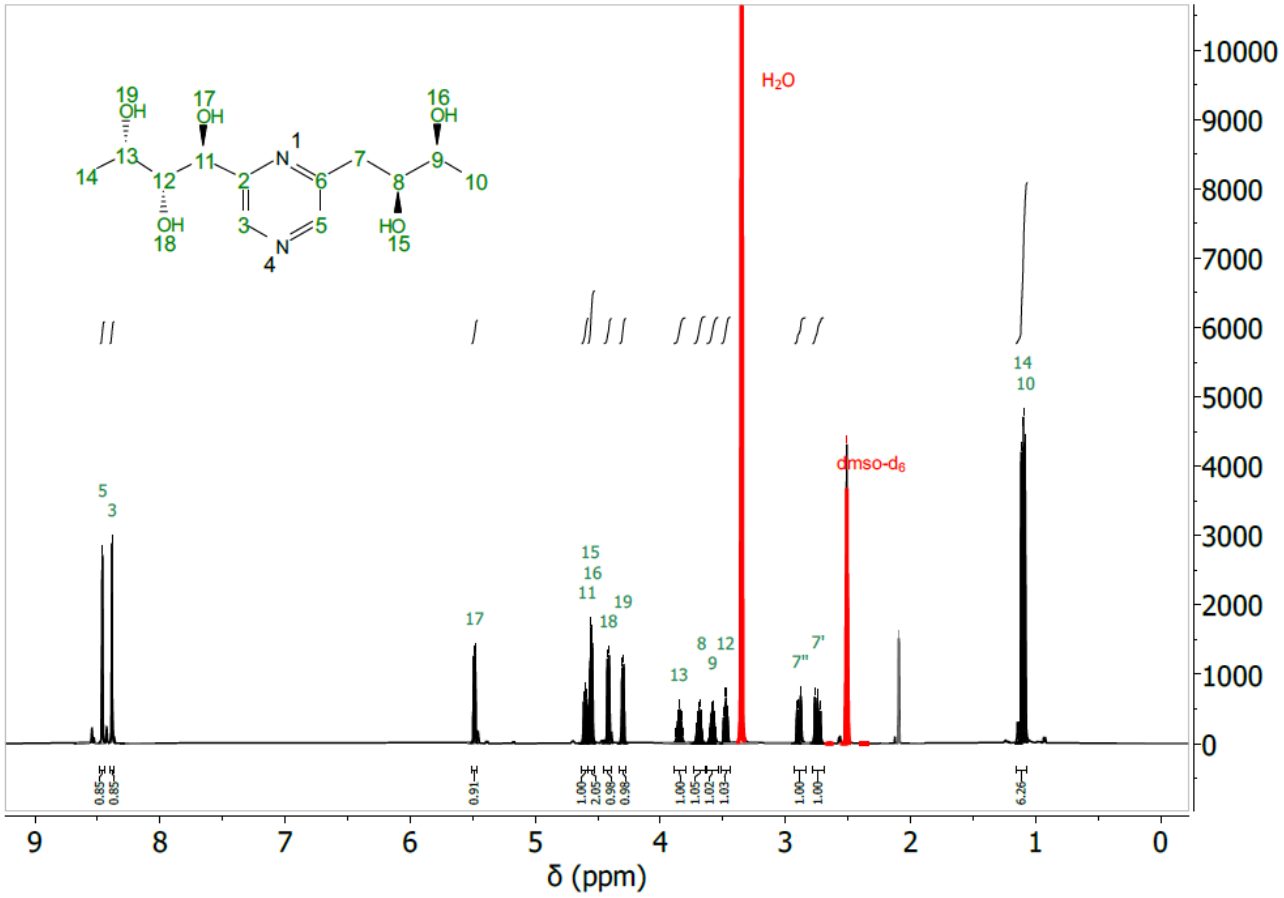

Figure S25: ^{1}H -NMR (400MHz, DMSO-d_6) for 2,6-DOFu from fucose

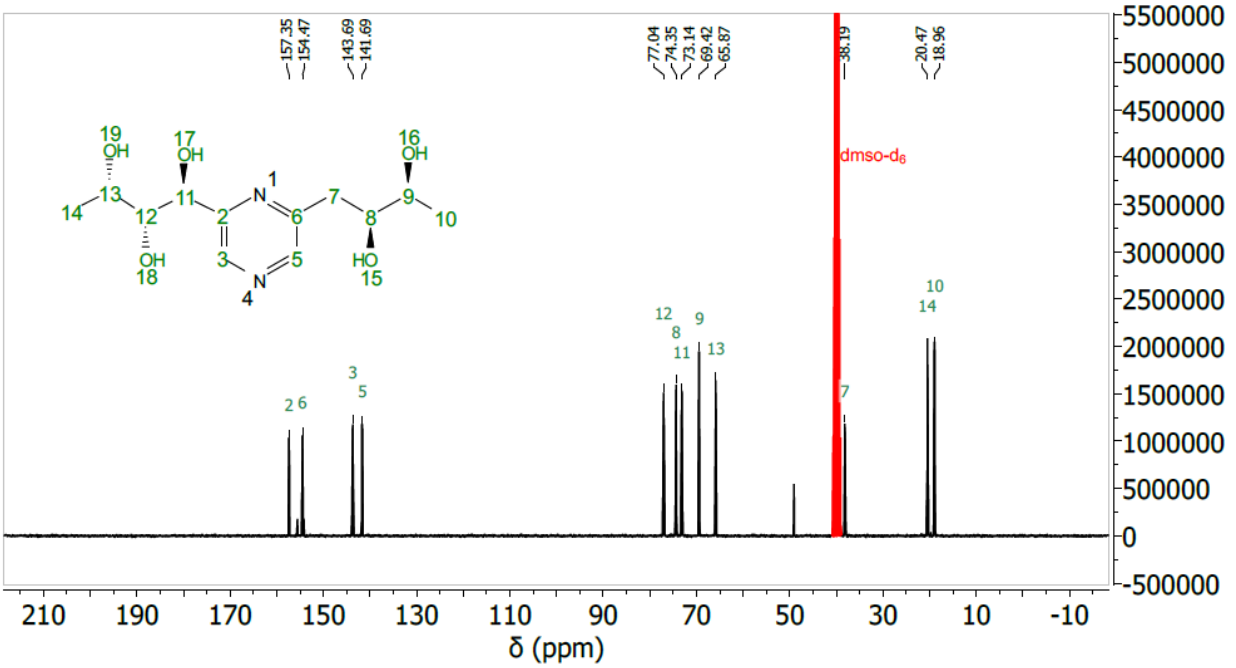

Figure S26: ^{13}C -NMR (400MHz, DMSO-d_6) for 2,6-DOFu from fucose

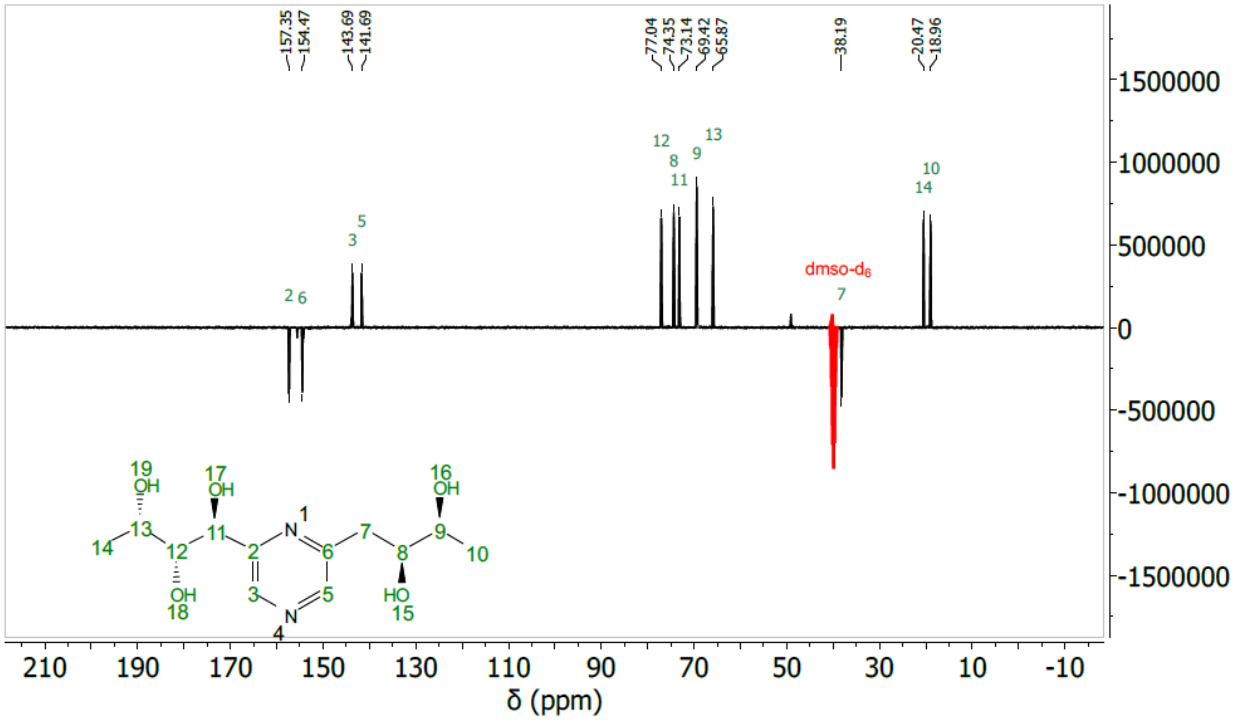

Figure S27: ^{13}C-APT-NMR (400MHz, DMSO-d_6) for 2,6-DOFu from fucose

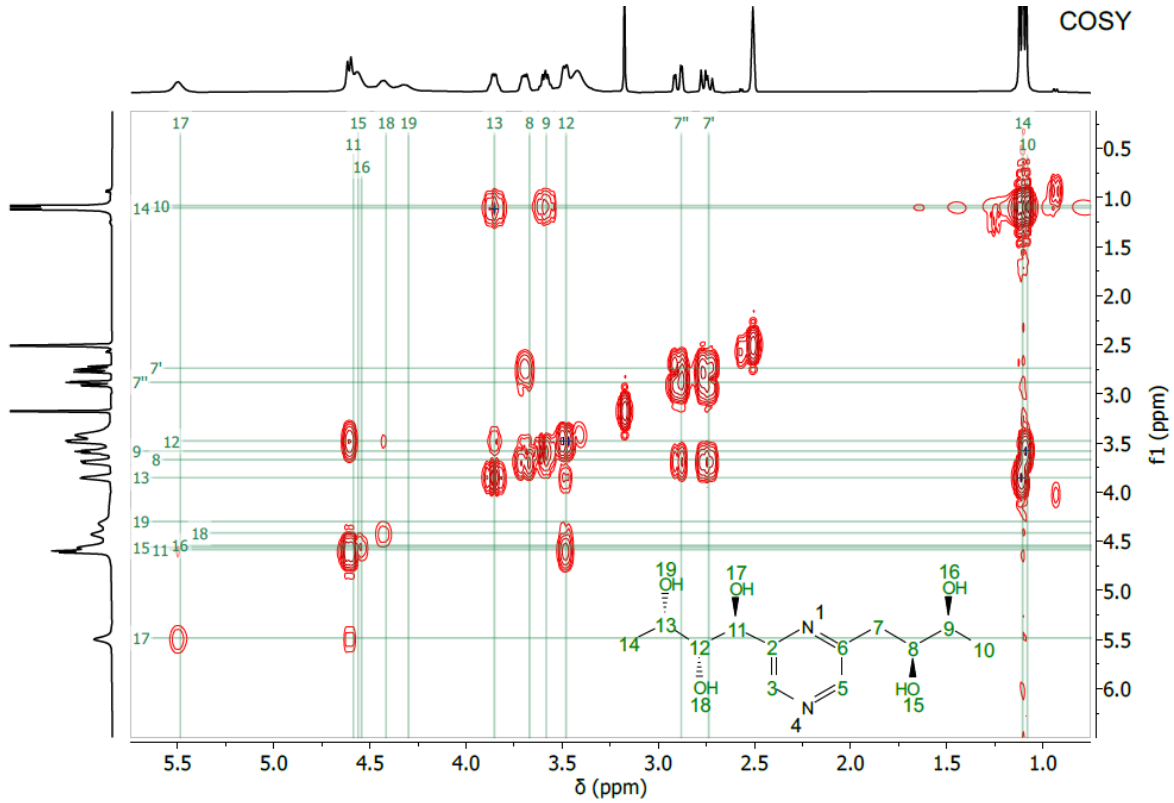

Figure S28: COSY-NMR (400MHz, DMSO-d₆) for 2,6-DOFu from fucose

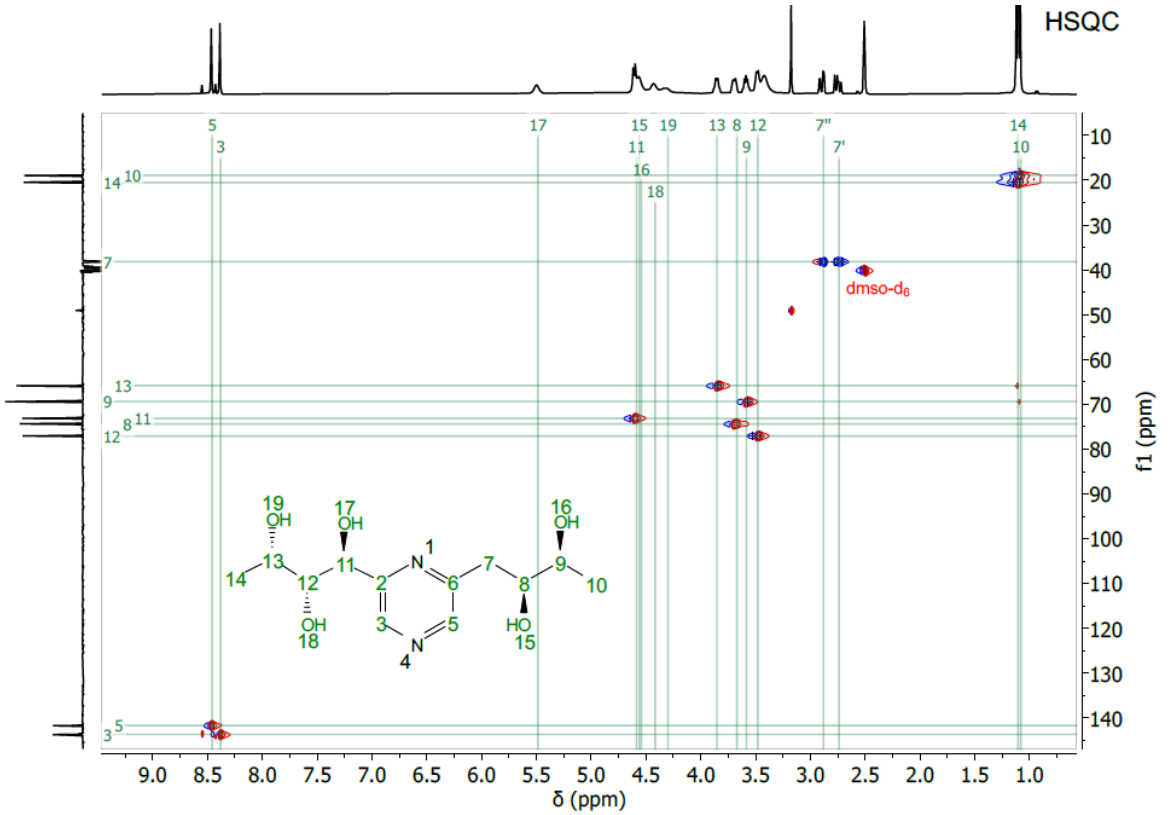

Figure S29: HSQC-NMR (400MHz, DMSO-d₆) for 2,6-DOFu from fucose

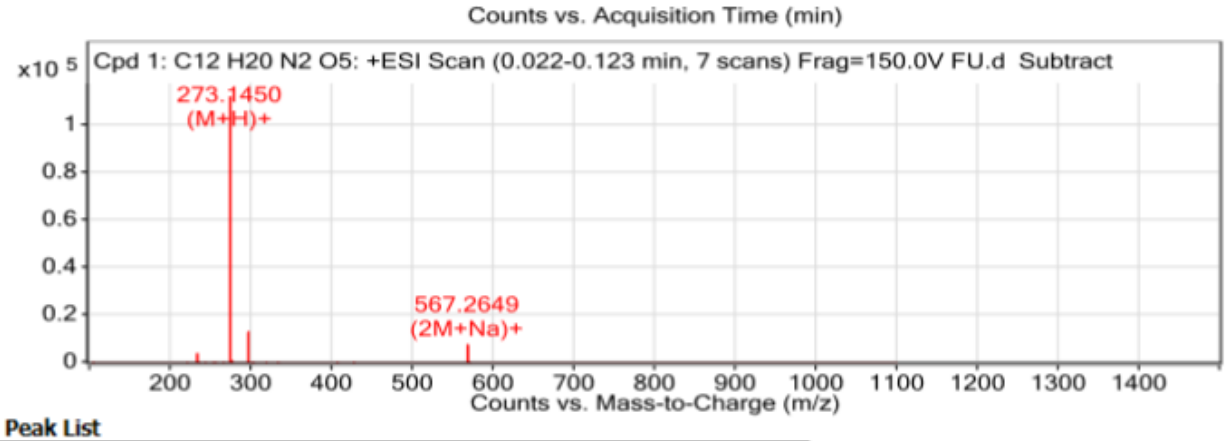

Peak List

m/z	z	Abund	Formula	Ion
255.1345	1	325	C12 H19 N2 O4	(M+H)+[-H2O]
273.145		114665	C12 H21 N2 O5	(M+H)+
273.3488		2166		
274.1479		11320	C12 H21 N2 O5	(M+H)+
275.15		1459	C12 H21 N2 O5	(M+H)+
295.1274	1	13940	C12 H20 N2 Na O5	(M+Na)+
296.1309	1	1815	C12 H20 N2 Na O5	(M+Na)+
549.2513	1	79	C24 H38 N4 Na O9	(2M+Na)+[-H2O]
567.2649	1	8131	C24 H40 N4 Na O10	(2M+Na)+
568.2676	1	1988	C24 H40 N4 Na O10	(2M+Na)+

Figure S30: HR-MS for 2,6-DOFu from fucose

S3. The reaction with levulinic acid for the synthesis of 5-methyl-2-pyrrolidone

S3.1. NMR analysis of crude

^{1}H NMR (400 MHz, DMSO) δ 7.72 (s, 1H), 3.61 (q, J = 6.1 Hz, 1H), 2.12 (p, J = 4.3 Hz, 3H), 1.48 (tdq, J = 8.0, 5.8, 2.3 Hz, 1H), 1.08 (d, J = 6.2 Hz, 3H).

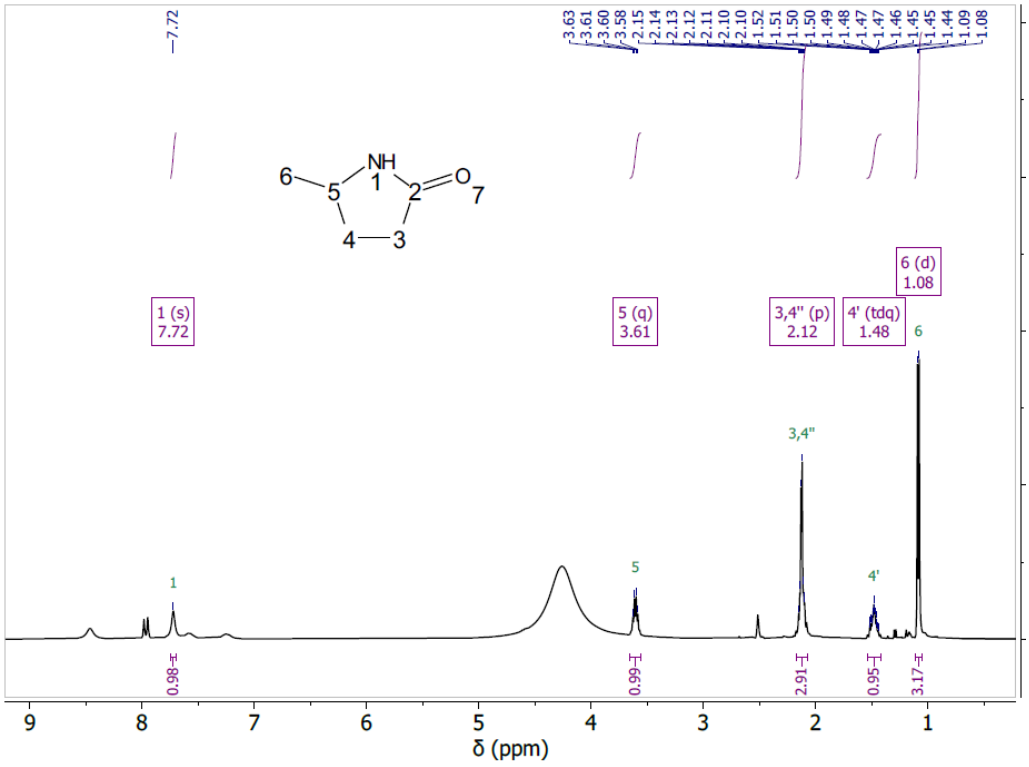

Figure S31: ^{1}H-NMR spectra in DMSO of the crude mixture and identification of 5MP.

S3.2. Conversion of ammonium formate into formamide

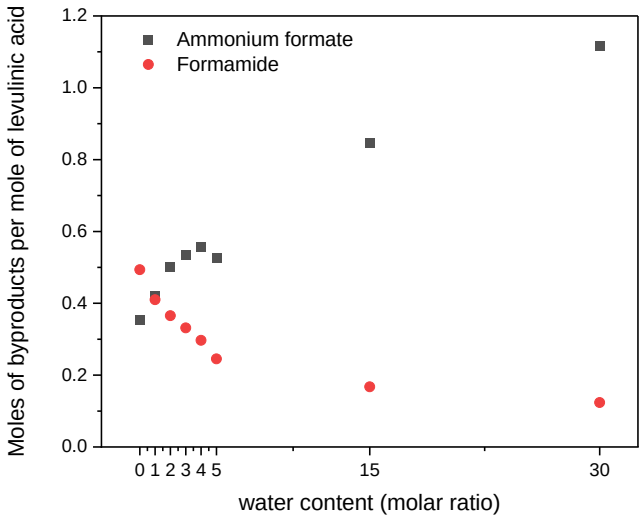

Figure S32: Moles of ammonium formate and formamide in the crude reaction mixture for varying amounts of added water.

S4. The reaction with organic acids and its use in the biorefinery

S4.1. REM characterization

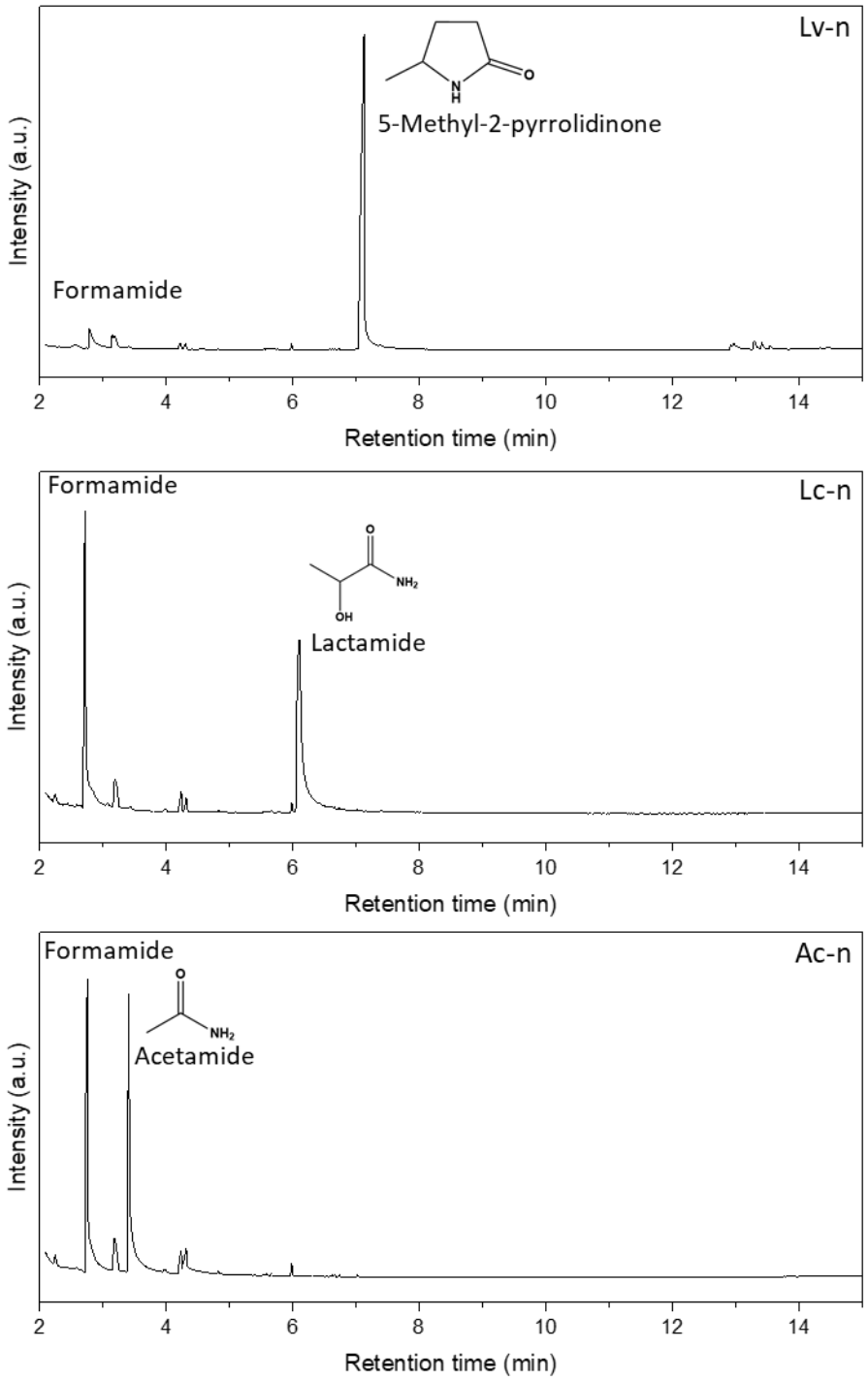

Figure S33: GC-MS results for REM components after the reaction. Organic acids are not detected in GC-MS due to their low boiling points.

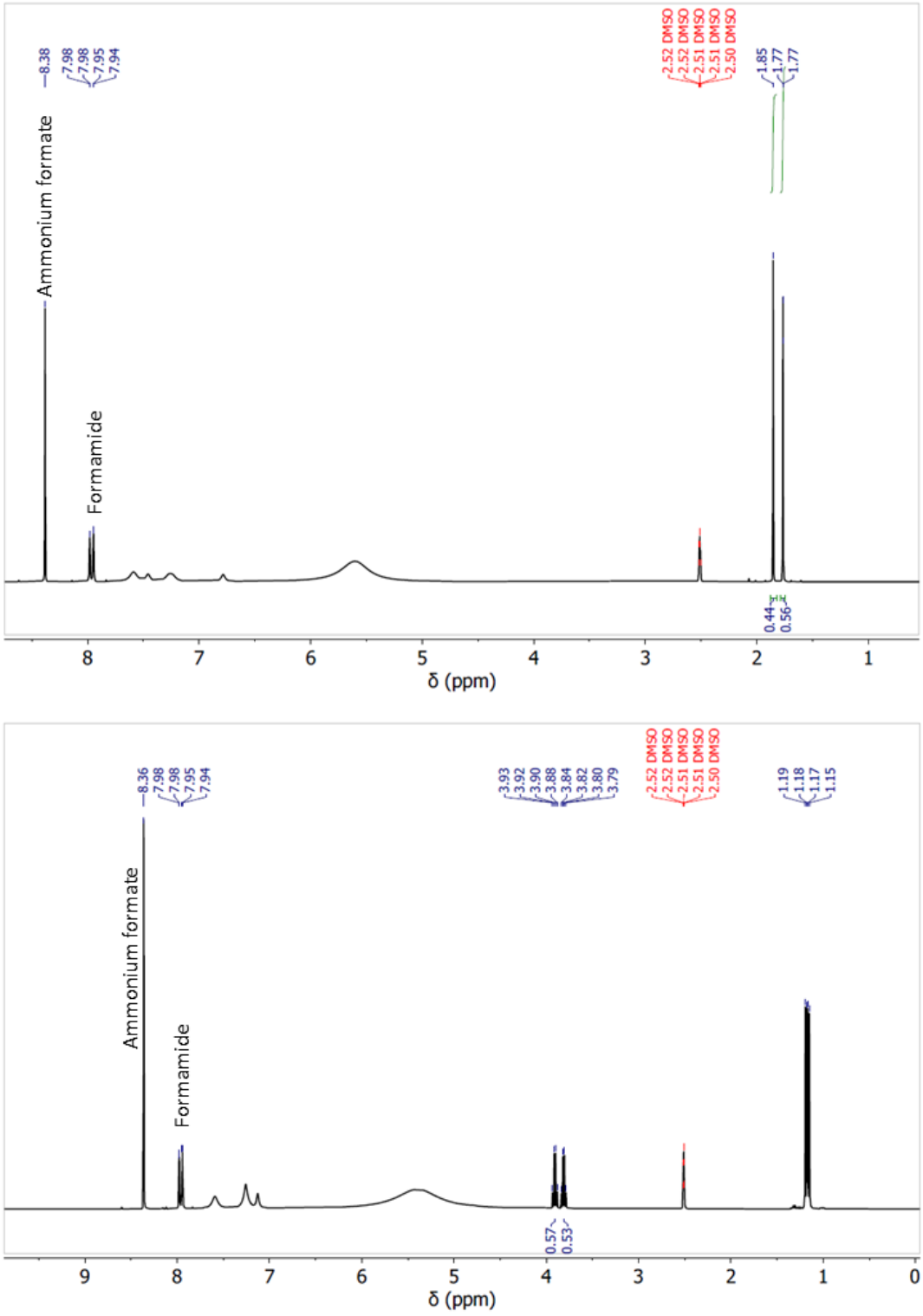

Figure S34: ^{1}H NMR in DMSO-d_6 of AcAc-n (top) and LacAc (bottom) after 2hours at 160°C. Product identification of LvAc based REM can be seen in Figure S31.

Acetic acid: ^{1}H NMR (400 MHz, DMSO) δ 1.85 (s, 1H).

Acetic amide: ^{1}H NMR (400 MHz, DMSO) δ 1.77 (s, 1H).

Lactic acid: ^{1}H NMR (400 MHz, DMSO) δ 3.91 (q, 1H), δ 1.17 (dd, 3H).

Lactamide: ^{1}H NMR (400 MHz, DMSO) δ 3.81 (q, 1H), δ 1.17 (dd, 3H).

S4.2. HSQC NMR of lignin samples

Table S4: Assignment of main Lignin ^{13}C–^{1}H Cross-Signals in the HSQC Spectra,

	δC/δH	**Assignment**
-OMe	56.7/3.7	C–H in methoxyls
β-O-4α	60.7/3.4	C_α–H_α in β-O-4 substructures
β-O-4β (H/G)	83.4/4.3	C_β–H_β in β-*O*-4 substructures linked to G and H units
β-O-4β (S)	85.6/4.1	C_β–H_β in β-*O*-4 substructures linked to S units
β-O-4γ	72.1/4.9	C_γ–H_γ in β-O-4 substructures
β'-O-4α	`81.6/4.5	C_α–H_α in β′-O-4 substructures (OEt instead of OH)
β-5α	87.4/5.5	C_α–H_α in phenylcoumaran substructures
β-5β	54.8/2.9	C_β–H_β in phenylcoumaran substructures
β-5γ	63.2/3.7	C_β–H_β in phenylcoumaran substructures
β-βα	85.1/4.6	C_α–H_α in resinol substructures
β-ββ	54.4/3.0	C_β–H_β in resinol substructures
β-βγ	71.3/4.2 and 3.8	C_γ–H_γ in resinol substructures
$S_{2,6}$	104.9/6.6	$C_{2,6}$–$H_{2,6}$ in syringyl units
$S_{2,6'}$	106.5/7.1	$C_{2,6}$–$H_{2,6}$ in oxidized (Cα=O) syringyl units
G_2	111.6/6.9	C_2–H_2 in guaiacyl units
G_5	115.5/6.7	C_5–H_5 in guaiacyl units
G_6	119.9/6.7	C_6–H_6 in guaiacyl units
$H_{2/6}$	126.6/7.0	$C_{2,6}$–$H_{2,6}$ in *p*-hydroxyphenyl units
Aldimine	161.4/8.1	Cα–Hα aldimine groups

The integrated signals were processed according to the following equations:

$$\text{total aromatic} = (S_{2/6} + S'_{2/6})/ 2 + (G_2 + G_5 + G_6 - H_{2/6}) / 3 + H_{2/6} / 2 \quad (S5)$$

$$\text{Ratio S} = 100 * ((S_{2/6} + S'_{2/6})/ 2) / \text{total aromatic} \quad (S6)$$

$$\text{Ratio G} = 100 * ((G_2 + G_5 + G_6 - H_{2/6}) / 3) / \text{total aromatic} \quad (S7)$$

The total number of linkages per 100 C9 units were all based on the signals of the α proton of the linkages. They were based on the following equations:

$$\beta\text{-O-4 linkages}/100\ \text{C9 units} = 100^{*}\ (\beta\text{-O-4}_{\alpha} + \beta'\text{-O-4}_{\alpha}) / \text{total aromatic} \quad (S8)$$

$$\beta\text{-5 linkages}/100\ \text{C9 units} = 100^{*}\ \beta\text{-5}_{\alpha} / \text{total aromatic} \quad (S9)$$

$$\beta\text{-}\beta\ \text{linkages}/100\ \text{C9 units} = 100^{*}\ \beta\text{-}\beta_{\alpha} / \text{total aromatic} \quad (S10)$$

$$\text{aldimines}/100\ \text{C9 units} = 100^{*}\ \text{aldimine} / \text{total aromatic}$$

Table S5: Integration results of main Lignin ^{13}C–^{1}H Cross-Signals in the HSQC Spectra,

	Organosolv	Le-n	Le-PG	Lac-PG	Lac-EG	Ac-PG	AC-EG
-OMe	24.71	26.16	37.65	94.95	48.29	48.43	39.06
β-O-4α	1.02	0.92	0.98	1.42	0.99	0.98	0.99
β-O-4β (H/G)	0.28	0.32	0.13	0.51	0.67	0.48	0.63
β-O-4β (S)	0.77	0.64	0.54	1.08	0.69	0.87	1.21
β-O-4γ	0.96	1.83	1.89	4.46	6.45	2.42	5.48
	0.33						
β-5α	0.24	0.06	0	0.12	0.18	0.03	0.04
β-5β	0.29						
β-5γ	0.68	0.20		0.33	0.39		
β-βα	0.35	0.35	0.49	1.25	0.73	0.79	0.63
β-ββ	0.41	0.39	0.52	1.63	0.83	0.9	0.8
β-βγ	0.64	0.5	1.2	2.34	1.36	1.3	1
S2,6	5.85	6.93	10.24	26.5	12.92	13.12	10.33
S2,6'	0.54						
G2	1.62	2.14	3.05	7.99	3.22	4.49	3.07
G5	1.84	2.3	3.23	8.35	4.42	4.21	3.42
G6	1.13	1.92	2.41	6.96	3.42	3.77	2.45
H2/6	0.09	0.03	0	0	0	0	0
Aldimine	0	1.09	1.06	4.19	1.97	2.22	1.58
Total aromatic	4.74	5.59	8.02	21.02	10.15	10.72	8.15
S(%)	67.4	62.0	63.9	63.0	63.7	61.2	63.4
G(%)	31.6	37.7	36.1	37.0	36.3	38.8	36.6
H(%)	0.9	0.3	0.0	0.0	0.0	0.0	0.0
β-O-4 linkages	28.5	16.5	12.2	6.8	9.8	9.1	12.2
β-β linkages	7.4	6.3	6.1	5.9	7.2	7.4	7.7
β-5 linkages	5.1						
Aldimine	0.0	19.5	13.2	19.9	19.4	20.7	19.4
-OMe	173.8	156.0	156.5	150.6	158.6	150.6	159.9

S5. The reaction with citric acid for the synthesis of an oligocitrazinic acid dye

S5.1. Synthesis in reactive eutectic mixture

DSC of REM, heated to different temperatures

Differential scanning calorimetry (DSC) of the mixture in the temperature range from -80 to +80 °C supports the formation of a one phase with the glass transition at -37.1 °C, bringing this system into the category of deep eutectics. Reaction mixtures, prepared at different reaction temperatures, indicate the change in composition.

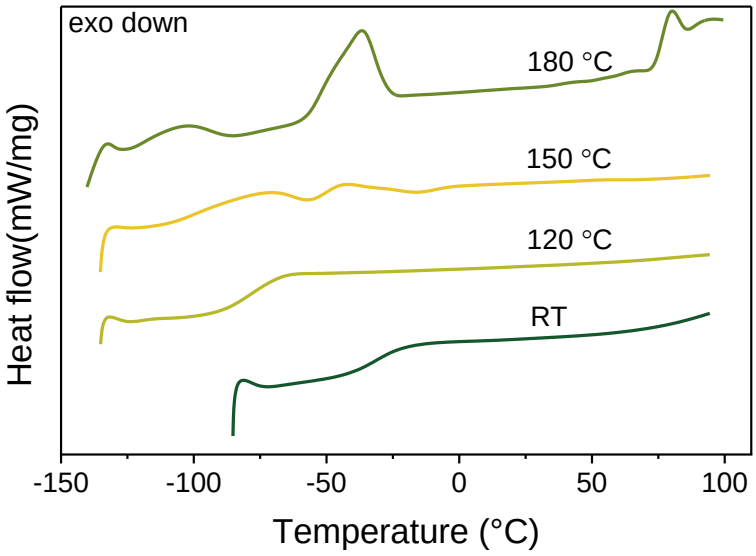

Figure S35: Differential scanning calorimetry (DSC) of the reactive eutectic mixture of ammonium formate and citric acid (2:1) at room temperature as well as after heating to different temperatures.

Synthesis in solution

While reaction in water does result in a different reaction pathway, reaction in ethylene glycol shows traces of the relevant product (indicated by the absorption maximum at 560nm). However, as shown by the reaction kinetics, selectivity is low.

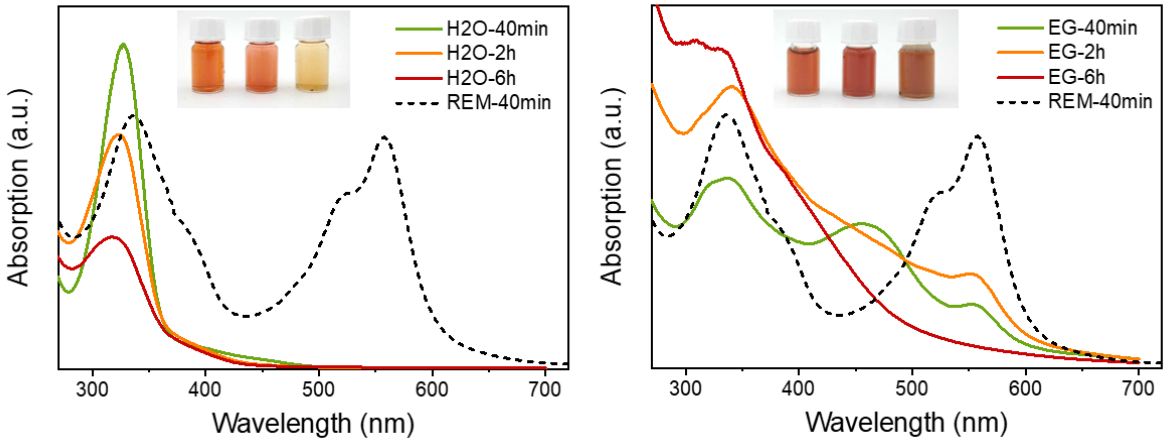

*Figure S36: UV-vis spectra of the reaction kinetics for the synthesis **in solvent** (left in water and right in ethylene glycol). The synthesis is performed in a microwave oven at 180°C.*

S5.2. Characterization of purified product

TEM

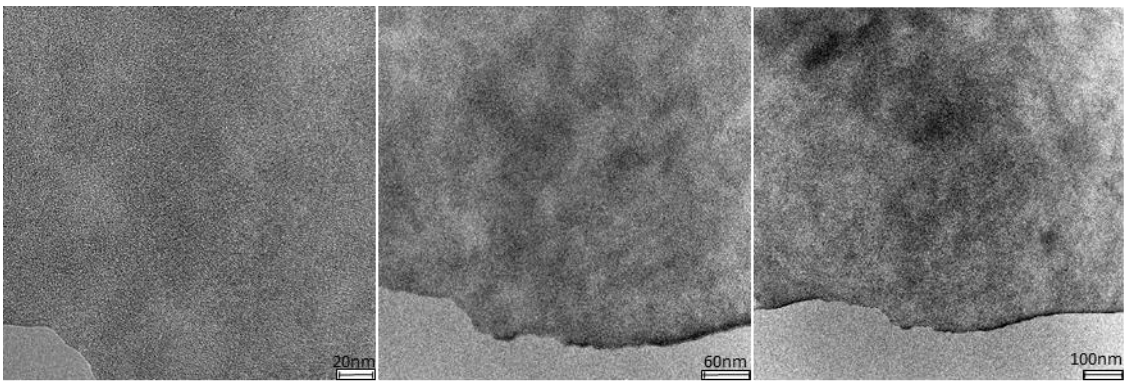

Figure S37: TEM images of purified oligo-CzA

EPR spectroscopy

Table S6: Concentration of unpaired electrons in oligo-CzA, measured over time in duplicate.

Sample	**mmol of spins/ g**			
	day 0	day 5	day 15	day 30
Sample1	0.0027	0.0038	0.0045	
Sample2	0.0026	0.0035	0.0041	0.0075

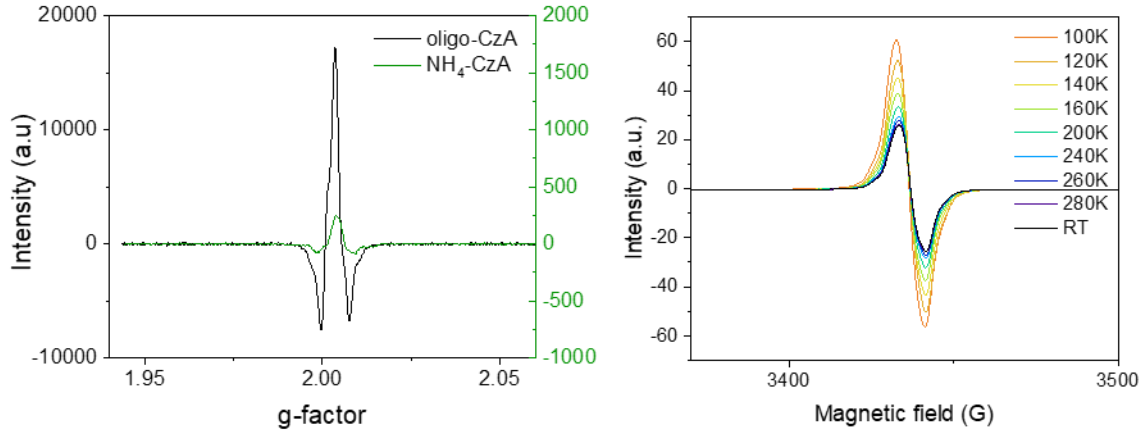

Figure S38: (left) g-factor for oligo-CzA as well as for NH_4-CzA; (right) variable temperature EPR for oligo-CzA

Variations of oligo-CzA

Synthesis in excess of AF: The reaction mixture is prepared with a molar ratio of 4:1 ammonium formate to CA. The remaining synthesis and purification procedure is the same.

Treatment with alkali salt: The purified oligo-CzA product is dissolved in NaOH or KOH solution, giving a pH around 11.5 and stirred overnight. The solution is neutralized with HCl and concentrated in the rotary evaporator. The product is precipitated with ethanol, washed several times, and dried in the vacuum oven at 40 °C overnight.

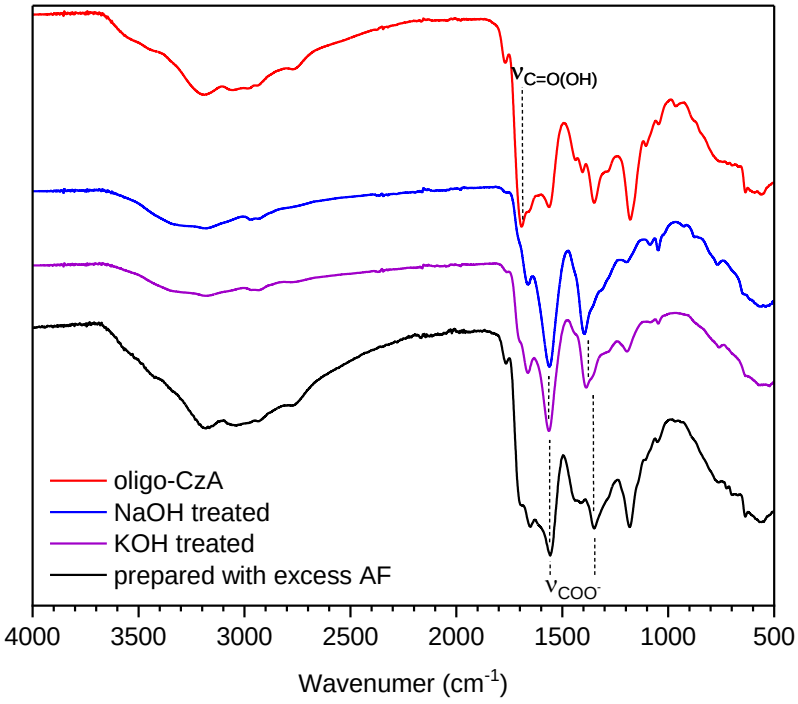

Figure S39: ATR-FTIR of oligo-CzA as well as alkali salt treated oligo-CzA and prepared with an excess of AF.

Semi-preparative HPLC

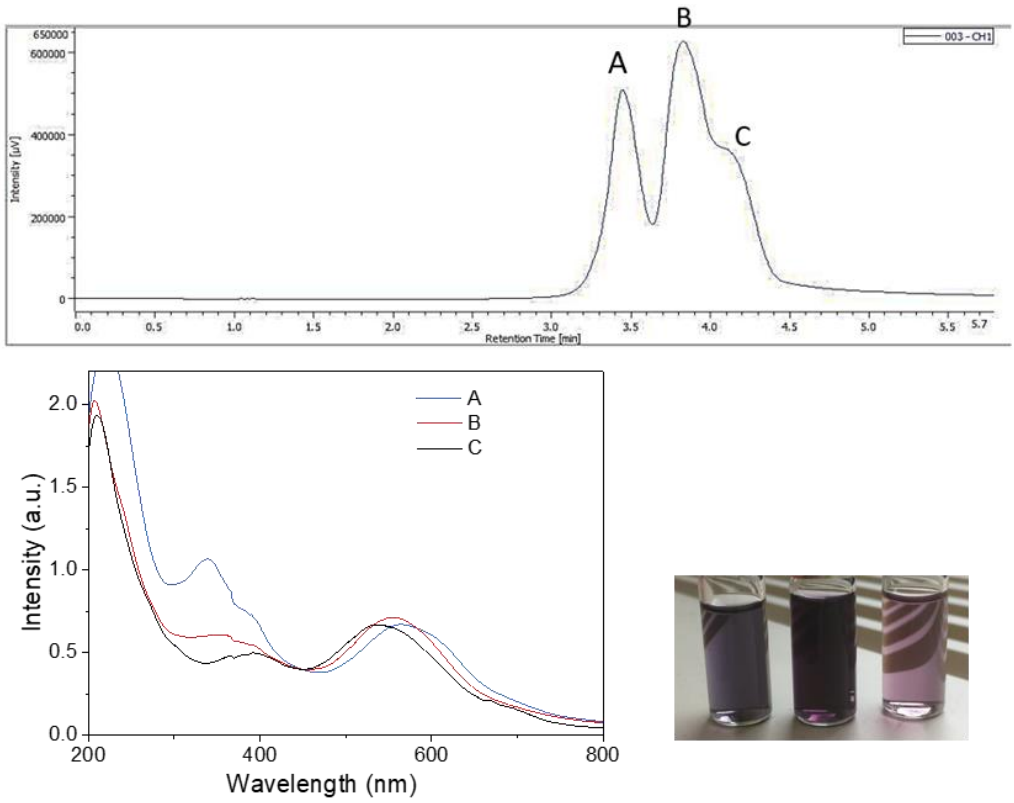

Figure S40: Semi-preparative HPLC of freshly prepared oligo-CzA. Separation is performed on a C18 column (ACE 5, C18 250x21.2) with a flow rate of 15 mL min^{-1}, a detection wavelength of 335 nm and a mobile phase consisting of 30% water and 70% methanol. The separated fractions are afterwards analysed with UV-vis spectroscopy.

Ammonia test

Ammonium ions can be detected in the purified product. This is done by the addition of concentrated sodium hydroxide solution onto a small portion of oligo-CzA powder. The consequential colour change of pH paper above the solution indicates the presence of released ammonia. The presence of ammonium ions in the material means, that we are dealing with an anionic dye where the ammonium ion represents the counter cation.

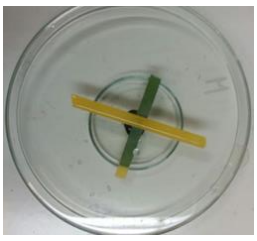

Figure S41. Positive ammonia test performed on oligo-CzA

XRD

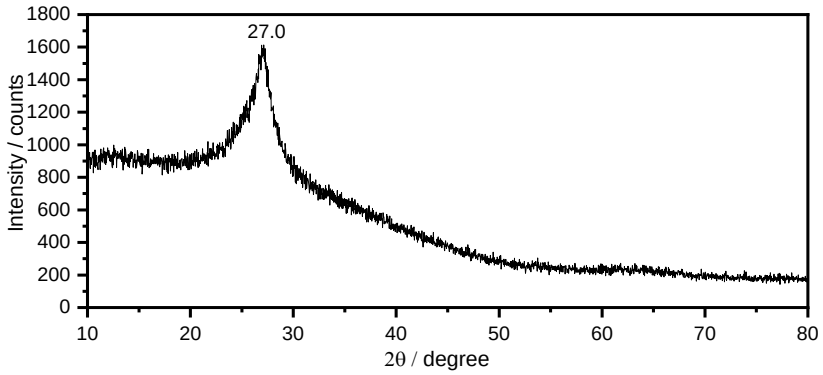

Figure S42: XRD of the precipitate formed after the colloid aging

UV-vis spectra of the dialysate

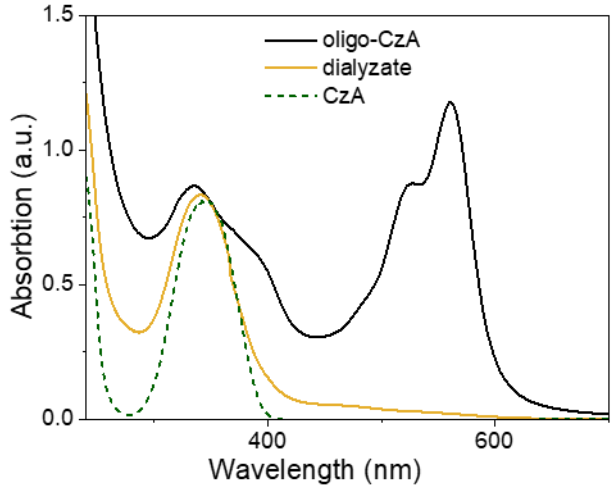

*Figure S43: Absorption spectrum of the dialysate from **oligo-CzA** (using a molecular weight cut-off of 1000 Da) compared to the absorption spectra of **oligo-CzA** as well as CzA. Note that the UV-vis spectra are recorded in ammonia water since CzA as well as the dried dialysate are not soluble in pure water. However, the prior dialysis is performed in pure water.*

Fluorescence Stokes shift

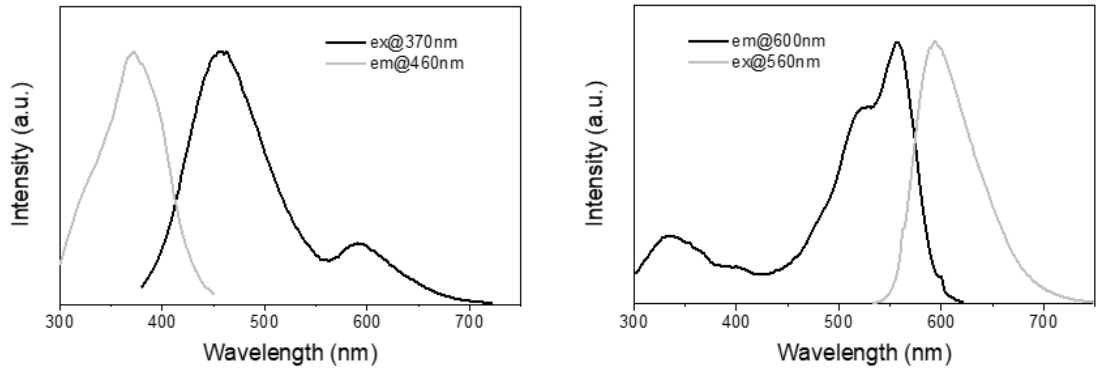

Figure S44: Stokes shift for ***oligo-CzA*** *in ammonia water*

Fluorescence decay

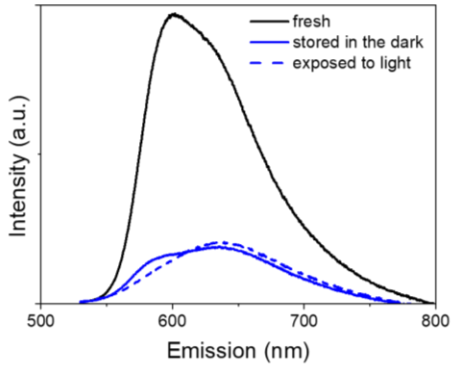

Figure S45: Emission spectra of ***oligo-CzA*** *in water for excitation at 520 nm, freshly prepared and after 90 min. stored in the dark as well as under light exposure.*

Fluorescence quantum yields

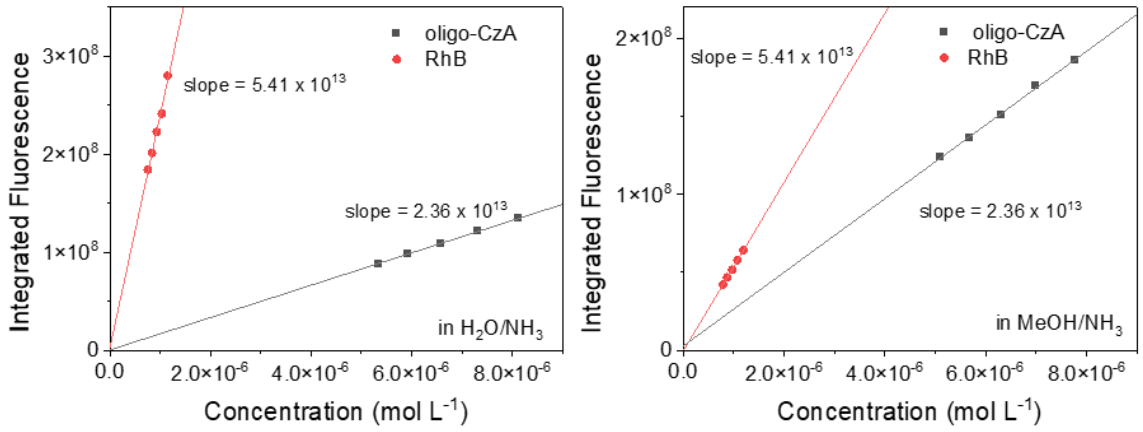

Figure S46: Determination of the fluorescence quantum yields of ***oligo-CzA,*** *using Rhodamine B as standard, in ammonia water or in ammonia in methanol.*

List of abbreviations

5MP	5-methyl-2-pyrrolidone
AcAc	Acetic acid
APT	Attached proton test
COSY	Correlation spectroscopy
DEPT	Distortionless enhancement by polarization
DES	Deep eutectic solvent
DOF	Deoxyfructosazine
DOFu	Deoxyfucosazine
DOR	Deoxyrhamnosazine
DSC	Differential scanning calorimetry
EG	Ethylene glycol
EPR	Electron paramagnetic resonance
FTIR	Fourier-transform infrared spectroscopy
FZ	Fructosazine
GC-MS	Gas chromatography – mass spectrometry
GPC	Gel permeation chromatography
HBA	Hydrogen bond acceptor
HBD	Hydrogen bond donor
HPLC-MS	High performance liquid chromatography - mass spectrometry
HMBC	Heteronuclear multiple bond correlation
HSQC	Heteronuclear single quantum coherence
ICP-OES	Inductively Coupled Plasma Optical Emission spectroscopy
LacAc	Lactic acid
LMM	Low melting mixtures
LvAc	Levulinic acid
MALDI-TOF	Matrix assisted laser desorption ionization - time of flight
NADES	Natural deep eutectic solvents
NMP	N-vinyl-2-pyrrolidone
NMR	Nuclear-magnetic resonance
PG	Propylene glycol
PVP	Polyvinylpyrrolidone
PXRD	Powder X-ray diffraction
REM	Reactive eutectic media
SEM	Scanning electron microscopy

SI	Supplementary information
TEM	Transmission electron microscopy
UV-vis	Ultraviolet-visible
XPS	X-ray photoelectron spectroscopy

References

1. Abbott, A. P., Boothby, D., Capper, G., Davies, D. L. & Rasheed, R. K. Deep Eutectic Solvents formed between choline chloride and carboxylic acids: Versatile alternatives to ionic liquids. *J. Am. Chem. Soc.* **126**, 9142–9147 (2004).

2. Gawande, M. B., Bonifácio, V. D. B., Luque, R., Branco, P. S. & Varma, R. S. Solvent-Free and Catalysts-Free Chemistry: A Benign Pathway to Sustainability. *ChemSusChem* **7**, 24–44 (2014).

3. Loupy, A. Solvent-free microwave organic synthesis as an efficient procedure for green chemistry. *Comptes Rendus Chim.* **7**, 103–112 (2004).

4. Chauvier, C. & Cantat, T. A Viewpoint on Chemical Reductions of Carbon-Oxygen Bonds in Renewable Feedstocks Including CO2 and Biomass. *ACS Catal.* **7**, 2107–2115 (2017).

5. Kani, N. C., Prajapati, A., Collins, B. A., Goodpaster, J. D. & Singh, M. R. Competing Effects of pH, Cation Identity, H2O Saturation, and N2 Concentration on the Activity and Selectivity of Electrochemical Reduction of N2 to NH3 on Electrodeposited Cu at Ambient Conditions. *ACS Catal.* **10**, 14592–14603 (2020).

6. Ojo, G. & Camarda, K. Sustainable Ammonia Production via Electrolysis and Haber-Bosch Process. in *32 European Symposium on Computer Aided Process Engineering* (eds. Montastruc, L. & Negny, S. B. T.-C. A. C. E.) vol. 51 229–234 (Elsevier, 2022).

7. Abranches, D. O., Silva, L. P., Martins, M. A. R., Pinho, S. P. & Coutinho, J. A. P. Understanding the Formation of Deep Eutectic Solvents: Betaine as a Universal Hydrogen Bond Acceptor. *ChemSusChem* **13**, 4916–4921 (2020).

8. van Osch, D. J. G. P., Dietz, C. H. J. T., Warrag, S. E. E. & Kroon, M. C. The Curious Case of Hydrophobic Deep Eutectic Solvents: A Story on the Discovery, Design, and Applications. *ACS Sustain. Chem. Eng.* **8**, 10591–10612 (2020).

9. Smith, E. L., Abbott, A. P. & Ryder, K. S. Deep Eutectic Solvents (DESs) and Their Applications. *Chem. Rev.* **114**, 11060–11082 (2014).

10. Hansen, B. B . *et al.* Deep Eutectic Solvents: A Review of Fundamentals and Applications. *Chem. Rev.* **121**, 1232–1285 (2021).

11. Ashworth, C. R., Matthews, R. P., Welton, T. & Hunt, P. A. Doubly ionic hydrogen bond interactions within the choline chloride–urea deep eutectic solvent. *Phys. Chem. Chem. Phys.* **18**, 18145–18160 (2016).

12. Hayler, H. J. & Perkin, S. The eutectic point in choline chloride and ethylene glycol mixtures. *Chem. Commun.* **58**, 12728–12731 (2022).

13. Kollau, L. J. B. M., Vis, M., van den Bruinhorst, A., Esteves, A. C. C. & Tuinier, R. Quantification of the liquid window of deep eutectic solvents. *Chem. Commun.* **54**, 13351–

13354 (2018).

14. Martins, M. A. R., Pinho, S. P. & Coutinho, J. A. P. Insights into the Nature of Eutectic and Deep Eutectic Mixtures. *J. Solution Chem.* **48**, 962–982 (2019).

15. Radošević, K. *et al.* Evaluation of toxicity and biodegradability of choline chloride based deep eutectic solvents. *Ecotoxicol. Environ. Saf.* **112**, 46–53 (2015).

16. Juneidi, I., Hayyan, M. & Mohd Ali, O. Toxicity profile of choline chloride-based deep eutectic solvents for fungi and Cyprinus carpio fish. *Environ. Sci. Pollut. Res.* **23**, 7648–7659 (2016).

17. Halder, A. K. & Cordeiro, M. N. D. S. Probing the Environmental Toxicity of Deep Eutectic Solvents and Their Components: An In Silico Modeling Approach. *ACS Sustain. Chem. Eng.* **7**, 10649–10660 (2019).

18. Yu, D., Xue, Z. & Mu, T. Deep eutectic solvents as a green toolbox for synthesis. *Cell Reports Phys. Sci.* **3**, 100809 (2022).

19. Posada, E. *et al.* Reline aqueous solutions behaving as liquid mixtures of H-bonded co-solvents: Microphase segregation and formation of co-continuous structures as indicated by Brillouin and 1H NMR spectroscopies. *Phys. Chem. Chem. Phys.* **19**, 17103–17110 (2017).

20. López-Salas, N. *et al.* Further Extending the Dilution Range of the “Solvent-in-DES” Regime upon the Replacement of Water by an Organic Solvent with Hydrogen Bond Capabilities. *ACS Sustain. Chem. & Eng.* **8**, 12120–12131 (2020).

21. López-Salas, N. *et al.* Looking at the ‘water-in-Deep-Eutectic-Solvent’ System: A Dilution Range for High Performance Eutectics. *ACS Sustain. Chem. Eng.* **7**, 17565–17573 (2019).

22. Smith, P. J., Arroyo, C. B., Lopez Hernandez, F. & Goeltz, J. C. Ternary Deep Eutectic Solvent Behavior of Water and Urea Choline Chloride Mixtures. *J. Phys. Chem. B* **123**, 5302–5306 (2019).

23. Sharepour, F., Bakhshi, H. & Rahimnejad, M. Separation of ethanol azeotropic mixture using deep eutectic solvents in liquid- liquid extraction process. *J. Mol. Liq.* **338**, 116637 (2021).

24. Oliveira, F. S., Pereiro, A. B., Rebelo, L. P. N. & Marrucho, I. M. Deep eutectic solvents as extraction media for azeotropic mixtures. *Green Chem.* **15**, 1326–1330 (2013).

25. Neubauer, M., Wallek, T. & Lux, S. Deep eutectic solvents as entrainers in extractive distillation – A review. *Chem. Eng. Res. Des.* **184**, 402–418 (2022).

26. Yuan, Z., Liu, H., Yong, W. F., She, Q. & Esteban, J. Status and advances of deep eutectic solvents for metal separation and recovery. *Green Chem.* **24**, 1895–1929 (2022).

27. Tang, S., Zhang, M. & Guo, M. A Novel Deep-Eutectic Solvent with Strong Coordination Ability and Low Viscosity for Efficient Extraction of Valuable Metals from Spent Lithium-

Ion Batteries. *ACS Sustain. Chem. Eng.* **10**, 975–985 (2022).

28. Kozhevnikova, A. V., Zinov'eva, I. V., Zakhodyaeva, Y. A., Baranovskaya, V. B. & Voshkin, A. A. Application of Hydrophobic Deep Eutectic Solvents in Extraction of Metals from Real Solutions Obtained by Leaching Cathodes from End-of-Life Li-Ion Batteries. *Processes* **10**, (2022).

29. Duan, L., Dou, L.-L., Guo, L., Li, P. & Liu, E.-H. Comprehensive Evaluation of Deep Eutectic Solvents in Extraction of Bioactive Natural Products. *ACS Sustain. Chem. Eng.* **4**, 2405–2411 (2016).

30. Kalyniukova, A. *et al.* Application of deep eutectic solvents for separation and determination of bioactive compounds in medicinal plants. *Ind. Crops Prod.* **172**, 114047 (2021).

31. Grozdanova, T. *et al.* Extracts of medicinal plants with natural deep eutectic solvents: enhanced antimicrobial activity and low genotoxicity. *BMC Chem.* **14**, 1–9 (2020).

32. Dai, Y., van Spronsen, J., Witkamp, G.-J., Verpoorte, R. & Choi, Y. H. Ionic Liquids and Deep Eutectic Solvents in Natural Products Research: Mixtures of Solids as Extraction Solvents. *J. Nat. Prod.* **76**, 2162–2173 (2013).

33. Pal Chowdhury, M., Makarewicz, C., Piezonka, H. & Buckley, M. Novel Deep Eutectic Solvent-Based Protein Extraction Method for Pottery Residues and Archeological Implications. *J. Proteome Res.* **21**, 2619–2634 (2022).

34. Bowen, H. *et al.* Application of deep eutectic solvents in protein extraction and purification. *Front. Chem.* **10**, 912411 (2022).

35. Meng, J. *et al.* Development of different deep eutectic solvent aqueous biphasic systems for the separation of proteins. *RSC Adv.* **9**, 14116–14125 (2019).

36. Martins, M. A. R. *et al.* Tunable Hydrophobic Eutectic Solvents Based on Terpenes and Monocarboxylic Acids. *ACS Sustain. Chem. Eng.* **6**, 8836–8846 (2018).

37. Song, Z. *et al.* Systematic Screening of Deep Eutectic Solvents as Sustainable Separation Media Exemplified by the CO2 Capture Process. *ACS Sustain. Chem. Eng.* **8**, 8741–8751 (2020).

38. Karami, B., Ghaemi, A. & Shahhosseini, S. Eco-Friendly Deep Eutectic Solvents Blended with Diethanolamine Solution for Postcombustion CO2 Capture. *Energy & Fuels* **36**, 945–957 (2022).

39. Kalhor, P. & Ghandi, K. Deep Eutectic Solvents for Pretreatment, Extraction, and Catalysis of Biomass and Food Waste. *Molecules* **24**, (2019).

40. Liu, Y. *et al.* Tunable and functional deep eutectic solvents for lignocellulose valorization. *Nat. Commun.* **12**, 1–15 (2021).

41. Xia, Q. *et al.* Multiple hydrogen bond coordination in three-constituent deep eutectic

solvents enhances lignin fractionation from biomass. *Green Chem.* **20**, 2711–2721 (2018).

42. Luo, T. *et al.* Innovative production of lignin nanoparticles using deep eutectic solvents for multifunctional nanocomposites. *Int. J. Biol. Macromol.* **183**, 781–789 (2021).

43. Jančíková, V. & Jablonský, M. The role of deep eutectic solvents in the production of cellulose nanomaterials from biomass. *Acta Chim. Slovaca* **15**, 61–71 (2022).

44. Choi, Y. H. *et al.* Are natural deep eutectic solvents the missing link in understanding cellular metabolism and physiology? *Plant Physiol.* **156**, 1701–1705 (2011).

45. Alcalde, R., Gutiérrez, A., Atilhan, M. & Aparicio, S. An experimental and theoretical investigation of the physicochemical properties on choline chloride – Lactic acid based natural deep eutectic solvent (NADES). *J. Mol. Liq.* **290**, 110916 (2019).

46. Craveiro, R., Mano, F., Paiva, A. & Duarte, A. R. C. Deep eutectic solvents: Exploring their role in nature. *Deep Eutectic Solvents Synth. Prop. Appl.* 95–110 (2019) doi:10.1002/9783527818488.ch6.

47. Aroso, I. M. *et al.* Dissolution enhancement of active pharmaceutical ingredients by therapeutic deep eutectic systems. *Eur. J. Pharm. Biopharm.* **98**, 57–66 (2016).

48. Hessel, V. *et al.* Sustainability of green solvents-review and perspective. *Green Chem.* **24**, 410–437 (2022).

49. Morrison, H. G., Sun, C. C. & Neervannan, S. Characterization of thermal behavior of deep eutectic solvents and their potential as drug solubilization vehicles. *Int. J. Pharm.* **378**, 136–139 (2009).

50. Lu, C., Cao, J., Wang, N. & Su, E. Significantly improving the solubility of non-steroidal anti-inflammatory drugs in deep eutectic solvents for potential non-aqueous liquid administration. *Medchemcomm* **7**, 955–959 (2016).

51. Hikmawanti, N. P., Ramadon, D., Jantan, I. & Mun'im, A. Natural Deep Eutectic Solvents (NADES): Phytochemical Extraction Performance Enhancer for Pharmaceutical and Nutraceutical Product Development. *Plants* vol. 10 (2021).

52. Dai, Y., Choi, Y. H. & Verpoorte, R. Chapter Fourteen - Honey in traditional Chinese medicine: A guide to future applications of NADES to medicines. in *Eutectic Solvents and Stress in Plants* (eds. Verpoorte, R., Witkamp, G.-J. & Choi, Y. H. B. T.-A. in B. R.) vol. 97 361–384 (Academic Press, 2021).

53. Dimitriu, L. *et al.* Honey and Its Biomimetic Deep Eutectic Solvent Modulate the Antioxidant Activity of Polyphenols. *Antioxidants* **11**, 2194 (2022).

54. Abbott, A. P., Capper, G., Davies, D. L. & Rasheed, R. Ionic liquids based upon metal halide/substituted quaternary ammonium salt mixtures. *Inorg. Chem.* **43**, 3447–3452 (2004).

55. Figueiredo, M. *et al.* Differential capacity of a deep eutectic solvent based on choline

chloride and glycerol on solid electrodes. *Electrochim. Acta* **54**, 2630–2634 (2009).

56. Abbott, A. P., El Ttaib, K., Frisch, G., McKenzie, K. J. & Ryder, K. S. Electrodeposition of copper composites from deep eutectic solvents based on choline chloride. *Phys. Chem. Chem. Phys.* **11**, 4269–4277 (2009).

57. Abbott, A. P., Capper, G., McKenzie, K. J. & Ryder, K. S. Electrodeposition of zinc–tin alloys from deep eutectic solvents based on choline chloride. *J. Electroanal. Chem.* **599**, 288–294 (2007).

58. Abbott, A. P., Capper, G., McKenzie, K. J. & Ryder, K. S. Voltammetric and impedance studies of the electropolishing of type 316 stainless steel in a choline chloride based ionic liquid. *Electrochim. Acta* **51**, 4420–4425 (2006).

59. Abbott, A. P., Capper, G., Swain, B. G. & Wheeler, D. A. Electropolishing of stainless steel in an ionic liquid. *Trans. IMF* **83**, 51–53 (2005).

60. Zhang, C., Zhang, L. & Yu, G. Eutectic Electrolytes as a Promising Platform for Next-Generation Electrochemical Energy Storage. *Acc. Chem. Res.* **53**, 1648–1659 (2020).

61. Tran, M. K., Rodrigues, M.-T. F., Kato, K., Babu, G. & Ajayan, P. M. Deep eutectic solvents for cathode recycling of Li-ion batteries. *Nat. Energy* **4**, 339–345 (2019).

62. Hammond, O. S., Edler, K. J., Bowron, D. T. & Torrente-Murciano, L. Deep eutectic-solvothermal synthesis of nanostructured ceria. *Nat. Commun.* **8**, 1–7 (2017).

63. Jhang, P. C., Chuang, N. T. & Wang, S. L. Layered zinc phosphates with photoluminescence and photochromism: Chemistry in deep eutectic solvents. *Angew. Chemie - Int. Ed.* **49**, 4200–4204 (2010).

64. Parnham, E. R., Drylie, E. A., Wheatley, P. S., Slawin, A. M. Z. & Morris, R. E. Ionothermal Materials Synthesis Using Unstable Deep-Eutectic Solvents as Template-Delivery Agents. *Angew. Chemie* **118**, 5084–5088 (2006).

65. Srivastava, S. Knoevenagel Condensation and Michael Addition in Bio-Renewable Deep Eutectic Solvent: Facile Synthesis of a Library of Bis-enol Derivatives. *ChemistrySelect* **5**, 799–803 (2020).

66. Pelliccioli, V. *et al.* Ligand-Free Suzuki–Miyaura Cross-Coupling Reactions in Deep Eutectic Solvents: Synthesis of Benzodithiophene Derivatives and Study of their Optical and Electrochemical Performance. *European J. Org. Chem.* **2020**, 6981–6988 (2020).

67. Cicco, L., Rodríguez-Álvarez, M. J., Perna, F. M., García-Álvarez, J. & Capriati, V. One-pot sustainable synthesis of tertiary alcohols by combining ruthenium-catalysed isomerisation of allylic alcohols and chemoselective addition of polar organometallic reagents in deep eutectic solvents. *Green Chem.* **19**, 3069–3077 (2017).

68. Cicco, L. *et al.* Programming cascade reactions interfacing biocatalysis with transition-metal catalysis in: Deep Eutectic Solvents as biorenewable reaction media. *Green Chem.* **20**, 3468–3475 (2018).

69. Ñíguez, D. R., Guillena, G. & Alonso, D. A. Chiral 2-Aminobenzimidazoles in Deep Eutectic Mixtures: Recyclable Organocatalysts for the Enantioselective Michael Addition of 1,3-Dicarbonyl Compounds to β-Nitroalkenes. *ACS Sustain. Chem. Eng.* **5**, 10649–10656 (2017).

70. Vidal, C., García-Álvarez, J., Hernán-Gõmez, A., Kennedy, A. R. & Hevia, E. Introducing deep eutectic solvents to polar organometallic chemistry: Chemoselective addition of organolithium and grignard reagents to ketones in air. *Angew. Chemie - Int. Ed.* **53**, 5969–5973 (2014).

71. Vadagaonkar, K. S., Kalmode, H. P., Prakash, S. & Chaskar, A. C. Greener [3+3] tandem annulation–oxidation approach towards the synthesis of substituted pyrimidines. *New J. Chem.* **39**, 3639–3645 (2015).

72. Vitale, P. *et al.* Streamlined Routes to Phenacyl Azides and 2,5-Diarylpyrazines Enabled by Deep Eutectic Solvents. *European J. Org. Chem.* **2019**, 5557–5562 (2019).

73. Ghosh, S. K. & Nagarajan, R. Deep eutectic solvent mediated synthesis of quinazolinones and dihydroquinazolinones: synthesis of natural products and drugs. *RSC Adv.* **6**, 27378–27387 (2016).

74. Kalmode, H. P., Vadagaonkar, K. S., Murugan, K., Prakash, S. & Chaskar, A. C. Deep eutectic solvent: a simple{,} environmentally benign reaction media for regioselective synthesis of 2{,}3{,}4-trisubstituted 1H-pyrroles. *RSC Adv.* **5**, 35166–35174 (2015).

75. Liu, F. *et al.* Catalytic deep eutectic solvents for highly efficient conversion of cellulose to gluconic acid with gluconic acid self-precipitation separation. *Chem. Commun.* **54**, 6140–6143 (2018).

76. Guajardo, N., Carlesi, C. & Aracena, Á. Toluene Oxidation by Hydrogen Peroxide in Deep Eutectic Solvents. *ChemCatChem* **7**, 2451–2454 (2015).

77. Lu, J., Li, X.-T., Ma, E.-Q., Mo, L.-P. & Zhang, Z.-H. Superparamagnetic CuFeO2 Nanoparticles in Deep Eutectic Solvent: an Efficient and Recyclable Catalytic System for the Synthesis of Imidazo[1,2-a]pyridines. *ChemCatChem* **6**, 2854–2859 (2014).

78. Marset, X., Pérez, J. M. & Ramón, D. J. Cross-dehydrogenative coupling reaction using copper oxide impregnated on magnetite in deep eutectic solvents. *Green Chem.* **18**, 826–833 (2016).

79. Guajardo, N. *et al.* Water as Cosolvent: Nonviscous Deep Eutectic Solvents for Efficient Lipase-Catalyzed Esterifications. *ChemCatChem* **9**, 1393–1396 (2017).

80. Gorke, J. T., Srienc, F. & Kazlauskas, R. J. Hydrolase-catalyzed biotransformations in deep eutectic solvents. *Chem. Commun.* 1235–1237 (2008) doi:10.1039/B716317G.

81. Carriazo, D., Gutiérrez, M. C., Ferrer, M. L. & del Monte, F. Resorcinol-Based Deep Eutectic Solvents as Both Carbonaceous Precursors and Templating Agents in the Synthesis of Hierarchical Porous Carbon Monoliths. *Chem. Mater.* **22**, 6146–6152 (2010).

82. Isik, M. *et al.* Innovative Poly (Ionic Liquid) s by the Polymerization of Deep Eutectic

Monomers. 1135–1142.

83. Mota-Morales, J. D. *et al.* Free-radical polymerizations of and in deep eutectic solvents: Green synthesis of functional materials. *Prog. Polym. Sci.* **78**, 139–153 (2018).

84. Pérez-García, M. G., Gutiérrez, M. C., Mota-Morales, J. D., Luna-Bárcenas, G. & del Monte, F. Synthesis of Biodegradable Macroporous Poly(l-lactide)/Poly(ε-caprolactone) Blend Using Oil-in-Eutectic-Mixture High-Internal-Phase Emulsions as Template. *ACS Appl. Mater. Interfaces* **8**, 16939–16949 (2016).

85. Coulembier, O. *et al.* Synthesis of poly(l-lactide) and gradient copolymers from a l-lactide/trimethylene carbonate eutectic melt. *Chem. Sci.* **3**, 723–726 (2012).

86. Carriazo, D., Serrano, M. C., Gutiérrez, M. C., Ferrer, M. L. & del Monte, F. Deep-eutectic solvents playing multiple roles in the synthesis of polymers and related materials. *Chem. Soc. Rev.* **41**, 4996–5014 (2012).

87. Wang, J., Zhang, S., Ma, Z. & Yan, L. Deep eutectic solvents eutectogels: progress and challenges. *Green Chem. Eng.* **2**, 359–367 (2021).

88. Ruiz-Olles, J., Slavik, P., Whitelaw, N. K. & Smith, D. K. Self-Assembled Gels Formed in Deep Eutectic Solvents: Supramolecular Eutectogels with High Ionic Conductivity. *Angew. Chemie - Int. Ed.* **58**, 4173–4178 (2019).

89. Hümmer, M. *et al.* Synthesis of (-)-menthol fatty acid esters in and from (-)-menthol and fatty acids – novel concept for lipase catalyzed esterification based on eutectic solvents. *Mol. Catal.* **458**, 67–72 (2018).

90. Siebenhaller, S. *et al.* Sustainable enzymatic synthesis of glycolipids in a deep eutectic solvent system. *J. Mol. Catal. B Enzym.* **133**, S281–S287 (2016).

91. Pöhnlein, M. *et al.* Lipase-catalyzed synthesis of glucose-6-O-hexanoate in deep eutectic solvents. *Eur. J. Lipid Sci. Technol.* **117**, 161–166 (2015).

92. Sirviö, J. A. & Heiskanen, J. P. Synthesis of Alkaline-Soluble Cellulose Methyl Carbamate Using a Reactive Deep Eutectic Solvent. *ChemSusChem* **10**, 455–460 (2017).

93. Sirviö, J. A., Visanko, M. & Liimatainen, H. Acidic Deep Eutectic Solvents As Hydrolytic Media for Cellulose Nanocrystal Production. *Biomacromolecules* **17**, 3025–3032 (2016).

94. Laitinen, O., Ojala, J., Sirviö, J. A. & Liimatainen, H. Sustainable stabilization of oil in water emulsions by cellulose nanocrystals synthesized from deep eutectic solvents. *Cellulose* **24**, 1679–1689 (2017).

95. Sirviö, J. A. & Visanko, M. Lignin-rich sulfated wood nanofibers as high-performing adsorbents for the removal of lead and copper from water. *J. Hazard. Mater.* **383**, 121174 (2020).

96. Sirviö, J. A., Ukkola, J. & Liimatainen, H. Direct sulfation of cellulose fibers using a reactive deep eutectic solvent to produce highly charged cellulose nanofibers. *Cellulose* **26**, 2303–

2316 (2019).

97. Jaekel, E. E., Sirviö, J. A., Antonietti, M. & Filonenko, S. One-step method for the preparation of cationic nanocellulose in reactive eutectic media. *Green Chem.* **23**, 2317–2323 (2021).

98. Gore, S., Baskaran, S. & Koenig, B. Efficient synthesis of 3,4-dihydropyrimidin-2-ones in low melting tartaric acid–urea mixtures. *Green Chem.* **13**, 1009–1013 (2011).

99. Allegretti, C. *et al.* Reactive Deep Eutectic Solvents (RDESs): A New Tool for Phospholipase D-Catalyzed Preparation of Phospholipids. *Catalysts* vol. 11 (2021).

100. Markushyna, Y., Völkel, A., Savateev, A., Antonietti, M. & Filonenko, S. One-pot photocalalytic reductive formylation of nitroarenes via multielectron transfer by carbon nitride in functional eutectic medium. *J. Catal.* **380**, 186–194 (2019).

101. Bakthadoss, M., Sivakumar, G. & Kannan, D. Solid-State Melt Reaction for the Domino Process: Highly Efficient Synthesis of Fused Tetracyclic Chromenopyran Pyrimidinediones Using Baylis−Hillman Derivatives. *Org. Lett.* **11**, 4466–4469 (2009).

102. Mayurachayakul, P., Niamnont, N., Chaiseeda, K. & Chantarasriwong, O. Catalyst- and Solvent-Free Synthesis of N-Acylhydrazones via Solid-State Melt Reaction. *Asian J. Org. Chem.* **11**, e202200117 (2022).

103. Mayurachayakul, P., Pluempanupat, W., Srisuwannaket, C. & Chantarasriwong, O. Four-component synthesis of polyhydroquinolines under catalyst- and solvent-free conventional heating conditions: mechanistic studies. *RSC Adv.* **7**, 56764–56770 (2017).

104. Bakthadoss, M. & Murugan, G. Highly Stereoselective Synthesis of Tricyclic Chromenoisoxazolidines by Intramolecular 1,3-Dipolar Cycloadditions. *European J. Org. Chem.* **2010**, 5825–5830 (2010).

105. Bakthadoss, M., Selvakumar, R. & Srinivasan, J. An efficient protocol for the synthesis of benzoheterocyclic compounds via solid-state melt reaction (SSMR). *Tetrahedron Lett.* **55**, 5808–5812 (2014).

106. Paul, S. & Lee, Y. R. Eco-friendly construction of highly functionalized chromenopyridinones by an organocatalyzed solid-state melt reaction and their optical properties. *Green Chem.* **18**, 1488–1494 (2016).

107. Dąbrowska, S., Chudoba, T., Wojnarowicz, J. & Łojkowski, W. Current Trends in the Development of Microwave Reactors for the Synthesis of Nanomaterials in Laboratories and Industries: A Review. *Crystals* vol. 8 (2018).

108. Priecel, P. & Lopez-Sanchez, J. A. Advantages and Limitations of Microwave Reactors: From Chemical Synthesis to the Catalytic Valorization of Biobased Chemicals. *ACS Sustain. Chem. Eng.* **7**, 3–21 (2019).

109. Gedye, R. *et al.* The use of microwave ovens for rapid organic synthesis. *Tetrahedron Lett.* **27**, 279–282 (1986).

110. Gedye, R. N., Rank, W. & Westaway, K. C. The rapid synthesis of organic compounds in microwave ovens. II. *Can. J. Chem.* **69**, 706–711 (1991).

111. Palma, V. *et al.* Microwaves and heterogeneous catalysis: A review on selected catalytic processes. *Catalysts* **10**, (2020).

112. Buttress, A. J. *et al*. Design and optimisation of a microwave reactor for kilo-scale polymer synthesis. *Chem. Eng. Sci. X* **2**, 100022 (2019).

113. Zheng, B., Fang, Z., Cheng, J. & Jiang, Y. Microwave-assisted Conversion of Carbohydrates into 5-Hydroxymethylfurfural Catalyzed by ZnCl2. **65**, 168–172 (2010).

114. Romano, P. N. *et al.* Microwave-Assisted Selective Hydrogenation of Furfural to Furfuryl Alcohol Employing a Green and Noble Metal-Free Copper Catalyst. *ChemSusChem* **9**, 3387–3392 (2016).

115. Li, X. *et al.* Sulfonated copolymers with SO3H and COOH groups for the hydrolysis of polysaccharides. *J. Mater. Chem.* **22**, 1283–1289 (2012).

116. Sweygers, N., Alewaters, N., Dewil, R. & Appels, L. Microwave effects in the dilute acid hydrolysis of cellulose to 5-hydroxymethylfurfural. *Sci. Rep.* **8**, 7719 (2018).

117. Jacob, J., Chia, L. H. L. & Boey, F. Y. C. Thermal and non-thermal interaction of microwave radiation with materials. *J. Mater. Sci.* **30**, 5321–5327 (1995).

118. De La Hoz, A., Díaz-Ortiz, A. & Prieto, P. *Microwave-assisted green organic synthesis*. *RSC Green Chemistry* vols 2016-Janua (The Royal Society of Chemistry, 2016).

119. Kuhnert, N. Microwave-Assisted Reactions in Organic Synthesis—Are There Any Nonthermal Microwave Effects? *Angew. Chemie Int. Ed.* **41**, 1863–1866 (2002).

120. Strauss, C. R. Microwave-Assisted Reactions in Organic Synthesis—Are There Any Nonthermal Microwave Effects? Response to the Highlight by N. Kuhnert. *Angew. Chemie Int. Ed.* **41**, 3589–3591 (2002).

121. Kappe, C. O., Pieber, B. & Dallinger, D. Microwave Effects in Organic Synthesis: Myth or Reality? *Angew. Chemie Int. Ed.* **52**, 1088–1094 (2013).

122. Dudley, G. B., Stiegman, A. E. & Rosana, M. R. Correspondence on Microwave Effects in Organic Synthesis. *Angew. Chemie Int. Ed.* **52**, 7918–7923 (2013).

123. Kappe, C. O. Reply to the Correspondence on Microwave Effects in Organic Synthesis. *Angew. Chemie Int. Ed.* **52**, 7924–7928 (2013).

124. Herrero, M. A., Kremsner, J. M. & Kappe, C. O. Nonthermal Microwave Effects Revisited: On the Importance of Internal Temperature Monitoring and Agitation in Microwave Chemistry. *J. Org. Chem.* **73**, 36–47 (2008).

125. Zhang, X., O. Hayward, D. & Michael P. Mingos, D. Apparent equilibrium shifts and hot-spot formation for catalytic reactions induced by microwave dielectric heating. *Chem. Commun.* 975–976 (1999) doi:10.1039/A901245A.

126. Zhang, X., Hayward, D. O. & Mingos, D. M. P. Effects of Microwave Dielectric Heating on Heterogeneous Catalysis. *Catal. Letters* **88**, 33–38 (2003).

127. Xu, W., Zhou, J., Su, Z., Ou, Y. & You, Z. Microwave catalytic effect: a new exact reason for microwave-driven heterogeneous gas-phase catalytic reactions. *Catal. Sci. Technol.* **6**, 698–702 (2016).

128. Ano, T. *et al.* Probing the temperature of supported platinum nanoparticles under microwave irradiation by in situ and operando XAFS. *Commun. Chem.* **3**, 86 (2020).

129. Duangkamol, C., Batsomboon, P., Stiegman, A. E. & Dudley, G. B. Microwave Heating Outperforms Conventional Heating for a Thermal Reaction that Produces a Thermally Labile Product: Observations Consistent with Selective Microwave Heating. *Chem. – An Asian J.* **14**, 2594–2597 (2019).

130. Kappe, C. O. My Twenty Years in Microwave Chemistry: From Kitchen Ovens to Microwaves that aren't Microwaves. *Chem. Rec.* **19**, 15–39 (2019).

131. Gou, D., Huang, K., Liu, Y., Shi, H. & Wu, Z. Investigation of Spatial Orientation and Kinetic Energy of Reactive Site Collision between Benzyl Chloride and Piperidine: Novel Insight into the Microwave Nonthermal Effect. *J. Phys. Chem. A* **126**, 2690–2705 (2022).

132. Antonio, C. & Deam, R. T. Can "microwave effects" be explained by enhanced diffusion? *Phys. Chem. Chem. Phys.* **9**, 2976–2982 (2007).

133. Bionic Laboratories BLG GmbH - A short overview of the core Bionic Technologies. https://www.bionic-world.net/index.php/en/technology.

134. Microwave Chemical Co. Ltd., Production plant. https://mwcc.jp/en/service_technology/productionplant.html.

135. Ramopoulos, V., Link, G., Soldatov, S. & Jelonnek, J. Industrial scale microwave applicator for high temperature alkaline hydrolysis of PET. *Proc. Int. Astron. Union* **10**, 709–716 (2018).

136. Eghbal Sarabi, F., Liu, J., Stankiewicz, A. I. & Nigar, H. Reverse traveling microwave reactor – Modelling and design considerations. *Chem. Eng. Sci.* **246**, 116862 (2021).

137. Taghian Dinani, S., Kubbutat, P. & Kulozik, U. Assessment of heating profiles in model food systems heated by different microwave generators: Solid-state (semiconductor) versus traditional magnetron technology. *Innov. Food Sci. Emerg. Technol.* **63**, 102376 (2020).

138. Leonelli, C. & Mason, T. J. Microwave and ultrasonic processing: Now a realistic option for industry. *Chem. Eng. Process. Process Intensif.* **49**, 885–900 (2010).

139. Stefanidis, G. D., Muñoz, A. N., Sturm, G. S. J. & Stankiewicz, A. A helicopter view of microwave application to chemical processes: reactions, separations, and equipment concepts. **30**, 233–259 (2014).

140. Sturm, G. S. J., Stankiewicz, A. I. & Stefanidis, G. D. Microwave Reactor Concepts: From

Resonant Cavities to Traveling Fields. in *Alternative Energy Sources for Green Chemistry* (The Royal Society of Chemistry, 2016). doi:10.1039/9781782623632-00093.

141. Bermúdez, J. M., Beneroso, D., Rey-Raap, N., Arenillas, A. & Menéndez, J. A. Energy consumption estimation in the scaling-up of microwave heating processes. *Chem. Eng. Process. Process Intensif.* **95**, 1–8 (2015).

142. Lu, X., Xi, B., Zhang, Y. & Angelidaki, I. Microwave pretreatment of rape straw for bioethanol production: Focus on energy efficiency. *Bioresour. Technol.* **102**, 7937–7940 (2011).

143. Barnard, T. M., Leadbeater, N. E., Boucher, M. B., Stencel, L. M. & Wilhite, B. A. Continuous-Flow Preparation of Biodiesel Using Microwave Heating. *Energy & Fuels* **21**, 1777–1781 (2007).

144. Choedkiatsakul, I., Ngaosuwan, K., Assabumrungrat, S., Mantegna, S. & Cravotto, G. Biodiesel production in a novel continuous flow microwave reactor. *Renew. Energy* **83**, 25–29 (2015).

145. Lertsathapornsuk, V., Pairintra, R., Aryusuk, K. & Krisnangkura, K. Microwave assisted in continuous biodiesel production from waste frying palm oil and its performance in a 100 kW diesel generator. *Fuel Process. Technol.* **89**, 1330–1336 (2008).

146. Moseley, J. D. & Woodman, E. K. Energy Efficiency of Microwave- and Conventionally Heated Reactors Compared at meso Scale for Organic Reactions. *Energy & Fuels* **23**, 5438–5447 (2009).

147. Razzaq, T. & Kappe, C. O. On the Energy Efficiency of Microwave-Assisted Organic Reactions. *ChemSusChem* **1**, 123–132 (2008).

148. Statistisches Bundesamt. *Energieverbrauch in der Industrie 2020 um 1,9 % gegenüber dem Vorjahr gesunken [Press release]*. https://www.destatis.de/DE/Presse/Pressemitteilungen/2021/12/PD21_551_435.html (2021).

149. Frauenhofer-UMSICHT. *Die Industriezukunft braucht dringend klimaneutrale Prozesswärme [Press release]*. https://www.umsicht.fraunhofer.de/de/presse-medien/pressemitteilungen/2022/waermewende-industrie.html (2022).

150. Arbeitsgruppe Erneuerbare Energien-Statistik (AGEE-Stat) am Umweltbundesamt. Erneuerbare Energien in Deutschland - Daten zur Entwicklung im Jahr 2020. *Umweltbundesamt* (2021).

151. Schüwer, D. & Schneider, C. Electrification of industrial process heat: Long-term applications, potentials and impacts. *Eceee Ind. Summer Study Proc.* **2018-June**, 411–422 (2018).

152. Amini, A., Latifi, M. & Chaouki, J. Electrification of materials processing via microwave irradiation: A review of mechanism and applications. *Appl. Therm. Eng.* **193**, 117003

(2021).

153. Long, B. L. *International Environmental Issues and the OECD 1950-2000: an historical perspective*. (OECD Publishing, 2000).

154. Stephan, D. G. & Atcheson, J. The EPA's approach to pollution prevention. *Chem. Eng. Prog.* **85**, 53–58 (1989).

155. Roberts, J. A. Creating Green Chemistry: Discursive Strategies of a Scientific Movement. 196 (2005).

156. Anastas, P. & Warner, J. C. *Green chemistry : theory and practice*. (Oxford University Press, Oxford (England), 1998).

157. Linthorst, J. A. An overview: origins and development of green chemistry. *Found. Chem.* **12**, 55–68 (2010).

158. Ratti, R. Industrial applications of green chemistry: Status, Challenges and Prospects. *SN Appl. Sci.* **2**, 263 (2020).

159. Anastas, P. Twenty Years OF Green Chemistry. *c&en chemical & engineering news* Volume 89, Issue 26 (2011).

160. Woodhouse, E. J. & Breyman, S. Green Chemistry as Social Movement? *Sci. Technol. Hum. Values* **30**, 199–222 (2005).

161. Anastas, P. T. & Kirchhoff, M. M. Origins, Current Status, and Future Challenges of Green Chemistry. *Acc. Chem. Res.* **35**, 686–694 (2002).

162. Winterton, N. Green chemistry: deliverance or distraction? *Clean Technol. Environ. Policy* **18**, 991–1001 (2016).

163. Winterton, N. The green solvent: a critical perspective. *Clean Technol. Environ. policy* **23**, 2499–2522 (2021).

164. Fenner, K. & Scheringer, M. The Need for Chemical Simplification As a Logical Consequence of Ever-Increasing Chemical Pollution. *Environ. Sci. Technol.* **55**, 14470–14472 (2021).

165. Glüge, J. *et al.* An overview of the uses of per- and polyfluoroalkyl substances (PFAS). *Environ. Sci. Process. Impacts* **22**, 2345–2373 (2020).

166. Persson, L. *et al.* Outside the Safe Operating Space of the Planetary Boundary for Novel Entities. *Environ. Sci. Technol.* **56**, 1510–1521 (2022).

167. Anastas, N. D. Connecting toxicology and chemistry to ensure safer chemical design. *Green Chem.* **18**, 4325–4331 (2016).

168. Zimmerman, J. B., Anastas, P. T., Erythropel, H. C. & Leitner, W. Designing for a green chemistry future. *Science (80-.).* **367**, 397–400 (2020).

169. Hellwig, M. & Henle, T. Baking, Ageing, Diabetes: A Short History of the Maillard Reaction.

Angew. Chemie Int. Ed. **53**, 10316–10329 (2014).

170. Nursten, H. E. *The Maillard Reaction*. (The Royal Society of Chemistry, 2005). doi:10.1039/9781847552570.

171. Agyei-Aye, K., Chian, M. X., Lauterbach, J. H. & Moldoveanu, S. C. The role of the anion in the reaction of reducing sugars with ammonium salts. *Carbohydr. Res.* **337**, 2273–2277 (2002).

172. Vollmuth, T. A. Caramel color safety – An update. *Food Chem. Toxicol.* **111**, 578–596 (2018).

173. Sengar, G. & Sharma, H. K. Food caramels: a review. *J. Food Sci. Technol.* **51**, 1686–1696 (2014).

174. Kort, M. J. Reactions of Free Sugars with Aqueous Ammonia. *Adv. Carbohydr. Chem. Biochem.* **25**, 311–349 (1970).

175. Nunes, F. M., Del Castillo, M. D. & Carbonero, F. Editorial: Food Melanoidins: Chemistry and Nutrition. *Front. Nutr.* **9**, (2022).

176. Tsuchida, H., Komoto, M. & Mizuno, S. Isolation and Identification of Polyhydroxyalkylpyrazines in Soy Sauce. *Nippon SHOKUHIN KOGYO GAKKAISHI* **37**, 154–161 (1990).

177. Magaletta, R. L. & Ho, C. T. Effect of Roasting Time and Temperature on the Generation of Nonvolatile (Polyhydroxyalkyl)pyrazine Compounds in Peanuts, As Determined by High-Performance Liquid Chromatography. *J. Agric. Food Chem.* **44**, 2629–2635 (1996).

178. Tsuchida, H., Morinaka, K., Fujii, S., Komoto, M. & Mizuno, S. Identification of novel non-volatile pyrazines in commercial caramel colors. *Dev. Food Sci.* **13**, 85–94 (1986).

179. Bhattacherjee, A., Hrynets, Y. & Betti, M. Fructosazine, a Polyhydroxyalkylpyrazine with Antimicrobial Activity: Mechanism of Inhibition against Extremely Heat Resistant Escherichia coli. *J. Agric. Food Chem.* **64**, 8530–8539 (2016).

180. Hrynets, Y., Bhattacherjee, A., Ndagijimana, M., Hincapie Martinez, D. J. & Betti, M. Iron (Fe2+)-Catalyzed Glucosamine Browning at 50 °c: Identification and Quantification of Major Flavor Compounds for Antibacterial Activity. *J. Agric. Food Chem.* **64**, 3266–3275 (2016).

181. Georges, B., Carry, J., Evers, M. & Filoche, B. Polyhydroxyalkylpyrazine derivatives, their preparation and medicaments comprising them. vol. 1 (2004).

182. Chesnokov, V., Gong, B., Sun, C. & Itakura, K. Anti-cancer activity of glucosamine through inhibition of N-linked glycosylation. *Cancer Cell Int.* **14**, 1–10 (2014).

183. Zhu, A., Huang, J. B., Clark, A., Romero, R. & Petty, H. R. 2,5-Deoxyfructosazine, a d-glucosamine derivative, inhibits T-cell interleukin-2 production better than d-glucosamine. *Carbohydr. Res.* **342**, 2745–2749 (2007).

184. Wu, S. *et al.* Conversions of Cellobiose and Inulin to Deoxyfructosazine in Aqueous Solutions. *CLEAN – Soil, Air, Water* **39**, 572–576 (2011).

185. Li, Y. & et al. A method of 2,5- deoxy fructosazine is prepared using fructose. (2019).

186. Jia, L., Wang, Y., Qiao, Y., Qi, Y. & Hou, X. Efficient one-pot synthesis of deoxyfructosazine and fructosazine from d-glucosamine hydrochloride using a basic ionic liquid as a dual solvent-catalyst. *RSC Adv.* **4**, 44253–44260 (2014).

187. Yingxiong Wang, Xianglin Hou, Lingyu Jia, Pengfei Liu, Y. Q. Preparation method and application of fructosazine. (2021).

188. Jezo, I. & Luzak, I. Aminolýza sacharózy (V) Reakcia sacharózy s vodným roztokom etanolaminu. *Chem. Pap.* **18**, 837–851 (1964).

189. Kuhn, R., Krüger, G., Haas, H. J. & Seeliger, A. Pyrazinbildung aus Aminozuckern. **644**, (1961).

190. Tsuchida, H., Kōmoto, M., Kato, H. & Fujimaki, M. Isolation of Deoxyfructosazine and Its 6-Isomer from the Nondialyzable Melanoidin Hydrolyzate. *Agric. Biol. Chem.* **39**, 1143–1148 (1975).

191. Tsuchida, H., Tachibana, S. & Komoto, M. Isolation and identification of 2-(d-threo-trihydroxypropyl)-5-(d-grycero-2′, 3′-dihydroxypropyl)pyr azine and its 6-isomer from the browning reaction between xylose and ammonium formate. *Agric. Biol. Chem.* **40**, 1241–1242 (1976).

192. Tsuchida, H., Tachibana, S., Kitamura, K. & Komoto, M. Formation of Deoxyfructosazine and Its 6-Isomer by the Browning Reaction between Fructose and Ammonium Formate. *Agric. Biol. Chem.* **40**, 921–925 (1976).

193. Filonenko, S., Voelkel, A. & Antonietti, M. Valorization of monosaccharides towards fructopyrazines in a new sustainable and efficient eutectic medium. *Green Chem.* **21**, 5256–5266 (2019).

194. Bhattacherjee, A., Hrynets, Y. & Betti, M. Fructosazine, a Polyhydroxyalkylpyrazine with Antimicrobial Activity: Mechanism of Inhibition against Extremely Heat Resistant Escherichia coli. *J. Agric. Food Chem.* **64**, 8530–8539 (2016).

195. Dai, Y., Witkamp, G. J., Verpoorte, R. & Choi, Y. H. Tailoring properties of natural deep eutectic solvents with water to facilitate their applications. *Food Chem.* **187**, 14–19 (2015).

196. Bashiardes, Georges; Carry, Jean-Christophe; Evers, Michel; Filoche, Bruno; Mignani, S. Preparation of polyhydroalkylpyrazines as hypoglycemics. (2000).

197. Sherwood, J., Farmer, T. J. & Clark, J. H. Catalyst: Possible Consequences of the N-Methyl Pyrrolidone REACH Restriction. *Chem* **4**, 2010–2012 (2018).

198. Jessop, P. G., Jessop, D. A., Fu, D. & Phan, L. Solvatochromic parameters for solvents of interest in green chemistry. *Green Chem.* **14**, 1245–1259 (2012).

199. Werpy T, Frye JG, Wang Y, Z. A. In Methods of making pyrrolidones. (2003).

200. Manzer, L. In Production of 5-methyl-n-aryl-2-pyrrolidone and 5-methyl-n-alkyl- 2-pyrrolidone. (2004).

201. Sun, Z., Chen, J. & Tu, T. NHC-based coordination polymers as solid molecular catalysts for reductive amination of biomass levulinic acid. *Green Chem.* **19**, 789–794 (2017).

202. Amarasekara, A. S. & Lawrence, Y. M. Raney-Ni catalyzed conversion of levulinic acid to 5-methyl-2-pyrrolidone using ammonium formate as the H and N source. *Tetrahedron Lett.* **59**, 1832–1835 (2018).

203. M. E. Hawkins, P. *et al.* Potent Bactericidal Antimycobacterials Targeting the Chaperone ClpC1 Based on the Depsipeptide Natural Products Ecumicin and Ohmyungsamycin A. *J. Med. Chem.* **65**, 4893–4908 (2022).

204. Iavicoli, I. *et al.* In vitro evaluation of the potential toxic effects of palladium nanoparticles on fibroblasts and lung epithelial cells. *Toxicol. Vitr.* **42**, 191–199 (2017).

205. Ledoux, A., Sandjong Kuigwa, L., Framery, E. & Andrioletti, B. A highly sustainable route to pyrrolidone derivatives - Direct access to biosourced solvents. *Green Chem.* **17**, 3251–3254 (2015).

206. Ma, T., Zhang, H. Y., Yin, G., Zhao, J. & Zhang, Y. Catalyst-free reductive amination of levulinic acid to N-substituted pyrrolidinones with formic acid in continuous-flow microreactor. *J. Flow Chem.* **8**, 35–43 (2018).

207. Wu, H., Dai, W., Saravanamurugan, S., Li, H. & Yang, S. Quasi-Catalytic Approach to N-Unprotected Lactams via Transfer Hydro-amination/Cyclization of Biobased Keto Acids. *ACS Sustain. Chem. Eng.* **7**, 10207–10213 (2019).

208. Pollard, C. B. & Young, D. C. The mechanism of the leuckart reaction. *J. Org. Chem.* **16**, 661–672 (1951).

209. Adrian, E. D. The mechanism of the nerves. *Nature* **123**, 167–169 (1929).

210. Webers, V. J., Bruce, W. F. & Bruce, W. F. Reaction: A Study of the Mechanism. **1954**, 1941–1943 (1980).

211. Loupy, A. *et al.* Towards the rehabilitation of the Leuckart reductive amination reaction using microwave technology. *Tetrahedron Lett.* **37**, 8177–8180 (1996).

212. Islam, M. K. *et al.* N-Methyl-2-pyrrolidone pre-treatment of lignocellulose for high lignin yield and cellulose digestibility. *Biomass Convers. Biorefinery* (2022) doi:10.1007/s13399-022-02655-2.

213. Bajwa, D. S., Pourhashem, G., Ullah, A. H. & Bajwa, S. G. A concise review of current lignin production, applications, products and their environmental impact. *Ind. Crops Prod.* **139**, 111526 (2019).

214. Tuck, C. O., Pérez, E., Horváth, I. T., Sheldon, R. A. & Poliakoff, M. Valorization of Biomass:

Deriving More Value from Waste. *Science (80-.).* **337**, 695–699 (2012).

215. Zakzeski, J., Bruijnincx, P. C. A., Jongerius, A. L. & Weckhuysen, B. M. The Catalytic Valorization of Lignin for the Production of Renewable Chemicals. *Chem. Rev.* **110**, 3552–3599 (2010).

216. Wang, H., Pu, Y., Ragauskas, A. & Yang, B. From lignin to valuable products–strategies, challenges, and prospects. *Bioresour. Technol.* **271**, 449–461 (2019).

217. Mittal, A. *et al*. Ammonia Pretreatment of Corn Stover Enables Facile Lignin Extraction. *ACS Sustain. Chem. Eng.* **5**, 2544–2561 (2017).

218. Bouxin, F. P., David Jackson, S. & Jarvis, M. C. Isolation of high quality lignin as a by-product from ammonia percolation pretreatment of poplar wood. *Bioresour. Technol.* **162**, 236–242 (2014).

219. Brandt, A., Gräsvik, J., Hallett, J. P. & Welton, T. Deconstruction of lignocellulosic biomass with ionic liquids. *Green Chem.* **15**, 550–583 (2013).

220. Sathitsuksanoh, N. *et al.* Lignin fate and characterization during ionic liquid biomass pretreatment for renewable chemicals and fuels production. *Green Chem.* **16**, 1236–1247 (2014).

221. Guo, Z. *et al.* Short-time deep eutectic solvent pretreatment for enhanced enzymatic saccharification and lignin valorization. *Green Chem.* **21**, 3099–3108 (2019).

222. Luterbacher, J. S. *et al.* Nonenzymatic Sugar Production from Biomass Using Biomass-Derived γ-Valerolactone. *Science (80-.).* **343**, 277–280 (2014).

223. Shi, T. *et al.* Aminated and amidated structures introduced by ethylenediamine pretreatment endow lignin with bright fluorescence. *Green Chem.* **24**, 9040–9054 (2022).

224. Xu, L. *et al.* High-solid ethylenediamine pretreatment to fractionate new lignin streams from lignocellulosic biomass. *Chem. Eng. J.* **427**, 130962 (2022).

225. Yu, O., Yoo, C. G., Kim, C. S. & Kim, K. H. Understanding the Effects of Ethylene Glycol-Assisted Biomass Fractionation Parameters on Lignin Characteristics Using a Full Factorial Design and Computational Modeling. *ACS Omega* **4**, 16103–16110 (2019).

226. Filipe, B. & Sampaio, C. Development of a propylene glycol-based organosolv process for biomass fractionation October 2019. (2019).

227. Bloom, D., Hoffman, C. & Soper, G. Methods for producing bioderived propylene glycol. vol. 2 (2017).

228. Rivas Torres, B. *et al.* Bio-derived ethylene glycol compositions for polyester bottle. vol. 1 1–29 (2022).

229. Margellou, A. G. *et al.* Catalytic fast pyrolysis of beech wood lignin isolated by different biomass (pre)treatment processes: Organosolv, hydrothermal and enzymatic hydrolysis. *Appl. Catal. A Gen.* **623**, 118298 (2021).

230. Luo, J., Zhou, Q.-Q., Montag, M., Ben-David, Y. & Milstein, D. Acceptorless dehydrogenative synthesis of primary amides from alcohols and ammonia. *Chem. Sci.* **13**, 3894–3901 (2022).

231. Jursic, B. S. & Zdravkovski, Z. A Simple Preparation of Amides from Acids and Amines by Heating of Their Mixture. *Synth. Commun.* **23**, 2761–2770 (1993).

232. Barbaro, P., Liguori, F., Oldani, C. & Moreno-Marrodán, C. Sustainable Catalytic Synthesis for a Bio-Based Alternative to the Reach-Restricted N-Methyl-2-Pyrrolidone. *Adv. Sustain. Syst.* **4**, 1900117 (2020).

233. Moreno-Marrodan, C., Liguori, F. & Barbaro, P. Sustainable processes for the catalytic synthesis of safer chemical substitutes of N-methyl-2-pyrrolidone. *Mol. Catal.* **466**, 60–69 (2019).

234. Luo, T. *et al.* Preparation and Characterization of Size-Controlled Lignin Nanoparticles with Deep Eutectic Solvents by Nanoprecipitation. *Molecules* vol. 26 (2021).

235. Dunlop, A. P. & Sherman, E. 5-Methyl-2-pyrrolidinone. *United States* (1954).

236. Faix, O. Classification of Lignins from Different Botanical Origins by FT-IR Spectroscopy. **45**, 21–28 (1991).

237. Chapter 2 - Structure and Characteristics of Lignin. in (eds. Huang, J., Fu, S. & Gan, L. B. T.-L. C. and A.) 25–50 (Elsevier, 2019). doi:https://doi.org/10.1016/B978-0-12-813941-7.00002-3.

238. Hu, X. *et al.* Surface passivated carbon nanodots prepared by microwave assisted pyrolysis: effect of carboxyl group in precursors on fluorescence properties. *RSC Adv.* **4**, 18818–18826 (2014).

239. Zhu, S. *et al.* Highly Photoluminescent Carbon Dots for Multicolor Patterning, Sensors, and Bioimaging. *Angew. Chemie Int. Ed.* **52**, 3953–3957 (2013).

240. Shi, W., Li, X. & Ma, H. A Tunable Ratiometric pH Sensor Based on Carbon Nanodots for the Quantitative Measurement of the Intracellular pH of Whole Cells. *Angew. Chemie Int. Ed.* **51**, 6432–6435 (2012).

241. Zhai, X. *et al.* Highly luminescent carbon nanodots by microwave-assisted pyrolysis. *Chem. Commun.* **48**, 7955–7957 (2012).

242. Wang, F. *et al.* Down- and up-conversion luminescent carbon dot fluid: inkjet printing and gel glass fabrication. *Nanoscale* **6**, 3818–3823 (2014).

243. Qu, S., Wang, X., Lu, Q., Liu, X. & Wang, L. A Biocompatible Fluorescent Ink Based on Water-Soluble Luminescent Carbon Nanodots. *Angew. Chemie Int. Ed.* **51**, 12215–12218 (2012).

244. Bin Yang, H. *et al.* Graphene quantum dots-incorporated cathode buffer for improvement of inverted polymer solar cells. *Sol. Energy Mater. Sol. Cells* **117**, 214–218 (2013).

245. Yang, H. Bin, Dong, Y. Q., Wang, X., Khoo, S. Y. & Liu, B. Cesium Carbonate Functionalized

Graphene Quantum Dots as Stable Electron-Selective Layer for Improvement of Inverted Polymer Solar Cells. *ACS Appl. Mater. Interfaces* **6**, 1092–1099 (2014).

246. Bian, J. *et al.* Carbon Dot Loading and TiO2 Nanorod Length Dependence of Photoelectrochemical Properties in Carbon Dot/TiO2 Nanorod Array Nanocomposites. *ACS Appl. Mater. Interfaces* **6**, 4883–4890 (2014).

247. Lin, X., Gao, G., Zheng, L., Chi, Y. & Chen, G. Encapsulation of Strongly Fluorescent Carbon Quantum Dots in Metal–Organic Frameworks for Enhancing Chemical Sensing. *Anal. Chem.* **86**, 1223–1228 (2014).

248. Dong, Y., Wang, R., Tian, W., Chi, Y. & Chen, G. "Turn-on" fluorescent detection of cyanide based on polyamine-functionalized carbon quantum dots. *RSC Adv.* **4**, 3701–3705 (2014).

249. Dong, Y. *et al.* Polyamine-Functionalized Carbon Quantum Dots as Fluorescent Probes for Selective and Sensitive Detection of Copper Ions. *Anal. Chem.* **84**, 6220–6224 (2012).

250. Yan, F. *et al.* Highly photoluminescent carbon dots-based fluorescent chemosensors for sensitive and selective detection of mercury ions and application of imaging in living cells. *Sensors Actuators B Chem.* **192**, 488–495 (2014).

251. Zhu, S. *et al.* Highly Photoluminescent Carbon Dots for Multicolor Patterning, Sensors, and Bioimaging. *Angew. Chemie Int. Ed.* **52**, 3953–3957 (2013).

252. Behrmann, A. & Hofmann, A. W. Ueber die Amide der Citronensäure; Umwandlung derselben in Pyridinverbindungen. *Berichte der Dtsch. Chem. Gesellschaft* **17**, 2681–2699 (1884).

253. Sell, W. J. & Easterfield, T. H. LXXIII.—Studies on citrazinic acid. Part I. *J. Chem. Soc. Trans.* **63**, 1035–1051 (1893).

254. Easterfield, T. H. & Sell, W. J. V.—Studies on citrazinic acid. Part II. *J. Chem. Soc. Trans.* **65**, 28–31 (1894).

255. Shadrin, A. E. Process E-6: laboratory processing of color reversible photographic films of the Ektachrome type. (1992).

256. Kasprzyk, W., Bednarz, S., Żmudzki, P., Galica, M. & Bogdał, D. Novel efficient fluorophores synthesized from citric acid. *RSC Adv.* **5**, 34795–34799 (2015).

257. Kasprzyk, W., Świergosz, T., Romańczyk, P. P., Feldmann, J. & Stolarczyk, J. K. The role of molecular fluorophores in the photoluminescence of carbon dots derived from citric acid: current state-of-the-art and future perspectives. *Nanoscale* **14**, 14368–14384 (2022).

258. Cadranel, A., Margraf, J. T., Strauss, V., Clark, T. & Guldi, D. M. Carbon Nanodots for Charge-Transfer Processes. *Acc. Chem. Res.* **52**, 955–963 (2019).

259. Ragazzon, G. *et al.* Optical processes in carbon nanocolloids. *Chem* **7**, 606–628 (2021).

260. Wang, C., Strauss, V. & Kaner, R. B. Carbon Nanodots for Capacitor Electrodes. *Trends Chem.* **1**, 858–868 (2019).

261. Shan, D., Hsieh, J.-T., Bai, X. & Yang, J. Citrate-Based Fluorescent Biomaterials. *Adv. Healthc. Mater.* **7**, 1800532 (2018).

262. Vallan, L. & Imahori, H. Citric Acid-Based Carbon Dots and Their Application in Energy Conversion. *ACS Appl. Electron. Mater.* (2022) doi:10.1021/acsaelm.2c01021.

263. Ren, J., Malfatti, L. & Innocenzi, P. Citric Acid Derived Carbon Dots, the Challenge of Understanding the Synthesis-Structure Relationship. *C* vol. 7 (2021).

264. Righetto, M. *et al.* Spectroscopic Insights into Carbon Dot Systems. *J. Phys. Chem. Lett.* **8**, 2236–2242 (2017).

265. Song, Y. *et al.* Investigation from chemical structure to photoluminescent mechanism: a type of carbon dots from the pyrolysis of citric acid and an amine. *J. Mater. Chem. C* **3**, 5976–5984 (2015).

266. Strauss, V., Wang, H., Delacroix, S., Ledendecker, M. & Wessig, P. Carbon nanodots revised: the thermal citric acid/urea reaction. *Chem. Sci.* **11**, 8256–8266 (2020).

267. Reckmeier, C. J. *et al.* Aggregated Molecular Fluorophores in the Ammonothermal Synthesis of Carbon Dots. *Chem. Mater.* **29**, 10352–10361 (2017).

268. Reckmeier, C. J. *et al.* Aggregated Molecular Fluorophores in the Ammonothermal Synthesis of Carbon Dots. *Chem. Mater.* **29**, 10352–10361 (2017).

269. Wang, W. *et al.* Shedding light on the effective fluorophore structure of high fluorescence quantum yield carbon nanodots. *RSC Adv.* **7**, 24771–24780 (2017).

270. Ensign, J. C. & Rittenberg, S. C. The formation of a blue pigment in the bacterial oxidation of isonicotinic acid. *Arch. Mikrobiol.* **51**, 384–392 (1965).

271. Sutthiwong, N., Fouillaud, M., Valla, A., Caro, Y. & Dufossé, L. Bacteria belonging to the extremely versatile genus Arthrobacter as novel source of natural pigments with extended hue range. *Food Res. Int.* **65**, 156–162 (2014).

272. Jana, B. *et al.* Carbon Nanodots for All-in-One Photocatalytic Hydrogen Generation. *J. Am. Chem. Soc.* **143**, 20122–20132 (2021).

273. Strauss, V. *et al.* Assigning Electronic States in Carbon Nanodots. *Adv. Funct. Mater.* **26**, 7975–7985 (2016).

274. Bourlinos, A. B. *et al.* Surface Functionalized Carbogenic Quantum Dots. *Small* **4**, 455–458 (2008).

275. Tang, B., Zhao, J., Xu, J.-F. & Zhang, X. Tuning the stability of organic radicals: from covalent approaches to non-covalent approaches. *Chem. Sci.* **11**, 1192–1204 (2020).

276. Murto, P. & Bronstein, H. Electro-optical π-radicals: design advances{,} applications and future perspectives. *J. Mater. Chem. C* **10**, 7368–7403 (2022).

277. Song, Q., Li, F., Wang, Z. & Zhang, X. A supramolecular strategy for tuning the energy level

of naphthalenediimide: Promoted formation of radical anions with extraordinary stability. *Chem. Sci.* **6**, 3342–3346 (2015).

278. Jinshi, L., Pingchuan, S., Zujin, Z. & Zhong, T. Ben. Through-Space Conjugation: A Thriving Alternative for Optoelectronic Materials. *CCS Chem.* **1**, 181–196 (2019).

279. Sanchez-Viesca, F. & Gomez, R. On the Sabanin-Laskowski Test for Citric Acid. *World J. Org. Chem.* **8**, 5–6 (2020).

280. Soltzberg, L. J., Hagar, A., Kridaratikorn, S., Mattson, A. & Newman, R. MALDI-TOF Mass Spectrometric Identification of Dyes and Pigments. *J. Am. Soc. Mass Spectrom.* **18**, 2001–2006 (2007).

281. Duff, D. G., Kirkwood, D. J. & Stevenson, D. M. The Behaviour of Dyes in Aqueous Solutions. I. The Influence of Chemical Structure on Dye Aggregation - a Polarographic Study. *J. Soc. Dye. Colour.* **93**, 303–306 (1977).

282. Bradley, D. F. & Wolf, M. K. Aggregation of Dyes Bound To Polyanions. *Proc. Natl. Acad. Sci.* **45**, 944–952 (1959).

283. Evans, R., Wearne, R. H. & Wallis, A. F. A. Molecular weight distribution of cellulose as its tricarbanilate by high performance size exclusion chromatography. *J. Appl. Polym. Sci.* **37**, 3291–3303 (1989).

284. Sluiter, A. *et al.* Determination of structural carbohydrates and lignin in Biomass - NREL/TP-510-42618. *Natl. Renew. Energy Lab.* 17 (2008).

285. Wong, W. R., Oliver, A. G. & Linington, R. G. Development of Antibiotic Activity Profile Screening for the Classification and Discovery of Natural Product Antibiotics. *Chem. Biol.* **19**, 1483–1495 (2012).

286. Hawkins, P. M. E. *et al.* Potent Bactericidal Antimycobacterials Targeting the Chaperone ClpC1 Based on the Depsipeptide Natural Products Ecumicin and Ohmyungsamycin A. *J. Med. Chem.* **65**, 4893–4908 (2022).

287. Gambino, M., Gaune, P., Nabavian, M., Gaune-Escard, M. & Bros, J. P. Enthalpie de fusion de l'uree et de quelques melanges eutectiques a base d'uree. *Thermochim. Acta* **111**, 37–47 (1987).

Acknowledgements

I would like to thank the following people, who have contributed in one way or another to this work:

My supervisor Markus Antonietti, who gave me the opportunity to pursue my doctoral work in his department at MPIKG and who provided guidance and feedback throughout this endeavor.

My daily supervisor Svitlana Filonenko – for her support and the fruitful and trusting relationship we built over the time.

All the MPIKG technicians that have enabled this work. Special thanks to Antje Völkel, Bolortuya Badamorj, Eva Settels, Jessica Brandt, Heike Runge, Marlis Gräwert, Olaf Niemeyer and Regina Rothe.

The current and former members of the Sustainable Solvents group: Tina Seemann, Rui Xu, Ekaterina Sheridan, Esther Jaekel, Vitalii Tkachenko, Natallia Doskaliuk, Alexander Volikov and Roberto Calmanti for their energy, understanding and help throughout this time. And to Ella Buchner for her infectious motivation and great help.

The whole colloids department for the open and friendly atmosphere. Special thanks to my colleagues Majd Al-Naji, Volker Strauß and Sylvain Rath, for valuable scientific advice and invaluable moral support.

Lastly, for their inspiration, love, wisdom, generosity and endless patience I am grateful to my parents Ulrich Schneider and Esther Schneider, Frank Schmid, Anna Schmid, Jonas Eichhorn and Selma Eichhorn.